UNIVERSITÄT ZU LÜBECK

From the Institute of Psychology I

of the University of Lübeck

Director: Prof. Dr. rer. nat Nico Bunzeck

Functional and structural changes in the progression of Alzheimer's disease: insights from human imaging

Dissertation

for Fulfillment of

Requirements

for the Doctoral Degree

of the University of Lübeck

from the Department of Natural Sciences

Submitted by:

Marthe Mieling

from Itzehoe (Germany)

Lübeck 2024

First referee: Prof. Dr. rer. nat. Nico Bunzeck

Second referee: Prof. Dr. med. Alexander Münchau

Date of oral examination: 04.12.2024

Approved for printing. Lübeck, 18.12.2024

Table of contents

Acknowledgments

Working on this doctoral dissertation has been a journey filled with challenges, growth, and moments of joy. For me, it's not merely about the title I aim for but the invaluable lessons I have learned along the way that hold the greatest meaning. It's important to acknowledge that this accomplishment was not solely achieved through my efforts alone but rather through the support and assistance of numerous people.

First and foremost, I extend my heartfelt appreciation to my esteemed supervisor, Prof. Dr. Nico Bunzeck, whose guidance, expertise, and unwavering support have been instrumental in shaping this research as well as my academic journey. Nico, your mentorship has been invaluable, and I am deeply grateful for your dedication and belief in my abilities. Furthermore, I would like to thank Prof. Dr. Alexander Münchau for his willingness to examine this work.

I extend my thanks to the co-authors of the articles. Your effort and contributions shaped this work. Sincere gratitude to the Alzheimer's Disease Neuroimaging Initiative and all individuals participating and being engaged in the studies. I am deeply thankful for the Institute of Psychology I and the members of the Lifespan group, for their support and the positive atmosphere, Mushfa Yousuf, Alexandra Sobczak, Tineke Steiger, Anne Ritz, Christa Marx, Tanja Kruse, Anne Herrmann, and Michaela Haller. Furthermore, I would like to thank Davina Biel, Veronica Rozynek, Mushfa Yousuf, and Andreja Stajduhar for their constructive feedback.

To my families Mieling and Teßmann, your support, encouragement, and companionship have been incomparable to me. Thank you for everything. Moreover, I thank the Schnelle family for their open-heartedness and assistance in the past few years.

To my cherished friends, Lydia and Melanie: your inspiration and understanding have been a source of comfort and strength. Thank you for always being there for me.

To my partner, Thies: your love, patience, and unconditional daily support have been my rock throughout this journey. I must also mention our beloved dog Bonschi, who has never left my side since my undergraduate studies in Klagenfurt.

To all those mentioned above and to countless others who have supported me in ways seen and unseen, thank you from the depths of my heart. This work would not have been possible without you.

Finally, to the reader: I thank you for your interest in this thesis.

Abstract

Structural and functional brain changes are associated with the progression of Alzheimer's disease (AD). However, the precise alterations remain poorly understood. In light of this and based on recent AD models, this thesis aims to investigate structural and functional changes across the progression of AD using different methodological approaches. In **study 1** gray matter volume (GM) reductions in the cholinergic basal forebrain's (BF) nucleus basalis of Meynert (NbM) and medial temporal lobe (MTL) were compared between healthy older adults (HC), those with mild cognitive impairment (MCI), and AD dementia patients using coordinate-based voxel-based-morphometry (VBM) magnetic resonance imaging (MRI) meta-analyses (including 54 experiments). Reduced GM was observed in the bilateral BF's NbM in AD dementia but limited in MCI. Notably, MCI and AD dementia patients exhibited less GM in the amygdala and hippocampus, indicating more pronounced effects in the amygdala in AD dementia. **Study 2** investigated relevant features contributing to the diagnostic status and disease progression of HC, MCI, and AD dementia. Therefore, volumetric brain information, socio-demographics, CSF status, and genotyping information from the Alzheimer's Disease Neuroimaging Initiative (ADNI) were analyzed using an XGBoost machine learning (ML) algorithm to classify HC, MCI, and AD dementia (n=568). Moreover, longitudinal classifications were made on HC converting to MCI and HC remaining cognitive normal (HC-converters vs. HC-stable, n=92), and MCI converting to AD dementia and MCI remaining MCI (MCI-converters vs. MCI-stable, n=378). The most relevant features for the classifications were CSF status, hippocampal volume, entorhinal thickness, and amygdala volume. Interestingly, while the hippocampus contributed to the conversion from healthy aging to MCI, in the conversion from MCI to AD dementia the entorhinal cortex (EC) was prominent. In **study 3**, iron accumulations in AD were explored, given that increased iron levels can be observed during healthy aging and are even more pronounced in AD with detrimental consequences. Thus, using effect size based meta-analyses (involving 22 *in vivo* MRI experiments), iron aggregation in the basal ganglia (putamen, globus pallidus, nucleus caudate), thalamus, and hippocampus in AD dementia compared to HC was examined and correlated with cognitive performance. Iron level increases were found in the basal ganglia, with the strongest effect in the putamen and the weakest in the thalamus. Iron deposition in the globus pallidus was negatively correlated with cognitive functioning in AD dementia. In **study 4**, resting-state MRI activity markers were

investigated using longitudinal data (baseline and two years later) based on CSF assays from ADNI (n=71), considering that functional brain changes often precede structural ones. Two region-of-interest (ROI) analyses revealed that at baseline the local activity, here fractional amplitude of low-frequency fluctuations (fALFF), differed between normal and abnormal CSF in the NbM but not EC. Furthermore, NbM's fALFF signal linearly decreased, corresponding to the CSF ratio (pTau/Aβ), reflecting the disease progression. Finally, NbM's baseline fALFF signal predicted the annual percentage signal change of fALFF in the EC, not vice versa, independent of CSF status. Finally, this thesis gives novel insights into the complex pathophysiology of AD, pinpointing the central role of the BF's NbM, MTL, and basal ganglia in the onset and progression of AD. Furthermore, the results suggest potential clinical implications for prevention and treatment as well as emphasize the necessity for future multimodal investigations.

German Abstract / Deutsche Zusammenfassung

Strukturelle und funktionelle Veränderungen des Gehirns werden mit dem Fortschreiten der Alzheimer Erkrankung (AD) in Verbindung gebracht. Die genauen Veränderungen sind jedoch nach wie vor nur unzureichend bekannt. Vor diesem Hintergrund und auf der Grundlage aktueller AD-Modelle zielt diese Arbeit darauf ab, strukturelle und funktionelle Veränderungen im Verlauf von AD mit verschiedenen methodischen Ansätzen zu untersuchen. In **Studie 1** wurde die Verringerung des Volumens der grauen Substanz (GM) im cholinergen Nucleus basalis von Meynert (NbM) des basalen Vorderhirns (BF) und im medialen Temporallappen (MTL) zwischen gesunden älteren Erwachsenen (HC), Patienten mit leichter kognitiver Beeinträchtigung (MCI) und AD-Demenzpatienten mit Hilfe von Metaanalysen der koordinaten- und voxelbasierten Morphometrie (VBM) Magnetresonanztomographie (MRT) verglichen (insgesamt 54 Experimente). Bei an AD-Demenz Erkrankten wurde eine Verringerung der GM in dem bilateralen NbM des BF beobachtet, bei MCI jedoch nur in geringem Maße. Insbesondere wiesen MCI- und AD-Demenz-Patienten weniger GM in der Amygdala und im Hippocampus auf, was auf ausgeprägtere Effekte in der Amygdala bei der AD-Demenz hinweist. In **Studie 2** wurden relevante Merkmale untersucht, die zum Diagnosestatus und zum Krankheitsverlauf von HC, MCI und AD-Demenz beitragen. Dazu wurden volumetrische Hirndaten, soziodemografische Daten, Liquorstatus und Genotypisierungsdaten aus der Alzheimer's Disease Neuroimaging Initiative (ADNI) mit Hilfe eines XGBoost-Algorithmus für maschinelles Lernen (ML) analysiert, um HC, MCI und AD-Demenz zu klassifizieren (n=568). Darüber hinaus wurden longitudinale Klassifizierungen von HC, die zu MCI konvertieren, und HC, die kognitiv normal bleiben (HC-Converters vs. HC-Stable, n=92), sowie MCI, die zu AD-Demenz konvertieren, und MCI, die MCI bleiben (MCI-Converters vs. MCI-Stable, n=378), vorgenommen. Die wichtigsten Merkmale für die Klassifizierung waren der Liquorstatus, das Hippocampusvolumen, die entorhinale Dicke und das Amygdalavolumen. Interessanterweise trug der Hippocampus zur Progression von gesundem Altern zu MCI bei, während bei dem Fortschreiten von MCI zur AD-Demenz der entorhinale Kortex (EC) im Vordergrund stand. In **Studie 3** wurde, angesichts der Tatsache, dass erhöhte Eisenspiegel bei gesundem Altern beobachtet werden können und bei AD mit schädigenden Folgen noch ausgeprägter sind, die Eisenanreicherung bei AD untersucht. Anhand von Metaanalysen auf der Grundlage von Effektgrößen (insgesamt 22 *in vivo* MRT-

Experimente) wurde die Eisenanhäufung in den Basalganglien (Putamen, Globus Pallidus, Nucleus Caudatus), im Thalamus und im Hippocampus bei AD-Demenz im Vergleich zu HC untersucht und mit der kognitiven Leistung korreliert. Erhöhte Eisenspiegel wurden in den Basalganglien festgestellt, wobei der stärkste Effekt im Putamen und der schwächste im Thalamus zu beobachten war. Die Eisenablagerung im Globus Pallidus zeigte eine negative Korrelation mit der kognitiven Leistungsfähigkeit der AD-Demenz. In der **Studie 4** wurden MRT-Aktivitätsmarker im Ruhezustand anhand von Längsschnittdaten (Ausgangswert und zwei Jahre später) auf der Grundlage von Liquoruntersuchungen von ADNI (n=71) untersucht, da funktionelle Hirnveränderungen häufig den strukturellen vorausgehen. Zwei Region-of-Interest (ROI) Analysen zeigten, dass sich die lokale Aktivität, hier die fraktionierte Amplitude der niederfrequenten Fluktuationen (fALFF), zu Studienbeginn zwischen normalem und abnormalem Liquor in dem NbM, nicht aber im EC unterschied. Darüber hinaus nahm das fALFF-Signal in dem NbM entsprechend dem Liquorverhältnis (pTau/Aβ) linear ab, was das Fortschreiten der Krankheit widerspiegelt. Schließlich sagte das fALFF-Basissignal des NbM die jährliche prozentuale Signaländerung des fALFF im EC voraus, nicht umgekehrt, und zwar unabhängig vom Liquorstatus. Zusammenfassend, gibt diese Arbeit neue Einblicke in die komplexe Pathophysiologie von AD und verweist auf die zentrale Rolle des NbM, des MTL und der Basalganglien bei der Entstehung und dem Fortschreiten von AD. Darüber hinaus deuten die Ergebnisse auf mögliche klinische Implikationen für Prävention und Behandlung hin und unterstreichen die Notwendigkeit künftiger multimodaler Untersuchungen.

Abbreviations

Aβ	Amyloid-β
AA	Alzheimer's Association
ACh	Acetylcholine
ADAS-Cog	Alzheimer's Disease Assessment Scale Cognitive
ADNI	Alzheimer's Disease Neuroimaging Initiative
ALE	Activation likelihood estimation
APOE	Apollipoprotein E
APP	Amyloid precursor protein
APSC	Annual percentage signal change
ATP	Adenosine triphosphate
BFCS	Basal forebrain cholinergic system
BOLD	Blood Oxygen Level-Dependent
CDRSB	Clinical Dementia Rating Scale
ChAT	Choline acetyl transferase
CSF	Cerebrospinal fluid
DARTEL	Diffeomorphic anatomical registration using exponential lie algebra
DMN	Default mode network
DPARSFA	Data Processing Assistant for Resting-State fMRI Advanced
EC	Entorhinal cortex
EF	Executive function
fALFF	Fractional amplitude of low-frequency fluctuations
FC	Functional connectivity
(f)MRI	(Functional) magnetic resonance imaging
FDRI	Field-dependent R2 increase
FEW	Family-wise error
GM	Grey matter
HC	Healthy controls
ICV	Intracranial volume
IDA	Image and Data Archive
LONI	Laboratory of Neuro Imaging

MCI	Mild cognitive impairment
MEM	Memory
ML	Machine learning
MMSE	Mini-Mental-State Examination
MNI	Montreal Neurological Institute
MoCA	Montreal-Cognitive-Assessment
MTL	Medial temporal lobe
NbM	Nucleus basalis of Meynert
NFTs	Neurofibrillary tangles
NIA	National Institute on Aging
PET	Positron emission tomography
PHFs	Paired helical filaments
pTau	Hyperphosphorylated Tau
QSM	Quantitative susceptibility mapping
RAVLT	Rey Auditory Verbal Learning Test
ReHo	Regional homogeneity
ROI	Region of interest
ROS	Reactive oxygen species
rsfMRI	Resting-state functional MRI
SCD	Subjective cognitive decline
SHAP	SHapley Additive exPlanations
SN/VTA	Substantia nigra/ventral tegmental area
SPM	Statistical Parametric Mapping toolbox
SWI	Susceptibility-weighted imaging
VBM	Voxel-based morphometry
WHO	World health organization
WM	White matter
XGBoost	Extreme gradient boosting

1 General Introduction

The global population is rising, life expectancy is increasing, and many countries are seeing a steady climb in the number of elderly individuals that make up their population (*WHO*|*Ageing and Health*, 2022). Considering aging as a primary risk factor for neurodegenerative diseases (Hou et al., 2019), the worldwide count of individuals living with dementia is projected to increase from 55 million in 2019 to 139 million by 2050, according to the World Health Organization (*WHO*|*Dementia*, 2021). Dementia has evolved into a progressively severe global health problem, placing substantial economic and health burdens on society and families (X. Li et al., 2022; Nichols et al., 2019). Alzheimer's disease (AD) is the leading cause of dementia, responsible for 60 to 80% of cases. It is associated with the progressive loss of cognitive functions and impaired memory, and its pathophysiological alterations can manifest years before diagnosis ('2023 Alzheimer's Disease Facts and Figures', 2023). Although healthy aging includes a moderate cognitive decline in specific domains (Deary et al., 2009), AD is characterized by more severe pathological deteriorations across multiple cognitive domains and a negative impact on quality of life (McKhann et al., 2011; Swerdlow, 2011). When referring to its progression, AD involves the continuum from normal cognition over mild cognitive impairment (MCI) to the debilitating symptoms characteristic of AD dementia in diagnostic terms (Davis et al., 2018). In the following, the expression 'AD progression' is explicitly used to describe the continuum of AD, while 'AD' alone refers to AD dementia in diagnostic terms. AD's progression encompasses specific pathophysiological changes reflecting current biomarkers, such as amyloid-β (Aβ) deposition, tau pathology, and neurodegeneration (Jack et al., 2018; Jack, Knopman, et al., 2010). Despite extensive research efforts, the precise underlying neuronal mechanisms of the onset and progression of AD remain partly elusive.

From a general perspective, it is crucial to improve the comprehension of these neuropathological changes in order to better prevent, predict, and treat AD (Dubois et al., 2023). In this context, this thesis examines biomarkers, including structural and functional brain changes, throughout AD progression. The following chapters provide a theoretical background on healthy and pathological aging, the pathogenesis and theories of AD, and the associated structural and functional brain changes due to AD. The research aims are then described, followed by the presentation of the studies and a discussion of the results.

2 Theoretical Background

2.1 Aging

With life expectancy increasing worldwide due to improved medical care and living standards (e.g., Hou et al., 2019), it is predicted that one out of six individuals will be 60 years or older by 2030 (*WHO*|*Ageing and Health*, 2022; Hou et al., 2019). The extension of lifespan brings with it the challenge of ensuring that these additional years are accompanied by a good quality of life (Martinez et al., 2021). This necessitates a deeper understanding of the aging process, both healthy and pathological, to mitigate age-related diseases and promote healthy aging.

Aging describes an irreversibly progressive decline in physiological integrity, resulting in compromised function and heightened vulnerability to death (Z. Li et al., 2021; López-Otín et al., 2013). This natural decline represents a major risk factor for developing common human pathologies such as cancer, diabetes, and cardiovascular and neurodegenerative diseases (e.g., Hou et al., 2019). Although numerous theories exist regarding the underlying causes of aging, there is currently no consensus (Da Costa et al., 2016). However, these theories can be categorized into a) program theories, which postulate the existence of internal and external programs shaping the aging process (Da Costa et al., 2016; Semsei, 2000); b) damage/error theories, which suggest that aging results from destructive factors inducing errors, mutations, regulatory dysfunctions, leading to dysfunction and senescence describing the gradual decline in bodily functions as time passes (Da Costa et al., 2016; Semsei, 2000); and c) combined theories, which integrate aspects from both theories above (Da Costa et al., 2016; Semsei, 2000). Despite these theories, the categorization of aging remains complex (Kirkwood, 2005) and subjective (Da Costa et al., 2016).

Research shows that the hallmarks of aging consist of different biological mechanisms that influence the pace of damage and resilience (compensating damage). Along these lines, telomere shortening, cellular senescence, epigenetic changes, mitochondrial dysfunctions, decreased autophagy, and proteostasis were identified (Ferrucci et al., 2020). Studies indicated an overall reduction of physical (Ferrucci et al., 2016; Ko et al., 2010; Stolz et al., 2024) and cognitive functions (Harada et al., 2013; Murman, 2015) with age as well as the interdependence between both (Bamidis et al., 2014; Rosano et al., 2005). Moreover, several brain changes are associated with healthy aging, such as alterations in neurotransmitters and

cells (Lee & Kim, 2022), brain atrophy (Dickstein et al., 2007), altered spontaneous brain activity (Montalà-Flaquer et al., 2023), and iron accumulation (J. Xu et al., 2012).

2.1.1 Cognitive changes associated with healthy aging

With advancing age, cognitive performance declines; however, interindividual differences exist regarding the onset, speed of progression, and the extent of its impact (Ghisletta et al., 2012; Ram et al., 2011). For instance, learning and memory, attention, decision speed, sensory perception (vision, hearing, touch, smell, taste), and motor coordination deteriorate with age (Mattson & Arumugam, 2018). It has been shown that memory impairment coincides with changes in brain areas relevant to memory function (Lee & Kim, 2022; Sikora et al., 2021). Similarly, structural and functional changes in the prefrontal cortex, medial temporal lobe (MTL) regions, and white matter tracts are associated with age-related cognitive deficits (Hedden & Gabrieli, 2004). Furthermore, age-related iron accumulation and demyelination in basal ganglia structures are strongly associated with verbal memory performance (Steiger & Bunzeck, 2017) and executive functioning (Biel et al., 2021).

Subjective cognitive decline (SCD) refers to a perceived memory worsening and other cognitive abilities without detectable neuropsychological deficits (Jessen et al., 2006) and is observed occasionally in nearly all elderly (Rabin et al., 2017; Slavin et al., 2010). SCD may serve as an early indicator of AD (Rabin et al., 2017) and predicts faster conversion to MCI and AD (Fernández-Blázquez et al., 2016). Due to the less noticeable symptoms, discriminating between cognitive decline in the initial phases of pathological aging and typical age-related cognitive worsening is challenging (Denver & McClean, 2018). Therefore, rather than categorizing healthy and pathological aging as distinct entities, it may be more insightful to consider them as two extremes along a continuum (Franceschi et al., 2018; Sikora et al., 2021).

2.2 Alzheimer's disease

Dementia refers to the broad term for a specific group of symptoms, including difficulties with memory, language, problem-solving, and other cognitive abilities. This neurodegenerative disease relies on different causes, reflecting unique neurophysiological changes. The most common cause of dementia is AD, accounting for 60% to 80% of all cases ('2023 Alzheimer's Disease Facts and Figures', 2023). It was estimated that the prevalence of AD in Europe is 5.05% (Niu et al., 2017). The progression of AD encompasses from normal cognitive over MCI to increasing severity of AD (Davis et al., 2018). Early AD symptoms include

difficulties in remembering past conversations, names, or events, apathy, and depression. This is followed by confusion, communication challenges, poor judgment, and behavioral changes. In the later stages of AD, walking, speaking, and swallowing problems occur ('2023 Alzheimer's Disease Facts and Figures', 2023). Despite promising advances in pharmacological treatments for AD in recent years (Conti Filho et al., 2023), it is essential to note that there are currently no curative therapies available (Cummings, 2021; Self & Holtzman, 2023).

Within AD progression, brain changes precede cognitive symptoms and cognitive as well as physical impairments gradually increase ('2023 Alzheimer's Disease Facts and Figures', 2023). Two hallmarks of brain alterations are the accumulation of Aβ into plaques outside neurons and the abnormal aggregation of tau protein into tangles within neurons (e.g., Gallardo & Holtzman, 2019). Many researchers support the notion that Aβ triggers or facilitates the pathologic tau spreading (e.g., Hanseeuw et al., 2019; C. Sato et al., 2018), which is closely associated with neurodegeneration, and this, in turn, leads to cognitive decline (Jack et al., 2013, 2018). The AT(N) framework categorizes the hallmarks Aβ (A), tau (T) and neurodegeneration (N) based on imaging or biofluids, allowing the identification of distinct disease stages as well as the interaction of the pathological processes (Jack et al., 2018). Importantly, the AT(N) framework describes the progression of AD biologically instead of syndromally and represents a research framework rather than clinical diagnostic guidelines (Jack et al., 2018). Many AD patients exhibit brain changes associated with one or more causes of dementia, a condition known as mixed dementia (Brenowitz et al., 2017; Kapasi et al., 2017). However, there is a lack of adequate, especially *in vivo*, biomarkers for diagnosing mixed pathology dementia (Kapasi et al., 2017).

Various guidelines exist for the clinical diagnosis of AD (for an overview see Tahami Monfared et al. (2023)). According to the recommendations from the National Institute on Aging (NIA) and the Alzheimer's Association (AA) in 2011, AD progression can be classified into three stages: a) preclinical AD linked with pathological brain changes due to AD but no cognitive symptoms, b) MCI involving subtle memory, language, and cognitive deterioration more pronounced than in healthy individuals, and c) AD that includes advanced cognitive impairment, memory loss and functional decline (Albert et al., 2011; McKhann et al., 2011; Sperling et al., 2011). Recent data has suggested that cognitive decline in AD occurs continuously over time, along with biomarker progression. Here, biomarkers serve as measures that indicate the presence or absence of AD or the risk of developing it. For instance,

in the preclinical phase, compensatory mechanisms in the brain maintain normal functioning; however, in MCI, these mechanisms fail due to neuronal damage, resulting in subtle symptoms that become more severe over the final AD stages ('2023 Alzheimer's Disease Facts and Figures', 2023). The recognition of continuity prompts a paradigm shift in understanding AD as a continuum rather than distinct clinical stages, a concept recognized but not formalized in the 2011 NIA-AA guidelines (Jack et al., 2018). Along the continuum from preclinical AD to full-blown AD, factors such as age, sex, genetics, CSF markers, and setting (research versus clinical) influence the duration of each phase, leading to variability in disease progression among individuals (Vermunt et al., 2019).

2.2.1 Genetics and environmental factors

The pathogenesis of AD involves a complex interplay of genetic predispositions, environmental factors, and neuropathological processes, leading to the progressive neurodegeneration characteristic of the disease (Scheiblich et al., 2020; H. Wang et al., 2021). Although not particularly central to this thesis, it is worth briefly mentioning genetic predispositions and environmental factors influencing AD progression, as it provides insights into the diverse factors affecting the disease.

Genetics play a role in the development of various forms of AD. For example, autosomal mutations in the amyloid precursor protein (APP), presenilin-1 (PSEN1), and presenilin-2 (PSEN2) were identified as accountable for the familial form of AD (Bateman et al., 2010; Mendez, 2019). Here, the typical onset for this form is under 65 years (Harvey, 2003). However, most AD cases are late-onset forms, lacking a clear familial clustering (Bellenguez et al., 2020). In these cases, a complex interplay between genetic and environmental factors is assumed (Lane et al., 2018). Various genes influence the biological processes involved in late-onset AD (Bellenguez et al., 2022). Among these, the Apolipoprotein E (APOE) ε4 allele (APOE4) stands out as the primary risk factor for late-onset AD (Yamazaki et al., 2019). The APOE gene is essential for lipid transportation and exists in three allelic variants (ε2 (APOE2), ε3 (APOE3) and ε4) (Husain et al., 2021). While APOE3 was found to have a neutral effect on the AD risk, APOE2 is associated with a decreased risk and APOE4 with an increased risk (see Yamazaki et al. (2019) for an overview). Furthermore, individuals with one or two copies of the APOE4 allele experience an earlier onset of late-onset AD (Corder et al., 1993; Verghese et al., 2011).

Numerous epidemiological studies, alongside *in vitro* and *in vivo* work using animal and cell models, explored diverse environmental factors as potential risks for AD (Migliore & Coppedè, 2009, 2022). However, these studies showed conflicting results and the data is often based on non-objective measurements, interviews, or other measurements that do not assess the dosage of environmental triggers (Migliore & Coppedè, 2022). For a comprehensive overview of environmental protective and risk factors for AD see Migliore & Coppedè (2022). For instance, western diet, vitamin D deficiency, pesticides, metals and metalloids, electromagnetic fields, and preventable factors such as depression, smoking, social isolation, low education, hearing impairment, physical inactivity, obesity, hypertension, and diabetes are associated with a higher risk of developing AD. In contrast, protective factors against AD include a Mediterranean diet, antioxidants, fruit and vegetables, caffeine, physical activity, anti-inflammatory drugs, cognitively demanding work, and high education (Migliore & Coppedè, 2022). Finally, genetic and environmental factors can interact and affect the probability of AD development (Dunn et al., 2019).

2.2.2 Alzheimer's disease theories

Over the years, different theories and models have been proposed for the pathogenesis of AD to describe the progression of pathological changes within the brain (Berry & Harrison, 2023; Therriault et al., 2022). Two prominent theories explaining the mechanisms of AD would be the cholinergic hypothesis, emphasizing the role of the basal forebrain (BF) cholinergic system (BFCS), and the amyloid hypothesis, focusing on Aβ pathology (Bartus, 2000; Berry & Harrison, 2023; Braak & Braak, 1991; Fernández-Cabello et al., 2020; M. J. Grothe et al., 2018; Mesulam, 2004b; Thal et al., 2002).

Between 1970 and 1980, the cholinergic hypothesis was prominent in AD research (Bartus et al., 1982; Berry & Harrison, 2023; Plotkin & Jarvik, 1986; Whitehouse et al., 1982). This hypothesis proposes that the loss of the cholinergic neurons in the BF, a subcortical brain region consisting of many small nuclei producing a variety of neurotransmitters (Mesulam et al., 1983; Woolf, 1991), notably Acetylcholine (ACh), contributes to cognitive decline (e.g., Berry & Harrison, 2023). This decline affects memory, learning, and attention in healthy aging but is even more pronounced in AD (Grothe et al., 2012; Mesulam, 2012; Muir, 1997). Along these lines, in AD reduced levels of choline acetyltransferase (ChAT) the final enzyme in the ACh synthesis pathway can be observed (Davies & Maloney, 1976). Moreover, memory and

attention deficits can be induced by pharmaceutical disruption of the basal BFCS (Broks et al., 1988; Safer & Allen, 1971).

Cholinergic neurons, such as the medial septal nucleus (Ch1), vertical and horizontal diagonal band nuclei (Ch2, Ch3), and the magnocellular complex (Ch4), which primarily comprises the Nucleus basalis of Meynert (NbM), build the BFCS (Mesulam et al., 1983). These project to numerous brain regions and receive reciprocal inputs and modulation from various subcortical systems. Considering that the NbM is recognized as the largest nucleus within the BF, it has been a primary target for investigation (Mesulam & Geula, 1988). It should be noted that providing an extensive delineation of the BFCS projections falls outside the scope of this thesis. However, in summary, the following projections can briefly be outlined. The prefrontal cortex and amygdala receive cholinergic input from the NbM (Mesulam et al., 1983), while the entorhinal cortex (EC) and hippocampus receive cholinergic inputs from the medial septum and vertical diagonal band nuclei (Mesulam et al., 1992; Mesulam & Geula, 1988). Reciprocally, the BFCS is modulated by other subcortical systems, such as the noradrenergic locus coeruleus, serotonergic dorsal raphe nucleus, and dopaminergic substantia nigra/ventral tegmental neurons (Bari et al., 2020; Gaykema & Zaborszky, 1997; Halberstadt & Balaban, 2008; Hornung, 2003; Rho et al., 2018; Zaborszky & Cullinan, 1996). Since 1990, AD research has shifted from the cholinergic hypothesis to the currently prevalent amyloid hypothesis. This shift is due to the findings of insufficient effects of acetylcholinesterase (AChE) inhibitors, which inhibit the enzyme AChE, thus increasing the levels of ACh in the synaptic gap (Colovic et al., 2013), and evidence supporting cortical Aβ pathology. Additionally, the role of Aβ and tau is not thoroughly considered (Berry & Harrison, 2023).

The amyloid hypothesis of AD describes the pathophysiological process that Aβ pathology triggers the spread of tau pathology from the MTL, including the transentorhinal and EC, to the hippocampus and following to other cortical regions, leading to neurodegeneration and cognitive decline (Braak & Braak, 1991; Corder et al., 2000; Duyckaerts et al., 1990; Jack et al., 2018; Jagust, 2018). The identification of genetic mutations in the genes APP, PSEN1, and PSEN2 supports this hypothesis (Goate et al., 1991; Rogaev et al., 1995; Schellenberg et al., 1992; Van Broeckhoven et al., 1992). Extracellular accumulations known as senile amyloid plaques consist of abnormally folded Aβ proteins comprising 40 or 42 amino acids (Aβ40 and Aβ42) derived from the APP metabolism. Aβ42 is more prevalent within plaques than Aβ40 due to its higher rate of fibrillization and insolubility

(Serrano-Pozo et al., 2011). This abnormal aggregation of Aβ peptides disrupts neuronal function, triggers neurotoxicity, and promotes synaptic dysfunction. However, ambiguity remains regarding both the physiological and pathological forms of Aβ, as well as the precise mechanism causing the pathology (‘2023 Alzheimer’s Disease Facts and Figures’, 2023; G. Chen et al., 2017). Increased Aβ is linked to the subsequent accumulation of tau abnormalities, which manifests as intraneuronal aggregates of hyperphosphorylated and misfolded tau proteins (pTau), known as neurofibrillary tangles (NFTs) (Bilgel et al., 2022; G. Chen et al., 2017; Jack et al., 2018). These structures primarily consist of paired helical filaments (PHFs) and occasionally exhibit variations such as straight filaments or hybrid forms (Crowther, 1991; Wegmann et al., 2010). Upon the death of tangle-bearing neurons, NFTs can transition into extraneuronal 'ghost' tangles, accompanied by the breakdown of dendrites and axons, known as neuropil threads (Serrano-Pozo et al., 2011). Tau pathology disrupts the transport of vital nutrients and molecules required for normal neuronal function and is closely associated with neuronal loss and cognitive impairment (‘2023 Alzheimer’s Disease Facts and Figures’, 2023; Bejanin et al., 2017).

Previous research indicated that Aβ and tau proteinopathies may trigger various neuronal alterations contributing to the progression of AD. For instance, Aβ and tau pathology initiate synaptic and mitochondrial dysfunction, demyelination, as well as brain atrophy due to cell loss. Additionally, both lead to inflammatory responses in glial cells, resulting in sustained neuroinflammation (e.g., Y. Chen & Yu, 2023; Kent et al., 2020; Van Der Kant et al., 2020; L. Wang et al., 2015). Furthermore, dysregulation of iron homeostasis reinforces the pathological cascade, highlighting the complex interplay between these proteinopathies and various cellular processes implicated in AD (e.g., Ayton et al., 2017; Spotorno et al., 2020). However, it is important to note that only a subset of potential alterations linked to the proteinopathology are presented here. The exact sequence of events and causal relationships in these processes remains not well understood, underscoring the complexity of AD and the challenges in capturing its underlying mechanisms (e.g., Y. Chen & Yu, 2023; Jack et al., 2018; Kent et al., 2020).

Although the amyloid hypothesis has gained substantial support, it faces difficulties in fully explaining AD pathology. Contradictory findings were observed, such as unsuccessful anti-Aβ clinical trials, the presence of Aβ in aged cognitively normal without AD, discrepancies between the clinical phenotype and neuropathology, and the involvement of other factors,

such as the BFCS (Berry & Harrison, 2023; Morris et al., 2018). The cholinergic evidence underlines the importance of integrating the role of the BFCS into the amyloid hypothesis (Berry & Harrison, 2023; Hampel et al., 2018). Interactions between the BFCS and Aβ pathology may bridge the cholinergic and amyloid hypotheses in AD, as highlighted in a recent review article (Berry & Harrison, 2023). This review article discusses bidirectional effects: increasing Aβ levels disrupt cholinergic transmission, while reduced cholinergic integrity accelerates the Aβ pathology, creating a detrimental cycle of compromised BFCS integrity and pathological processes (Berry & Harrison, 2023).

In AD, the proteinopathies Aβ and pTau are assumed to spread along the neural projection system to prone brain regions (Warren et al., 2013) and across anatomically and functionally connected brain regions (de Calignon et al., 2012; Grothe et al., 2018; Hanseeuw et al., 2019; L. Liu et al., 2012; Sepulcre et al., 2018; J. W. Wu et al., 2016). Despite differences, comparisons between the BFCS and MTL structures, like the hippocampus, highlight a common susceptibility to AD pathology (Berry & Harrison, 2023). Hence, both regions share characteristics such as the continual demand for synaptic plasticity based on their contribution to memory and attention processes (Hasselmo, 2006; Suh et al., 2011). However, it remains unclear whether these shared characteristics imply shared mechanisms of vulnerability to AD pathology (Berry & Harrison, 2023).

2.3 Structural and functional brain changes in Alzheimer's disease

Evidence from mouse models of AD (de Calignon et al., 2012; Khan et al., 2014; L. Liu et al., 2012; J. W. Wu et al., 2016) and human patients (Grothe et al., 2018; Hanseeuw et al., 2019; Sepulcre et al., 2018) underscores the spreading of Aβ and tau pathologies with alterations in both brain structure and function throughout the disease progression. Interestingly, it has been hypothesized that with structural degeneration in older adulthood, there is a functional compensation to maintain functioning that, however, breaks down in pathological aging, such as AD, due to more pronounced structural degeneration (Bunzeck et al., 2024). In the following, structural changes in gray matter (GM), iron, and functional changes in resting-state functional magnetic resonance imaging (fMRI) will be presented.

2.3.1 Gray matter

The GM includes neuronal cell bodies (somata), synapses, glial cells, capillaries, dendrites, and unmyelinated axons. It is distributed across the brain and throughout the spinal

cord. Specifically, in the brain, it is located both cortically and in various subcortical brain regions, such as the thalamus, subthalamus, hypothalamus, and basal ganglia, which include structures like the putamen, nucleus accumbens, globus pallidus, and septal nuclei. Unlike GM, white matter (WM) is structured into bundles of primarily myelinated axons, forming tracts that facilitate communication between different functional GM networks across the brain (Kolb & Whishaw, 2003; Purves, 2008; Wen & Chklovskii, 2005). Structural MRI studies revealed reduced GM volume and cortical thickness in multiple brain areas in preclinical AD, which were strongly associated with cognitive impairment (Lombardi et al., 2020; Suzuki et al., 2019; Vemuri & Jack, 2010).

The relevance of the BF is emphasized by studies combining *in vivo* anatomical MRI with CSF assessments of Aβ and pTau, showing more pronounced GM loss in the NbM than EC in cognitively healthy individuals with abnormal compared to normal CSF biomarkers (Schmitz & Spreng, 2016). Along these lines, as stated in the pathological staging model, the baseline volume of the NbM has been shown to predict longitudinal degeneration of the EC. However, the EC predicted the degeneration in temporal and parietal cortices, suggesting a trans-synaptic propagation of Aβ originating from the NbM (Fernández-Cabello et al., 2020; Schmitz & Spreng, 2016). These findings align with animal work, adding a crucial upstream connection to the subsequent spread from the EC to other MTL structures, including the hippocampus, and further to more distant neocortical brain regions, such as the posterior parietal cortex (de Calignon et al., 2012; Khan et al., 2014; L. Liu et al., 2012; J. W. Wu et al., 2016). Although the cholinergic BF is recognized for its role in AD, empirical evidence, especially *in vivo* remains limited. Therefore, **study 1** addresses this limitation by investigating structural differences across the disease progression using a meta-analytic approach.

Due to the prevailing assumption of the amyloid hypothesis, *in vivo* structural MRI studies mostly focused on abnormalities in the MTL and cortical regions. For instance, volume (Karas et al., 2004) and shape (Gerardin et al., 2009) differences were found in the hippocampus and variations in hippocampal subfields in patients with MCI and AD compared to age-matched healthy controls (Frisoni et al., 2010). Similarly, for example the EC, amygdala, as well as frontal and parietal cortices are affected by GM volume loss as AD progresses (Z. Wu et al., 2021). Moreover, machine learning (ML) studies successfully classified HC, MCI, and AD patients using structural MRI information (Basaia et al., 2019; Rathore et al., 2017; Sarica et al., 2017). These classifications mainly were based on volumetric differences of the

hippocampus, amygdala, EC, precuneus, cingulate gyrus, and the rostral and caudal regions within the medial frontal lobe, indicating a GM loss in MCI and AD compared to HC (Böhle et al., 2019; Diogo et al., 2022; Pan et al., 2020; Rondina et al., 2018; Son et al., 2017). While the MTL plays an important role in ML based classifications of AD, neurodegenerative processes affect the entire brain (Diogo et al., 2022), a consideration that has not been fully explored. Furthermore, only limited studies exist on the classification of AD progression or lack information on contributing features. Therefore, **study 2** aims to address this gap by employing ML based classification techniques on brain integrity (volume and thickness), as well as additional features, such as sociodemographic information, CSF assays, and APOE4 genotyping for AD progression.

2.3.2 Iron

There are two types of iron in the human body: heme and non-heme. Heme iron is essential in transporting oxygen via hemoglobin throughout the circulatory system. In contrast, intracellular non-heme iron is essential for various physiological functions, such as cellular energy production through adenosine triphosphate (ATP) synthesis, axonal myelination, and neurotransmitter synthesis (Todorich et al., 2009; Zecca et al., 2004). The iron metabolism is regulated by various proteins, governing its uptake, storage, and utilization (Mills et al., 2010; Reinert et al., 2019). Despite the intricate regulatory mechanisms, disruptions in iron homeostasis can occur, particularly with advancing age, leading to detrimental effects on cellular function (Lillig et al., 2008; Tian et al., 2022). Dysregulation of the iron metabolism can result in oxidative stress. Free ferrous iron (Fe2+) interacts with hydrogen peroxide, generating reactive oxygen species (ROS) through the Fenton reaction (H. C. Sutton & Winterbourn, 1989). This can further exacerbate iron dysregulation, forming a destructive feedback loop promoting oxidative damage (Altamura & Muckenthaler, 2009; Horowitz & Greenamyre, 2010; Mastroberardino et al., 2009). Finally, neuroinflammation can be triggered, and potentially ferroptosis, an iron-depending programmed cell death (Dixon et al., 2012; H. Long et al., 2023; Ward et al., 2022).

In the context of AD, a *post-mortem* meta-analysis revealed increased non-heme iron levels in the basal ganglia structures, cingulate cortex, frontal, parietal, and temporal lobe areas in AD compared to HC individuals (Tao et al., 2014). Moreover, *in vivo* neuroimaging studies, which offer the potential for a clearer connection to cognitive impairment and

provide novel insights into paramagnetic brain iron (Haacke et al., 2005; Tran et al., 2022), observed accumulated non-heme iron particularly in the basal ganglia, thalamus, and hippocampus (Damulina et al., 2020; Ding et al., 2009; Du et al., 2018; H.-G. Kim et al., 2017; Kuchcinski et al., 2022). Therefore, individuals with MCI and AD showed increased iron levels correlated with cognitive decline and structural brain atrophy (Ayton et al., 2017; Du et al., 2018; H.-G. Kim et al., 2017; Y. Moon et al., 2016; A. Yang et al., 2022). Moreover, *post-mortem* and *in vivo* studies revealed a link between elevated iron levels and the presence of tau and Aβ pathology (Ayton et al., 2017; Spotorno et al., 2020; Van Bergen et al., 2016; Van Duijn et al., 2017; Bulk et al., 2018). However, *in vivo* imaging meta-analytic findings regarding increased iron levels in AD brains are lacking, particularly in relation to cognitive decline. Accordingly, **study 3** investigates the iron accumulation in AD compared to HC using meta-analyses in the basal ganglia regions, hippocampus, and thalamus.

2.3.3 Resting-state fMRI

fMRI represents a non-invasive marker of brain activity by measuring blood oxygen level-dependent signals (Cai et al., 2020; Huang et al., 2020; Logothetis & Wandell, 2004; Xing et al., 2021). Previous studies detected changes in connectivity across various brain networks in AD patients (Dennis & Thompson, 2014). For example, decreased connectivity within the default mode network (DMN) and altered functional connectivity (FC) between the DMN and salience network were found in preclinical AD (A. P. Schultz et al., 2017). Along these lines, broad-scale dynamic network disruptions were linked to cognitive decline and to the presence of molecular biomarkers associated with AD as well as genetic risk factors (Q. Wang et al., 2021). Furthermore, prominent functional resting-state activity markers, such as FC between brain regions, regional homogeneity (ReHo), and fractional amplitude of low-frequency fluctuations (fALFF) assessing local functioning of specific brain regions, could classify cognitively normal adults with and without Aβ burden, reflecting sensitivity to AD pathology (S.-M. Wang et al., 2021). However, there is only a limited number of studies investigating these functional activity markers, which show partly divergent effects, such as an activity increase or decrease in various brain regions reflecting possible compensatory effects to maintain an adequate level of cognitive performance (He et al., 2007; Y. Liu et al., 2014; S.-M. Wang et al., 2021; Zeng et al., 2019; Zhang et al., 2012). Building upon the pathological staging model (Fernández-Cabello et al., 2020; Schmitz & Spreng, 2016) outlined previously, which

identified structural degeneration in the NbM predicting the degeneration in the EC, and considering that functional brain changes often precede structural brain changes (Johnson et al., 2012; Sperling, 2011; Warren & Moustafa, 2023), **study 4** investigates the functional properties of the NbM and EC.

2.4 Research aim

Previous studies have identified alterations in biomarkers along the AD progression, challenging the prevailing amyloid hypothesis and prompting investigations on an overlap with the cholinergic hypothesis (Berry & Harrison, 2023). Consequently, neuropathological changes were observed in key regions such as the cholinergic BF, MTL, and basal ganglia. Despite these findings, the neurophysiology of AD remains not fully understood. Thus, the aim of this thesis is to gain insights into the underlying pathophysiology of AD progression using structural and functional MRI measures, as well as different analysis methods (i.e., meta-analyses, ML based classification, and functional activity marker analyses). Explicitly, four **specific goals** associated with four individual studies were outlined:

Study 1 further investigates the exact nature of structural degeneration of the BF and interconnected MTL. Structural differences, specifically GM volume, were compared between HC and MCI as well as HC and AD patients using a coordinate-based meta-analytic approach. We expected GM volume reductions in the cholinergic BF and MTL in MCI and AD compared to HC.

In **study 2**, we examined the predictive value of volumetric brain information (i.e., volume and thickness), socio-demographics, CSF, and APOE4 genotype information for AD onset and progression. Therefore, utilizing a ML based extreme-gradient boosting algorithm, classifications were performed cross-sectionally on diagnostic groups (i.e., HC, MCI, and AD) and longitudinally on converters (HC to MCI and MCI to AD) to identify crucial features for these classifications. Based on the work described above, reduced volumes and thicknesses were expected in the MTL and, with disease progression, other cortical regions.

In **study 3**, we tested the hypothesis that iron accumulations are a characteristic hallmark of AD and relate to cognitive decline. Hence, a meta-analytical approach was used to compare iron levels in HC and AD patients and further the relationship between iron levels and cognitive decline in AD was investigated. Increased iron levels were hypothesized in AD patients compared to HC, with an expected correlation between iron accumulation with

neuropsychological performance indicating higher iron load associated with worse performance.

Study 4 aims to characterize how functional activity markers in the BF's NbM relate to those in the EC depending on CSF assays along the progression of AD (including HC, MCI, and AD). Based on the previous findings of the pathological staging model mentioned above, we hypothesized that the NbM precedes and predicts functional changes in the EC using longitudinal fMRI resting-state data. Moreover, a reduction in disease severity in local spontaneous brain activity was expected.

In the subsequent sections, the methods employed in each of the four studies will be described, followed by the presentation of their respective manuscripts. Finally, the general discussion will provide a summary of the findings, their integration as well as the limitations and future directions. Figure 2.1 gives an overview of the studies which are included in this thesis. The specific hypotheses of the studies have been elaborated in detail in the manuscripts (please refer to sections 4-7).

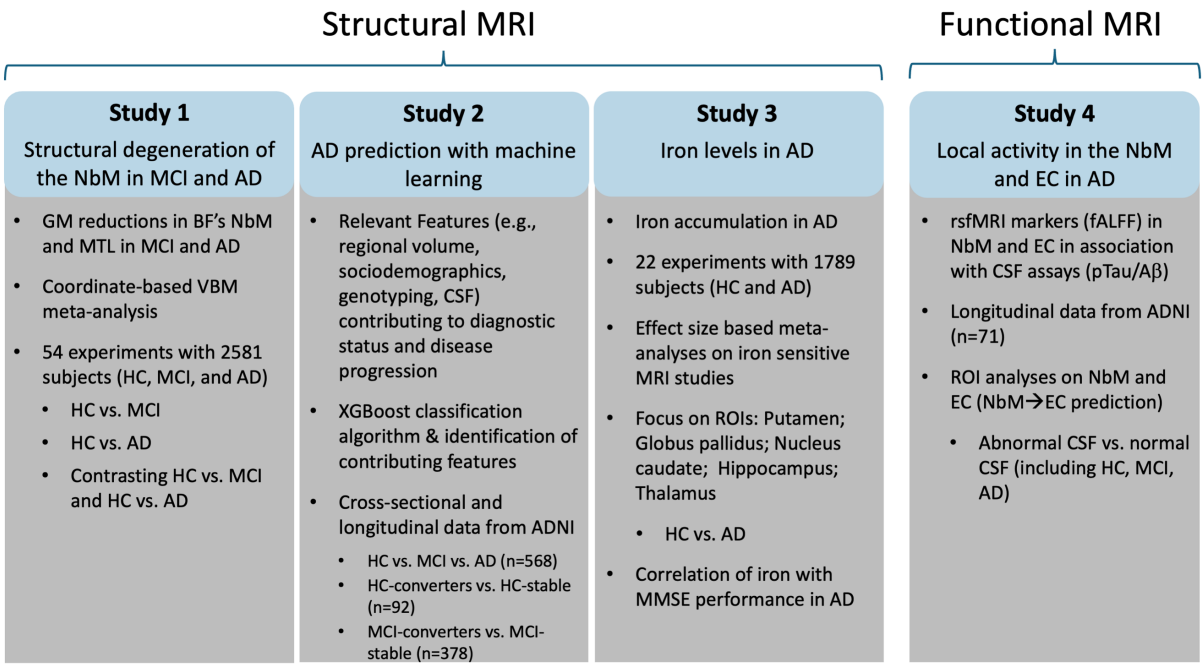

Figure 2.1 Overview of all four studies included in this thesis to gain insights into the underlying pathophysiology of AD progression. Studies 1-3 were based on structural MRI and study 4 focused on functional MRI. Studies 1 and 3 involved meta-analyses using data from previous research. Abbreviations: AD=Alzheimer's disease; ADNI=Alzheimer's Disease Neuroimaging Initiative; Aβ=Amyloid-β; BF=Basal forebrain; CSF=Cerebrospinal fluid; EC=Entorhinal cortex; fALFF=Fractional amplitude of low-frequency fluctuations; GM=Gray matter; HC=Healthy controls; MCI=Mild cognitive impairment; MMSE=Mini-Mental-State Examination; NbM=Nucleus basalis of Meynert; pTau=Hyperphosphorylated Tau, ROI=Region of interest; rsfMRI=Resting-state functional magnetic resonance imaging; VBM=Voxel-based morphometry; XGBoost=Extreme gradient boosting

3 General methods

3.1 Magnetic resonance imaging (MRI)

Magnetic resonance imaging (MRI) is a non-invasive imaging technique utilizing magnetic fields to acquire images of anatomical structures and physiological processes within a body (Hussain et al., 2022; Serai et al., 2021). Over the past decades, MRI imaging has increased utilization and refinement of (Hussain et al., 2022; Kabasawa, 2022). In this thesis, structural and functional MRI data were analyzed. While a detailed presentation of the principles of MRI is beyond the scope of this work, the subsequent section will offer an overview of the structural and functional MRI methods employed in the articles. Detailed explanations of MRI principles can be found elsewhere (e.g., Weishaupt et al., 2014; Serai et al., 2021).

Structural MRI offers insights into brain structure, encompassing shape, size, and integrity assessments (Bischoff-Grethe & Fennema-Notestine, 2023). Different methods can be applied to investigate structural MRI properties, which will be outlined below. While various methods exist regarding the analysis of structural brain characteristics, in this work, the focus lies on voxel-based morphometry (VBM), extracted GM volume and cortical thickness by FreeSurfer, an open-source software package for processing, analyzing, and visualizing brain images (https://surfer.nmr.mgh.harvard.edu/), and iron sensitive MRI.

VBM typically includes a voxel-wise comparison of local GM volume between two groups of subjects. Therefore, data processing involves the spatial normalization of high-resolution images from all subjects into a common stereotactic space. Subsequently, GM segmentation is conducted on the spatially normalized images, followed by spatial smoothing. Parametric statistical tests are then applied voxel-wise to compare the smoothed GM images from the two groups (Ashburner & Friston, 2000). Here, the results, i.e., VBM coordinates from specific studies were utilized and further analyzed using a coordinate based meta-analytic approach (**study 1**, see below for more information, 3.2). A common alternative to VBM is cortical reconstruction and volumetric segmentation using FreeSurfer, documented and freely available for download online (http://surfer.nmr.mgh.harvard.edu/). The technical details of the processing are available in previous publications (Dale et al., 1999; Dale & Sereno, 1993; Fischl et al., 2001, 2002, 2004b, 2004a; Fischl & Dale, 2000; Han et al., 2006; Jovicich et al., 2006; Reuter et al., 2010, 2012; Ségonne et al., 2004). Briefly, the processing steps involve motion correction (Reuter et al., 2010), removal of non-brain tissue (Ségonne et

al., 2004), intensity normalization (Sled et al., 1998), automated Talairach transformation, segmentation and parcellation (Fischl, 2012; Fischl et al., 2002, 2004a). Based on the Desikan-Killany atlas (Desikan et al., 2006) and the subcortical whole brain segmentation (Fischl et al., 2002, 2004a) the scans were processed and extracted features provided by ADNI (processed by the Tosun laboratory at the University of California-San Francisco, see https://adni.loni.usc.edu/data-samples/data-types/mri/) as a component of the shared data-set and further analyzed using ML (**study 2**, see below for more information on ML, 3.3).

Numerous MRI sequences are sensitive to iron, including T2, T2*, T2', R2, R2*, R2', field-dependent R2 increase (FDRI), phase imaging, and susceptibility-weighted imaging (SWI) (Haacke et al., 2005; Langkammer et al., 2014) along with quantitative susceptibility mapping (QSM) (Langkammer et al., 2012). However, not all methods are equally sensitive and specific in iron detection. For instance, T2 and R2 show substantial limitations, such as susceptibility to interference from other factors like water, thereby impacting their efficacy in iron detection (Haacke et al., 2005; Langkammer et al., 2010, 2012). Importantly, no iron-sensitive MRI data has been acquired for this thesis. Instead, the data and results from previously published studies were analyzed using effect size based meta-analyses (**study 3**, see below for more information on meta-analyses, 3.2).

fMRI detects brain activity by identifying changes in blood flow and oxygenation levels, utilizing the Blood Oxygen Level-Dependent (BOLD) contrast (Ogawa et al., 1990). For instance, when brain regions get activated (e.g., because of a task), these require more energy, resulting in an increased demand for oxygen and nutrients. To meet this demand, the blood flow increases. This, in turn, leads to a longer T2* relaxation time of the surrounding water, contributing to the observed signal elevation in T2*-weighted images (Glover, 2011; Weishaupt et al., 2014). Two basic approaches are involved in fMRI: task-based fMRI and resting-state fMRI (rsfMRI). Task-based fMRI monitors brain activity in subjects performing a specific cognitive or motor exercise. Therefore, changes in blood flow and oxygenation levels associated with this performance are detected, allowing to map the brain regions involved. In contrast, rsfMRI examines spontaneous neural activity while subjects rest without actively engaging in any specific activity. This approach can reveal regional brain activity or FC patterns between different brain regions, providing insights into intrinsic brain networks (Glover, 2011; Lee et al., 2013; Weishaupt et al., 2014; Yuan et al., 2021). Since **study 4** of this thesis employs rsfMRI, a brief overview of the measures and properties used will be given. These include

fractional amplitude of low-frequency fluctuation (fALFF), regional homogeneity (ReHo), and ROI-to-ROI FC.

fALFF measures spontaneous local brain activity by assessing the amplitude of low-frequency fluctuations (ALFF). It represents the ratio of total amplitude within the low-frequency range (0.01-0.1 Hz) to the amplitude across the entire detectable frequency range (Biswal et al., 1995; Zou et al., 2008; Zuo et al., 2010). ReHo evaluates local connectivity within brain regions by measuring regional synchronization among neighboring voxels (Zang et al., 2004), assuming that structurally neighboring voxels exhibit functional homogeneity (Jiang & Zuo, 2016). ReHo is quantified using Kendall's coefficient of concordance (KCC) (Kendall & Gibbons, 1990), with larger values indicating higher local synchronization. ROI to ROI FC assesses the temporal dependence between anatomically separated brain regions, reflecting functional communication and shared functions (Biswal et al., 1995; Lowe et al., 1998, 2000; van den Heuvel & Hulshoff Pol, 2010).

3.2 Magnetic resonance imaging based meta-analyses

Many neuroimaging studies suffer from small sample sizes, leading to underpowered analyses and false positive results (Button et al., 2013). Results can be influenced by experimental as well as analytic procedures and replication studies are rare. Moreover, it is challenging to overlook all published findings due to numerous neuroimaging studies (Button et al., 2013; Eklund et al., 2016; Wager et al., 2007). Performing a neuroimaging meta-analysis might address these issues since it stands out as a powerful method for combining various results unbiasedly (Cieslik et al., 2018).

Neuroimaging meta-analysis methods can be categorized as image-based and coordinate-based. Image-based meta-analyses use the full statistical images from the original publications, whereas the coordinate-based meta-analyses utilize the x, y, z coordinates (in certain instances their z-statistic) of the peak location, resulting from the analysis in the respective study. Since whole-brain statistical images are rarely shared and most studies report their results in standardized coordinates, coordinate based meta-analyses can address more research questions and allow the inclusion of many of the published neuroimaging articles. Notably, the results should be based on a whole-brain analysis without a correction for small volume (Cieslik et al., 2018). However, to investigate differences on a region-of-interest (ROI) level, effect size-based meta-analysis can be carried out. Here, effect sizes

between groups across studies are compared and an overall effect size can be generalized beyond the included studies (Borenstein et al., 2009).

3.3 Machine learning

ML is a specific approach coming from computer science. It is applied in data mining and classification tasks, facilitating the process of generalization and optimization (Martínez-Florez et al., 2021; X.-D. Zhang, 2020). ML has become a valuable tool in MRI data analysis, for example, aiding in image segmentation, disease classification, and treatment outcome prediction (Gassenmaier et al., 2021). In this thesis in **study 2**, extreme gradient boosting (XGBoost) was employed for binary and multi-class classification tasks involving various categorical and numeric variables, specifically sociodemographic, brain volumetric, CSF, and genotyping data. XGBoost represents a gradient-boosting-based algorithm that uses decision trees as its base model (Chen & Guestrin, 2016). It functions as a supervised algorithm, meaning it learns from labeled data consisting of input-output pairs during training (Chen & Guestrin, 2016; X.-D. Zhang, 2020). XGBoost is a powerful and valid tool for investigating the combination of different classes of variables (e.g., biomarkers, MRI data, neuropsychological test results) (Franciotti et al., 2023). Moreover, XGBoost demonstrated strong performance in various regression and classification tasks, such as predicting brain age and classifying brain tumors (Hashmi & Osman, 2022; Kaufmann et al., 2019; Lange et al., 2020). A model-agonistic explanation approach can be used to interpret the XGBoost classifications and gain insights into its internal mechanisms. Specifically, in this thesis, SHAP (SHapley Additive exPlanations) was employed to calculate and visualize the contribution of each input feature to the XGBoost binary and multi-class model's prediction (Mosca et al., 2022).

4 Structural Degeneration of the Nucleus basalis of Meynert in Mild Cognitive Impairment and Alzheimer's disease – Evidence from an MRI-based Meta-Analysis

This chapter refers to **study 1**, investigating the structural degeneration of the NbM in MCI and AD (see section 2.4, Fig. 2.1). It has been formally integrated into the dissertation's style for consistency. The content corresponds to the following publication:

Mieling, M., Meier, H., & Bunzeck, N. (2023). Structural Degeneration of the Nucleus basalis of Meynert in Mild Cognitive Impairment and Alzheimer's Disease – Evidence from an MRI-based Meta-Analysis. Neuroscience & Biobehavioral Reviews, 105393. https://doi.org/10.1016/j.neubiorev.2023.105393

Author's contributions

MM and NB conceived the study. MM ad HM analyzed the data. MM and NB wrote the manuscript and revised it.

Abstract

Recent models of Alzheimer's Disease (AD) suggest that neuropathological changes of the medial temporal lobe (MTL), especially entorhinal cortex (EC), are preceded by degenerations of the cholinergic Nucleus basalis of Meynert (NbM). Evidence from imaging studies in humans, however, is limited. Therefore, we performed an activation-likelihood estimation meta-analysis on whole brain voxel-based morphometry (VBM) MRI data from 54 experiments and 2581 subjects in total. It revealed, compared to healthy older controls, reduced gray matter (GM) in the bilateral NbM in AD, but only limited evidence for such an effect in patients with mild cognitive impairment (MCI), which typically precedes AD. Both patient groups showed less GM in the amygdala and hippocampus, with hints towards more pronounced amygdala effects in AD. We discuss our findings in the context of studies that highlight the importance of the cholinergic basal forebrain (BF) in learning and memory throughout the life span, and conclude that they are partly compatible with pathological staging models suggesting initial and pronounced structural degenerations within the NbM in the progression of AD.

Introduction

Anatomy and function of the cholinergic basal forebrain

The basal forebrain (BF) cholinergic system is a subcortical structure located in the frontal cortex. It can be subdivided into four nuclei with predominantly cholinergic neurons, namely, the medial septal nucleus (Ch1), the vertical and horizontal limb of the diagonal band of Broca nuclei (Ch2, Ch3), and the magnocellular complex (Ch4), which mainly includes the Nucleus basalis of Meynert (NbM) (Mesulam et al., 1983). The NbM is considered to be the largest of the BF's nuclei with ca. 13-14 mm from anterior-posterior and 16-18 mm from medial-lateral (Mesulam & Geula, 1988), and has, therefore, been targeted both in animal and human imaging studies. Functionally, the NbM plays an essential role in the modulation of complex behaviors and cognition through the communication with limbic structures and the entire neocortex (Mesulam et al., 1983), which we further explain below. Finally, cholinergic neurons within the NbM are complexly branched and, important for the understanding of life-long development, the axonal arborizations and synapses are required to remodel continuously due to their principal role in learning, memory and attention (Hasselmo, 2006; Mitsushima et al., 2013; Schmitz & Duncan, 2018; H. Wu et al., 2014).

Acetylcholine (ACh) has long been identified as a powerful neuromodulator that is involved in the regulation of neural activity in distant brain regions and thereby serves several functions, including learning and memory (Picciotto et al., 2012). For instance, the processing of novel stimuli is associated with neural responses in the monkey cholinergic BF (Wilson & Rolls, 1990) as well as increases in fronto-cortical and hippocampal acetylcholine levels in rats (Acquas et al., 1996). Further, high levels of ACh in the rat perirhinal cortex during the encoding of novel information promote memory performance, but they have a detrimental effect on consolidation (Winters et al., 2006) (see Gais and Born (2004), for a similar effect in humans). Compatible with this observation, the removal of cholinergic inputs to the perirhinal cortex impairs object recognition in rodents (Winters & Bussey, 2005).

In humans, pharmacological stimulation of cholinergic activity by acetylcholinesterase inhibition leads to a change in neural novelty signals within the MTL, including the parahippocampal cortex and hippocampus (Bunzeck et al., 2014). In electrophysiological studies, also in humans, cholinergic stimulation led to a shift in novelty responsive brain regions from medio-temporal to prefrontal areas, which suggests that the influence of the

MTL and prefrontal regions in novelty processing is mediated by acetylcholine levels (Eckart & Bunzeck, 2013). Indeed, cholinergic antagonists can impair working memory (Aigner & Mishkin, 1986) and the encoding of novel information in explicit memory tasks (Sherman et al., 2003). In contrast, cholinergic agonists can have opposite effects (Buccafusco et al., 2005). Finally, acetylcholine also modulates attentional processing (Bauer et al., 2012; Hasselmo & Sarter, 2011) as well as human working memory and subsequent familiarity based recognition (Eckart et al., 2016) via changes in neural oscillations.

While the involvement of ACh in cognition, especially learning and memory, is widely accepted, the underlying mechanisms are still under debate. In this regard several effects of ACh within the MTL seem particularly important (Hasselmo, 2006). For instance, ACh enhances the afferent input from dentate gyrus and EC to CA3 (Giocomo and Hasselmo, 2005; Radcliffe et al., 1999); ACh is closely related to hippocampal theta rhythm (Bland and Oddie, 2001; Siok et al., 2006), which was linked to mnemonic processes (Herweg 2020); ACh can increase synaptic plasticity within hippocampal CA1 region (Adams et al., 2004; Huerta and Lisman, 1993) and EC (Cheong et al., 2001); and finally, ACh can enhance encoding related spike activity for novel information in the EC (Klink and Alonso, 1997). Computational models suggest (Gluck et al., 2005; Myers et al., 1996) that cholinergic projections from the BF, in particular the medial septum, to the hippocampus influence suppression of synaptic transmission within the hippocampus and the neocortex. This suppression is selective in as much it affects intrinsic, recurrent collaterals (such as CA1 and CA3) more strongly than external afferents (such as from the EC to CA1) of the hippocampal formation (Hasselmo et al., 1995; Myers et al., 1996).

Together, the BF, including the NbM, is a major source of cholinergic projections to the MTL and neocortex. Thereby, it has the potential to promote cognitive functions, including learning and memory, via the modulation of spike activity, neural oscillations and network properties (Picciotto et al., 2012; Záborszky et al., 2018).

Age related changes of the basal forebrain

Structural degenerations of the BF can be observed during healthy aging, which leads to cognitive impairment (Düzel et al., 2010; Heys et al., 2010; Mesulam, 2004a). While this can be distinguished from more prominent pathological changes in mild cognitive impairment (MCI) and Alzheimer's disease (AD), it is also clear that healthy and pathological aging can be

described on a continuum and, therefore, understanding developmental trajectories is essential. For instance, aged rats showed significant atrophy and a loss of cholinergic BF neurons (de Lacalle et al., 1996), which, in another study, closely related to specific cognitive impairments, including spatial learning (Fischer et al., 1989). Further, magnocellular BF cholinergic neurons are vulnerable to intraneuronal amyloid-β (Aβ) accumulation even in cognitively unimpaired healthy older humans, as shown in a *post-mortem* study (Baker-Nigh et al., 2015).

With regard to disease progression, MCI is typically defined by mild cognitive problems, including memory and language, that are more pronounced than healthy age-related changes, but only minimally interfere with daily life. People with MCI are at higher risk of developing AD, which is characterized by even more pronounced cognitive impairments and structural degenerations (Jessen et al., 2014; Petersen et al., 2018). Physiologically, the prevailing view on the development of AD is that deposits of Aβ and p-Tau first occur in the trans-entorhinal cortex and EC, located within the MTL, followed by the hippocampus and other cortical regions (Braak & Braak, 1991; Corder et al., 2000; Duyckaerts et al., 1990). Therefore, previous MRI studies in humans have often focused on structural abnormalities of these brain regions using voxel-based morphometry (VBM), or similar measures (Ashburner & Friston, 2000), and more recently, positron emission tomography (PET), that allows to quantify Aβ and pTau *in vivo* (Jagust, 2018). They could show that the volume (Karas et al., 2004) and shape (Gerardin et al., 2009) of the hippocampus as well as hippocampal subfields (Hett et al., 2019) differ between MCI and AD patients as compared to age-matched healthy controls (Frisoni et al., 2010). Similar but more heterogeneous effects have been observed in the EC, amygdala, and frontal and parietal cortex (Arrondo et al., 2022).

The focus on MTL regions as origin of AD has been challenged by histologic studies (Geula & Mesulam, 1996; Mesulam et al., 2004; Schliebs & Arendt, 2011) and *in vivo* imaging that shows early pathological changes in the NbM (Grothe et al., 2012, 2013). Specifically, the BF was suggested as one of the first sub-cortical regions affected by neuronal loss (Davies & Maloney, 1976; P. J. Whitehouse et al., 1981), possibly due to accumulation of Aβ and pTau, which is followed by decreased levels of ACh (Rajmohan & Reddy, 2017). This, in turn, could interfere with neuronal signaling, especially in memory encoding (Atri et al., 2004) and attentional processing (Ballinger et al., 2016). Therefore, major damages of cholinergic neurons of the BF in AD not only leads to a 90-95% loss in cortical ACh activity but also

cognitive and behavioral impairments (Ballinger et al., 2016; Geula et al., 2021). Finally, in advanced AD neural loss is more pronounced in the NbM as compared to layer-II EC (Arendt et al., 2015). Based on these findings, a recent view suggests the NbM as early origin of structural degeneration followed by the EC and other cortical brain regions. In humans, direct evidence comes from anatomical MRI studies in combination with measures of Aβ and pTau (Fernández-Cabello et al., 2020; Schmitz & Spreng, 2016). They revealed more pronounced NbM GM loss in cognitively healthy humans depending on abnormal vs normal CSF biomarkers (Fernández-Cabello et al., 2020; Schmitz et al., 2020; Schmitz & Spreng, 2016). Importantly, NbM baseline volumes predicted longitudinal EC degenerations, implying a trans-synaptic spread of Aβ starting in the NbM (Fernández-Cabello et al., 2020; Schmitz & Spreng, 2016). This conclusion is compatible with work in animals and adds a crucial upstream link to the subsequent spread from EC to other MTL structures, including the hippocampus, and more distant neocortical brain regions such as the posterior parietal cortex (de Calignon et al., 2012; Khan et al., 2014; L. Liu et al., 2012; J. W. Wu et al., 2016). Apart from these and other studies (Arrondo et al., 2022; Colloby et al., 2014; Fernández-Cabello et al., 2020; Jessen et al., 2006; Kerbler et al., 2015; Kilimann et al., 2014; Schmitz et al., 2018; Schmitz & Spreng, 2016) showing structural degenerations of the BF *in vivo* with MRI, others have demonstrated reduced structural integrity of cholinergic white matter pathways in AD (Nemy et al., 2023; Schumacher et al., 2022).

Research Question and hypotheses

Despite the prominent view of a role of the cholinergic BF in AD, empirical evidence is limited, especially *in vivo*, and a meta-analytic investigation is missing. Here, we assumed that AD and MCI are characterized by smaller NbM volumes as compared to healthy controls (HC). More specifically, we hypothesized that patients with MCI show less GM in the NbM compared to age-matched HC (HC>MCI, hypothesis 1); patients with AD show less GM in the NbM compared to age-matched HC (HC>AD, hypothesis 2); and patients with MCI or AD show less GM in the MTL (EC and hippocampus, hypothesis 3) compared to age-matched HC (HC>MCI/AD). To this end, we employed an activation likelihood estimation (ALE) meta-analytic approach on the basis of recently published whole brain voxel-based morphometry (VBM) MRI data. This allowed us to focus on the NbM and EC, and, in a more exploratory

fashion, other brain regions, such as temporoparietal areas, which have also been associated with AD (Fernández-Cabello et al., 2020).

Methods

Literature search and selection

This work followed the PRISMA 2020 guidelines (Page et al., 2021) and is in accordance with suggestions by Müller et al. (2018) for Neuroimaging Meta-Analyses (see Table S1.1). More specifically, a systematic review was conducted based on the VBM BrainMap database using the search application Sleuth (version 3.0.4) (Fox et al., 2005; Fox & Lancaster, 2002; Vanasse et al., 2018). Here, the rationale is to identify those studies with convergence regarding brain volume reductions in MCI and AD compared to HC; therefore, literature review and statistical analyses (see below) were run separately for HC>MCI and HC>AD (Eickhoff et al., 2009; Vanasse et al., 2018).

The search included all whole-brain VBM studies in the database until Aug. 16, 2022 – these were 1316 publications with 4345 experiments (Fox et al., 2005; Fox & Lancaster, 2002; Vanasse et al., 2018). Here, the term experiment refers to a single analysis conducted in a given publication (Turkeltaub et al., 2012). Applying a specific category selection in Sleuth (see Table S1.1) and specific inclusion and exclusion criteria (Table 4.1) resulted in 22 publications with 33 experiments for the contrast HC>MCI. However, only 16 publications (17 experiments) remained after a more careful inspection (Table S1.2, Fig. 4.1.). For the contrast HC>AD, the initial search resulted in 71 publications, with 103 experiments but after a detailed inspection only 37 publications (37 experiments) could be included in the analysis (Table S1.2, Fig. 4.1).

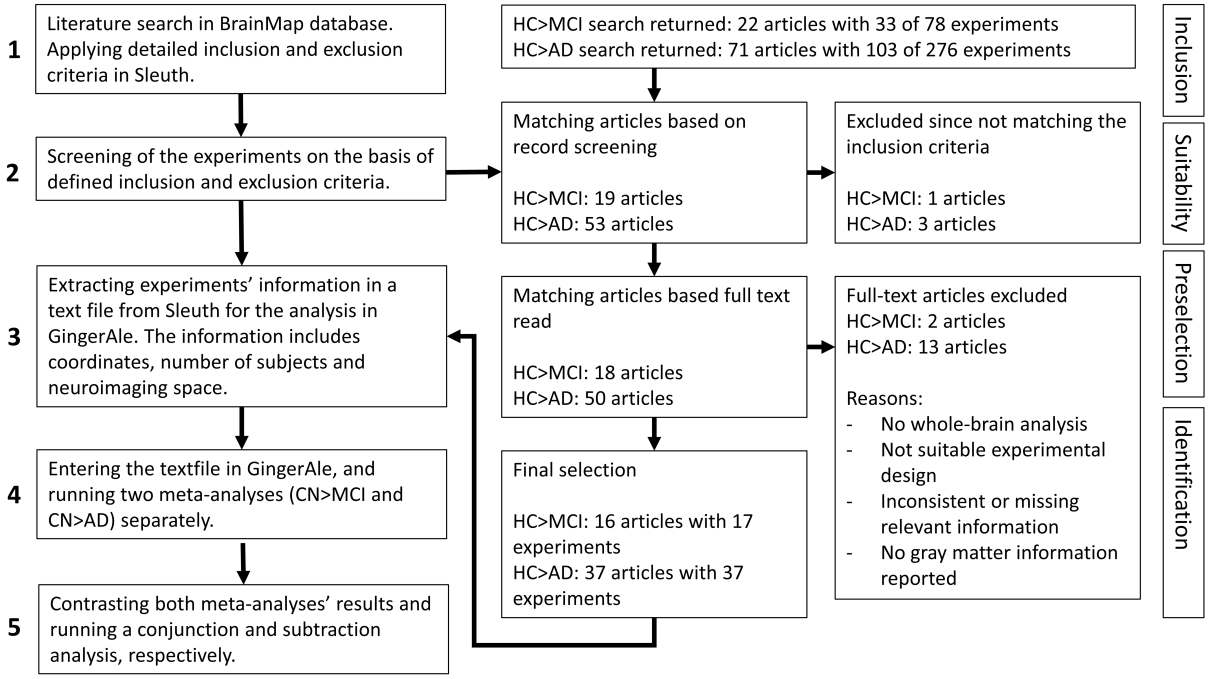

Figure 4.1. Flowchart of the steps performed in the meta-analysis.

Table 4.1. Inclusion and exclusion criteria for the systematic literature research

Inclusion criteria	Exclusion criteria
Study contrasted MCI vs HC or AD vs HC.	Study did not contrast MCI vs HC or AD vs HC, e.g., MCI vs AD.
MCI/AD and HC were matched regarding age, gender, education etc.	MCI/AD and HC were not matched regarding age, gender, education etc. or compared with patients other than MCI/AD.
Patient groups were clearly defined and if necessary summarized, e.g., "early AD" or "late AD".	Several subgroups of AD were defined (e.g., early/late AD) and analyzed separately.
Study was based on one temporal measurement per patient. In longitudinal studies, the first MRI acquisition was selected.	Multiple measurements across time for each subject included in one analysis.
Analysis and report of GM based whole brain VBM.	Other analysis than GM based whole brain VBM, e.g., region of interest (ROI) analysis or correlation analysis.

In total, structural MRI data from 347 MCI patients with 462 matching controls, and 799 AD patients with 973 matching controls were analyzed. Therefore, data from 1146 patients were compared with 1435 healthy older adults. A possible sample overlap between the studies was avoided by applying appropriate exclusion criteria in BrainMap, and additional cross-checks with the primary literature. Specifically, this included the sample characteristics, author affiliations and scanning locations. Note, however, that in the HC>MCI meta-analysis, two experiments from Bozzali et al. (2006) were included, contrasting MCI retrospective converters and non-converters with healthy controls separately. Here, these experiments were treated as independent analyses due to different MCI groups involved, the focus on coordinate-based contrasts, and no other coding possibility of the experiments (Turkeltaub et al., 2012). Additionally, in four studies (Bozzali et al., 2006; Hämäläinen et al., 2007; Rami et al., 2009; Shiino et al., 2006) the same HCs were contrasted against MCI and AD, respectively; here they were entered into both meta-analyses HC>MCI and HC>AD, respectively. However, study-specific biases are unlikely due to the number of included experiments (see Fig. 4.1) (Heckner et al., 2021; Turkeltaub et al., 2012).

MRI scanners included field strengths from 1.0 to 3.0 Tesla, for one study the field strength was unknown, and all incorporated studies performed a VBM whole brain analysis (Ashburner & Friston, 2000; Mechelli et al., 2005), typically with SPM, MedX or FSL. A possible bias resulting from different MRI scanner field strengths (Tardif et al., 2009) was investigated using a chi-squared test. It revealed no significant effects, indicating no systematic differences in MRI field strength in the two meta-analyses ($\chi^2(3) = 1.55$, $p = 0.67$, Cramer's $V = 0.168$).

About 80 percent of the studies reported their findings in MNI and 20 percent in Talairach reference space. Ten of 17 experiments used voxel- or cluster-wise corrected p-values in the HC>MCI comparison, the remaining seven used uncorrected p-values. In the HC>AD comparison 30 of 37 experiments used corrected p-values and seven used uncorrected p-values. All information is listed in detail in Table S1.2 and Table S1.3.

Two researchers (M.M. and H.M.) independently inspected each study individually with regard to the inclusion and exclusion criteria, based on the abstract, title, information provided by Sleuth, and finally, a full text read. Disagreements were, if required, discussed with a third researcher (N.B.). The final selection of included publications and experiments, respectively, with further study-specific information is shown in Tables S1.2 and S1.3.

Statistical analysis

Activation likelihood estimation (ALE)

The activation likelihood estimation (ALE) meta-analytic approach was used to investigate the convergence of VBM results from all included whole-brain experiments (Eickhoff et al., 2009, 2012; Turkeltaub et al., 2012; Vanasse et al., 2018). ALE is implemented in BrainMap's application GingerALE (version 3.0.2) (Eickhoff et al., 2009, 2012; Turkeltaub et al., 2012) and represents a coordinate-based neuroimaging meta-analyses technique. Here, in a first step, all reported Talairach coordinates were automatically converted to MNI space by the implemented algorithm icbm2tal (Laird et al., 2010; Lancaster et al., 2007). All other studies, i.e., those that already provided MNI coordinates, were not further converted. Second, the ALE random-effects algorithm treated all included coordinates of maximum activation, called foci, as spatial Gaussian probability distributions weighted by the number of subjects (Eickhoff et al., 2009; Laird et al., 2009). Further, the probability distributions of the foci from the specific experiment are summarized per voxel, resulting in a model activation (MA) map. Here, the voxel-wise MA values were calculated based on the maximum probability of any focus in the given experiment (Eickhoff et al., 2012; Turkeltaub et al., 2012). The voxel-wise union of these MA maps results in ALE scores on a voxel level. Accordingly, ALE scores represent the convergence of results across studies instead of foci. Third, to statistically evaluate the degree of convergence across studies, ALE scores are compared to an empirical null distribution of random spatial associations between all MA maps (Eickhoff et al., 2009, 2012). Here, our results were thresholded at $p<0.05$ with 1,000 permutations (cluster-level) corrected for multiple comparisons by the family-wise error (FWE) and an cluster-forming (uncorrected) $p<0.001$ (Eickhoff et al., 2016). Again, this approach was conducted separately for the meta-analysis HC>MCI and HC>AD.

Additionally, to investigate the differences and common effects of the two meta-analyses HC>MCI and HC>AD, their results were combined in a contrast analysis ([HC>MCI]>[HC>AD] and [HC>AD]>[HC>MCI]) and a conjunction analysis (HC>MCI and HC>AD), respectively. Therefore, the conjunction included computing the voxel-wise-minimum based on the HC>MCI and HC>AD ALE images resulting from initial meta-analysis (Eickhoff et al., 2011; Laird et al., 2005). The subtraction resulted in a new ALE image for each dataset, which was then subtracted from the other and compared to the true data. Finally,

after permutations, a final voxel-wise p-value image is created and then z-scored to represent significance rather than the direct ALE subtraction (Eickhoff et al., 2011; Laird et al., 2005). Note that different sample sizes between the meta-analyses were corrected for the conjunction and contrast (Eickhoff et al., 2011). The results were thresholded at $p<0.01$ (uncorrected) and 10,000 permutations.

Significant clusters and associated brain regions will be reported based on the probabilistic cytoarchitectonic human brain maps as implemented in the SPM Anatomy Toolbox Version 3.0 (Eickhoff et al., 2005, 2006, 2007; Heckner et al., 2021) (available from https://www.fz-juelich.de/en/inm/inm-7/resources/jubrain-anatomy-toolbox).

Region-of-Interest analyses

On the basis of our a priori hypotheses (see introduction), we performed post-hoc region-of-interest (ROI) analyses for the NbM and EC, separately, using the whole-brain ALE meta-analysis approach. The ROIs for both regions were generated for the left and right hemisphere as well as one bilateral ROI for the NbM and one bilateral ROI for the EC. This was done in MNI space using the SPM Anatomy Toolbox Version 3.0 (Eickhoff et al., 2005, 2006, 2007) (available from https://www.fz-juelich.de/en/inm/inm-7/resources/jubrain-anatomy-toolbox). Specifically, the NbM was defined using previous published probabilistic maps labeled as Ch4 (Zaborszky et al., 2008), and the EC was derived from the previously published probability map (Amunts et al., 2005). The mean p-values of the NbM and EC were extracted at a threshold of 50% probability from the uncorrected p-value maps (resulting from the analyses HC>MCI and HC>AD, respectively) using Marsbar (Brett et al., 2002) implemented in the SPM toolbox (SPM 12, https://www.fil.ion.ucl.ac.uk/spm/) for MATLAB®. Note that this approach allows the extraction of p-values from each ROI but no other statistical values such as standard deviations or individual data points.

Results

The HC>MCI meta-analysis included 17 experiments from 16 studies, and the HC>AD meta-analysis included 37 experiments from 37 studies. The mean age of the subjects ranged from 62 to 76 years (HC>MCI) and 59 to 83 years (HC>AD), respectively. For both meta-analyses, the patient groups were matched to the HC regarding age and gender. See Table S1.2 and S1.3, respectively, for further information on sociodemographics

HC > MCI

The meta-analysis HC>MCI revealed two significant clusters (Table 4.2, Fig. 4.2A). The first cluster was driven by seven studies and included the right amygdala and right hippocampus. The second cluster was driven by four studies and included the left hippocampus and left amygdala.

HC > AD

The meta-analysis HC>AD revealed six significant clusters (Table 4.2, Fig. 4.2B). The first cluster was driven by twenty studies and included the right amygdala and right hippocampus. The second cluster was driven by eighteen studies and included the left amygdala, left hippocampus and EC. The third cluster was driven by eleven studies and included the left hippocampus and left thalamus. The fourth cluster was driven by eight studies and included the right hippocampus. The fifth cluster was driven by seven studies and included the right angular gyrus and right lateral occipital cortex (LOC). The sixth cluster was driven by four studies and included the left and right thalamus.

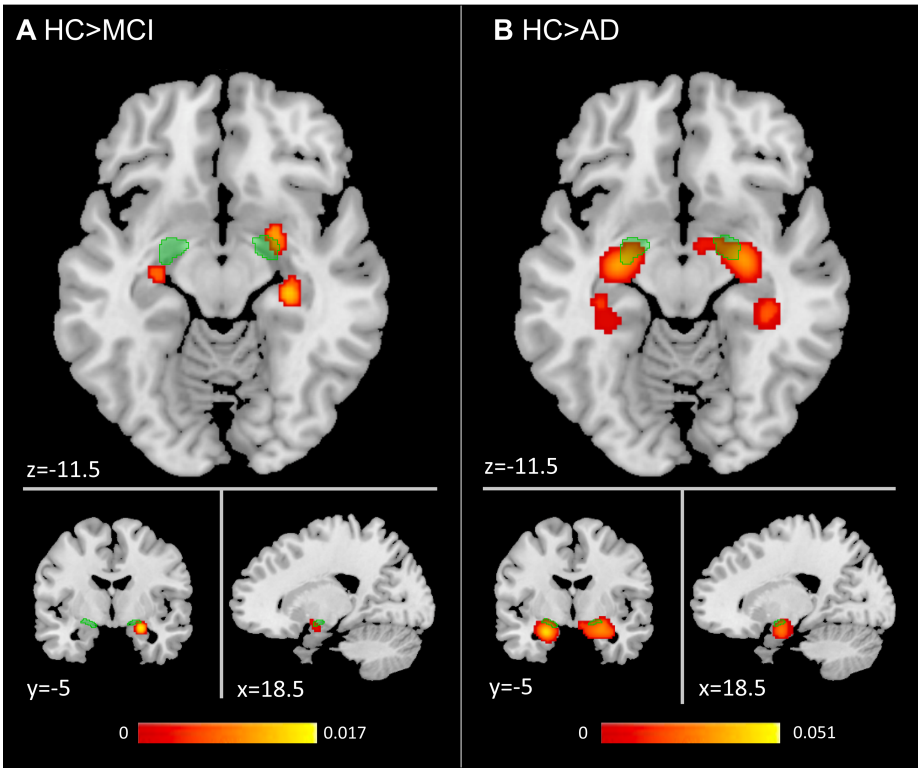

Figure 4.2. Results of meta-analyses HC>MCI (A) and HC>AD (B). Clusters represent significant convergence across experiments in GM reductions. Cluster-level $p<0.05$, family-wise error corrected with a cluster-forming threshold $p<0.001$. The color bar represents the activation likelihood estimation (ALE) scores. The light green region indicates the NbM. Clusters were overlaid onto a T1 weighted template image.

Table 4.2. Results of the ALE meta-analysis for the contrasts HC>MCI and HC>AD. Significant clusters, their sizes (in voxels, 2x2x2 mm), peaks, regional assignment (probability in %) and cytoarchitectonic probabilities (in %) are based on the Jülich Brain atlas. Additionally, we also report the contributing studies, based on GingerALE. Abbreviations, R: Right; L: Left; CA: Cornu Ammonis; DG: Dentate Gyrus; HATA: Hippocampus-Amygdala-Transition Area; EC: Entorhinal Cortex; LOC: Lateral Occipital Cortex; Area FG3=Fusiform Gyrus; Area PGa (IPL)= Rostral region in the Angular Gyrus (Inferior Parietal Lobe); Area PGp (IPL)= Caudal region in the Angular Gyrus (Inferior Parietal Lobe)

ALE Meta-Analysis and significant clusters	Size (in voxel)	Peak MNI Coordinates (x, y, z)	Cytoarchitectonic probability	Contributing studies
HC>MCI				
# Cluster 1 **CA1** 58.5% CA 1 23.9% DG 17.6 % Subiculum	282	28, -10, -28	58.9% R Hippocampus 30.2% R Amygdala	Bai et al. (2008), Barbeau et al. (2008), Bell-McGinty et al. (2005), Hämäläinen et al. (2007), Z. Long et al. (2016), Pennanen et al. (2005), Shiino et al. (2006)
# Cluster 2 **CA1** 41.6 % CA 1 37.8% DG 20.6% Subiculum	121	-26, -14, -26	92.5% L Hippocampus 3.8% L Amygdala	Bell-McGinty et al. (2005), Gold et al. (2010), Hämäläinen et al. (2007), Shiino et al. (2006)
HC>AD				
# Cluster 1 **CA1** 48.0% CA1 38.0% DG 13.9 Subiculum	690	28, -12, -26	37.3 % R Hippocampus 34.1% R Amygdala	Baron et al. (2001), Boxer et al. (2003), Bozzali et al. (2006, 2012), Dashjamts et al. (2011), Farrow et al. (2007), Frisoni et al. (2002), Gili et al. (2011), Hämäläinen et al. (2007), Irish et al. (2013, 2016), Ishii et al. (2005), Kanda et al. (2008), S. Kim et al. (2011), Matsuda et al. (2002), Ohnishi et al. (2001), Rami et al. (2009), Rémy et al. (2005), Shiino et al. (2006), S. Xie et al. (2006)

# Cluster 2 **Subiculum** 45.6% Subiculum 31.8% EC 12.8% CA1 9.5% HATA	576	-18, -10, -28	41.4% L Hippocampus 38.4% L Amygdala	Baron et al. (2001), Bozzali et al. (2006), Dashjamts et al. (2011), Di Paola et al. (2007), Farrow et al. (2007), Frisoni et al. (2002), Guo et al. (2010), Hall et al. (2008), Hämäläinen et al. (2007), Ishii et al. (2005), Kanda et al. (2008), S. Kim et al. (2011), Ohnishi et al. (2001), Rémy et al. (2005), Shiino et al. (2006), Wei et al. (2020), Whitwell et al. (2007), S. Xie et al. (2006)
# Cluster 3 **DG** 57.5% CA1 42.5% DG	286	-36,-28,-14	45.5% L Hippocampus 11.2% L Thalamus	Bozzali et al. (2012, 2006), Brenneis et al. (2004), Dashjamts et al. (2011), Di Paola et al. (2007), Frisoni (2002), Guo et al. (2010), Hämäläinen et al. (2007), Matsuda et al. (2002), Rémy et al. (2005), Shiino et al. (2006)
# Cluster 4 30.9% CA1 1.7% Area FG3	224	36, -36, -12	27.5% R Hippocampus	Baron et al. (2001), Brenneis et al. (2004), Dashjamts et al. (2011), Frisoni et al. (2002), Hämäläinen et al. (2007), Matsuda et al. (2002), Rémy et al. (2005), Shiino et al. (2006)
# Cluster 5 **Area PGa (IPL)** 42.5% Area PGa (IPL) 21.6% Area PGp (IPL)	155	54, -58, 26	62.3% R Angular Gyrus 32.0% R LOC, superior division	Brenneis et al. (2004), Frisoni (2002), Hämäläinen et al. (2007), Kanda et al. (2008), Rémy et al. (2005), Shiino et al. (2006), Wei et al. (2020)
# Cluster 6 **Not specified**	151	0,-14,-2	48.0% L Thalamus 40.3% R Thalamus	Bozzali et al. (2006), Hämäläinen et al. (2007), Rami et al. (2009), Rémy et al. (2005)

Contrast and conjunction analyses

The conjunction of both meta-analyses (HC>AD & HC>MCI) showed two significant clusters. The first was driven by eleven experiments and included the right amygdala and right hippocampus (Table 4.3, Fig. 4.3A). The second cluster was driven by nine experiments and included in the left hippocampus and left amygdala (Table 4.3, Fig. 4.3A).

Finally, the contrast of both meta-analyses (HC>AD minus HC>MCI) revealed a significant effect in the left amygdala (Table 4.3, Fig. 4.3B), which was driven by two studies. This indicates more pronounced GM differences in AD (<HC) as compared to MCI (<HC). The reverse contrast (HC>MCI minus HC>AD) revealed no significant effects.

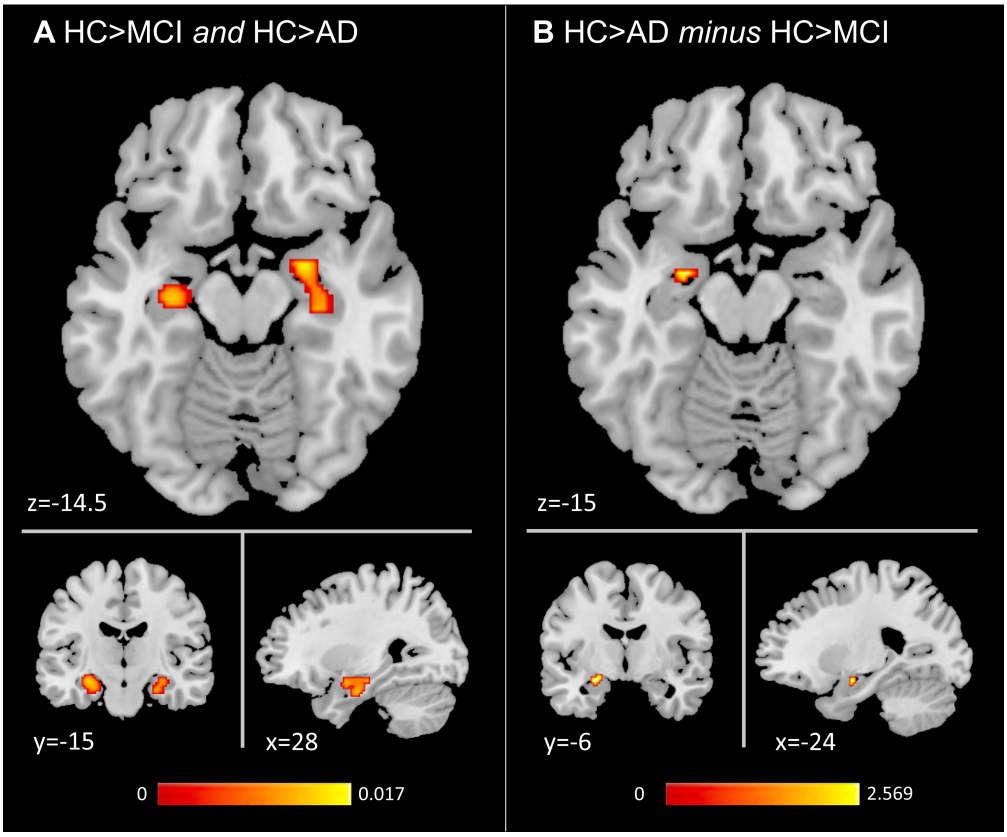

Figure 4.3. Results of the conjunction (A) and contrast analyses (B)**.** A) shows the conjunction image (p<0.01, uncorrected) of both meta-analyses (HC>MCI and HC>AD), and color bar indicating the activation likelihood estimation scores. B) shows the results of the subtraction HC>AD *minus* HC>MCI (p<0.01, uncorrected), and the color bar reflects the z scores. Clusters were overlaid onto a T1 weighted template image.

Table 4.3. Results of the meta-analyses for the conjunction HC>MCI AND HC>AD as well as the contrast HC>MCI MINUS HC>AD. Significant clusters, their sizes (in voxels, 2x2x2 mm), peaks, regional assignment (probability in %) and cytoarchitectonic probabilities (in %) are based on the Jülich Brain atlas. Additionally, we also report the contributing studies, based on GingerALE. Abbreviations, R: Right; L: Left; CA: Cornu Ammonis; DG: Dentate Gyrus; BF: Basal Forebrain

ALE Meta-Analysis	Size (in voxel)	Peak MNI Coordinates (x, y, z)	Cytoarchitectonic probability	Contributing studies
HC>MCI *AND* HC>AD				
# Cluster 1 **CA1** 48.0% CA1 38.0% DG 13.9% Subiculum	174	28, -12, -26	57.7% R Hippocampus 39.1% R Amygdala	Bai et al. (2008), Barbeau et al. (2008), Frisoni et al. (2002), Hämäläinen et al. (2007, 2 experiments), Irish et al. (2016), Ishii et al. (2005), S. Kim et al. (2011), Pennanen et al. (2005), Shiino et al. (2006, 2 experiments)
# Cluster 2 **CA1** 59.2% CA1 29.1% DG 8.4% Subiculum 1.5% Amygdala (ventro-medial)	116	-24, -14, -24	92.2% L Hippocampus 4.0% L Amygdala	Bell-McGinty et al. (2005), Farrow et al. (2007), Gold et al. (2010), Guo et al. (2010), Hämäläinen et al. (2007), S. Kim et al., (2011), Rémy et al. (2005), Wei et al. (2020)
HC>AD *MINUS* HC>MCI				
# Cluster 1 **Amygdala (centromedial)** 41.9% Amygdala (centro-medial) 15.2% Amygdala (intermediate fiber bundles) 13.8% Amygdala (laterobasal) 12.9% BF (Ch4) 12.0% Amygdala (internale medial fiber bundles)	13	-24, -6, -14	100% L Amygdala	Frisoni (2002), Hall et al. (2008)

ROI analysis

To further investigate possible GM differences in the NbM, a more liberal post-hoc ROI analysis based on the uncorrected p-value maps was carried out. It revealed a significant effect for the comparison HC>AD (p=0.007, Table 4.4) but not HC>MCI (p=0.122, Table 4.4). For the sake of completeness, in Table 4.4, we also report the p-values for the left and right NbM, which indicates a borderline significant effect in the right but not left NbM (p=0.073) for the comparison HC>MCI. In the EC, the analyses revealed no significant effects for HC>MCI (p=0.223) and HC>AD (p=0.208).

Table 4.4. Results of the post-hoc ROI analysis. Listed are the average p-values extracted from the uncorrected p-value map of both meta-analyses (HC>MCI and HC>AD) for both the Nucleus basalis of Meynert (NbM) and Entorhinal cortex (EC). * indicates p<0.01.

Contrast and ROI	p-value
HC>MCI	
L NbM	0.165
R NbM	0.073
Bilateral NbM	0.122
L EC	0.335
R EC	0.089
Bilateral EC	0.223
HC>AD	
L NbM	0.012
R NbM	0.001*
Bilateral NbM	0.007*
L EC	0.121
R EC	0.312
Bilateral EC	0.208

Discussion

We investigated structural abnormalities, with a focus on the cholinergic BF (NbM) and MTL, in MCI and AD patients compared to HC using the whole brain ALE meta-analytic approach. Our analyses included 53 previously published whole brain MRI studies with 54 experiments, and revealed less GM in the NbM of AD patients but only weak evidence in MCI. Furthermore, MCI and AD both showed, compared to HC, reduced GM in the MTL, including the hippocampus and amygdala, with hints towards more pronounced amygdala effects in AD. As such, our findings provide novel evidence in favor of the notion that structural degeneration of the cholinergic BF and interconnected MTL play a critical role in the progression of AD.

The cholinergic BF is a core region involved in complex behaviors and cognition, including attention and learning, through the modulation of neural activity in distant brain regions (Picciotto et al., 2012; Záborszky et al., 2018). It is also known to degenerate during healthy aging and AD, as shown in *post-mortem* and *in vivo* imaging studies. For instance, in healthy older adults, the BF integrity, as measured with MRI based magnetization transfer ratio (MTR), closely related to verbal learning and working memory performance (Düzel et al., 2010). Importantly, in AD these structural changes appear to be much more pronounced, as reported in individual MRI studies (Hall et al., 2008; Whitwell et al., 2007), and evident in our post-hoc ROI analysis based on the whole-brain estimated uncorrected p-value maps (Table 4.4), which further points towards a critical role of the BF, especially the NbM, in the disease progression. Indeed, *post-mortem* studies in AD have identified pathological changes of the NbM, including accumulations of Aβ and pTau, as early features that are associated with cognitive decline (Contestabile, 2011; Mesulam, 2004b; Schliebs & Arendt, 2011). This selective vulnerability might be explained by the large projecting axons with wide arbors expanding vast distances in the central nervous system (X. Li et al., 2018; Mesulam & Geula, 1988; H. Wu et al., 2014). With regard to AD progression, previous studies suggest that pathologies of the BF precede those within other cortical regions, especially the EC and hippocampus. In humans, such a view is supported by longitudinal MRI studies showing that the BF volume predicts atrophy in the EC, which was further moderated by AD specific proteinopathies (Fernández-Cabello et al., 2020; Schmitz & Spreng, 2016). Finally, there is also evidence for reduced NbM volumes in patients with MCI and preclinical AD, which underlines the notion of a characteristic disease progression (Grothe et al., 2012; Hall et al., 2008; Kilimann et al., 2014; Muth et al., 2010).

In our meta-analysis, NbM GM reductions in MCI were only marginally significant (p=0.073, Table 4.4), which is contrary to our hypothesis and the pathological staging model (Fernández-Cabello et al., 2020; Schmitz & Spreng, 2016). While this is difficult to interpret, at least two explanations seem to be relevant. First, the number of included experiments for the meta-analysis HC>MCI (n=17) was much smaller as compared to HC>AD (n=37). Therefore, the null-finding could simply reflect a power problem, which could be addressed in future studies by searching more or other databases. Second, since NbM atrophy in MCI is not as pronounced as in AD, it is much more difficult to detect it with MRI based VBM. Indeed, not the entire NbM but posterior parts of it seem to be particularly vulnerable to the early stages of AD (Arendt et al., 1985; Doucette et al., 1986; Grothe et al., 2012, 2013; Kilimann et al., 2014; A. K. L. Liu et al., 2015; Vogels et al., 1990), which further calls for more fine-grained microstructural MRI measures such as multiparameter mapping (Leutritz et al., 2020) (see below).

Compared to healthy controls, both patient groups showed significant GM reductions in the amygdala with cautious evidence for more pronounced effects in AD (Table 4.3, Fig. 4.3). This is, again, in line with individual studies that drive the effect (Hall et al., 2008; S. Kim et al., 2011) and others that also show early structural degenerations within the amygdala (Planche et al., 2022; Poulin et al., 2011; Ramos Bernardes da Silva Filho et al., 2017). From an anatomical point of view, the amygdala represents a central target region of NbM projections, including a high density of cholinergic axons (Mesulam & Geula, 1988; Mesulam et al., 1992), and functionally it is prominent for its role in processing emotional information (Dolan, 2002; LeDoux, 2003) but also memory formation and consolidation (Rutishauser et al., 2010; Yousuf et al., 2021). For instance, cholinergic stimulation in healthy middle aged humans reduced activity in the right amygdala for successful versus unsuccessful spatial context retrieval (Kukolja et al., 2009), which is in line with others suggesting that high levels of ACh promote encoding but interfere with retrieval (Winters et al., 2006). With regard to AD, a longitudinal study in humans could show that amygdala degeneration and abnormal memory-related alpha oscillations, as measured with electroencephalography (EEG), predict the conversion to AD (Prieto del Val et al., 2016). Further, fMRI based functional connectivity (FC) between the NbM and amygdala during resting state was increased with neuropathology as indicated by Aβ and tau PET (Zeng et al., 2022). This is in line with other PET studies on the spread of Aβ and tau (Insel et al., 2020), as well as MRI studies in MCI and AD showing that NbM atrophy covaries with atrophy in innervating regions, including the amygdala (Cantero et al., 2016;

Schmitz et al., 2018). Therefore, the loss of cholinergic inputs to the amygdala, together with a trans-synaptic spread of tau, might facilitate and accelerate AD pathology (Clavaguera et al., 2009; de Calignon et al., 2012; Khan et al., 2014).

As expected, both meta-analyses (HC>MCI and HC>AD) revealed significant hippocampal GM atrophy in AD and MCI compared to HC. However, in the EC a significant effect was observed only in AD (Table 4.2, second cluster, 31.8% probability based on the Jülich Brain atlas) and not MCI. Note that our post-hoc ROI analysis did not confirm the effect in AD possibly since it was spatially limited to a small portion of the rather large EC. In any case, these findings are only partly compatible with another prevailing model suggesting the trans-entorhinal cortex as origin of AD pathology (Braak & Braak, 1991; Corder et al., 2000; Duyckaerts et al., 1990). Together with an arguably stronger effect in the NbM in AD, this could be interpreted as evidence in favor of the view that NbM pathology precedes EC pathology (e.g., Schmitz and Spreng, 2016; Fernández-Cabello et al., 2020). However, the absence of structural degenerations in EC might also have methodological reasons, see below. Therefore, more fine-grained MRI based methods should be used, preferably in combination with larger samples and longitudinal designs, to further address this important issue.
The significant GM effect in the hippocampus in AD and MCI was driven by large numbers of studies (Table 4.3) and confirms, on a meta-analytic level, its involvement in AD pathology and its important role in early AD detection (Good et al., 2002; Hett et al., 2019; Planche et al., 2022; Wolz et al., 2011).

With regard to the BF, the hippocampus (and EC) receives a high density of cholinergic axons, which mainly originate in the medial septum and vertical diagonal band nuclei (i.e. Ch1 and Ch2, Mesulam and Geula, 1988; Mesulam et al., 1992); this is in contrast to the amygdala, which receives cholinergic innervations from NbM (i.e. CH4) (Mesulam et al., 1983). Here, we focused in the NbM due to its early vulnerability in AD but the hodological separation between BF nuclei and specific projection sites in the MTL points towards another fruitful avenue in future research to fully understand healthy and pathological age-related development.

Apart from cortical projections, the cholinergic system is interconnected with subcortical regions that are part of the dopaminergic mesolimbic system and play a central role in the encoding and consolidation of novel information into long-term memory (Bunzeck et al., 2014; Lisman et al., 2011; Lisman & Grace, 2005). For instance, substantia nigra/ventral tegmental area (SN/VTA) dopamine neurons receive cholinergic projections from the

laterodorsal and pedunculopontine (PPT) tegmental nuclei, which modulate their activity via muscarinic and nicotinic receptors (Futami et al., 1995; Oakman et al., 1995). Therefore, systemic injections of the nonselective muscarinic antagonist scopolamine increased dopamine release into the striatum in rats (Chapman et al., 1997; Miller & Blaha, 2004), and cholinergic agonists, and the other hand, attenuated the striatal dopamine efflux (Miller & Blaha, 2004). In humans, both the dopamine precursor levodopa and the acetylcholinesterase inhibitor galantamine modulated hemodynamic activity in the SN/VTA and MTL during novelty processing (Bunzeck et al., 2014). Therefore, these and other studies (e.g., Mark et al., 2011; Threlfell et al., 2012) point towards a close structural and functional interaction between the cholinergic and dopaminergic system.

Importantly and similar to the cholinergic system, the dopaminergic mesolimbic system also undergoes age-related changes (Backman et al., 2006; Guitart-Masip et al., 2016) but their common effect on cognition and behavior across the life span remain little understood. For instance, the structural integrity of the SN/VTA, as measured with MRI based magnetization transfer ration, was reduced in healthy older adults (Bunzeck et al., 2007) and correlated with learning abilities (Düzel et al., 2008). Moreover, age-related iron accumulation and demyelination in basal ganglia structures are closely related to verbal memory (Steiger & Bunzeck, 2017) and executive functioning (Biel et al., 2021). Along these lines, microstructural brain changes, in particular iron depositions, are not only a hallmark of healthy but also pathological aging. In fact, excessive iron depositions have long been observed in AD and Parkinson's Disease (PD) (Guan et al., 2022; Loeffler et al., 1995; Sian-Hülsmann et al., 2011), which points towards a dysfunction of brain iron homeostasis (Ward et al., 2014). From a mechanistic point of view, this could have neurotoxic effects via oxidative stress, which accelerates neurodegeneration (Ward et al., 2014). More specifically, enhanced iron levels have been linked to Aβ and tau in AD (Rogers et al., 2008; Yamamoto et al., 2002), and α-synuclein and Lewy body aggregation in PD (Ostrerova-Golts et al., 2000).

Together, cognitive deficits during healthy and pathological aging can have complex etiologies involving both the cholinergic and dopaminergic system (Amalric et al., 2021). Therefore, future studies in humans might leverage recent advances in microstructural MRI and PET imaging to focus on several open questions, including interactions. Another line of research might focus on functional brain changes in AD, which often precede structural

degenerations (Johnson et al., 2012; Sperling, 2011; Warren & Moustafa, 2023) and could involve compensational mechanisms (Cabeza et al., 2018) to promote cognition.

Finally, our meta-analytic approach has several strengths but also limitations, which both could guide future research. First, we focused on the convergence across experiments on the basis of previously published whole-brain VBM studies that are included in the BrainMap database. Currently, these are limited to ca 20-30% of all published neuroimaging studies. While this may be considered a limitation, the advantage is that BrainMap's database allows a fast and less error-prone search and data extraction (Cieslik et al., 2018). As such, it represents a powerful tool to provide robust and generalizable results (Heckner et al., 2021). The disadvantage of our whole brain approach is that we could not integrate original studies with a region of interest approach showing significant structural changes in the BF (e.g., Arrondo et al., 2022; Colloby et al., 2014; Fernández-Cabello et al., 2020; Jessen et al., 2006; Kerbler et al., 2015; Kilimann et al., 2014; Schmitz et al., 2018; Schmitz and Spreng, 2016) or reduced structural integrity of cholinergic white matter pathways in AD (Schumacher et al. 2022, Nemy et al., 2023).

Second, the NbM is a rather small brain structure but not all original studies were specifically optimized with regard to spatial resolution and imaging analysis. For instance, too large voxels in combination with inappropriate smoothing kernels might „wash-out" possible effects. Nevertheless, it is important to note that the voxel size (typically 1x1x1 mm or slightly larger) and smoothing kernel (approximately 8-12 mm full width at half maximum) employed in most studies should be sufficient to detect signals in the NbM. Third, the meta-analysis HC>MCI only included 17 experiments, which is at the lower end of recommendations (17-20) to achieve adequate power to detect even small effects (Eickhoff et al., 2016). Fourth, the contrast and conjunction analyses did not include a minimum cluster size (Eickhoff et al., 2009, 2011, 2012; Turkeltaub et al., 2012). This is particularly relevant for the rather small amygdala effect (Table 4.3, 13 voxels, which correspond to 104 mm^3, driven by two studies), which, therefore, needs to be interpreted with caution.

Fifth, participants were included in the analyses solely based on their clinical status. To avoid possible heterogeneity (e.g. by including preclinical AD cases in the group of healthy controls), the AT(N) framework, which incorporates Aβ (A), tau (T), and neurodegenerative (N), could have been used (Jack et al., 2018). However, in most studies, these markers were not assessed, and larger sample sizes would be necessary to include at least three groups (A-

T-, A+T-, A+T+), with typically imbalanced distributions (see, e.g., Zeng et al. (2022)). Additionally, other forms of dementia were excluded based on the specified exclusion criteria in BrainMap that were validated by cross-checking the original literature. Finally, the direct comparison of MCI>AD (rather than HC>MCI vs HC>AD) might have been helpful, but a search in BrainMap's database revealed only four studies, which is not suitable to perform a statistical meta-analysis (Eickhoff et al., 2016).

In conclusion, using the ALE meta-analytic approach, involving 54 experiments and 2581 subjects, our study provides novel evidence for structural degenerations of the NbM in AD patients, but only limited evidence in MCI. In both patient groups, the hippocampus and amygdala showed GM reductions, with hints towards more pronounced amygdala effects in AD. As such, our findings provide novel insights into the role of the cholinergic BF and interconnected MTL in AD.

5 Predicting MCI and Alzheimer's disease on structural brain integrity with machine learning

This chapter corresponds to **study 2** and focuses on the prediction of MCI and AD using various features (see section 2.4, Fig. 2.1). It has been formally integrated into the dissertation's style for consistency. The manuscript has been submitted to a peer-reviewed journal. The content corresponds to the following preprint:

Mieling, M.[↑]*, Yousuf, M.*[↑]*, & Bunzeck, N. (2023). Predicting MCI and Alzheimer's disease on structural brain integrity with machine learning.*
https://doi.org/10.31219/osf.io/8dtcm

[↑]shared First Autorship

Author's contributions

MM, MY and NB conceived the study. MM and MY analyzed the data. MM, MY and NB wrote the manuscript and revised it.

Abstract

Machine learning (ML) on structural MRI data revealed that a classification along the Alzheimer's disease continuum is possible. However, the contributing brain regions, also in comparison to other features such as demographics and proteinopathology, remain little understood. Therefore, we utilized Alzheimer's Disease Neuroimaging Initiative (ADNI) data in combination with an extreme-gradient-boosting algorithm and SHAP (SHapley Additive exPlanations) values on cognitively normal (HC) older adults, older adults with mild cognitive impaired (MCI) and Alzheimer's disease (AD) patients. Our analyses included one cross-sectional multi-class classification of HC vs. MCI vs. AD (n=568), and two longitudinal binary-class classifications of HC who converted to MCI vs. those remaining healthy (HC-converters vs. HC-stable, n=92), and MCI who converted to AD vs those remaining MCI (MCI-converters vs. MCI-stable, n=378). Classifications included bilateral volumes of 46 brain regions and thickness of 34 brain regions, CSF status of Aβ and pTau ratio, demographics and genetic data (APOE4). All classifications exceeded chance-level with a global accuracy of 70-77%, and precision of 61-83%. The most important features included CSF status, hippocampal volume, entorhinal thickness and amygdala volume with a clear dissociation: while the hippocampus

contributed to the conversion from healthy aging to MCI, the EC played a more prominent role in the conversion from MCI to full-blown AD. As such, our findings demonstrate a novel way to make explainable predictions of the trajectories of healthy and pathological aging, and they provide novel evidence in favor of a dissociation of medial temporal lobe (MTL) brain regions in the progression of AD.

Introduction

Structural brain integrity has long been associated with cognitive abilities across the adult lifespan (Biel et al., 2021; Hedden & Gabrieli, 2004; Mesulam, 2004a). While a distinction can be made between healthy vs. pathological changes in mild cognitive impairment (MCI) and Alzheimer's disease (AD), it is also clear that age-related changes can be described on a continuum rather than one-off events, and, therefore, understanding developmental trajectories is essential. In this regard, machine learning (ML) (Brossollet et al., 2023) offers novel ways to systematically investigate the contribution and developmental changes of complex feature constellations, including brain regions, proteinopathology or genetic factors; however, longitudinal studies with cognitively normal (HC) older adults, MCI and AD patients are scares. Filling this apparent gap, and to identify fingerprints of complex feature constellations in the context of AD progression, was the goal of this work.

Apart from typical neurodegeneration, especially within medial temporal lobe (MTL) regions, such as the hippocampus and EC, the progression of AD is associated with accumulation of amyloid-β (Aβ) and hyperphosphorylated tau (pTau) (Jack et al., 2018; Jack & Holtzman, 2013; Olsson et al., 2016). These neuropathologies may all serve as biomarkers, but the initial stages of AD often manifest without noticeable symptoms, making it challenging to identify them early on (Jack et al., 2018). Previous research indicates that the progression of AD is distinguished by the dissemination of structural brain degeneration, which is influenced by Aβ and pTau proteinopathology, quantified based on cerebrospinal fluid (CSF) assays. Accordingly, initial structural degeneration spreads from subcortical brain regions, such as the nucleus basalis of Meynert (NbM) but also possibly the locus coeruleus (Beardmore et al., 2021), to the EC moderated by CSF status (Fernández-Cabello et al., 2020; Schmitz & Spreng, 2016). Importantly, this is followed by a spread of neural degeneration from the EC to temporal and parietal brain regions, which can be detected *in vivo* by structural MRI (Fernández-Cabello et al., 2020) even in preclinical AD. For instance, in subjects with preclinical AD (i.e., cognitively normal and abnormal Aβ and pTau biomarkers) showed more

atrophy in the EC than cognitively healthy (i.e., cognitively normal, normal Aβ and pTau biomarker) (Fernández-Cabello et al., 2020). Hence, the development of AD can be described on a continuum encompassing normal aging, initial pathological shifts in biomarkers, followed by the onset of mild symptoms as seen in MCI, finally leading to the development of full-blown AD (Jack et al., 2018). In this regard, CSF status and MRI measures of structural brain integrity appear to be important biomarkers (Counts et al., 2017; Jack & Holtzman, 2013).

Previous studies have already used different ML approaches to classify high-performing cognitively normal (HC), MCI, and AD patients based on structural MR images (Basaia et al., 2019; Rathore et al., 2017; Sarica et al., 2017). Classification accuracies in binary classifications ranged from 80-100% for HC vs AD, 60-90% for HC vs. MCI, and 50-85% for AD vs MCI (Pellegrini et al., 2018; Tanveer et al., 2020). These effects were often based on lower volumes in MCI and AD as compared to HC in specific brain regions, which is in line with the prevailing view on the etiological and neuroscientific comprehension of AD (Böhle et al., 2019; Diogo et al., 2022; Pan et al., 2020; Rondina et al., 2018; Son et al., 2017). These include the hippocampus, amygdala, EC, precuneus, cingulate gyrus, as well as the rostral and caudal regions within the medial frontal lobe (Grueso & Viejo-Sobera, 2021). Despite the apparent specificity, especially within the MTL, AD encompasses widespread neurodegenerative processes throughout the entire brain (Diogo et al., 2022), which have not fully been addressed. Along these lines, research on ternary classifications of HC vs. MCI vs. AD, and longitudinal studies on the disease progression, involving the conversion from HC to MCI or MCI to AD, are scares or do not provide information on the contributing features (i.e., brain regions) of the classification (e.g., Basaia et al., 2019; Beheshti et al., 2017; Lim et al., 2022; Ocasio & Duong, 2021; Pellegrini et al., 2018; Sarica et al., 2017).

Therefore, we utilized data from the Alzheimer's Disease Neuroimaging Initiative (ADNI) to examine how differences in brain integrity (volume and thickness) and additional features, such as CSF status, age, sex, education, and APOE4 genotyping, contribute to the classification of HC vs. MCI vs. AD (cross sectional, analysis 1). In a second step, we performed a longitudinal binary-class classification of HC older adults who later converted to MCI vs those that remained healthy (i.e., HC-converters vs. HC-stable, analysis 2), and MCI patients that later converted to AD vs those that remained MCI (i.e., MCI-converters vs. MCI-stable, analysis 3). All three analyses were based on state-of-the-art XGBoost (eXtreme Gradient Boosting) ML algorithm, and the assessment of SHAP (SHapley Additive exPlanations) values to pinpoint the

contributing features for the classification models. We expected that the integrity of MTL brain regions, especially the hippocampus and EC, contribute to the distinction of HC, MCI and AD, and, importantly, they would allow a precise prediction of the disease progression.

Material and Methods

ADNI data

Data used in the preparation of this article were obtained from the Alzheimer's Disease Neuroimaging Initiative (ADNI) database (adni.loni.usc.edu). ADNI was launched in 2003 as a public-private partnership, led by Principal Investigator Michael W. Weiner, MD, to test whether serial magnetic resonance imaging (MRI), positron emission tomography (PET), other biological markers, and clinical and neuropsychological assessment can be combined to characterize the progression of mild cognitive impairment (MCI) and early Alzheimer's disease.

Participants and diagnoses

We included participants based on their diagnosis as HC, MCI and AD at the time point of MRI measurement. The assignment of diagnoses was conducted by the ADNI Clinical Core, which categorized individuals into three groups: HC (Clinical dementia rating [CDR]=0, Mini Mental State Examination [MMSE]=24-30), MCI (CDR=0.5, MMSE=24-30), and AD (CDR=0.5-1, MMSE=20-26). These classifications are commonly used in clinical trials to assess cognitive and functional measures (Aisen et al., 2010, 2015). For more information on the diagnostic procedure and in- and exclusion criteria, please see http://adni.loni.usc.edu.

For the first analysis (HC vs. MCI vs. AD, Fig. 5.1A), the disease classification was based on a participants' baseline measures. In the longitudinal analyses 2 (HC-converters vs HC-stable, Fig. 5.1B) and 3 (MCI-converters vs MCI-stable, Fig. 5.1C), for the converters (HC-converters and MCI-converters) the latest available measurement as HC before the conversion to MCI (minimum 4 months), and AD (minimum 4 months), respectively, was selected. Therefore, the term „longitudinal" refers to the diagnostic information rather than changes in MRI measures. For HC-stable and MCI-stable, the earliest available measurement was chosen (e.g., baseline information or if MCI converted from HC, then the first measurement associated with MCI), and time of stability was assessed by the time interval between the earliest available measurement and the last available ADNI visit. These participants remained stable for at least one measurement or longer and did not undergo

conversion in their follow-up visits recorded by ADNI. For all analyses, participants with reverting diagnoses (e.g., MCI to HC, or AD to MCI) were excluded.

Participants were only included with available high-quality FreeSurfer MRI, CSF drawings, and genotyping data acquired in close proximity with their neuropsychological assessment (<6 months ago). For more specific information regarding the criteria for inclusion and exclusion in ADNI, see http://adni.loni.usc.edu. Table S2.1 gives an overview of the participants' demographics, information on APOE4 genotype and harmonized CSF assay. Table S2.3 shows neuropsychological test results.

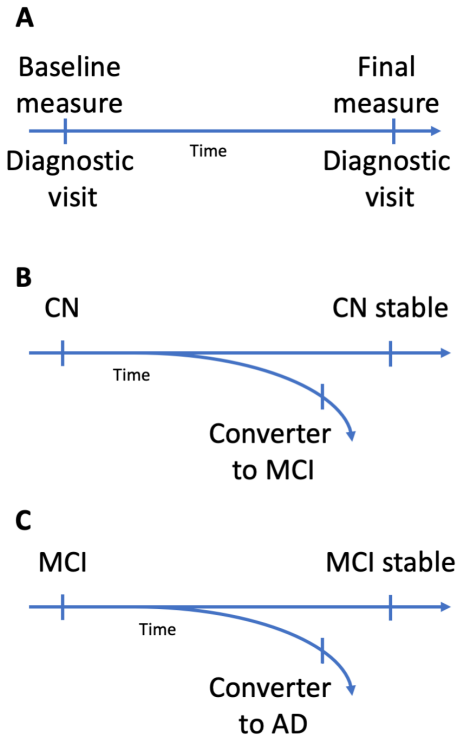

Figure 5.1 Schematic illustration of the experimental design and analyses. All subjects underwent at least two diagnostic visits, including a baseline measure and follow-up (A). In a first cross-sectional analysis, cognitively normal (HC) older adults were compared against patients with mild-cognitive impairment (MCI) and patients with Alzheimer's disease (AD). B) depicts analysis 2 with HC that either remained stable over all follow-ups or developed a MCI at a following measure. C) Analysis 3 with MCI patients who remained stable and MCI patients who later converted to AD.

MRI acquisition and FreeSurfer processing

The participants' MRI scans were obtained at various sites equipped with 1.5 and 3.0 Tesla scanners, following the standardized monitoring protocols of ADNI; see http://adni.loni.usc.edu for more information. The T1 images were processed using the cross-sectional pipeline (Fischl & Dale, 2000) provided by FreeSurfer (Ezzati et al., 2020) (version 4.3, 5.1 and 6.0, https://surfer.nmr.mgh.harvard.edu/). FreeSurfer is an open-source software package for processing, analyzing, and visualizing brain images (https://surfer.nmr.mgh.harvard.edu/). The features were extracted based on the Desikan-Killany atlas (Desikan et al., 2006) and the subcortical whole brain segmentation (Fischl et al., 2002, 2004a). The final results were provided by ADNI (processed by the Tosun laboratory at the University of California-San Francisco, see https://adni.loni.usc.edu/data-samples/data-types/mri/) as a component of the shared data-set.

In ADNI 1/GO, FreeSurfer version 4.3 encompassed data acquired from 1.5 Tesla scanners, version 5.1 included data from 3.0 Tesla scanners in ADNI GO/2, and version 6.0 integrated data from 3.0 Tesla scanners in ADNI 3. We merged FreeSurfer results, recognizing a potential bias (Mofrad, Lundervold, & Lundervold, 2021), however, FreeSurfer morphometric techniques have displayed strong test-retest reliability across various scanner manufacturers and field strengths (Han et al., 2006). Due to a limited number of participants in analyses 2 and 3, we combined data from 1.5 Tesla and 3.0 Tesla scanners, including all available FreeSurfer versions. In analysis 1, which had a sufficient number of participants, we adopted a more stringent approach by only including data from 3.0 Tesla scanners, utilizing the newer FreeSurfer versions 5.1 and 6.0. Further, we corrected for scanner manufacturer to mitigate bias and used only cross-sectional data.

The methods for identifying and calculating regional brain volume and thickness using FreeSurfer have been previously described (Fischl et al., 2002). Briefly, the volumes of brain regions were corrected for intracranial volume (ICV) by dividing the regions of interest (ROI) of the left and right hemispheres by the ICV. In the following, ICV-corrected bilateral ROI volumes were averaged; a similar approach was adopted for ROI thicknesses. Only MRI scans that exhibited exceptional overall segmentation and successfully passed ADNI's quality assessment were included. We only included FreeSurfer information with no missing values for each participant. In total, volume information on 46 bilateral brain regions and average

thickness information on 34 bilateral brain regions (see Table S2.2) served as input for our XGBoost classification model.

CSF biomarker

AD's neuropathology involves the accumulation of Aβ, leading to plaques, and pTau, resulting in neurofibrillary tangles (Palmqvist et al., 2016; Shaw et al., 2009). We included CSF samples obtained through a fully automated Elecsys® protocol for Aβ and pTau measurements related to MRI acquisition dates to comprehend their association with structural degeneration and diagnostic classification. Aβ 1-42 and pTau181 values were extracted for each participant. It is important to note that the Elecsys® protocols are still being developed, and the reported results are restricted to a specific technical limit (>1700 pg/mL). Higher values beyond this limit were extrapolated from the calibration curve solely for research purposes, not diagnostics. For additional information on CSF draws and analyses see http://adni.loni.usc.edu.

In this study, we included both proteins in the classification models as a previously established pTau/Aβ ratio to depict the pathological processes of both proteins, demonstrating high concordance with PET measures and clinical diagnoses (Hansson et al., 2018). Analysis 1 involved CSF, while analysis 3 was run with and without CSF, as CSF data were available only for a limited number of participants (n=44). Analysis 2, however, was run only without CSF due to the limited number of participants with CSF data (n=16). Therefore, descriptive CSF values were presented in Table S2.1 for this analysis.

APOE genotyping

The Apolipoprotein E (APOE) gene's ε4 allele is widely recognized as the most influential genetic risk factor for non-familial AD (Corder et al., 1993), and it is related to the grey matter atrophy in AD spectrum (Spampinato et al., 2011). To better understand the diagnostic classification relying on structural ROIs, we incorporated APOE4 genotyping as a variable, factoring in the count of APOE4 alleles (0, 1 or 2) (Gupta et al., 2019). A blood sample was collected during the screening or baseline visit for APOE genotyping, and the analysis of genotypes followed standard procedures (Saykin et al., 2010).

Neuropsychological assessment

The participants' cognitive performance was investigated using a comprehensive neuropsychological test battery. Here, we included the validated memory (MEM) and

executive function assessments, as determined by confirmatory factor analysis (Crane et al., 2012; Gibbons et al., 2012). The memory scores encompassed the Alzheimer's Disease Assessment Scale, Logical Memory test, MMSE, and Rey Auditory Verbal Learning Test (RAVLT). The executive function scores were derived from the Category Fluency, Digit Span Backwards, Digit Symbol Substitution, Trails A and B, and Clock Drawing tests (Crane et al., 2012; Gibbons et al., 2012). Furthermore, to gain a more comprehensive understanding of the participants' cognitive profiles, we also included the Montreal-Cognitive-Assessment (MoCA), the Sum of Boxes in the Clinical Dementia Rating Scale (CDRSB), and the Alzheimer's Disease Assessment Scale Cognitive (ADAS-Cog 13) (see specific details below).

Ensemble model: XGBoost

For binary and multi-class classification, XGBoost version 1.6.2 (https://xgboost.readthedocs.io/en/latest/python/) was used (Chen & Guestrin, 2016) in Python version 3.9.12 (Rossum & Drake, 2010) and scikit-learn version 1.0.2 (Pedregosa et al., 2012) on Jupyter Notebook version 6.4.12 (Kluyver et al., 2016) running on Windows 11. XGBoost is a gradient-boosting based algorithm that uses decision trees as its base model (T. Chen & Guestrin, 2016), and it has been recently shown to perform well in various regression and classification tasks, including predicting brain age and classifying brain tumors (Hashmi & Osman, 2022; Kaufmann et al., 2019; Lange et al., 2020). Splitting data into training and testing sets is a common practice in ML to assess a trained model's performance on unseen test datasets. In the current study, XGBoost models were trained on 65% of the stratified data and then evaluated on the remaining 35%. A grid search was performed to optimize the hyper parameters of an XGBoost model by using a 5-fold cross-validation, which included imaging data (volume and thickness), CSF, demographics (age and sex), and genotyping features as inputs. Optimizing hyper parameters aims to find the best set of hyper parameters resulting in high performing XGBoost models. Balanced accuracy was used as the scoring metric for multi-class classification analysis that comprises imbalanced data. Balanced accuracy accounts for imbalanced class distributions, i.e., it gives equal weight to each class regardless of the number of samples within each class (García et al., 2009; Moreno-Ibarra et al., 2021). Furthermore, the scoring metric accuracy was used for binary classification analyses that comprise the balanced data. Finally, SHAP version 0.41.0 (https://shap.readthedocs.io/en/latest/) was used to calculate and visualize the contribution

of each input feature to the XGBoost binary and multi-class model's prediction (Mosca et al., 2022).

In ML, precision, recall, and F1-score are metrics used to evaluate the performance of classification models. The F1 score, a metric combining precision and recall, is vital for evaluating classification models as it balances their ability to classify positive instances and minimize false positives correctly. Precision measures the accuracy of positive predictions, while recall evaluates the model's capability to capture all positive instances, collectively providing a comprehensive evaluation of model performance. Additionally, global accuracy, which assesses the overall correctness of classifications across all classes, offers an overall view of model effectiveness (Goutte & Gaussier, 2005; Hicks et al., 2022).

ADNI dataset classification

We conducted three analyses based on the subjects' cognitive status provided by ADNI; individual subjects were only included once in any of the analyses. In the first analysis, a cross-sectional multi-class classification was performed by concatenating subjects with normal cognition (HC), MCI, and AD into one group (n=568). The CSF values of each subject were included as input in the first multi-class classification analysis. In the second analysis, a longitudinal binary classification was performed by concatenating HC-stable and HC-converters into one group (n=92); here, no CSF values were included as input due to the low number of available data (see above). Third, a longitudinal binary classification was carried out by concatenating the MCI-stable and MCI-converters into one group; here, we performed one analysis with (n=88) and one without CSF (n=378). As mentioned above, all three analyses included brain volume and thickness, demographics and genetics (APOE4).

The optimized hyperparameters for the first analysis were: gamma = 0.01, learning_rate = 0.05, max_depth = 3, min_child_weight = 3, n_estimators = 250, colsample_bytree = 1, subsample = 0.7; for the second analysis: gamma = 0, learning_rate = 0.001, max_depth = 1, min_child_weight = 5, n_estimators = 150, colsample_bytree= 0.7, subsample =1; the third analysis with CSF: gamma = 0, learning_rate = 0.01, max_depth = 1, min_child_weight = 3, n_estimators = 200, colsample_bytree = 1, subsample = 0.5; and for the third without CSF: gamma = 0.3, learning_rate = 0.1, max_depth = 6, min_child_weight = 3, n_estimators = 50, colsample_bytree =0.7, subsample = 1.

Ethics approval and consent to participate

Each center collecting data for ADNI provided an IRB (Institutional Review Board) approval and meets ADNI's requirements. Informed consent was obtained from all ADNI participants (for more information at http://adni.loni.usc.edu). The analyses presented here were approved by the local Ethics Committee of the University of Lübeck and carried out after ADNI's recommendations including the approval of the manuscript before submitting to a journal.

Data availability

All data from this study can be obtained freely upon request from the Image and Data Archive (IDA) operated by the Laboratory of Neuro Imaging (LONI) at https://ida.loni.usc.edu. Our analysis code is available at OSF: https://osf.io/ajwct/?view_only=4f2012b70a3b4ea18ac85e847767657d.

Results

Diagnoses and neuropsychological tests

For each of the three analyses, one-way ANCOVAs on the neuropsychological assessments, corrected for age, sex, and education (in years), were carried out. As expected, in cross-sectional analysis 1, significant differences emerged between HC, MCI, and AD (all tests $p<0.001$) with significantly lower cognitive performance in MCI and AD (Table S2.3). In longitudinal analysis 2, the HC-converters converted after, on average, 15 months (SD=8.35) and the HC-stables remained stable for, on average, 31.1 months (SD=31.2). The HC-converters scored lower on ADNI MEM ($F(1,87)=9.88$, $p=0.002$, Table S2.3) and ADAS-Cog 13 ($F(1,87)=14.44$, $p<0.001$, Table S2.3); however, for the other cognitive assessments, there were no significant differences ($p>0.05$, Table S2.3). In longitudinal analysis 3, MCI-converters converted, on average, after 9.53 months (SD=5.85), and the MCI-stables remained stable for, on average, 52.5 months (SD=93.5). The MCI-converters had lower scores in all neuropsychological assessments compared to MCI-stable (Table S2.3).

ADNI dataset classification results

XGBoost model performances for each analysis are reported in Table 5.1 For analysis 1 (HC vs MCI vs AD , Fig. 5.2A), the XGBoost model for the cross sectional multi-class classification achieved an overall global accuracy (i.e., classification accuracy) of 71%, and the model's f1-

scores were 76% for HC, 55% for MCI, and 83% for AD. SHAP revealed the following features with the highest predictive value in the classification: CSF status, hippocampus volume, and EC thickness (Fig. 5.2B). These features showed lower values across the three groups (Fig. 5.2C).

Table 5.1. XGBoost model performance for each analysis.

	precision	**recall**	**f1-score**	**macro average**	**global accuracy of the model**	**N_{Test}**
Analysis 1 (with CSF status)						
HC	72 %	81 %	76 %			95
MCI	61 %	50 %	55 %	71 %	71 %	68
AD	83 %	83 %	83 %			36
Analysis 2 (without CSF status)						
HC stable	72 %	81 %	76 %	76 %	76 %	16
HC converter	80 %	71 %	75 %			17
Analysis 3 (with CSF status)						
MCI stable	74 %	88 %	80 %	77 %	77 %	16
MCI converter	83 %	67 %	74 %			15
Analysis 4 (without CSF status)						
MCI stable	68 %	74 %	71 %	70 %	70 %	66
MCI converter	72 %	66 %	69 %			67

The precision, recall, f1-score, macro-average, global accuracy of the model and N_{Test} (the number of subjects included in the testing set) or each analysis separately. Abbreviations: HC=Cognitive normal; MCI=Mild cognitive impairment, AD=Alzheimer's disease, CSF=Cerebro Spinal Fluid

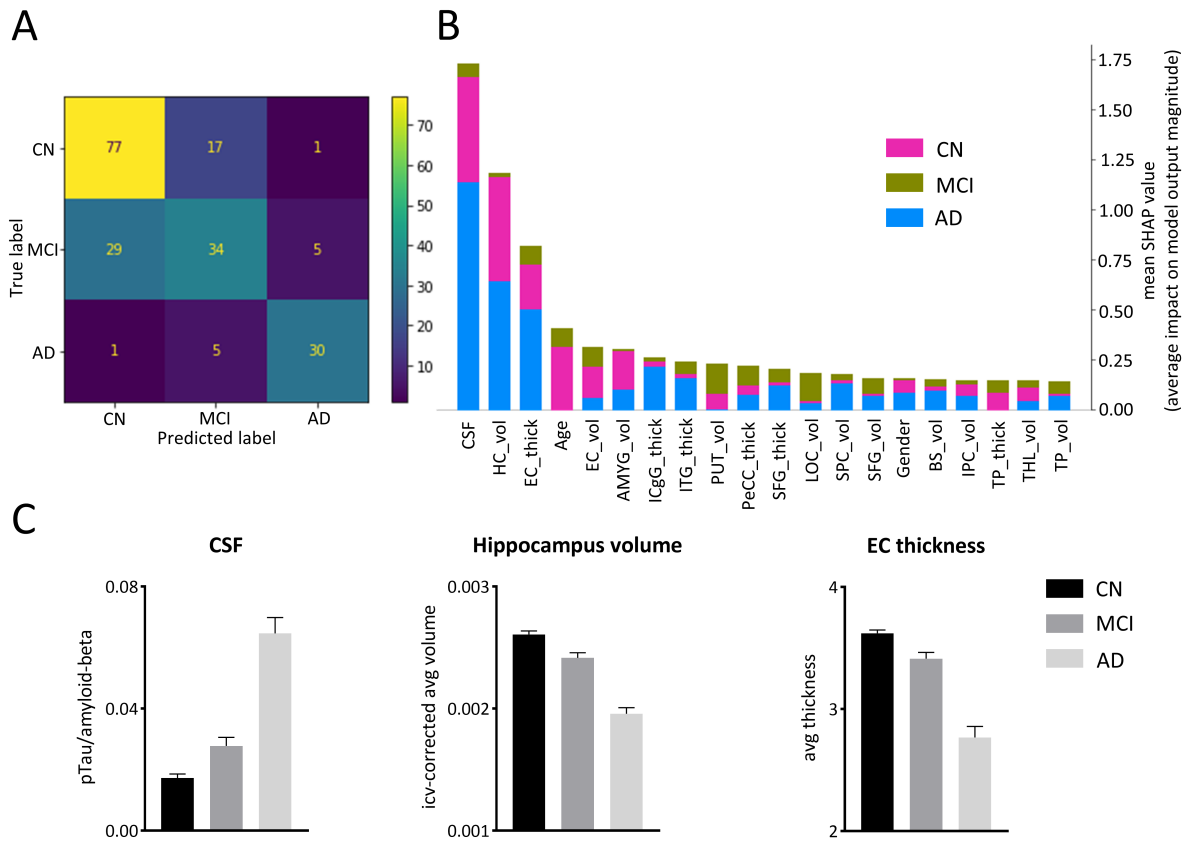

Figure 5.2. Analysis 1, cross-sectional classification of HC vs MCI vs AD. A) Displays the confusion matrix, visually representing the accuracy and misclassification of predictions among the groups. B) Features a SHAP plot highlighting key features and their respective impact magnitude on class predictions. C) Displays the three dominant features: CSF status, hippocampus volume and EC thickness. Abbreviations: SHAP = SHapley Additive exPlanations; CSF = Cerebrospinal Fluid; HC_vol = hippocampus volume; EC_thick = enthorinal cortex thickness; AMYG_vol = amygdala volume; ICgG_thick = isthmus of cingulate gyrus thickness; ITG_thick = inferior temporal gyrus thickness; PUT_vol = putamen volume; PeCC_thick = pericalcarine cortex thickness; SFG_thick = superior frontal gyrus thickness; LOC_vol = lateral occipital cortex volume; SPC_vol = superior parietal cortex volume; SFG_vol = superior frontal gyrus volume; BS_vol = brain stem volume; IPC_vol = inferior parietal cortex volume; TP_thick = temporal pole thickness; THL_vol = thalamus volume; TP_vol = temporal pole volume

For analysis 2 (HC-stable vs. HC-converter, Fig. 5.3A), the XGBoost model for longitudinal binary-class classification achieved an overall global accuracy of 76%, and the model's f1-scores were 76% for HC-stable and 75% for HC-converters. SHAP revealed the following features with the highest predictive value in the classification task: hippocampus volume, insula thickness, and superior temporal gyrus thickness (Fig. 5.3B). These brain regions showed lower values (i.e., volume and thickness, respectively) in HC-converters compared to HC-stable (Fig. 5.3C).

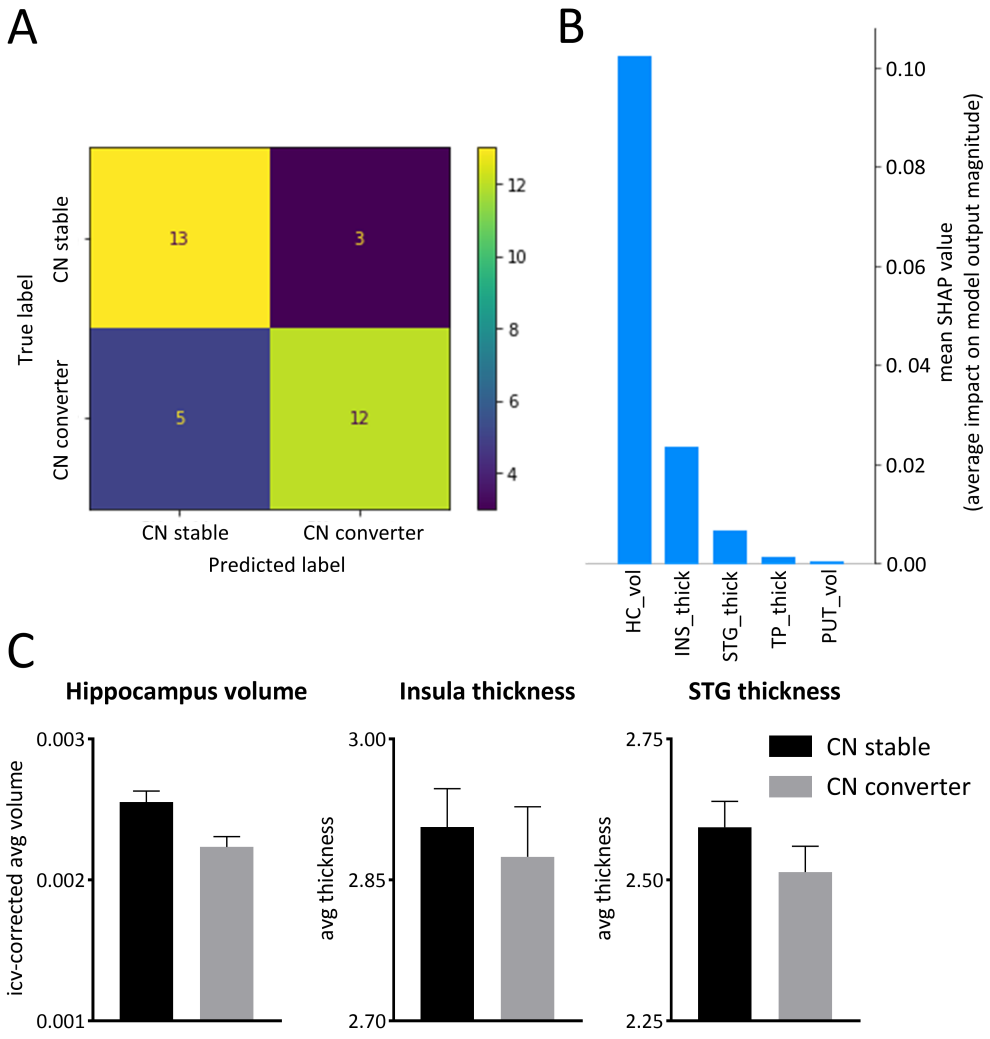

Figure 5.3. Analysis 2, longitudinal classification of HC stable vs HC converters. A) Displays the confusion matrix, visually representing the accuracy and misclassification of predictions among the groups. B) Features a SHAP plot highlighting key features and their respective impact magnitude on class predictions. C) Emphasizes the three dominant features: hippocampus volume; insula thickness; superior temporal gyrus (STG) thickness. Abbreviations: SHAP = SHapley Additive exPlanations; HC_vol = hippocampus volume; INS_thick = insula thickness; TP_vol = temporal pole volume; PUT_vol = putamen volume

For analysis 3 (MCI-stable vs MCI-converter, Fig. 5.4A), the XGBoost model for longitudinal binary-class classification achieved an overall global accuracy of 77%, and the model's f1-score were 80% for the MCI-stable and 74% for the MCI-converters. SHAP revealed the following features with the highest predictive value in the classification task: EC thickness, CSF status, and amygdala volume (Fig. 5.4B). Again, these features showed lower values in MCI-converters compared to MCI-stable (Fig. 5.4C). Finally, the same XGBoost model for binary-class classification without CSF status (Fig. 5.5A) showed an overall global accuracy of 70%, and the model's f1-score were 71% for MCI-stable and 69% for MCI-converters. SHAP revealed the following features with the highest predictive value in the classification task: EC thickness, amygdala volume, and cuneus volume (Fig. 5.5B). Again, these features showed lower values in MCI-converters compared to MCI-stable (Fig. 5.5C).

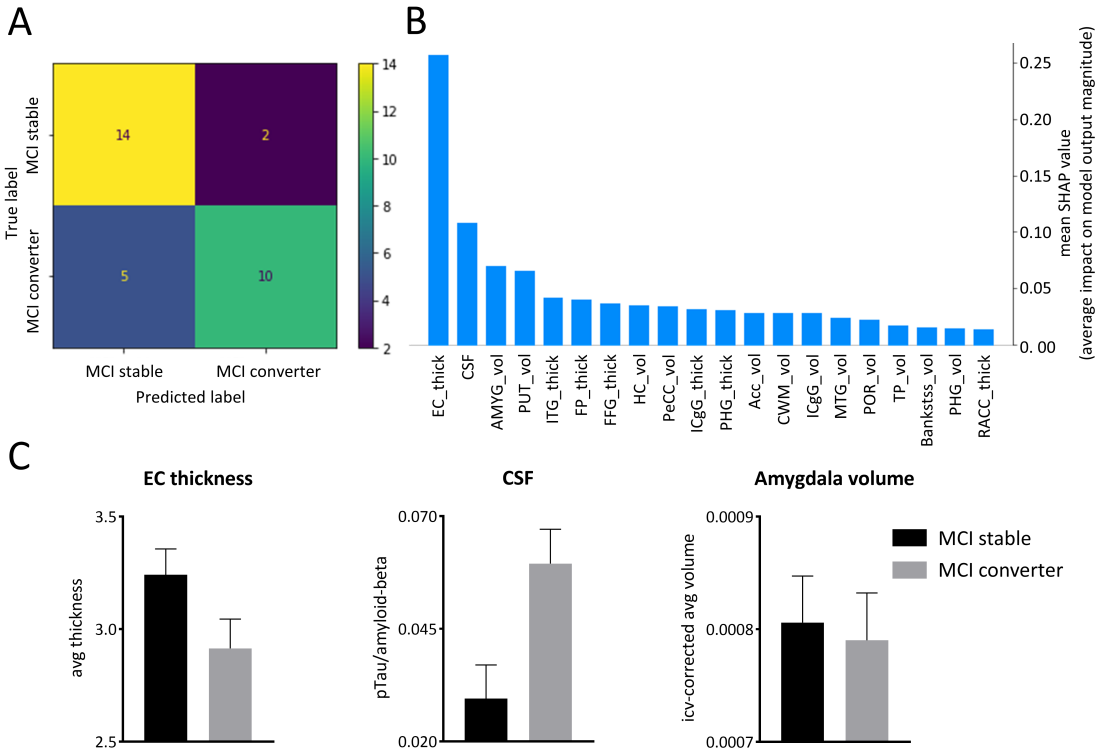

Figure 5.4. Analysis 3, longitudinal classification of MCI stable vs MCI converters, including CSF status. A) Displays the confusion matrix, visually representing the accuracy and misclassification of predictions among the groups. B) Features a SHAP plot highlighting key features and their respective impact magnitude on class predictions. C) Emphasizes the three dominant features: entorhinal cortex thickness, CSF status and amygdala volume. Abbreviations: SHAP = SHapley Additive exPlanations; CSF = Cerebrospinal Fluid; EC_thick = enthorinal cortex thickness; AMYG_vol = amygdala volume; PUT_vol = putamen volume; ITG_thick = inferior temporal gyrus thickness; FP_thick = frontal pole thickness; FFG_thick = fusiform gyrus thickness; HC_vol = hippocampus volume; PeCC_vol = pericalcarine cortex volume; ICgG_thick = isthmus of cingulate gyrus thickness; PHG_thick = parahippocampal gyrus thickness; ACC_vol = accumbens area volume; CWM_vol = cerebellum white matter volume; ICgG_vol = isthmus of cingulate gyrus volume; MTG_vol = middle temporal gyrus volume; POR_vol= pars orbitalis volume; TP_vol = temporal pole volume; Bankstss_vol = banks of the superior temporal sulcus volume; PHG_vol = parahippocampal gyrus volume; RACC_thick = rostral anterior cingulate cortex thickness

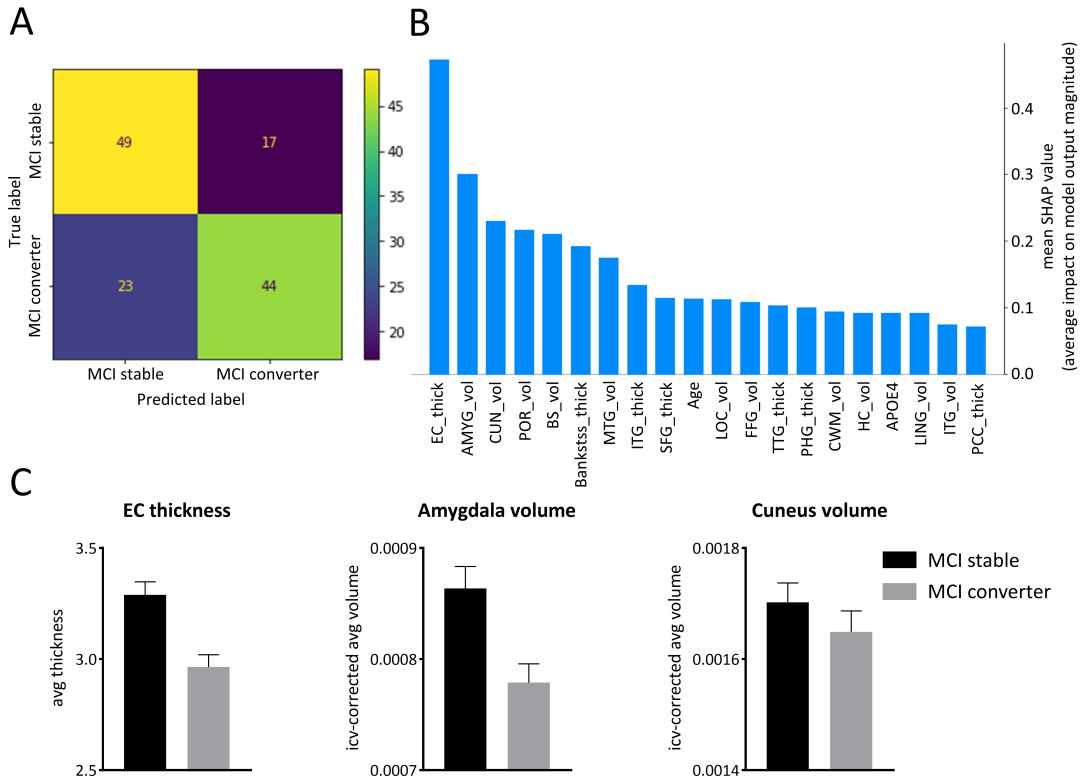

Figure 5.5. Analysis 4, longitudinal classification of MCI stable vs MCI converters, not including CSF. A) Displays the confusion matrix, visually representing the accuracy and misclassification of predictions among the groups. B) Features a SHAP plot highlighting key features and their respective impact magnitude on class predictions. C) Emphasizes the three dominant features: entorhinal cortex thickness, amygdala volume and cuneus volume. Abbreviations: SHAP = SHapley Additive exPlanations; EC_thick = enthorinal cortex thickness; AMYG_vol = amygdala volume; CUN_vol = cuneus volume; POR_vol = Pars orbitalis_volume; BS_vol = brain stem volume; Bankstss_thick = banks of the superior temporal sulcus thickness; MTG_vol = middle temporal gyrus volume; ITG_thick = inferior temporal gyrus thickness; SFG_thick = superior frontal gyrus thickness; LOC_vol = lateral occipital cortex volume; FFG_vol = fusiform gyrus volue; TTG_thick = transverse temporal gyrus thickness; PHG_thick = parahippocampal gyrus thickness; CWM_vol = Cerebellum white matter volume; HC_vol = hippocampus volume; APOE4 = Apolipoprotein E4; LING_vol = lingual gyrus volume; ITG_vol = inferior temporal gyrus volume; PCC_thick = posterior cingulate cortex thickness

Discussion

We investigated the underlying principles of Alzheimer's disease progression based on longitudinal diagnostic information, structural MRI data, APOE4, CSF status and sociodemographics from healthy older adults, individuals with MCI and patients with AD. Using a state-of-the-gradient-boosting based ML algorithm, we can show that a multi-class classification of HC vs. MCI vs. AD is prominently driven by CSF status (i.e., proteinopathology), hippocampal volume, and entorhinal thickness, which confirms previous work and demonstrates the feasibility of our approach. As a novel main observation, the accurate classification of a conversion from HC to MCI was mainly driven by hippocampal volume followed by thickness of the insula and superior temporal gyrus; the accurate classification of a conversion from MCI to AD was primarily based on thickness of the EC followed by CSF status and amygdala volume. While this indicates a more prominent role of the hippocampus in the conversion from HC to MCI and EC from MCI to AD, our findings also show that, in comparison, other brain regions are less important for the classification. Therefore, our findings give novel insights into the developmental trajectories of AD, and they show novel ways to employ ML in the context of neuropsychiatric disorders.

Our cross-sectional multi-class classification of HC, MCI and AD achieved a global accuracy of 71%, which is comparable with previous research showing similar accuracies ranging from 59-77% (Diogo et al., 2022; Pellegrini et al., 2018; Tanveer et al., 2020). Importantly, the three most relevant features of the classification were CSF ratio, hippocampal volume, and entorhinal thickness, followed by age and other features with comparably much lower predictive value (Fig. 5.2B). With regard to proteinopathology, Aβ and pTau have long been associated with AD ('2023 Alzheimer's Disease Facts and Figures', 2023), and individual CSF status can be superior compared to other features derived from structural MRI, FDG-PET and APOE (Gupta et al., 2019; L. Xie et al., 2023). This might be due to the fact that CSF biomarkers represent distinct biochemical aspects of AD pathology (Vemuri et al., 2009) and provide complementary information to structural MRI measures (Gupta et al., 2019). Therefore, abnormalities in CSF biomarkers, specifically Aβ, can precede neurodegeneration, including structural MRI changes and cognitive impairment (Jack et al., 2018; Jack & Holtzman, 2013), which is compatible with our observation of a reliable cross-sectional classification driven by CSF status (Schaeverbeke et al., 2021). Importantly, our classification approach (in all analyses) was based on a combination of several features, which

appears to be the most reliable method of classifying the AD spectrum (Gupta et al., 2019). Along these lines, hippocampal volume and EC thickness were the second and third most prominent features that contributed to a reliable cross-sectional classification. Specifically, both brain regions showed more pronounced volume and thickness, respectively, in HC, followed by MCI and AD, which resembles the disease progression (Fig. 5.2C) (Kulason et al., 2020; Maruszak & Thuret, 2014). It also aligns with past studies using ML, in which hippocampal features and the EC strongly contribute to AD classification (Diogo et al., 2022). Finally, previous VBM studies comparing HC vs. AD also revealed significant differences in grey matter within the MTL, including hippocampus (Baron et al., 2001; Hirao et al., 2006; Rombouts et al., 2000), EC (Di Paola et al., 2007; Frisoni, 2005; Ishii et al., 2005) and amygdala (Shiino et al., 2006; Whitwell, 2009), which underlines the importance of MTL brain regions in the development of AD, which will be discussed in more detail below.

Note that precision and recall in the cross-sectional multiclass classification of all three groups, MCI was associated with the lowest model's accuracy (f1-score of 55%), followed by cognitively normal older adults (76%) and then AD patients (83%, Table 5.1). This finding is compatible with previous reports of lower classifier performance for MCI (Basaia et al., 2019; Pellegrini et al., 2018), and can be explained by the notion that MCI is clinically heterogeneous with distinct but less pronounced brain atrophy compared to AD (Basaia et al., 2019). Cross-sectional classifications can only portrait group differences, but it cannot characterize longitudinal or developmental changes. Together with the fact that not all healthy older adults develop MCI, and not all MCI patients progress to AD, it is important to understand the underlying and contributing factors (Mieling et al., 2023). Here, our longitudinal binary classification of HC-converters vs. HC-stable revealed the hippocampus volume in particular, but also the thickness of the insula and superior temporal gyrus (Fig. 5.3B), as the three most prominent features contributing to an accurate classification. In all three regions, healthy older adults that subsequently developed MCI showed a significantly lower volume and thickness, respectively, compared to those who remained HC and therefore did not develop MCI (Fig. 5.3C). While this highlights the importance of the MTL in the development of MCI, it is interesting to note that only the hippocampus but not the EC emerged as significant feature in our analysis (Albert et al., 2018; Mofrad, Lundervold, Vik, et al., 2021). While this could be due to the rather low number of subjects in this analysis (n=46 in each group), our classification model reflected a global accuracy of 76%, which is comparable with previous

work reporting similar accuracies between 70-78% (Albert et al., 2018; Mofrad, Lundervold, & Lundervold, 2021; Mofrad, Lundervold, Vik, et al., 2021).

The contribution of the insula and superior temporal gyrus, with lower thicknesses in HC converters, is in line with cross-sectional VBM study results showing lower GM thickness in HC compared to MCI (Cheng et al., 2018). While cortical thinning originates in temporal brain regions (Cheng et al., 2018; Julkunen et al., 2010; Singh et al., 2006) (see below) and is associated with neuropsychological performance (Cheng et al., 2018), the role of the insula is less clear. However, in the progression of AD it is also affected by proteinopathies (Bonthius et al., 2005). Moreover, structural degeneration of the insula impacts on various functions such as olfaction (Christen-Zaech et al., 2003), gustation, anatomic self-control, self-awareness and emotion, which possibly contributes to the diverse symptoms of AD (Augustine, 1996; Bonthius et al., 2005; Y. Moon et al., 2014).

Compatible with the observation of reduced hippocampal volumes, HC-converters showed significantly worse memory functioning (MEM). Indeed, the hippocampus plays a central role in learning and memory with declines in structure and function even in healthy older adults (Fotuhi et al., 2012). While there were no significant differences in executive functioning or the MMSE, performances in other tests, however, point towards rather global differences in cognitive abilities (Table S2.3). For instance, the MoCA, which was lower in HC-converters, quantifies several cognitive domains, including visuospatial/executive abilities, language and verbal abilities, memory as well as attention (Freitas et al., 2013). Importantly, both groups showed, on average, MoCA values higher than a cut-off value of 22 indicating their normal cognitive abilities (Freitas et al., 2013). Therefore, both groups are, from a clinical perspective, cognitively unimpaired, and they do not show significant brain atrophy; yet, healthy older adults who later develop MCI show lower grey matter volume, especially in the hippocampus, together with lower scores in several cognitive tests. While this observation does not allow a clear conclusion on whether structural degeneration precedes cognitive decline, which has been suggested before (Jack et al., 2018; Jack & Holtzman, 2013), they clearly show that both factors – hippocampal volume and cognitive abilities – can provide significant biomarkers to predict the developmental trajectories in cognitively normal older adults. Therefore, this finding is of high clinical relevance and adds novel insights to the limited number of studies on the conversion from HC to MCI (Albert et al., 2018; Karaman et al., 2022;

Mofrad, Lundervold, & Lundervold, 2021; Mofrad, Lundervold, Vik, et al., 2021; Yue et al., 2021).

Our longitudinal binary classification with MCI patients who converted (MCI-converters) and MCI patients who remained stable (MCI-stable) had global accuracies ranging from 70% (excluding CSF) to 77% (with CSF, Table 5.1), which is comparable to others reporting accuracies ranging from 74-89% (Muhammed Niyas & Thiyagarajan, 2023). In our case, EC thickness and amygdala volume were the two most prominent features in both classification scenarios, with more pronounced reductions in MCI-converters compared to MCI-stable (Fig. 5.4B-C and 5.5B-C). The EC is considered a critical relay for the communication between the neocortex and hippocampus, and, therefore, plays a critical role in several cognitive processes, including learning and memory (Moscovitch et al., 2016; H. Schultz et al., 2015). With regard to AD progression, the EC appears to be one of the first brain regions affected, which could lead to memory impairments. For instance, deposits of Aβ and p-tau first occur in the trans-entorhinal and EC, which is followed by the hippocampus and other cortical regions e.g., (Braak & Braak, 1991). MRI studies confirm this picture by demonstrating that volume (Karas et al., 2004) and shape (Gerardin et al., 2009) of the hippocampus as well as hippocampal subfields (Hett et al., 2019) differ as a function of disease progression (for a review see Frisoni et al. (2010)). There are similar but more heterogeneous effects in the EC and the amygdala (Arrondo et al., 2022), and therefore, it is not surprising that both brain regions were the best predictors for the conversion from MCI to AD in our study.

Interestingly, when CSF status was included, the EC still emerged as the most predictive feature followed by CFS status (Fig. 5.4B), which could have important implications for the clinical context. In fact, whole brain MRIs are much less invasive than CSF drawings and bear a much lower risk of potential side effects. Physiologically, this possibly reflects a stronger atrophy of the EC as compared to CFS based accumulations of proteinopathies in the disease progression. In other words, while Aβ and p-tau accumulations are particularly pronounced in the early stages, this could be followed by more pronounced neurodegeneration of the EC in the following stages from MCI to AD, which is compatible with the ATN framework (Jack et al., 2018). In any case, it is important to note that our ML approach does not compare the effects of different features but combines them resulting in accurate classifications. Finally, the model without CSF status revealed the cuneus (Fig. 5.5B) as third most relevant contributing feature, which is in line with previous classifications of MCI-converters vs. MCI-stable (Suk et al., 2015;

T. Zhang et al., 2021). Indeed, the cuneus is associated with processing visual information, integrating sensory information, and cognitive processes including attention, learning and memory (Cabeza et al., 2002; Makino et al., 2004) and its atrophy has been associated with an increased risk of AD (B.-S. Wu et al., 2021).

Finally, we would like to point out the following limitations. First, our analysis focused on volumetric and thickness data based on the 2010 Desikan-Killiany atlas (Desikan et al., 2006), which excludes some subcortical brain regions (Fischl et al., 2002, 2004a), such as the nucleus basalis of Meynert (NbM), which might play a central role in the progression of AD (Fernández-Cabello et al., 2020; Mieling, Göttlich, et al., 2023; Mieling, Meier, et al., 2023; Schmitz & Spreng, 2016). Second, ADNI data was measured at multiple sites with diverse MRI scanners, which we addressed by only pre-selecting high-quality data and including scanner manufacturers as covariates in our analyses. Third, not all analyses included CSF status (analysis 2, Fig. 5.3), or the number of subjects was limited (analysis 3, Fig. 5.4). Fourth, we focused on participants with stable diagnoses and sound information on the conversion (with rather short conversion times), omitting potential reversions (Feng et al., 2021). Fifth, a model with more features, such as clinical, cognitive, genetic, PET and CSF status, could enhance model accuracies (Vieira et al., 2017), but this would require more data points (i.e., subjects). These aspects, together with alternative but mutually exclusive concepts, such as the AT(N) framework (Jack et al., 2018), should be considered in future work.

To conclude, ML in combination with structural MRI data, sociodemographic, CSF status and genetic information allows a precise and explainable classification along the AD continuum. Our findings indicate that the hippocampus plays a prominent role in the conversion from healthy aging to MCI; the EC, on the other hand, contributes more to the conversion from MCI to full-blown AD. As such, our study gives novel insights into the developmental trajectories from healthy to pathological aging by suggesting a dissociation of specific MTL brain regions. This, in turn, could contribute to earlier and more accurate diagnoses and interventions.

6 Globus pallidus iron relates to cognitive impairment in Alzheimer's disease: Evidence from MRI-based meta-analysis

This chapter corresponds to **study 3** and investigates iron accumulations in AD (see section 2.4, Fig. 2.1). It has been formally integrated into the dissertation's style for consistency. The manuscript has been submitted to a peer-reviewed journal. The content corresponds to the following preprint:

Mieling, M., Wiskow, C., & Bunzeck, N. (2024). Globus pallidus iron relates to cognitive impairment in Alzheimer's disease: Evidence from MRI-based meta-analysis. https://doi.org/10.31219/osf.io/xta8m

Author's contributions

MM and NB conceived the study. MM and CW analyzed the data. MM and NB wrote the manuscript and revised it.

Abstract

Iron plays an essential role in brain metabolism and, therefore, cognitive functioning. However, region specific iron level increases during healthy and, even more so, pathological aging, in particular Alzheimer's disease, can have detrimental effects. Although this notion has been supported by several single studies, meta-analytic evidence of a relationship between iron levels, as measured with *in vivo* MRI, and Alzheimer's disease (AD) is still missing. We used a meta-analytic approach of 22 *in vivo* MRI experiments with, in total, 685 AD patients and 1104 healthy controls (HC). All studies employed iron sensitive markers, such as R2* or QSM, and reported effects in specific brain regions, including the putamen, caudate nucleus, globus pallidus, hippocampus, and thalamus, that were further analyzed here. We also investigated the relationship between iron levels in AD and cognitive performance as measured with the Mini-Mental-Status-Examination (MMSE). In all regions of interest, higher iron level were significant in AD compared to HC, with most pronounced effects in the putamen followed by the caudate. Importantly, only in the globus pallidus iron levels showed a negative correlation with MMSE performance in AD patients. Our results provide unique evidence for the notion that iron level increases, especially within basal ganglia structures, which provide a hub for cognitive information processing, are a characteristic hallmark of AD. While this may relate to

neurodegeneration, amyloid plaques and tau pathologies, our findings suggest that iron level increases can help to explain and possibly predict cognitive decline in AD.

Introduction

Non-heme iron is essential for several metabolic processes, ensuring normal brain functioning and behavior (Crichton, 2001; Hallgren & Sourander, 1958). However, increased cerebral iron levels were not only reported in healthy older adults (Biel et al., 2021; Steiger et al., 2016) but also patients suffering from Alzheimer's Disease (AD) and mild-cognitive impaired (MCI) (Ayton et al., 2017; Du et al., 2018; H.-G. Kim et al., 2017; Y. Moon et al., 2016). Therefore, regionally specific excessive iron could lead to cognitive decline (Ayton et al., 2020; A. Yang et al., 2022) and structural brain atrophy (A. Yang et al., 2022). In fact, iron level increases have been linked with cognitive abilities, as measured with the Mini-Mental-Status-Examination (MMSE) or Montreal-Cognitive-Assessment (MoCa) (D. Li et al., 2020; X. Liu et al., 2021; D. Wang et al., 2014; A. Yang et al., 2022). Moreover, several *post-mortem* and *in vivo* studies provided evidence for a co-localization of iron and tau (Ayton et al., 2020; Bulk et al., 2018; Spotorno et al., 2020) as well as amyloid pathology (Van Bergen et al., 2016; Van Duijn et al., 2017) suggesting a direct relationship. While iron promotes oxidative stress (Floyd & Carney, 1993; Gutteridge, 1992) and aggregation of amyloid-β (Aβ) peptide (Mantyh et al., 1993), they both (iron and oxidative stress) mediate Aβ toxicity (Rottkamp et al., 2001). Conversely, iron promotes tau phosphorylation (Wan et al., 2019) and the aggregation of hyperphosphorylated tau into neurofibrillary tangles (S. S. Rao & Adlard, 2018; Yamamoto et al., 2002) .

A previous *post-mortem* meta-analysis, published in 2014, revealed higher iron levels in the putamen, caudate nucleus, globus pallidus, amygdala, cingulate cortex, as well as the frontal, parietal, and temporal lobe in AD patients compared to healthy controls (HC) (Tao et al., 2014). While this is an important finding, *in vivo* neuroimaging methods potentially allow a much clearer link to cognitive decline as well as novel insights on the basis of paramagnetic brain iron (Haacke et al., 2005; Tran et al., 2022). For instance, most studies comparing iron levels of AD vs HC using MRI reported significant iron level increases in basal ganglia structure, the amygdala, thalamus, and hippocampus (e.g., Damulina et al., 2020; Ding et al., 2009; Du et al., 2018; H.-G. Kim et al., 2017; Kuchcinski et al., 2022). However, meta-analytic evidence, especially with respect to a possible relationship of increased iron levels and impaired cognitive abilities in AD, is missing.

To this end, we performed random-effects meta-analyses on previously published data using iron-sensitive MRI *in vivo*, such as T2*, T2', R2*, R2', field-dependent R_2 increase (FDRI), susceptibility-weighted imaging (SWI), and quantitative susceptibility mapping (QSM) (Haacke et al., 2005; Langkammer et al., 2012, 2014). All included studies reported a comparison of AD patients vs age-matched HC for either one or more brain regions: putamen, caudate nucleus, globus pallidus, hippocampus, and thalamus (e.g., Damulina et al., 2020; Ding et al., 2009; Du et al., 2018; H.-G. Kim et al., 2017; Kuchcinski et al., 2022; Tao et al., 2014). For every brain region, a single random-effects model was calculated, and, in a subsequent step, the relationship between iron levels and cognitive performance (i.e. MMSE scores) in AD patients was investigated via linear regression.

Methods

Literature search and selection

This study followed the PRISMA (Preferred Reporting Items for Systematic Reviews and Meta-Analyses) 2020 guidelines (Page et al., 2021), see Figure 6.1. In detail, a systematic literature search was performed at https://pubmed.ncbi.nlm.nih.gov by using the search terms "MRI" AND "iron" AND "Alzheimer" OR "MRI iron Alzheimer" to find original MRI studies on brain iron in AD patients and healthy age-matched controls (see below for details on MRI sequences). The search included all potentially relevant and published studies until Nov. 27, 2023 – these were 317 original studies assessed in our preselection. Subsequently, titles and abstracts were screened, and, as a result, 263 articles were excluded, since they did not meet our inclusion criteria. The remaining 54 original studies were examined in more detail by two independent researchers (M.M. and C.W.) based on a full-text reading with regard to the inclusion and exclusion criteria.

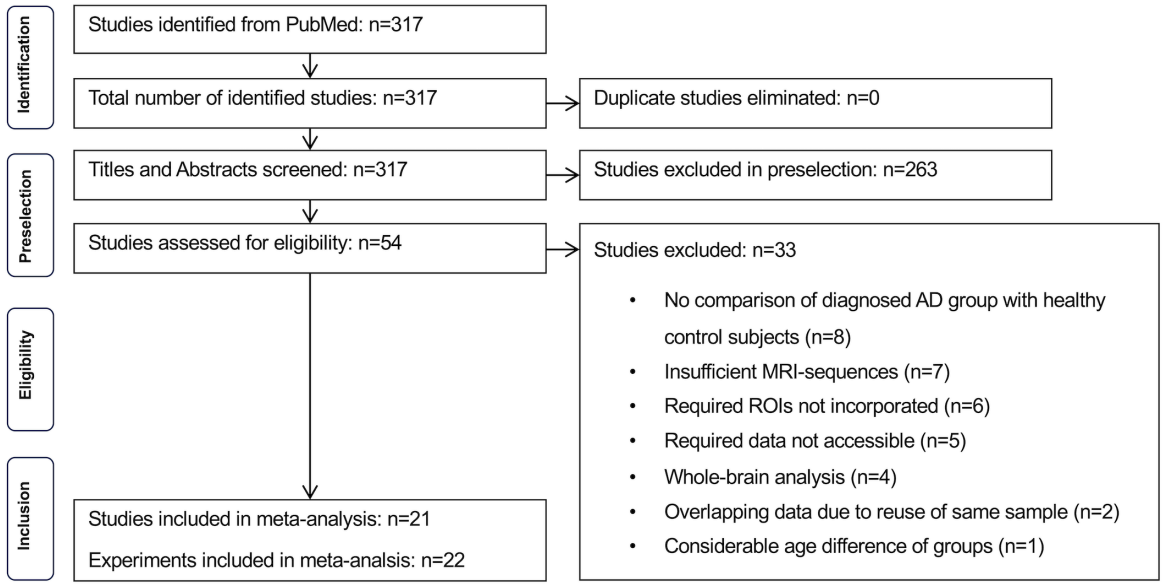

Figure 6.1. Flowchart of the steps performed in the meta-analysis.

The inclusion criteria comprise (1) AD patients were diagnosed according to well-established criteria, (2) the comparison of AD patients with HC, (3) no considerable age difference between AD patients and HC, (4) the data analysis was based on predetermined regions of interest (ROIs), (5) namely one or more of the following ROIs: putamen, caudate nucleus, globus pallidus, hippocampus or thalamus, (6) an iron-sensitive MRI-sequence was used for instance T2*, T2', R2*, R2', FDRI, SWI, and QSM. Articles were excluded based on the following criteria: (1) using T2 or R2 MRI sequence (Haacke et al., 2005; Langkammer et al., 2010, 2012), (2) review articles, (2) post-mortem studies, (3) animal models, (4) re-analysis of previously used data (i.e., repeated use of the same sample), and (5) missing data information. If a study included multiple independent experiments constituting a single analysis (Turkeltaub et al., 2012), these were incorporated and designated to separate experiments. If necessary, a third researcher (N.B.) was consulted.

The final selection of included articles and study-related information can be found in Table 6.1. Cross-checking with the original literature prevented potential sample overlap between the studies. This refers to sample characteristics, author affiliations, and scanning locations.

Participants

Participants were included and grouped based on their diagnoses explicitly reported in the original articles. The AD group met the diagnostic criteria for probable or possible AD, mostly in alignment with the National Institute of Neurological and Communicative Disorders and Stroke - Alzheimer's Disease and Related Disorders Association (NINCDS-ADRDA) or the National Institute on Aging and Alzheimer's Association (NIA-A) (McKhann et al., 2011). Moreover, in all original articles AD patients and HC were matched with regard to sex and age, which we further tested across studies using independent t-tests. Participants were scanned at various scanner field strengths. For instance, FDRI was applied at field strengths of 0.5 Tesla and 1.5 Tesla, Phase imaging and R2' were performed using a 1.5 Tesla scanner, while all other sequences were implemented at a field strength of 3 Tesla (see Table 6.1).

Meta-analyses

Overview

Our analyses were based on the following steps, that will be explained in more detail below. First, the effect sizes (Cohen's d) of group differences in iron levels were calculated for all available ROIs on the basis of their mean values and standard deviations (SD). Second, five random-effects meta-analyses were computed separately for each ROI (putamen, caudate nucleus, globus pallidus, hippocampus, and thalamus). Third, we assessed a possible relationship between iron level differences between groups (effect sizes) and memory performance (MMSE). Our calculations are available at the Open Science Framework (OSF, https://tinyurl.com/3u9n6cwh).

Effect size calculation – Cohen's d

The effect size (Cohen's d), bias-corrected for small sample sizes, was calculated for each ROI and original study based on mean values and SD (Hedges & Olkin, 1985). In five studies, mean (Luo et al., 2018) and SD (Higgins et al., 2003) were missing and therefore had to be calculated based on the given median (Cogswell et al., 2021; Damulina et al., 2020) or interquartile range (IQR) (Cogswell et al., 2021; Damulina et al., 2020; Guan et al., 2022). In five studies (Cogswell et al., 2021; Du et al., 2018; Guan et al., 2022; X. Liu et al., 2021; Qin et al., 2011), the mean and SD of the MRI data, or median and IQR, respectively, were not available in numerical data but they were shown in figures. Therefore, PlotDigitizer™ (*PlotDigitizer: Free Online App*, n.d.)

was used to extract the data (Aydin & Yassikaya, 2022). If the relevant values were separately reported for the right and left hemispheres, the average of both was calculated.

MRI-based markers of iron levels need to be interpreted carefully (Haacke et al., 2005). For some markers, high values indicate high iron levels (e.g., R2* (Damulina et al., 2020), QSM (Tiepolt et al., 2020), see Table 6.1 for all MRI methods used in the original studies), but for others low values indicate low iron levels (here T2* in msec (W.-J. Moon et al., 2012), phase values measured as radians (Ding et al., 2009), SWI (Gao et al., 2017; D. Wang et al., 2013, 2014)). Therefore, effect sizes had to be negated (multiplied by -1) when they were based on phase image (Ding et al., 2009), SWI (Gao et al., 2017; D. Wang et al., 2013, 2014), and T2* (W.-J. Moon et al., 2012). As a result, here positive effect sizes indicate higher iron levels in AD compared to HC, while negative effect sizes indicate higher iron levels in HC compared to AD.

Finally, individual effect sizes were used to calculate the mean overall effect across all studies. Values of 0.2, 0.5, and 0.8 indicate small, medium, and large effects, respectively (Cohen, 2013).

Random-effects models

Following Borenstein et al. (2009), for each ROI a single random-effects model was calculated. To ensure high overall effect precision, individual effect sizes were weighted by each study's inverted total variance. Significance testing of the weighted overall mean effect size (d*) was based on z-scores and corresponding p-values (two-tailed). We also calculated 95% confidence intervals and I^2 statistics to quantify heterogeneity (Borenstein et al., 2009; Higgins et al., 2003). I^2 indicates inconsistency across study results and represents the percentage of heterogeneity within the total variance of the primary studies (Borenstein et al., 2009; Higgins et al., 2003). It can be compared across different meta-analyses and ranges from 0 to 100. More specifically, it differentiates between low (25%), moderate (50%), and high (75%) heterogeneity (Higgins et al., 2003). Moreover, funnel plots were created and Egger regressions were performed (Egger et al., 1997) to address possible publication biases (Lin & Chu, 2018; A. J. Sutton, 2000). A funnel plot represents each study's effect sizes against standard errors, with an asymmetry indicating a publication bias (Lin & Chu, 2018; Peters et al., 2007; Sterne & Egger, 2001). Egger's regression detects publication bias based on the funnel plot by assessing the relationship between standardized effect estimates and their standard error (Egger et al., 1997; Lin & Chu, 2018). Here, we generated funnel plots and

conducted Egger's regressions using effect sizes and results from the random effect models within "Meta-Essentials: Workbooks for meta-analysis" (Version 1.4) (Suurmond et al., 2017).

Outliers were identified as data points exceeding 1.5 times the interquartile range (IQR) above the third or below the first quartile (Tukey, 1977). To enhance the robustness of the findings, the analyses were rerun after identifying and excluding any outliers detected.

Relationship between brain iron deposition and cognition in Alzheimer's disease

To investigate possible links between iron accumulations in AD and cognitive impairment, five correlation analyses were conducted in Jamovi (2.3.21) (*The Jamovi Project (2023). Jamovi (Version 2.3) [Computer Software].*, 2023). Here, effect sizes for our five ROIs, indicating iron level increases in AD compared to HC, were correlated with the AD MMSE scores from the original studies. Specifically, we used z-scored MMSE values and effect sizes in combination with Spearman's rank correlation (Spearman's Rho) due to the rather small sample size and since it is more robust against outliers (Rousselet & Pernet, 2012). Since we predicted a negative correlation between iron levels and cognitive performance, we did not apply a correction for multiple comparison in this analysis.

Results

Study characteristics

Overall, we included 685 AD patients and 1104 HC from 21 studies with 22 experiments (see Fig. 6.1). One study investigated two independent age groups of AD patients and HC, representing two individual analyses (Turkeltaub et al., 2012). Therefore, this study was included in the meta-analyses with both experiments (D. Wang et al., 2014). For the separate five ROI meta-analyses, 20 experiments were included for the putamen, 19 for the caudate nucleus, 19 for the globus pallidus, 11 for the hippocampus, and 10 for the thalamus (see Table 6.1 for an overview of the included experiments with more detailed information).

Although individual studies reported age-matched AD and HC groups, a t-test across studies revealed significant age differences ($t(36)=-2.12$, $p=0.041$). Accordingly, AD patients were slightly older (mean=70.67 years, SD=4.56) than HC (mean=67.75 years, SD=3.89). Note that three experiments from two studies (Ayton et al., 2017; D. Wang et al., 2014) did not report detailed information on age and could, therefore, not be included in our analysis. Mean sex ratios (female/male) of AD patients and HC were 1.78 (SD=1.74) and 1.77 (SD=1.22), respectively, with no significant differences across studies as assessed by a Mann-Whitney U

test due to the violation of normal distribution (U=191, p=0.629). One study (Ayton et al., 2020) did not report the sex for both groups and another (Bartzokis et al., 2004) solely for the AD group. Both studies were not included in our analysis.

Random effects meta-analyses

Putamen

The random-effects model for the putamen included 20 experiments from 19 studies (see Table 6.1). In all original experiments, the weighted mean effects were positive and statistical testing across studies revealed a highly significant positive effect indicating higher iron levels in AD vs HC (d*=0.89, p<0.001, CI [0.62, 1.16], Fig. 6.2A, Table 6.2). Heterogeneity testing revealed high heterogeneity of I^2=81.00%. After removing two outliers (H.-G. Kim et al., 2017; D. Li et al., 2020), the weighted mean effect was still highly significant but it showed a slightly reduced effect size (d*=0.74, p<0.001, CI (0.51, 0.97), I^2=72.67).

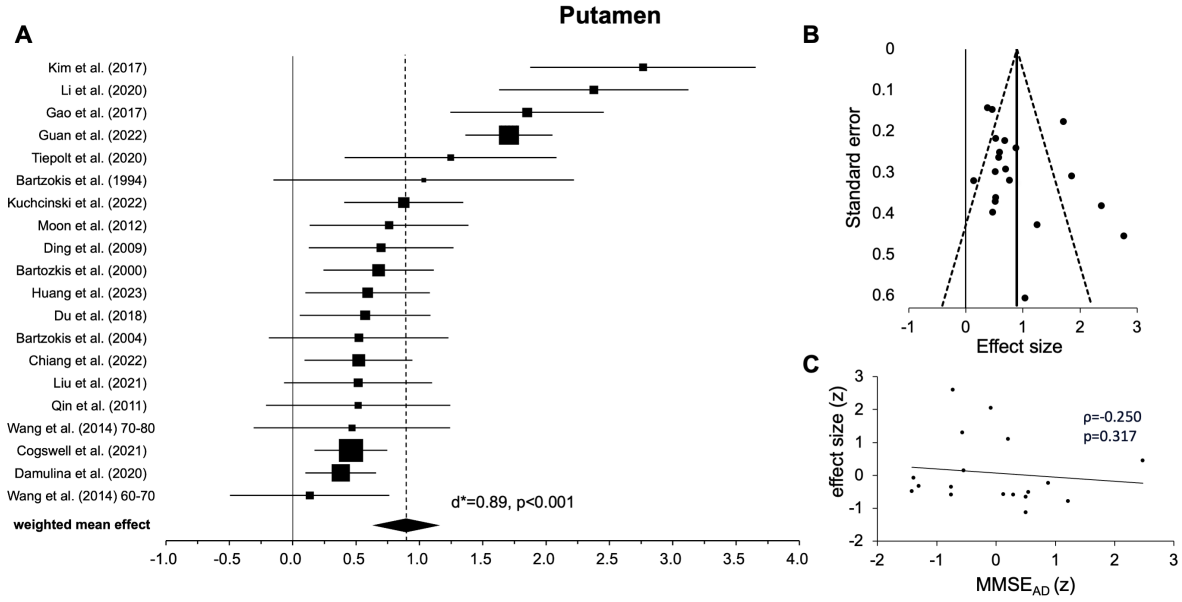

Figure 6.2. Results for the putamen. A) forest plot of group comparisons for Alzheimer's disease patients vs healthy controls. Squares represent the computed effect sizes of the original studies, the squares' size indicate the relative size of the sample studied, and the diamond represents the weighted mean effect. The width of the diamond as well as the horizontal lines of the squares indicate a study's 95% confidence intervals. B) Funnel plot: the dots mark the individual study, the dashed line the 95% confidence interval, and the vertical straight line the overall effect. C) Spearman correlation of the iron differences (effect size) and mean Mini-Mental-State-Examination (MMSE) scores.

Caudate nucleus

The random-effects model for the caudate nucleus included 19 independent experiments from 18 original studies (see Table 6.1). While most weighted mean effects were positive, three experiments (Chiang et al., 2022; Cogswell et al., 2021; D. Wang et al., 2014) showed negative effects. However, statistical testing across experiments revealed a highly significant positive effect, again suggesting higher iron levels in AD vs HC (d*=0.61, p<0.001, CI [0.35, 0.87], Fig. 6.3A, Table 6.2). Heterogeneity testing revealed high heterogeneity of I^2=79.53%. After removing one outlier (X. Liu et al., 2021), the effect remained highly significant (d*=0.53, p<0.001, CI [0.29, 0.77], I^2=75.34%).

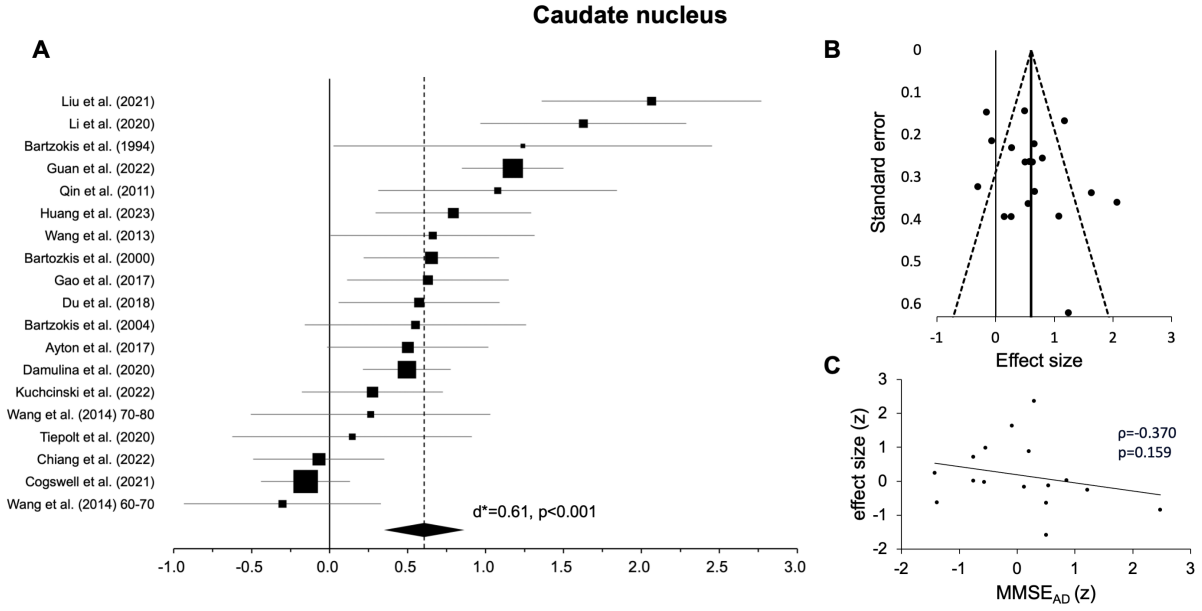

Figure 6.3. Results for the caudate nucleus. A) forest plot of group comparisons for Alzheimer's disease patients vs healthy controls. Squares represent the computed effect sizes of the original studies, the squares' size indicate the relative size of the sample studied, and the diamond represents the weighted mean effect. The width of the diamond as well as the horizontal lines of the squares indicate a study's 95% confidence intervals. B) Funnel plot: the dots mark the individual study, the dashed line the 95% confidence interval, and the vertical straight line the overall effect. C) Spearman correlation of the iron differences (effect size) and mean Mini-Mental-State-Examination (MMSE) scores.

Globus pallidus

For the globus pallidus, 19 independent experiments from 18 studies were included in the random-effects model (see Table 6.1). Except from five experiments (Bartzokis et al., 2004; Chiang et al., 2022; Du et al., 2018; W.-J. Moon et al., 2012; Tiepolt et al., 2020), all others showed positive weighted mean effects. Statistical analysis revealed a highly significant effect indicating higher iron levels in AD vs HC (d*=0.44, p=0.001, CI [0.19, 0.69], Fig. 6.4A, Table 6.2); again, heterogeneity was rather high (I^2=78.59%). After excluding one outlier (D. Li et al., 2020) the results remained statistically significant (d*=0.34, p=0.002, CI [0.13, 0.55], I^2=68.41%).

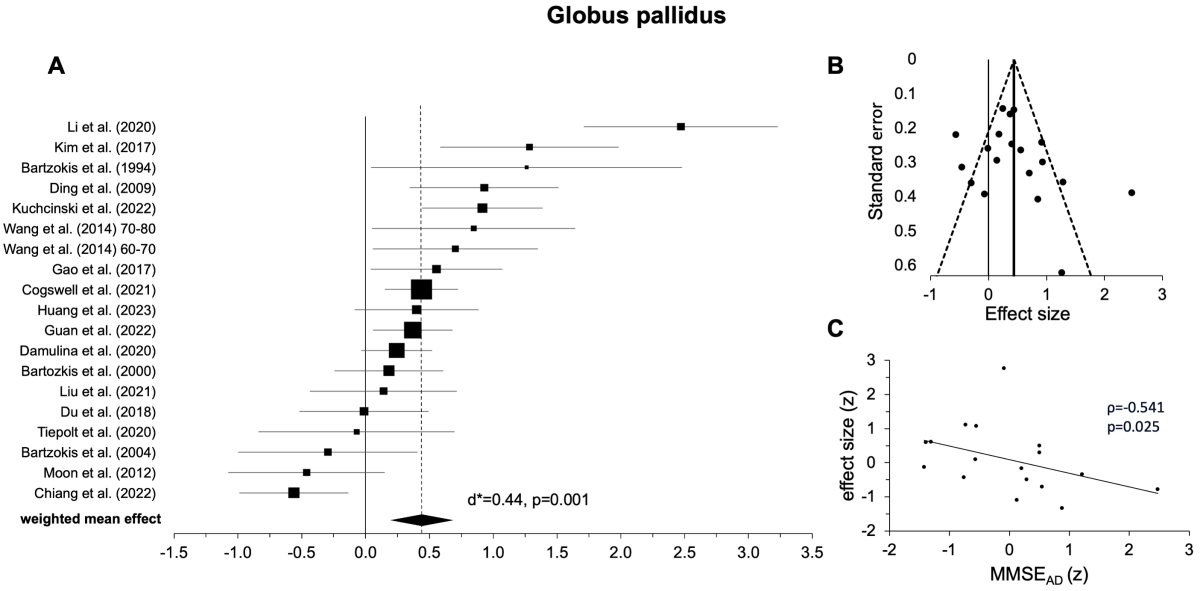

Figure 6.4. Results for the globus pallidus. A) forest plot of group comparisons for Alzheimer's disease patients vs healthy controls. Squares represent the computed effect sizes of the original studies, the squares' size indicate the relative size of the sample studied, and the diamond represents the weighted mean effect. The width of the diamond as well as the horizontal lines of the squares indicate a study's 95% confidence intervals. B) Funnel plot: the dots mark the individual study, the dashed line the 95% confidence interval, and the vertical straight line the overall effect. C) Spearman correlation of the iron differences (effect size) and mean Mini-Mental-State-Examination (MMSE) scores.

Hippocampus

The random-effect model for the hippocampus included only 11 experiments from 11 studies (see Table 6.1). All but one experiment (Ayton et al., 2020) showed positive mean weighted effects and, across experiments, statistical testing revealed a highly significant positive effect. Again, this indicates higher iron levels AD vs HC (d*=0.70, p=0.004, CI [0.23, 1.18], Fig. 6.5A, Table 6.2); heterogeneity was high (I^2=88.43%). After excluding one outlier (H.-G. Kim et al., 2017), the results remained significant but the effect size was rather small (d*=0.37, p=0.016, CI [0.07, 0.68], I^2=70.89%).

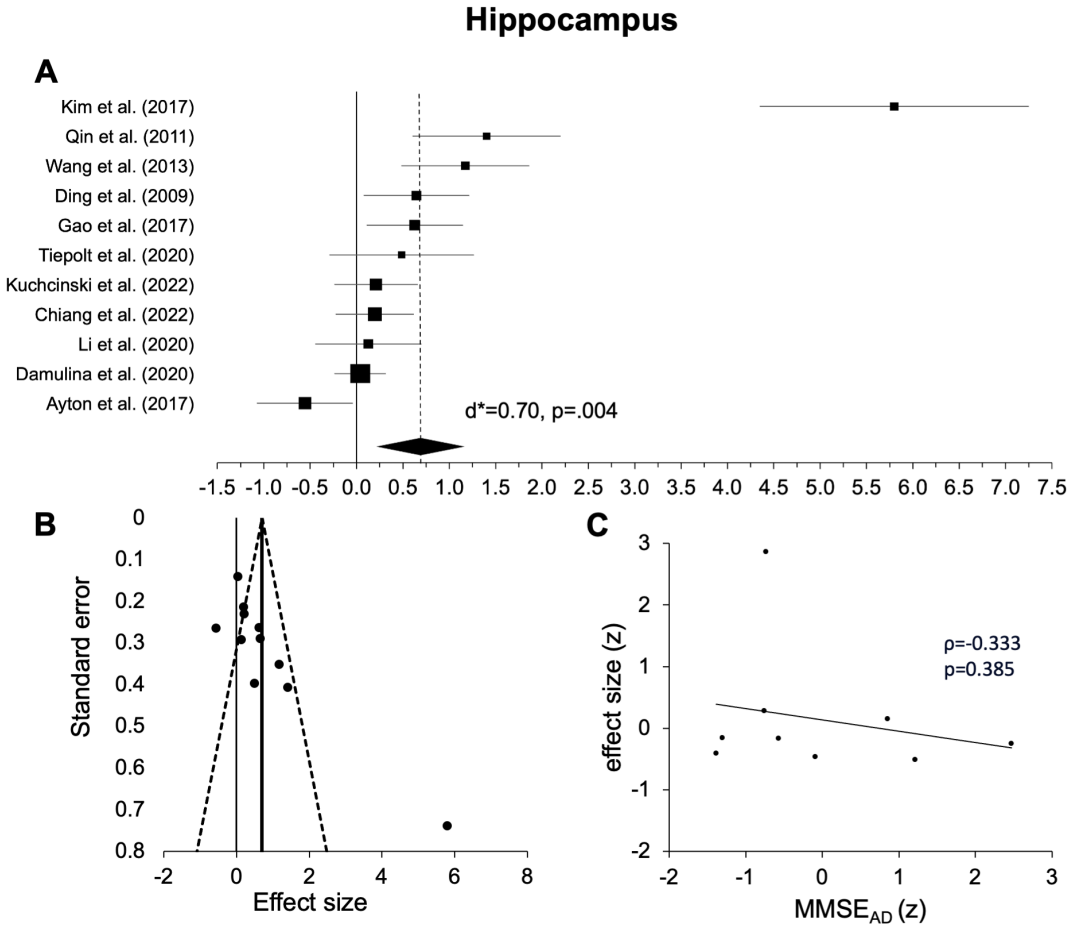

Figure 6.5. Results for the hippocampus. A) forest plot of group comparisons for Alzheimer's disease patients vs healthy controls. Squares represent the computed effect sizes of the original studies, the squares' size indicate the relative size of the sample studied, and the diamond represents the weighted mean effect. The width of the diamond as well as the horizontal lines of the squares indicate a study's 95% confidence intervals. B) Funnel plot: the dots mark the individual study, the dashed line the 95% confidence interval, and the vertical straight line the overall effect. C) Spearman correlation of the iron differences (effect size) and mean Mini-Mental-State-Examination (MMSE) scores.

Thalamus

The random-effects model for the thalamus involved only 10 experiments from 10 studies (see Table 6.1). While three weighted means were negative (Cogswell et al., 2021; Damulina et al., 2020; Du et al., 2018) the remaining seven were positive. Across experiments, statistical testing revealed a significant positive effect (d*=0.74, p=0.024, CI [0.1, 1.38], Fig. 6.6A, Table 6.2), also indicating higher iron levels in AD vs HC. Again, heterogeneity was high (I^2=94.25). After excluding one outlier (H.-G. Kim et al., 2017), the analysis revealed no significant effect (d*=0.39, p=0.16, CI [-0.16, 0.94]), and higher heterogeneity of the data (I^2=92.2%).

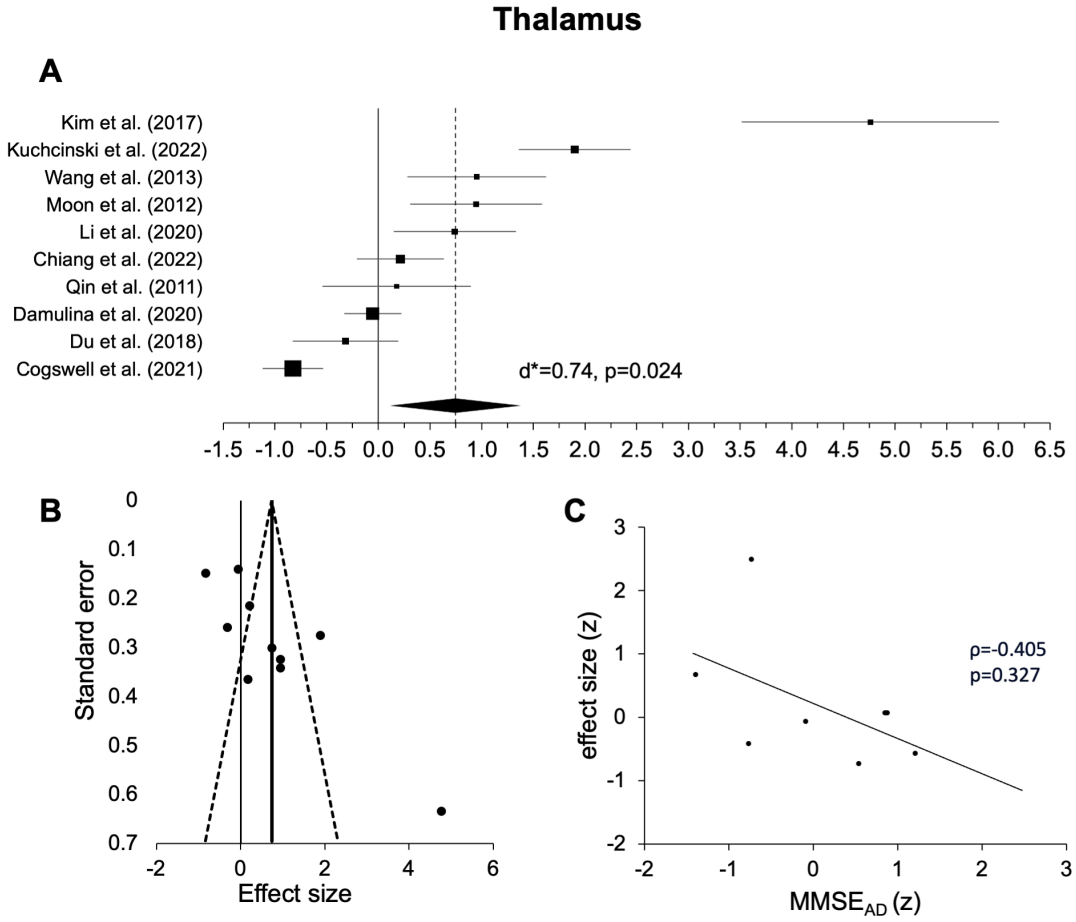

Figure 6.6. Results for the thalamus. A) forest plot of group comparisons for Alzheimer's disease patients vs healthy controls. Squares represent the computed effect sizes of the original studies, the squares' size indicate the relative size of the sample studied, and the diamond represents the weighted mean effect. The width of the diamond as well as the horizontal lines of the squares indicate a study's 95% confidence intervals. B) Funnel plot: the dots mark the individual study, the dashed line the 95% confidence interval, and the vertical straight line the overall effect. C) Spearman correlation of the iron differences (effect size) and mean Mini-Mental-State-Examination (MMSE) scores.

Publication bias

Upon visual inspection, data points in most ROIs showed a symmetric distribution around the weighted mean effect (Fig. 6.2-6B), indicating no publication bias. However, for the hippocampus (Fig. 6.5B) and thalamus (Fig. 6.6B), the funnel plots showed some degree of asymmetry. In line with this impression, Egger's regression revealed a significant effect for the hippocampus ($p<0.001$) and thalamus ($p=0.001$), indicating a publication bias, but not for the putamen ($p=0.144$, Fig. 6.2B), caudate nucleus ($p=0.203$, Fig. 6.3B) and pallidum ($p=0.118$, Fig. 6.4B).

Correlations between brain effect sizes and MMSE in Alzheimer's disease

Correlation analyses of the effects sizes (z-scored) and MMSE performance (z-scored) in AD revealed a significant negative effect only in the globus pallidus ($r(15)=-0.541$, $p=0.025$, Fig. 6.4C, Table 6.3). For the other ROIs, the effects were not statistically significant ($p>0.05$, Fig. 6.2,3,5,6C, Table 6.3). To further investigate this effect, we repeated the correlational analysis with iron effect sizes (z-scored) and MMSE effect sizes (resulting from a comparison of AD vs HC, z-scored). It also revealed a statistically significant effect ($r(12)=-0.569$, $p=0.037$). Note, however, in this latter analysis three experiments had to be excluded (Bartzokis et al., 2004; Guan et al., 2022; Kuchcinski et al., 2022) due to missing MMSE information in the HC group.

Table 6.1. Overview of the study characteristics of all included experiments. Abbreviations: AD: Alzheimer's disease. HC: healthy controls; MMSE: Mini-Mental-State-Examination; PUT: putamen; HC: caudaute nucleus; GP: globus pallidus; HIP: hippocampus; THAL: thalamus

Authors and titles	Method	Participants										Effect size (d)				
		AD						HC				PUT	HC	GP	HIP	THAL
		Group discription	Diagnosis	N	Age (mean ± SD)	Sex (f/m)	MMSE	N	Age	Sex (f/m)	MMSE					
Ayton et al. (2017)	QSM; 3T	probable/possible AD	NINCDS-ADRDA	19	-	-	-	64	-	-	-	-	0.501	-	-0.557	-
Bartzokis et al. (2000)	FDRI; 0.5T. 1.5T	probable/possible AD	NINCDS-ADRDA	31	75.6 ± 6.7	1.214	17.3 ± 7.39	68	68.8 ± 5.3	0.889	28.4 ± 0.92	0.678	0.652	0.182	-	-
Bartzokis et al. (1994)	FDRI; 0.5T. 1.5T	probable AD; mild to moderate AD	NINCDS-ADRDA	5	72.6 ± 3.97	0	17.8 ± 5.45	8	72.5 ± 4.5	0	28.6 ± 1.19	1.034	1.239	1.261	-	-
Bartzokis et al. (2004)	FDRI; 0.5T. 1.5T	probable/possible AD; onset >70 years	NINCDS-ADRDA	10	81.6 ± 3.4	0	19.4 ± 5.4	36	68.7 ± 4.9	-	-	0.52	0.55	-0.296	-	-
Chiang et al. (2022)	QSM; 3T	cognitively impaired	exclusion of other etiologies; neurological examination. neuropsychological assessment. laboratory data. MRI	68	72 ± 8.4	1.519	-	32	69 ± 9.9	2.556	-	0.52	-0.07	-0.562	0.197	0.212
Cogswell et al. (2021)	QSM; 3T	amnestic dementia	NIA-AA	56	68; IQR 61-77	1.074	-	296	69 IQR 59-76	0.762	-	0.459	-0.155	0.438	-	-0.827
Damulina et al. (2020)	R2*; 3T	probable/possible AD	DSM-IV. NINCDS-ADRDA	100	73 ±9	1.381	22; IQR 18.5-25	100	73 ±9	1.5	28; IQR 27-29	0.378	0.495	0.243	0.04	-0.054
Ding et al. (2009)	Phase; 1.5T	probable AD	NINCDS-ADRDA	26	70.96 ± 8.55	2.25	16.0 ± 3.9	24	69.40 ± 11.38	1.667	29.4 ± 1.0	0.697	-	0.93	0.645	-
Du et al. (2018)	QSM; 3T	mild to moderate AD	NINCDS-ADRDA	30	68.3 ± 6.6	2.333	20.4 ± 2.4	30	66.2 ± 7.8	2	28.0 ± 1.3	0.571	0.573	-0.013	-	-0.319
Gao et al. (2017)	SWI; 3T	probable AD	DSM-IV. NINCDS-ADRDA	30	74.83 ± 4.52	1.5	17.76 ± 4.15	30	72.86 ± 5.75	1.308	28.73 ± 1.11	1.849	0.63	0.555	0.628	-
Guan et al. (2022)	QSM; 3T	probable AD	NINCDS-ADRDA	51	68.7 ± 8.7	0.889	19.6 ± 3.9	189	61.4 ± 7.8	1.423	-	1.706	1.174	0.37	-	-
	QSM; 3T	AD	NIA-AA	43	62.63 ± 8.10	2.301	20.3 ± 1.89	27	58.70 ± 8.99	1.7	27.30 ± 2.20	0.5904	0.793	0.4003	-	-
H.-G. Kim et al. (2017)	QSM; 3T	probable AD; mild AD	NINCDS-ADRDA	19	69.79 ± 10.27	8.5	17.37 ± 3.42	19	65.37 ± 6.26	5.333	28.16 ± 1.89	2.765	-	1.283	5.799	4.761
Kuchcinski et al. (2023)	QSM; 3T	EOAD; probable AD; typical AD (tADMRI)	NIA-AA	34	60.6 ± 4	1.267	15.8 ± 6	43	62.0 ± 4.3	1.867	-	0.876	0.274	0.915	0.211	1.9
D. Li et al. (2020)	QSM; 3T	probable AD	NIA-AA	22	71.5 ± 8.4	1.444	18.9 ± 3.4	25	69.3 ± 5.2	1.5	29.7 ± 0.6	2.376	1.627	2.47	0.127	0.739
X. Liu et al. (2021)	QSM; 3T	AD	NINCDS-ADRDA	30	68.37 ± 6.734	2.75	19.8 ± 3.925	19	66.68 ± 8.564	2.8	28 ± 1.856	0.516	2.064	0.139	-	-
W.-J.Moon et al. (2012)	T2*; 3T	AD	NINCDS-ADRDA	21	72.1 ± 6.5	2.5	21.2 ± 3.8	21	68.9 ± 5.3	4.25	28.0 ± 1.2	0.76	-	-0.462	-	0.944
Qin et al. (2011)	R2'; 1.5T	probable AD	NINCDS-ADRDA	15	69.8	1.143	17.3	15	70.0	1.143	30	0.516	1.077	-	1.403	0.177
Tiepolt et al. (2020)	QSM; 3T	cognitive impairment + Aβ PET-positive	NINCDS-ADRDA	16	69 ± 9	3	25 ± 2	11	65 ± 3	1.75	30 ± 1	1.246	0.144	-0.070	0.487	-
D. Wang et al. (2014)	SWI; 3T	probable AD; age 60-70 years	NINCDS-ADRDA	20	-	0.818	20.3 ± 2.98	19	-	0.9	28.22 ± 0.97	0.134	-0.303	0.702	-	-
D. Wang et al. (2014)	SWI; 3T	probable AD; age 70-80 years	NINCDS-ADRDA	19	-	0.818	20.3 ± 1.89	10	-	0.9	27.84 ± 2.47	0.467	0.262	0.846	-	-
D. Wang et al. (2013)	SWI; 3T	probable AD	NINCDS-ADRDA	20	73.37 ± 9.81	0.758	21.15 ±1.23	18	70.52 ± 6.91	1.087	28.22 ± 0.87	-	0.66	-	1.173	0.951

Table 6.2. Overview of the results of the region of interest (ROI) random-effects models for comparing Alzheimer's disease vs. healthy control participants. Displayed are the number of experiments (k) included. the weighted mean effects (d*) of each ROI. 95% confidence intervals (CI). Z-values. and p-values as well as the heterogeneity indicators I^2 and their 95% confidence intervals.

	k	d*	CI (95%) $_d$	Z	p	I^2	CI (95%) $_{I^2}$
Putamen	20	0.89	0.62 - 1.16	6.49	<.001	81.00	71.54 – 87.31
Caudate nucleus	19	0.61	0.35 - 0.87	4.61	<.001	79.53	68.74 – 86.59
Globus pallidus	19	0.44	0.19 - 0.69	3.44	.001	78.59	67.14 - 86.05
Hippocampus	11	0.70	0.23 - 1.18	2.88	.004	88.43	81.28 - 92.85
Thalamus	10	0.74	0.10 - 1.38	2.26	.024	94.25	91.31 - 96.19

Table 6.3. Correlations between the region-of-interests' original studies' effect sizes and the MMSE mean of the Alzheimers disease (AD) group.

	MMSE mean AD group		
	Spearman's Rho	p-value	N
Putamen	-0.250	0.317	18
Caudate nucleus	-0.370	0.159	16
Globus pallidus	-0.541	0.025*	17
Hippocampus	-0.333	0.385	9
Thalamus	-0.405	0.327	8

The correlations (Spearmans' Rho) between the original studies' effect sizes for the brain regions (putamen. caudate nucleus. globus pallidus. hippocampus. and thalamus) with the Mini-Mental-State-Examination (MMSE) mean of the Alzheimer's disease (AD) groups from the original studies. Presented are the p-value (* <0.05) and N reflecting the included number of experiments (in that both MMSE scores for AD and the effect sizes were available).

Discussion

We leveraged the power of a meta-analytic approach to investigate the relationship of regional brain iron levels and cognitive abilities in Alzheimer's disease (AD). We employed data from 22 studies encompassing 1789 participants, including 685 patients diagnosed with Alzheimer's disease and 1104 age-matched healthy controls (HC). As expected, in AD iron levels were significantly higher in the putamen, caudate nucleus, and globus pallidus, but also hippocampus and less robust the thalamus. Importantly, iron accumulation in the globus pallidus, a basal ganglia hub with a critical role in several cognitive processes, was negatively associated with cognitive performance as measured with the MMSE. Therefore, our results provide unique evidence across a wide range of studies *in vivo* that iron accumulation in the basal ganglia is a characteristic feature in AD that contributes to cognitive decline.

Iron plays a central role in maintaining normal brain functioning, contributing to myelination (Bartzokis, 2011; Todorich et al., 2009), neurotransmitter synthesis (Zecca et al., 2004), and oxygen regulation (Crichton, 2001). However, excessive iron levels can induce oxidative stress and inflammation (Zecca et al., 2004), demyelination (Steiger et al., 2016), and ferroptosis, an iron-dependent form of cell death (Doll & Conrad, 2017), and therefore, promote the progression of AD. From a developmental perspective, brain iron accumulates over the lifespan (Aquino et al., 2009; Bartzokis et al., 1997; Biel et al., 2021; Hallgren & Sourander, 1958; Khattar et al., 2021; D. Li et al., 2020; Yim et al., 2022) with inter regional variations and particularly high levels in the basal ganglia (Haacke et al., 2005; Hallgren & Sourander, 1958; Koeppen, 1995). This pattern appears to reflect region specific needs in iron to meet metabolic demands (Mills et al., 2010). The excessive iron deposition in AD may, therefore, closely relate to dysregulations in iron metabolism and transport (Dusek et al., 2022), but also vascular hemorrhages and microbleeds (Dusek et al., 2022; Nikseresht et al., 2019), as well as neuroinflammation (Nikseresht et al., 2019). Moreover, *post-mortem* and *in vivo* studies revealed a co-localization of iron and tau (Ayton et al., 2020; Bulk et al., 2018; Spotorno et al., 2020) as well as Aβ pathology (Van Bergen et al., 2016; Van Duijn et al., 2017). In line with this observation, a positive correlation of MRI susceptibility has been shown for both Aβ (Cogswell et al., 2021; Van Bergen et al., 2016) and tau (Choi et al., 2018; Cogswell et al., 2021; Spotorno et al., 2020) PET in the basal ganglia, underscoring the importance of iron increases in AD.

Our results of iron accumulations in the putamen, caudate nucleus, and globus pallidus are consistent with this prior research and a meta-analysis investigating *post-mortem* iron accumulations in these brain regions (Tao et al., 2014). In comparison, the most pronounced effect was observed in the putamen as suggested by a large weighted effect size (Cohen, 2013) indicating a contribution by all original studies (Fig. 6.2A and Table 6.1). Although still highly significant, the random-effects model for the caudate nucleus showed a medium-weighted effect size with all but three studies (Chiang et al., 2022; Cogswell et al., 2021; D. Wang et al., 2014) contributing to the effect (Fig. 6.3A and Table 6.1). Finally, the random-effects model for the globus pallidus, again highly significant, had a rather small weighted effect size, and all but five studies (Bartzokis et al., 2004; Chiang et al., 2022; Du et al., 2018; W.-J. Moon et al., 2012; Tiepolt et al., 2020) contributed to the effect. Taken together, for the investigated basal ganglia structure, putamen, caudate nucleus, and globus pallidus, almost all included studies reported higher iron levels in AD compared to HC, which led to highly significant effects in our meta-analysis. Egger's regression and visual inspection of the funnel plots (Fig. 6.2-4B) did not indicate any publication bias for these regions, which further underlines the robustness of our findings.

Outside the basal ganglia, we observed significant effects in the hippocampus (Fig. 6.5A) and the thalamus (Fig. 6.6B) also, at the first glance, indicating higher iron levels in AD compared to HC. However, the thalamus effect did not remain significant after removing one outlier, and in the thalamus as well as the hippocampus a publication bias was detected (Fig. 6.5,6.6B). Together with a small-weighted effect sizes, this casts doubt on the reliability of the thalamus and hippocampus effect. However, both analyses were based on a small number of studies (10 for the thalamus and 11 for the hippocampus), indicating a possible power problem. Yet, our finding is in line with a previous *post-mortem* meta-analysis that also did not reveal statistically significant iron effects in AD in the thalamus ($p=0.16$) or hippocampus ($p=0.056$) (albeit with even fewer original studies compared to our work, $n>8$) (Tao et al., 2014).

Based on several single studies, we predicted a negative relationship between iron levels and cognitive performance in AD (D. Li et al., 2020; X. Liu et al., 2021; D. Wang et al., 2014; A. Yang et al., 2022). This has been confirmed specifically in the globus pallidus (Fig. 6.4C), further indicating that local increases in iron levels lead to cognitive impairments not only in healthy older adults (Biel et al., 2021; Steiger et al., 2016) but also AD. From a

mechanistic point of view, this can be explained by a central role of the pallidum in cognitive information processing. Specifically, to encode novel information into long-term memory, the hippocampal SN/VTA-loop model (Lisman et al., 2011; Lisman & Grace, 2005) suggests that a hippocampal novelty signal is sent to SN/VTA dopamine (DA) neurons via a polysynaptic path including the ventral pallidum before DA-neurons back-project to the hippocampus. While iron is required for DA synthesis (Zecca et al., 2004), an accumulation of it can impair DA production (Hare & Double, 2016; Zecca et al., 2004). Therefore, excessive iron levels within the bilateral pallidum may account for an imbalance of the loop, leading to impairments in declarative learning and memory. Furthermore, basal ganglia structures and DA have been associated with motivation, decision-making, and non-declarative memory functioning (Foerde & Shohamy, 2011), which may also contribute to MMSE performance. Indeed, a negative relationship between iron deposition in the globus pallidus and MMSE scores in 60-80 year old AD patients has been reported before (D. Wang et al., 2014). Despite this theoretical view and empirical evidence, our rather weak (but hypothesized) negative correlation (Fig. 6.4C) could be explained by the use effect sizes and mean MMSE values from the original studies, which may neglect individual data points potentially leading to reduced power.

Finally, some other limitations, that may guide future research, need to be considered. First, iron measures were averaged from both hemispheres, streamlining our analysis but neglecting possible lateralization effects (X. Xu et al., 2008). Second, we observed rather high heterogeneity in all random effect models (Higgins et al., 2003), which, despite strict inclusion and exclusion criteria (see methods), could be driven by differences in MRI sequences and field strengths (Daugherty & Raz, 2013; Haacke et al., 2005; Langkammer et al., 2014), regions of interest definitions, and sample characteristics (e.g. different stages of AD). To further substantiate our findings, however, all analyses were repeated without outliers, when necessary, and we also report empirical measures for potential publication biases (Fig. 6.2-6.6B). Third, although all individual studies included age-matched HC, across studies a slight but significant age difference was detected (Table 6.1), which might have biased the results. Fourth, all studies included used a cross-sectional design, which allows between group comparisons but, strictly speaking, not the description of developmental and disease specific changes. Longitudinal designs may help to address this important point. Fourth, in the original studies participants were included solely based on their clinical status. Future work could be

based on other approaches, especially the AT(N) framework, that includes markers of Aβ (A), tau (T), and neurodegeneration (N) (Jack et al., 2018). This would allow to explore differences (or changes) in iron levels more precisely as well as possible relationships with other imaging markers as derived by positron emission tomography (PET) (Cogswell & Fan, 2023), structural MRI (J. R. Sato et al., 2010) and functional MRI (Quevenco et al., 2017; Van Bergen et al., 2016).

Based on *in vivo* MRI studies and a meta-analytic approach, our results indicate higher iron levels in the putamen, caudate nucleus and globus pallidus, but also hippocampus and (less robust) in the thalamus, in AD patients. Together with a negative correlation of iron markers and MMSE scores in the globus pallidus, our work refines and provides further evidence for the notion that increased iron levels, especially in the basal ganglia, are a characteristic hallmark of AD, which can contribute to cognitive impairments. As such, our findings not only give novel insights into the pathogenesis of AD, but they also highlight the potential role of iron as a relevant marker in the diagnosis and possibly treatment of AD.

7 Basal forebrain activity predicts functional degeneration in the entorhinal cortex in Alzheimer's disease

This chapter refers to **study 4** and addresses the local activity of the NbM and EC (see section 2.4, Fig. 2.1). It has been formally integrated into the dissertation's style for consistency. The content corresponds to the following publication:

Mieling, M., Göttlich, M., Yousuf, M., & Bunzeck, N. (2023). Basal forebrain activity predicts functional degeneration in the entorhinal cortex in Alzheimer's disease. Brain Communications, 5(5), fcad262. https://doi.org/10.1093/braincomms/fcad262

Author's contributions

MM and NB conceived the study. MM, MG and MY analyzed the data. MM and NB wrote the manuscript and revised it. MG and MY gave further constructive feedback on the manuscript.

Abstract

Recent models of Alzheimer's disease suggest the nucleus basalis of Meynert (NbM) as an early origin of structural degeneration followed by the entorhinal cortex (EC). However, the functional properties of NbM and EC regarding amyloid-β (Aβ) and hyperphosphorylated tau remain unclear. We analyzed resting-state functional (rs)fMRI data with CSF assays from the Alzheimer's Disease Neuroimaging Initiative (ADNI, n=71) at baseline and two years later. At baseline, local activity, as quantified by fractional amplitude of low-frequency fluctuations (fALFF), differentiated between normal and abnormal CSF groups in the NbM but not EC. Further, NbM activity linearly decreased as a function of CSF ratio, resembling the disease status. Finally, NbM activity predicted the annual percentage signal change in EC, but not the reverse, independent from CSF ratio. Our findings give novel insights into the pathogenesis of Alzheimer's disease by showing that local activity in NbM is affected by proteinopathology and predicts functional degeneration within the EC.

Introduction

The basal forebrain's (BF) nucleus basalis of Meynert (NbM) has recently been suggested as an early origin of structural degeneration in Alzheimer's disease followed by the entorhinal cortex (EC) and other cortical brain regions (Fernández-Cabello et al., 2020; Schmitz & Spreng, 2016). For instance, grey matter loss was more prominent in the NbM compared to the EC in cognitively healthy humans with an abnormal CSF biomarker of amyloid-β (Aβ) and hyperphosphorylated Tau (pTau) (Schmitz & Spreng, 2016). Moreover, the NbM's baseline volume predicted the longitudinal structural degeneration in the EC, further suggesting a trans-synaptic spread of Aβ starting in the NbM (Fernández-Cabello et al., 2020; Schmitz & Spreng, 2016). This observation in humans is in line with animal work and adds a crucial upstream link to the subsequent spread from EC to other medial temporal lobe (MTL) structures, including the hippocampus, and more distal neocortical brain regions such as the posterior parietal cortex (de Calignon et al., 2012; Fernández-Cabello et al., 2020; Khan et al., 2014; L. Liu et al., 2012; J. W. Wu et al., 2016). Importantly, evidence in favor of such a pathological staging model is mainly limited to anatomical studies, and, therefore, the functional properties of both the NbM and EC during the disease progression of Alzheimer's disease in humans remain unclear.

Since functional brain changes in Alzheimer's disease often precede structural degeneration, we investigated the functional properties of the NbM and EC, including their functional connectivity (FC). To this end, we used data from the Alzheimer's Disease Neuroimaging Initiative (ADNI) and performed a longitudinal region of interest (ROI) analysis over 2 years, focusing on regional and interregional resting-state functional MRI (rsfMRI) properties. In detail, we analyzed (a) the fractional amplitude of low-frequency fluctuations (fALFF) to quantify spontaneous neuronal activity (Biswal et al., 1995; Zou et al., 2008; Zuo et al., 2010), (b) regional homogeneity (ReHo) reflecting the synchronicity of neural activity between a voxel and its neighboring voxels (Zang et al., 2004), and finally (c) the FC between NbM and EC. While all three measures may help to gain new insights into Alzheimer's disease progression, we initially focused on fALFF given its established role (S.-M Wang et al., 2021; L. Yang et al., 2018; X. Zhang et al., 2021), and report ReHo and FC analyses in the supplementary material S3.

In the first step, baseline signals and longitudinal functional changes were compared based on harmonized CSF assays of Aβ and pTau in NbM and EC. Subsequently, we

investigated functional changes in disease progression using the CSF markers. Finally, we tested the competing models NbM→EC vs. EC→NbM on a functional level. Our main hypothesis was that functional signals in the NbM predict functional change in EC, which would provide further evidence supporting the pathological staging model from NbM to EC. From a more general perspective, we aimed to provide new insights into the underlying functional properties of Alzheimer's disease, which may contribute to further developing markers and treatment strategies.

Materials and methods

ADNI data

Data used in the preparation of this article were obtained from the Alzheimer's Disease Neuroimaging Initiative (ADNI) database (adni.loni.usc.edu). ADNI was launched in 2003 as a public-private partnership, led by Principal Investigator Michael W. Weiner, MD, to test whether serial magnetic resonance imaging (MRI), positron emission tomography (PET), other biological markers, and clinical and neuropsychological assessment can be combined to characterize the progression of mild cognitive impairment (MCI) and early Alzheimer's disease.

Since rsfMRI was not acquired in all ADNI cohorts, here data were combined from ADNI-GO, ADNI-2 (ADNI-GO/2) and ADNI 3, downloaded from the Image and Data Archive (IDA) platform run by the Laboratory of Neuro Imaging (LONI) (https://ida.loni.usc.edu). Specifically, we only selected data from participants with CSF biomarkers, and two rsfMRI scans acquired with a delay of two years with the same MR scanner and head coil to ensure within-subject comparability.

Image acquisition

Participants were scanned at multiple sites equipped with 3-Tesla MRI scanners according to unified ADNI monitoring protocols (Jack, Bernstein, et al., 2010). To ensure maximum compatibility between the measurements, we followed ADNI's recommendations and included only the basic rsfMRI version but not advanced version of ADNI 3 since it is not compatible with ADNI-GO/2. Moreover, all participants here were examined with the same scanner and head coil for both time points, t1 and t2 (https://adni.loni.usc.edu/methods/mri-tool/mri-analysis/). Further, we only included MRI data with excellent, good, or fair quality.

For further information on image acquisition, see the supplementary material S3 and http://adni.loni.usc.edu.

Data preprocessing

Considering their specific scanning parameters such as TR, slice order, and volume number, all data were preprocessed with the Data Processing Assistant for Resting-State fMRI Advanced (DPARSFA, http://rfmri.org/dpabi) toolbox version 5 (release 5.2_210501), which is based on the Statistical Parametric Mapping toolbox (SPM 12, https://www.fil.ion.ucl.ac.uk/spm/) for MATLAB®. It started with the removal of the first ten volumes and subsequently included the following steps a) slice time correction; b) spatial realignment; c) T1 co-registration to the mean functional image; d) CSF, gray and white matter tissue segmentation, and spatial normalization using diffeomorphic anatomical registration using exponential lie algebra (DARTEL) (Ashburner, 2007) for T1 images; e) regression of nuisance variables; f) normalization to MNI space and resampling to an isotropic voxel size of 3 mm of the functional images using the parameters estimated by DARTEL (see supplementary material S3 for a detailed description).

To reduce the influence of excessive head motion, participants exhibiting more than 3.0 mm of maximum movement and a 3.0-degree rotation angle were discarded. Further, images were visually inspected after co-registration, segmentation, and normalization to guarantee high quality. This included a specific focus on signal loss and artifacts in our regions of interest (NbM, EC) by overlaying a ROI mask in standardized space; especially, the EC represents a region that might often be affected by artifacts (Olman et al., 2009). For a detailed description of the preprocessing steps, excluded participants, ROI definition, and rsfMRI analyses for fALFF, ReHo, and the functional connectivity, see supplementary material S3.

CSF biomarker

Alzheimer's disease neuropathology includes the accumulation of Aβ resulting in plaques and pTau leading to neurofibrillary tangles (Palmqvist et al., 2016; Shaw et al., 2009). To better understand how both relate to functional degeneration in NbM and EC, we followed previous studies (Fernández-Cabello et al., 2020; Schmitz & Spreng, 2016) and used ADNI's CSF samples, produced with a fully automated Elecsys® protocol of Aβ and pTau from the first measurement (t1). For each participant, we extracted Aβ 1-42 and pTau181 values. Since the

protocols by Elecsys® are still under development, the results are restricted to a specific technical limit (>1700 pg/mL). Higher values were provided by extrapolation of the calibration curve for research purposes only but not diagnostics. Further information on CSF draws and analyses can be found at http://adni.loni.usc.edu.

Here, we analyzed both proteins by using a previously established ratio of pTau/Aβ, which is known to highly concord with PET measures and clinical diagnoses (Hansson et al., 2018; Schindler et al., 2018). Based on these findings, the standardized and cross-validated cut-off of 0.028 was used to divide the participants into an abnormal (pTau/Aβ≥ 0.028) and a normal (pTau/Aβ<0.028) CSF group (Fernández-Cabello et al., 2020; Hansson et al., 2018; Schindler et al., 2018). Importantly, no participant classified with Alzheimer's disease had a normal CSF ratio, but a few (n=10) participants classified with MCI did, which indicates an unclear etiology. Nevertheless, we included them based on biological instead of a syndromal grouping (Jack et al., 2018).

Neuropsychological assessment and clinical diagnosis

All participants underwent a comprehensive neuropsychological test battery. Here, t1 scores are used, including validated memory (MEM) and executive function (EF), based on a confirmatory factor analysis (Crane et al., 2012; Gibbons et al., 2012). Memory scores include the Alzheimer's disease Assessment Scale, Logical Memory test, Mini-Mental-State Examination (MMSE), Rey Auditory Verbal Learning Test (RAVLT). EF scores are based on the Category Fluency, Digit Span Backwards, Digit Symbol Substitution, Trails A and B, and the Clock Drawing tests (Crane et al., 2012; Gibbons et al., 2012). We were also interested in the Montreal-Cognitive-Assessment (MoCA), Sum of Boxes in the Clinical Dementia Rating Scale (CDRSB) and the Alzheimer's Disease Assessment Scale Cognitive (ADAS-Cog 13) to get a deeper understanding of the participants' cognitive profiles (see below).

Furthermore, we included participants' t1 diagnosis made by the ADNI Clinical Core: cognitive normal (HC) (CDR=0, MMSE=24-30), mild cognitive impairment (MCI) (CDR=0.5, MMSE=24-30), and Alzheimer's disease (CDR=0.5-1, MMSE=20-26). These classifications represent widely used cognitive and functional measures in clinical trials (Aisen et al., 2010, 2015; Weiner et al., 2017). Further information regarding diagnostic is available at http://adni.loni.usc.edu.

Participants

We included rsfMRI data from ADNI-GO/2 and ADNI 3 – but, importantly, only those that also offered a subject's CSF draw (see below) temporally related to a rsfMRI acquisition (e.g., a participant's screening MRI and baseline lumbar punction measurement). This measurement served as t1 measurement in the analyses. To maximize the number of subjects, the second measurement was selected after an interval of 1.5 years ±12 months (t2) (Fernández-Cabello et al., 2020). Further details on inclusion and exclusion criteria for participating in ADNI are available under http://adni.loni.usc.edu. In total, 153 participants for ADNI-GO/2 and 141 for ADNI 3 (only basic rsfMRI version) fulfilled our inclusion criteria. However, a large proportion had to be excluded mainly based on fMRI data quality (see supplementary material S3). Thus, data from n=71 participants were analyzed, which could be further subdivided into those with normal CSF (nCSF, n=37) and abnormal CSF (aCSF, n=34) values (Table 7.1).

Table 7.1 gives an overview of the participants' demographics, as well as information on APOE4 genotype and harmonized CSF assay, and Table 7.2 shows the neuropsychological test results at baseline (t1).

Ethics approval and consent to participate

Each center collecting data for ADNI provided an IRB (Institutional Review Board) approval and meets ADNI's requirements. Informed consent was obtained from all ADNI participants (for more information at http://adni.loni.usc.edu). The analyses presented here were approved by the local Ethics Committee of the University of Lübeck and carried out after ADNI's recommendations including the approval of the manuscript before submitting to a journal.

Table 7.1. Participants' demographics and information on APOE4 genotype and harmonized CSF assays

	Normal CSF	**Abnormal CSF**	**Test - χ^2/ t**
n (total)=71	37	34	χ^2=0.127, p=0.722
ADNI-GO/2 (n=44) / 3 (n=27)	17/20	27/7	χ^2=8.420, p=0.004**
HC (n=32) / MCI (n=28) / AD(n=11)	27/10/0	5/18/11	χ^2=28.335, p<0.001***
Manufacturer Philips (n=52) / Siemens (n=11) / GE (n=8)	24/8/5	28/3/3	χ^2=2.959, p=0.228
Age	70.51 (6.23)	72.71 (7.18)	t=-1.376 p=0.173
Female (n=44) / Male (n=27)	22/15	22/12	χ^2=0.207, p=0.649
Education (in years)	16.59 (2.44)	15.91 (2.25)	t=1.222, p=0.226
Interscan interval			
In months	22.03 (5.0)	18.74 (6.9)	t=2.294 p=0.025*
In days	685.35 (151.15)	587.76 (210.43)	t=2.227, p=0.03*
APOE 4 (0/1/2)	28/8/1	5/21/8	χ^2=27.224, p<0.001***
Aβ	1430.64 (521.29)	637.22 (187.1)	t=8.670, p <0.001***
pTau	18.42 (4.83)	40.81 (17.76)	t=-7.114, p<0.001***

Information of the final sample from ADNI-GO/2 and ADNI-3 grouped by CSF. Means and standard deviation (SD) are represented and the respective t-test or chi-square test to investigate possible group differences. Baseline clinical diagnosis: HC=cognitive normal; MCI=mild cognitive impairment; AD=Alzheimer's disease. Age and education were assessed in years. APOE4 status: no allel / 1 allel / 2 allels. Aβ amyloid-β in pg/ml as concentration of the amyloid-β 1-42 peptide. pTau=in pg/ml as CSF concentration of hyperphosphorylated tau. *p<0.05, **p<0.01, ***p<0.001

Statistical analyses

Mixed ANCOVA

Mixed ANCOVAs were carried out for all measures separately (i.e., fALFF, ReHo) to compare baseline signals and the annual percentage signal change (APSC, see below) between regions (NbM and EC as a within-subject factor) and CSF groups (normal and abnormal as a between-subject factor). Covariates such as age, sex, education, ADNI cohort, and scanner manufacturer were included to adjust for different scan protocols and other potential scanner-related differences. All 2x2 (region x CSF group) mixed ANCOVAs were carried out in IBM SPSS statistics version 25 (SPSS) with type III sums of squares, and within-subject effects were interpreted without covariates (Schneider et al., 2015).

Linear regression of disease status based on CSF marker

To better understand the relationship between disease status and functional MRI properties, CSF ratios (see section CSF biomarker) and functional MRI signals were considered in a linear regression model in SPSS. The functional MRI signal served as dependent variable, and CSF ratio as independent variable. The regression was run with the z-scored data. Subsequently, the dependent overlapping correlations of NbM vs EC with CSF ratio were compared using cocor (Diedenhof & Musch, 2015; Silver et al., 2004).

Robust regression

To minimize the influence of outliers, especially in the APSC, robust regression models were carried out in MATLAB® R2020b with fitlm using the bisquare weight function with the default tuning constant. The same covariates as for the mixed ANCOVA were included in the model. Finally, the predictive models (NbM→EC and EC→NbM) were tested for each CSF group (normal and abnormal) and each functional property (fALFF and ReHo). The data was z-scored before entering the analysis to ensure comparability of the APSC and baseline signal.

Moderation analyses of independent samples

Moderation analyses were carried out in SPSS using the PROCESS macro (Hayes, 2017) for fALFF and ReHo investigating whether CSF group assignment moderates the spread (NbM→EC vs. EC→NbM) of functional degeneration. Here, CSF group was used as a dichotomous moderator variable. For the construction of products mean-centering was

applied, and the heteroscedasticity consistent standard error HC3 (Davidson-MacKinnon) was applied.

Annual percentage signal change (APSC)

The following formula (Cavedo et al., 2017; Fernández-Cabello et al., 2020) was used to assess longitudinal APSC in fALFF and ReHo. It accounts for the days between both measurements and minimizes the influence of differences between both measurements within a subject.

$$APSC=\left(\frac{Change\ baseline\ (t2-t1)\ signal)}{Baseline\ signal}\right)x\left(\frac{365}{Interscan\ interval\ in\ days}\right)\ x\ 100$$

Results

CSF grouping strategy and neuropsychological assessments

Based on the CSF grouping strategy, we investigated how aCSF and nCSF groups performed in neuropsychological tests. For each test, one-way fixed effect ANOVAs were carried out with CSF group as factor and age, sex, and education as covariates. As expected, the nCSF group is less affected by cognitive impairment than the aCSF group (see Table 7.2).

Table 7.2. Neuropsychological test results at baseline, compared by CSF normal vs. abnormal

Neuropsychological testing	CSF groups (mean (SD)) Normal	Abnormal	F- value	P- value
MEM score	0.88 (0.6)	-0.08 (0.97)	F(1,66)=23.4	<0.001*
EF score	1.02 (0.76)	-0.16 (1.1)	F(1,66)=23.8	<0.001*
MMSE	29.08 (1.12)	25.82 (3.5)	F(1,66)=23.35	<0.001*
ADAS-Cog 13	9.8 (4.8)	22.89(14.26)	F(1,66)=26.82	<0.001*
CDRSB	0.3 (0.55)	2.63 (2.36)	F(1,66)=34.73	<0.001*
MoCA	25.89 (2.34)	20.91 (5.72)	F(1,66)=22.5	<0.001*
Clock drawing	4.76 (0.55)	4.03 (1.22)	F(1,66)=8.73	0.004*

The mean values with standard deviation (SD) for normal vs. abnormal CSF groups. The abnormal CSF group showed worse performance in all neuropsychological tests. MEM: memory function score; EF: executive function score; MMSE: Mini-Mental State Examination; ADAS-Cog 13: Alzheimer's Disease Assessment Scale- Cognition Subscale, 13 tasks; CDRSB: Clinical Dementia Rating Scale; MoCA: Montreal-Cognitive-Assessment; Clock drawing: clock drawing test

* significant after Bonferroni correction $p<0.05/n$ (n=7 tests).

Lower fALFF values at baseline in aCSF vs. nCSF in NbM but not EC

Baseline fALFF values were compared in NbM and EC further subdivided into CSF groups using a 2x2 mixed ANCOVA. We found a main effect of CSF group ($F(1,63)=7.943$, $p=0.006$, partial $\eta^2=0.112$, Fig. 7.1B), that was driven by lower fALFF values in participants with abnormal CSF, and a significant region x CSF group interaction ($F(1,63)=4.623$, $p=0.035$, partial $\eta^2=0.068$, Fig. 7.1B), that was driven by a more pronounced fALFF reduction in the NbM. Post-hoc analyses showed that a significant difference in fALFF between nCSF vs aCSF was only observed in NbM ($t(69)=3.141$, $p=0.002$) but not EC ($t(69)=1.856$, $p=0.068$). There was no main effect of region ($F(1,69)=2.643$, $p=0.109$, partial $\eta^2=0.037$, Fig. 7.1B).

Annual percentage signal change in fALFF does not differentiate between CSF groups or regions

We used a 2x2 mixed ANCOVA to investigate whether the longitudinal indices of APSC in fALFF of the NbM and EC differentiated between CSF normal vs. abnormal groups. There was no significant main effect of CSF group ($F(1,63)=2.077$, $p=0.154$, partial $\eta^2=0.032$, Fig. 7.1C), or region ($F(1,69)=0.499$, $p=0.482$, partial $\eta^2=0.007$, Fig. 7.1C), and no significant group x region interaction ($F(1,63)=0.367$, $p=0.547$, partial $\eta^2=0.006$, Fig. 7.1C) in APSC fALFF.

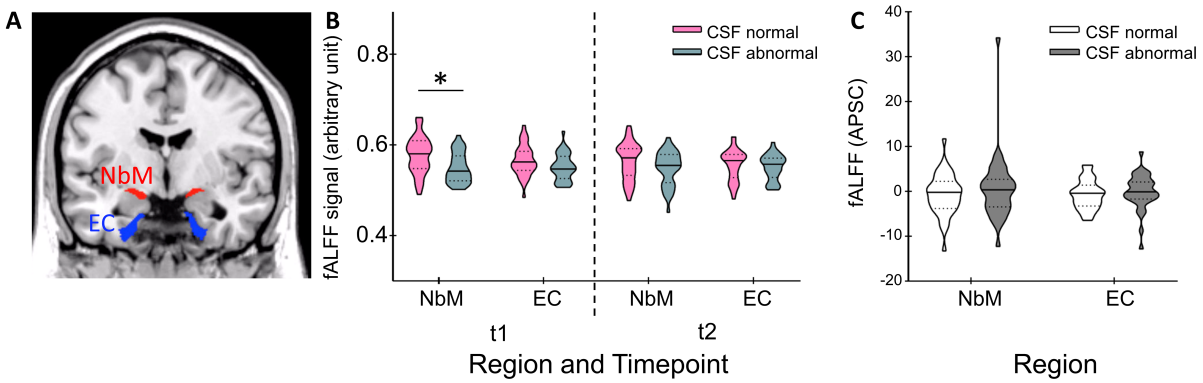

Figure 7.1. Regions of interests (ROIs), baseline and follow-up signal, and annual percentage signal change for fALFF. A) ROIs for the nucleus basalis of Meynert (NbM) (red) and entorhinal cortex (EC) (blue) on a coronal slice of a T1-weighted standard brain template. Violin plots representing the participants' B) baseline fALFF signals at time point 1 (t1) and fALFF signals at the follow-up measurement (t2) for normal CSF (n=37) and abnormal CSF (n=34). A mixed ANCOVA revealed a main effect of CSF ($F(1,63)=7.943$, $p=0.006$) and a significant region x CSF group interaction ($F(1,63)=4.623$, $p=0.035$). C) shows the participants' annual percentage signal change (APSC) in both regions again for normal CSF (n=37) and abnormal CSF (n=34). For the APSC, the mixed ANCOVA did not reveal significant effects. The horizontal lines represent medians and dotted lines interquartile ranges. *$p<0.01$.

NbM's fALFF relates to CSF ratio

In a next step, we used linear regressions on baseline fALFF values from NbM and EC, respectively, with CSF ratio as independent variable. It revealed a significant linear effect in the NbM (R^2=0.12, F(1, 69)=9.437, p=0.003, Fig. 7.2A) but not EC (R^2=0.031, F(1, 69)=2.206, p=0.142, Fig. 7.2B). A direct comparison of both correlations (NbM vs EC, one-tailed, which was justified by our a priori hypotheses) revealed a significant difference that was driven by a more negative correlation in NbM compared to EC (z=-1,94; p=0.0262; 95% CI: -0.3429 to 0.0015). Additionally, we analyzed both linear regressions independently for Aβ and pTau (Fig. S3.1). It revealed significant effects in NbM (pTau: R^2=0.057, F(1, 69)=4.19, p=0.044, Fig. S3.1A; Aβ: R^2=0.09, F(1, 69)=6.784, p=0.011, Fig. S3.1C) but not in EC (pTau: R^2=0.022, F(1, 69)=1.556, p=0.217, Fig. S3.1B; Aβ: R^2=0.003, F(1, 69)=0.234, p=0.63, Fig. S3.1D).

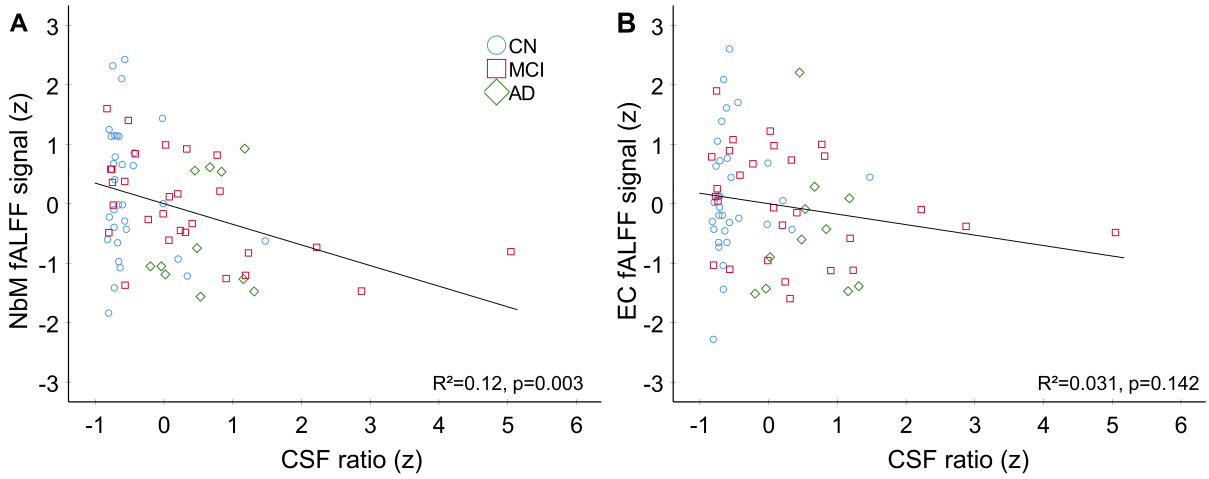

Figure 7.2. Linear regression for z-scored fALFF signal at baseline (t1) against z-scored CSF ratio for nucleus basalis of Meynert (NbM). (A) and entorhinal cortex (EC) (B). For the sake of visualization, the groups are plotted in different colors and shapes representing individual data points, blue circle for HC (n=32), red square for MCI (n=28) and green rhombus for AD (n=11). The linear regression was significant only in the NbM (A) (R^2=0.120, F(1, 69)=9.437, p=0.003) but not EC (B) (R^2=0.031, F(1, 69)=2.206, p=0.142), indicating a region-specific decrease in functional activity and proteinopathology.

Baseline signal in NbM predicts annual percentage signal change in EC fALFF

To further address the temporal changes in Alzheimer's disease progression, we examined whether the baseline signal in one region predicts the APSC in the other region. Here, in a first step, we used robust regression modeling for both competing models separately for nCSF vs. aCSF. They revealed no significant effect for NbM→EC in aCSF (R^2=0.263, F(7, 26)=1.33, p=0.277, Fig. 7.3A, Table S3.1), and no significant effect for NbM→EC in nCSF (R^2=0.296, F(7, 29)=1.74, p=0.138, Fig. 7.3B, Table S3.1). Similarly, there was no significant effect for EC→NbM in aCSF (R^2=0.137, F(7, 26)=0.587, p=0.76, Fig. 7.3D, Table S3.1), and no significant effect for EC→NbM in nCSF (R^2=0.175, F(7, 29)=0.88, p=0.534, Fig. 7.3E, Table S3.1).

In a second step, we analyzed both groups together by including CSF group in the two competing regression models. Importantly, we observed a statistically significant effect for the model NbM→EC (R^2=0.235, F(8, 62)=2.39, p=0.026, Fig. 7.3C, Table S3.1), with NbM as a significant predictor of EC's APSC (r=-0.3751, t(62)=-3.1445, p=0.003, confidence interval (CI): -0.6136 to -0.1366). The other regression model EC→NbM did not show a significant effect (R^2= 0.0884, F(8, 62)=0.751, p=0.646, Fig. 7.3F, Table S3.1). Replacing CSF as dichotomous predictor by the continuous CSF ratio did not change the results (i.e. significant effects for the model NbM→EC, p=0.021, but not EC→NbM, p=0.466).

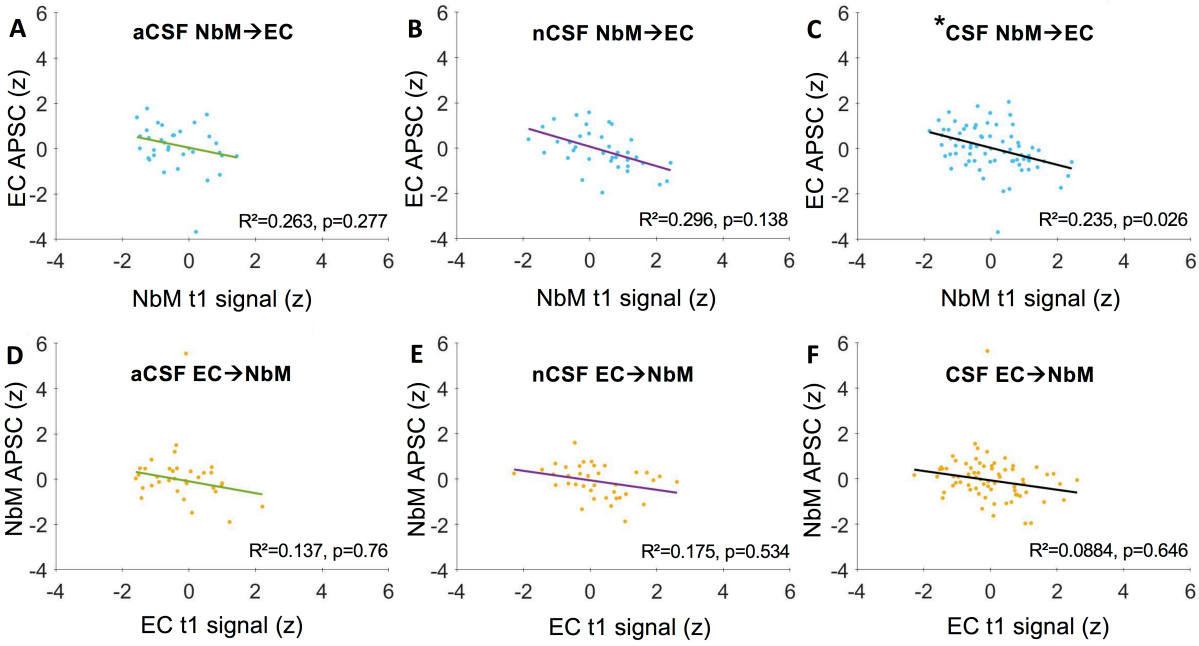

Figure 7.3. Baseline signal in the nucleus basalis of Meynert (NbM) predicts annual percentage signal change in the entorhinal cortex (EC) fALFF. Plots for robust regression models for NbM→EC (A, B, C), and EC→NbM (D, E, F). X-axis indicates z-scores for baseline (t1) signal and y-axis indicates z-scored APSC. There was a significant effect for NbM→EC (C, R^2=0.235, F(8, 62)=2.39, p=0.026), with NbM as a significant predictor of EC's APSC (r=-0.3751, t(62)=-3.1445, p=0.003). There was no significant effect for EC→NbM (R^2=0.0884, F(8, 62)=0.751, p=0.646). Each data point represents an individual value. aCSF=abnormal CSF (n=34); nCSF=normal CSF (n=37); CSF=CSF normal and abnormal included as a variable (n=71). *p<0.05. CSF group does not moderate the relationship of NbM and EC in fALFF

Finally, we performed two moderation analyses. The first model included baseline fALFF NbM as independent variable, fALFF EC APSC as dependent variable and CSF group as moderator. The model was statistically significant (R^2=0.2215, F(9,61)=3.4009, p=0.0019), with a significant direct effect of NbM→EC (t(61)=-3.442, p=0.001), but, no significant moderator effect (t(61)=0.4095, p=0.6836), which is in line with the robust regression analysis.

The second model included baseline fALFF EC as independent variable, fALFF NbM APSC as dependent variable and CSF group as moderator. The model was not statistically significant (R^2=0.0965, F(9,61)=0.7857, p=0.6303), which, again, is in line with the robust regression analysis.

The results for ReHo (Fig. S3.2A, S3.2B, S3.3, Table S3.2) and FC (Fig. S3.2C) can be found in the supplementary material S3.

Discussion

We investigated the functional properties of the human NbM and EC in relation to the disease progression of Alzheimer's disease based on longitudinal rsfMRI data and CSF markers of Aβ and pTau. With a focus on fALFF, our data provide evidence that spontaneous local brain activity in the NbM, but not EC, is reduced with CSF ratio, and, importantly, it predicts the annual percentage signal change in the interconnected EC independently from proteinopathology. As such, our findings extend previous anatomical studies in humans and animals by providing novel physiological insights into the pathological staging model of Alzheimer's disease suggesting the NbM as an early origin for subsequently affected brain regions possibly via a trans-synaptic mechanism.

Local spontaneous brain activity, as quantified by fALFF, was reduced in the NbM at baseline in the abnormal CSF group (Fig. 7.1B), and there was a linear reduction in fALFF activity with CSF-ratio (Fig. 7.2A). Importantly, both relationships were only observed in the NbM but not in the EC (Fig. 7.2B), which further underlines that the NbM is specifically vulnerable to Alzheimer's disease progression. In fact, pTau and Aβ are two proteins that have been associated with Alzheimer's disease (Alzheimer's Association, 2021) and the NbM is particularly vulnerable to the early accumulation of pTau (Braak & Del Tredici, 2011, 2015; Mesulam, 2004) and Aβ deposition (Baker-Nigh et al., 2015). This may be due to the fact that cholinergic BF neurons have rather large axons and arbors reaching into the entire central nervous system with high metabolic demands for maintenance, reparation, and transportation (H. Wu et al., 2014). At the same time, simply due to their sizes, they are more vulnerable to toxins (Mattson & Magnus, 2006), which may further promote disease progression.

The pathological staging model suggests a structural degeneration spreading from the NbM to the EC, which adds a crucial upstream link to Alzheimer's degeneration (Fernández-Cabello et al., 2020). Our functional data support such a view by showing that the NbM's baseline fALFF signal predicted the APSC in the EC (Fig. 7.3C) but not the reverse (Fig. 7.3F). Interestingly, this effect was independent of CSF status, which was further supported by the absence of a moderating effect of CSF. While this is compatible with a specific spread from NbM to EC, it also indicates that the putative functional consequences, namely changes in neural activation, are unrelated to pTau and Aβ. This apparently differs from anatomical changes from NbM to EC that were more pronounced in subjects with abnormal CSF

(Fernández-Cabello et al., 2020). From a physiological point of view, a trans-synaptic spread of proteins between anatomically interconnected brain regions is possible and has been shown in several animal studies. For instance, aggregates of tau can propagate from the EC to other limbic regions, including the dentate gyrus and hippocampal CA fields, followed by neocortical brain regions including the parietal cortex (de Calignon et al., 2012; Khan et al., 2014; L. Liu et al., 2012; Walker et al., 2013). *In vitro*, this can be enhanced by neural activity (J. W. Wu et al., 2016), which might help to explain why CSF status did not moderate the relationship between NbM activity and longitudinal changes in EC activity in our study. While this needs to be further investigated using larger and independent samples, our study is the first to show *in vivo* in humans that a neural signal in NbM can serve as a predictive marker for functional changes in the anatomically interconnected EC across healthy controls, MCIs and Alzheimer's disease patients.

Although fALFF is a prominent marker of spontaneous local brain activity (Zou et al., 2008; Zuo et al., 2010), only a limited number of studies used fALFF to investigate Alzheimer's disease. Importantly, previous work did not specifically focus on the NbM and EC but other, typically larger brain regions. It showed, for instance, decreased fALFF signals in the bilateral middle frontal and left precuneus in participants with positive Aβ (S.-M. Wang et al., 2021). In preclinical Alzheimer's disease, increases and decreases in fALFF were reported in the right inferior frontal gyrus (S.-M. Wang et al., 2021; Zeng et al., 2019), and in prodromal Alzheimer's disease lower fALFF signals could be shown in the bilateral precuneus, right middle frontal gyrus, right precentral gyrus, and postcentral gyrus. Finally, in Alzheimer's disease fALFF was increased in the right fusiform gyrus, MTL and inferior temporal gyrus, but decreased in the bilateral precuneus, left posterior cingulate cortex, left cuneus and superior occipital gyrus (Zeng et al., 2019). These partly divergent effects of fALFF associated with Alzheimer's disease might be explained by compensatory effects to maintain an adequate level of cognitive performance (Zeng et al., 2019), and could be a functional hallmark of neural aging (Cabeza et al., 2018) that needs further attention. Furthermore, since no significant effects in ReHo and FC were detected (see supplementary material S3), fALFF seems to be a particularly sensitive marker. Together, fALFF is highly sensitive to changes in neural activity associated with Alzheimer's disease even in rather small brain regions and therefore offers a useful marker in future studies.

Our analyses specifically focused on the functional properties of the human NbM and EC but no other interconnected brain regions that, according to the pathological staging model, follow the EC. These may include the parahippocampal cortex and hippocampal structures, as well as the parietal cortex (de Calignon et al., 2012; Fernández-Cabello et al., 2020; Khan et al., 2014; L. Liu et al., 2012; Walker et al., 2013). Along these lines, we included functional signals averaged from both hemispheres, which simplified our analyses, but it neglected possible lateralization effects (Banks et al., 2018; H. Liu et al., 2018). The NbM is most likely not the source of Alzheimer's disease pathology. In fact, post-mortem histology revealed the locus coeruleus as highly vulnerable to early degeneration even before the NbM (Beardmore et al., 2021; Zarow et al., 2003). Here, we did not include the locus coeruleus in our analyses since the rsfMRI data did not provide the necessary special resolution to extract a reliable signal from this rather small brain region (Beissner, 2015).

Finally, ADNI is a large multicenter study offering a rich and unique dataset. This also means that our rsfMRI data come from different MR scanners, possibly leading to a bias in image quality and extracted signal. Therefore, we only included high-quality data based on comparable protocols and within-subject measurements from the same scanner. We also employed appropriate covariates in our statistical models, and differences in scanning parameters (e.g., slice order or number of volumes) were accounted for during preprocessing (Badhwar et al., 2020; Teipel et al., 2017). Further, our main findings are based on analyses including a measure of APSC, which is robust against within-subject variability, e.g., because of the MR scanner. Along these lines, another possibility of analyzing our data would be based on the AT(N) framework, which includes markers of Aβ, tau (T) and neurodegeneration (N) (Jack et al., 2018). However, this requires a much larger sample of subjects than n=71, since at least three groups would need to be included (A-T-, A+T-, A+T+), and their distribution is typically unbalanced (see, e.g., Zeng et al. 2022). Furthermore, the necessary cut-off values, which are often based on PET but in some studies CSF, are not well defined (Jack et al., 2018). Finally, we wanted to analyze our data as similar as possible to Fernández-Cabello et al. (2020) in order to be comparable.

Functional activity in the human BF decreased with proteinopathology and predicted the functional decline within the interconnected EC independent from CSF status. As such, our findings extend the pathological staging model of Alzheimer's disease by giving novel insights into the functional properties of the underlying brain regions. From a more general

perspective, fALFF appears to be a suitable marker to further investigate functional brain changes associated with the progression of Alzheimer's disease.

8 General discussion

The aim of this thesis was to gain insights into the pathophysiology of AD progression. Therefore, four specific goals, examined by, respectively, four individual studies, have been formulated: investigating the exact nature of structural degeneration of the BF and interconnected MTL in MCI and AD patients (**study 1**); examining the predictive value of volumetric brain information (i.e., volume and thickness), socio-demographics, CSF, and APOE4 genotype status for AD onset and progression (**study 2**); testing the hypothesis that iron accumulations are a characteristic hallmark of AD and relate to cognitive decline (**study 3**); characterizing how functional activity markers in the BF relate to those in the EC depending on CSF assays along the progression of AD (including HC, MCI, and AD) (**study 4**). In the following, the findings of the respective studies (see sections 4-7) will be presented and discussed, with subsequent integration from a more general perspective based on current theories. Finally, implications and limitations with future directions will be elaborated.

8.1. Summary of findings

Based on our four studies, we could gain new insights into the underlying pathophysiology of AD progression. In **study 1** (Mieling, Meier, et al., 2023), using a coordinate-based VBM meta-analytic approach on 54 experiments and 2581 subjects, GM volume reductions in the cholinergic BF's NbM and MTL were compared between HC and MCI, as well as HC and AD. The meta-analyses revealed decreased GM in the bilateral BF's NbM in AD compared to HC. However, limited evidence was found for GM reductions in MCI compared to HC. Both MCI and AD patient groups showed less GM in the amygdala and hippocampus, with possibly more pronounced effects in the amygdala in AD.

In **study 2** (Mieling, Yousuf, et al., 2023), volumetric brain information (i.e., volume and thickness), socio-demographics, CSF assays (pTau/Aβ), and genotype information were analyzed using an XGBoost ML algorithm to classify cross-sectionally HC, MCI, and AD patients (n=568) and determine which factors best detect diagnostic states. Moreover, classifications were made within a longitudinal design on HC-to-MCI-converters and HC remaining stable (n=92) as well as MCI-to-AD-converters and MCI remaining stable (n=378), aiming to identify relevant features for the disease progression. The analyses achieved a global accuracy of 70-77%, and precision of 61-83%. The most important features were CSF status, hippocampal volume, EC thickness, and amygdala volume with a clear dissociation: while the hippocampus

contributed to the conversion from healthy aging to MCI, the EC played a more prominent role in the conversion from MCI to AD.

In **study 3** (Mieling et al., 2024), using a meta-analytical approach on 22 *in vivo* MRI experiments encompassing 1789 individuals, iron accumulation in the basal ganglia (putamen, globus pallidus, nucleus caudate), thalamus, and hippocampus in AD compared to HC was examined. Increased iron levels were found in the basal ganglia, with the strongest effect in the putamen, followed by the nucleus caudate. Notably, only the iron accumulation in the globus pallidus was negatively correlated with MMSE performance in AD.

In **study 4** (Mieling, Göttlich, et al., 2023) resting-state activity markers of local spontaneous brain activity, specifically fALFF, were investigated using longitudinal data (at baseline and two years later) based on CSF assays from ADNI (n=71). Two ROI analyses revealed a difference between normal and abnormal CSF at baseline in the NbM but not EC. Moreover, the local activity in the NbM linearly decreased, corresponding to the CSF ratio (pTau/Aβ), mirroring the disease progression. Finally, the baseline fALFF signal in the NbM predicted the annual percentage signal change of fALFF in the EC, but not vice versa, and independent of CSF status.

Gaining an understanding of the pathophysiological changes of AD progression requires considering both structural and functional brain alterations. This is particularly relevant given that structural degeneration is associated with neural compensation throughout adulthood (see Bunzeck et al. (2024) for an overview). Therefore, in the following, the findings of our four studies will be linked and discussed in the context of current theories.

8.2. Early degeneration of the basal forebrain's nucleus basalis of Meynert

The pathological staging model postulates that degeneration of the NbM occurs early and precedes the degeneration of the EC, which is associated with proteinopathies (Fernández-Cabello et al., 2020; Schmitz & Spreng, 2016). However, our understanding remains limited and there is a lack of structural meta-analytic and functional evidence. Therefore, **study 1** focused on investigating the exact nature of structural degeneration of the BF and interconnected MTL in patients with MCI and AD, using a meta-analytic approach. The results revealed GM volume reductions in the NbM in AD, supporting the notion of degeneration in this region. Interestingly, while decreases in GM volume in the EC have been revealed in previous studies (e.g., Fernández-Cabello et al., 2020), these were only partly observed in AD and were absent in MCI, suggesting that degeneration in the NbM precedes

degeneration in the EC. Based on these structural findings, **study 4** aimed to characterize how functional activity markers in the BF relate to those in the EC depending on CSF assays along the progression of AD (including HC, MCI, and AD). Remarkably, the local activity of the NbM linearly decreased with CSF assays. Moreover, it predicted the annual percentage signal change in the EC, not vice versa, independent of CSF status. Therefore, our results from **study 4** extend the pathological staging model to a functional level, supporting the link between proteinopathies and the NbM, as well as the spread of degeneration from NbM to EC. As such, our results emphasize the crucial role of the BF's NbM in AD, demonstrating both structural degeneration and functional alterations in this region.

Despite the evidence for the pathological staging model, our data also revealed limited support. Specifically, in **study 1**, we would have expected a reduction in GM volume in the NbM during earlier stages of AD, such as MCI, but this was only minimally observed. This discrepancy might be attributed to methodological reasons, as further addressed in the study's discussion (see section 4). In essence, the small number of included experiments in the comparison HC vs. MCI might lead to a lack of power and possibly limited spatial effects to a smaller portion of the NbM might not be detectable. Consequently, more precise microstructural MRI measures, such as multiparameter mapping (Leutritz et al., 2020), ideally combined with larger samples might address these methodological limitations.

Previous observations have shown that the spread of degeneration from NbM to EC is more pronounced in individuals with abnormal CSF and further moderated by CSF assays (Fernández-Cabello et al., 2020). While **study 1** did not include CSF assays due to missing data, the findings from **study 4** revealed that the prediction of neural activity from NbM's baseline signal to EC's annual percentage signal change is unrelated to pTau and Aβ. A possible explanation might be that the trans-synaptic spread of proteins between anatomically interconnected brain regions can be enhanced by neural activity as shown *in vitro* (J. W. Wu et al., 2016). Future studies with larger and independent samples need to investigate this further.

Considering that in **study 1** no longitudinal data was available, and in **study 4**, we focused exclusively on the NbM and EC, future studies should explore longitudinally how the degeneration spreads across the entire brain. This includes examining the spreading from the EC to more cortical regions, as suggested by the pathological staging model (Fernández-Cabello et al., 2020). Moreover, the NbM is unlikely to be the origin of AD pathology. For

instance, post-mortem histology has shown that the locus coeruleus represents an early vulnerability to degeneration before the NbM (Beardmore et al., 2021; Zarow et al., 2003). Due to the limited rsfMRI resolution in our study (Beissner, 2015), the locus coeruleus was not analyzed. This underscores the need to focus on that region in the future.

8.3. Bridging the amyloid and cholinergic hypotheses

A recent review article (Berry & Harrison, 2023) highlighted the importance of bridging the amyloid and cholinergic hypotheses (see section 2.2.2). While the pathological staging model, supported by both our structural and functional findings mentioned above, contributes to establishing such a connection by focusing on subsequent degenerative events from the BF's NbM to the EC related to proteinopathies, there is still a need to integrate both hypotheses (Berry & Harrison, 2023). Therefore, in the following, our findings will be addressed in the context of both the cholinergic and amyloid hypotheses.

Aiming to investigate the predictive value of volumetric brain information (i.e., volume and thickness), socio-demographics, CSF, and genotype for AD onset and progression, the results from **study 2** emphasize the importance of the MTL brain regions in AD, supporting the amyloid hypothesis. Specifically, in the cross-sectional classification of HC, MCI, and AD, hippocampal volume and EC thickness were identified as relevant features, with decreases in the measures resembling the disease progression (Kulason et al., 2020; Maruszak & Thuret, 2014). The longitudinal classifications revealed a dissociation of MTL regions, indicating that the hippocampus contributes to the conversion from HC to MCI, while the EC plays a pivotal role in the conversion from MCI to AD. These findings are only partly compatible with the amyloid hypothesis, assuming a spread from the transentorhinal and EC to the hippocampus and more cortical with disease progression (Braak & Braak, 1991; Corder et al., 2000; Duyckaerts et al., 1990; Jack et al., 2018; Jagust, 2018). Despite potential methodological limitations, such as a limited number of participants impacting this finding (further discussed in section 5), future longitudinal research on these brain regions is needed to exhibit the underlying mechanisms.

Supporting the cognitive consequences resulting from a spread of proteinopathology (Jack et al., 2018; Jagust, 2018) as proposed by the amyloid hypothesis, HC-converters showed significantly worse memory functioning (MEM) compared to HC-stable, aligning with the finding of reduced hippocampal volume in HC-converters. This result is thoroughly reviewed in the discussion section of **study 2**. Concisely, healthy older adults who later developed MCI

showed lower grey matter volume, particularly in the hippocampus, together with lower scores in several cognitive tests. Although based on our data, it remains inconclusive whether structural degeneration precedes cognitive decline, as suggested before (Jack et al., 2018; Jack & Holtzman, 2013), hippocampal volume and cognitive abilities can offer noteworthy biomarkers for predicting MCI in cognitively healthy older adults.

Studies 1 and **2** highlight the crucial role of the degeneration of the hippocampus and amygdala in the progression of AD, aligning with previous studies (e.g., Y.L. Rao et al., 2022; Stouffer et al., 2024). It was shown that the hippocampus and amygdala were affected by GM volume reductions in MCI and AD, with presumably stronger reductions in the amygdala in AD (**study 1**). Additionally, the hippocampal volume was highly relevant in classifying HC, MCI, and AD cross-sectionally and, as already discussed above, in the longitudinal classification of HC-converters and HC-stable. When classifying MCI-converters and MCI-stable longitudinally, the amygdala emerged as the second most important feature without CSF and the third most relevant feature with CSF included (**study 2**). These findings suggest that the amyloid and cholinergic hypotheses may be linked. Both regions are affected by the trans-synaptic spreading of proteinopathies as suggested by the amyloid hypothesis (Braak & Braak, 1991; Corder et al., 2000; Duyckaerts et al., 1990; Jack et al., 2018; Jagust, 2018), and both receive cholinergic input, which underlines the involvement of the BFCS. While the hippocampus receives a high density of cholinergic axons from the medial septum and vertical diagonal band nuclei (Ch1 and Ch2) (Mesulam et al., 1992; Mesulam & Geula, 1988), the amygdala is innervated from the NbM (Ch4) (Mesulam et al., 1983). This aligns with previous studies indicating that BF atrophy is selectively associated with atrophy in their target regions, including the hippocampus and the amygdala (Cantero et al., 2016, 2020). Thus, degeneration of the BF, specifically here, the NbM, may lead to a spread and acceleration of the AD pathology (Fernández-Cabello et al., 2020; Schmitz & Spreng, 2016). It is important to note that we focused solely on the NbM due to its early vulnerability to AD. However, including the other BFCS nuclei, such as Ch1 and Ch2, could provide further insights into their roles in AD progression and enhance the understanding of the disease.

The BFCS is interconnected with other subcortical systems beyond the cholinergic innervations to the MTL and amygdala, for example, the noradrenergic locus coeruleus, serotonergic dorsal raphe nucleus, and the dopaminergic substantia nigra/ventral tegmental neurons (Bari et al., 2020; Gaykema & Zaborszky, 1997; Halberstadt & Balaban, 2008;

Hornung, 2003; Rho et al., 2018; Zaborszky & Cullinan, 1996). These interconnections may influence the spread of AD pathology, while AD pathology itself may impact these interconnections (Berry & Harrison, 2023). As such, the dysfunction of one brain region may cascade across interconnected regions, contributing to the complexity of AD pathology and underlining the relevance of both the cholinergic and amyloid hypotheses (e.g., Fernández-Cabello et al., 2020; Schmitz et al., 2018; Schmitz & Spreng, 2016). Therefore, future work should focus on exploring the intricate interplay between these brain regions and their associated neurotransmitter systems in the context of AD pathology.

The BF was not included in **study 2** because the focus was on the 2010 Desikan-Killiany atlas (Desikan et al., 2006). Therefore, no conclusions can be drawn regarding the contribution of the NbM. This aspect can be addressed in subsequent studies that incorporate the structural information of the NbM in their analyses. It would be relevant to explore further the overlap between the cholinergic and amyloid hypotheses, including investigating the bidirectional effects of proteinopathies and degeneration in the BF and MTL regions. For instance, longitudinal investigations could provide insights into shared characteristics of the BF and MTL regions, such as the hippocampus (Berry & Harrison, 2023). Furthermore, since NbM's local activity represents a promising marker for detecting functional brain changes associated with AD pathology (**study 4**), and considering that incorporating various features such as clinical, cognitive, genetic, PET, and CSF status has been demonstrated to increase model accuracies (Vieira et al., 2017), it would be beneficial to replicate the analyses of **study 2**, with additional features (e.g., functional MRI, PET, and cognitive markers) on larger samples. This approach could offer increased statistical power and give a deeper understanding of the observed brain changes. In summary, our functional and structural results suggest a link between the cholinergic and amyloid hypothesis, emphasizing the vulnerability of the BF and MTL regions to AD pathology.

8.4. Insights into biomarker-based classification of Alzheimer's disease

The pathological staging model and the cholinergic as well as amyloid hypothesis are based on findings from various biomarkers, which have become increasingly important in AD research and diagnosis (Jack et al., 2016). A current approach to integrating biomarkers represents the AT(N) framework (Jack et al., 2018) (see 2.2). From a broader perspective, our findings not only support such a classification system but further highlight the relevance of neurodegeneration biomarkers, the (N) component, which will be discussed in the following.

It is important to note that the (N) component presents certain limitations. Unlike components A and T, it is less clear to what extent neurodegeneration can be attributed to AD or other comorbid conditions. Therefore, (N) has been placed in parenthesis (Jack et al., 2018). As such, there is a need for investigations into the (N) component's implications for AD diagnosis and treatment.

Our cross-sectional and longitudinal analyses in **study 2** underscore the importance of the proteinopathies Aβ and tau, corresponding to the categories A and T in the AT(N) framework. In the classification of HC, MCI and AD, CSF information emerged as the most relevant feature, consistent with previous studies indicating that CSF biomarkers can outperform other features obtained from structural MRI, PET and APOE (Gupta et al., 2019; L. Xie et al., 2023), capturing distinct biochemical aspects of AD pathology (Vemuri et al., 2009) and providing complementary information to structural MRI measures (Gupta et al., 2019). This might lead to preceding abnormalities in CSF biomarkers, specifically Aβ, before neurodegeneration, including structural MRI changes and cognitive impairment (Jack et al., 2018; Jack & Holtzman, 2013). Hereby, blood plasma biomarkers have gained importance, especially due to their less invasive nature compared to CSF drawings (Delaby et al., 2022). It was shown that cognitive performance correlates with plasma biomarkers, particularly pTau, underlining that blood plasma represents a valuable tool to facilitate data acquisition. Thus, utilizing blood plasma instead of CSF drawings may be advantageous in future studies (Toniolo et al., 2024).

In the longitudinal analysis of **study 2** investigating MCI-converters and MCI-stable, the EC remained the most relevant feature in the prediction when the CSF status was included. The CSF assays served as the second predictive feature, which could have critical clinical implications considering that MRI is less invasive than CSF drawings. From a physiological perspective, the EC atrophy might be stronger than the accumulation of Aβ and pTau captured with CSF in disease development. In broader terms, while proteinopathologies might be predominant in earlier AD stages, neurodegeneration of the EC can occur in the following conversion from MCI to AD, supported by the AT(N) framework (Jack et al., 2018). However, it should be noted that the ML approach combines features, leading to accurate classifications rather than comparing their effects individually. Such a comparison, preferably in longitudinal designs, could be addressed in subsequent work.

Besides alterations in GM and thickness as well as local activity, iron measured using MRI has gained relevance as a potential biomarker for neurodegeneration (Ficiarà et al., 2021), but meta-analytic evidence from *in vivo* imaging studies is missing. Therefore, using meta-analyses, **study 3** tested the hypothesis that iron accumulations are a characteristic hallmark of AD and relate to cognitive decline. Our findings of iron accumulations in the basal ganglia, along with the observed negative correlation between increased iron levels in the globus pallidus and cognitive performance in AD, support the notion that iron is a hallmark of AD and closely related to cognitive function. This implies that iron serves as a crucial indicator of neurodegeneration in AD, extending the (N) component within the AT(N) framework. The globus pallidus is a central element of the substantia nigra (SN)/ventral tegemental area (VTA) hippocampus loop, relevant for modulating dopamine (DA) release in response to novelty, thereby influencing memory formation and encoding new information into long-term memory (Lisman et al., 2011; Lisman & Grace, 2005). While iron is essential for DA synthesis (Zecca et al., 2004), an excessive deposition can lower DA production (Hare & Double, 2016; Zecca et al., 2004). For instance, it was shown that excessive iron accumulation can lead to cognitive impairment in healthy older adults (Biel et al., 2021; Steiger et al., 2016). Therefore, the accumulation of iron within the bilateral pallidum may disrupt the loop, resulting in declarative learning and memory impairments, suggesting a link between iron levels in the basal ganglia and disruptions in the dopaminergic system.

The dopaminergic system, including the SN/VTA, receives cholinergic projections that modulate its activity via muscarinic and nicotinic receptors (Futami et al., 1995; Oakman et al., 1995). For instance, in rat models, the nonselective muscarinic antagonist scopolamine enhanced dopamine release into the striatum (Chapman et al., 1997; Miller & Blaha, 2004), while cholinergic agonists diminished it (Miller & Blaha, 2004). In humans, during novelty processing, the dopamine precursor levodopa and the AChE inhibitor galantamine altered hemodynamic activity in the SN/VTA and MTL (Bunzeck et al., 2014). Therefore, the dopaminergic and cholinergic systems are closely related (e.g., Mark et al., 2011; Threlfell et al., 2012). Our findings, as previously discussed, support the role of the BFCS in the spread of degeneration across interconnected brain regions, such as the MTL and amygdala, within the progression of AD. This mechanism could also extend to the globus pallidus via dopaminergic pathways, suggesting that alterations in the BFCS (**studies 1** and **4**) could potentially impact the iron levels within the basal ganglia (**study 3**). More specifically, compromised cholinergic

function could exacerbate iron dysregulation through its connections to the dopaminergic system. Understanding the complex interplay among iron accumulation, the dopaminergic system, and the BFCS is crucial for gaining insight into the pathophysiology of AD and developing therapeutic targets, highlighting the need for further research to explore these interactions more thoroughly.

Beyond the basal ganglia, the meta-analysis within **study 3** revealed significant effects in the hippocampus and the thalamus, indicating higher iron levels in AD compared to HC. However, these effects were partly inconsistent, and a publication bias was observed for both. To better understand the involvement of the hippocampus and thalamus, as well as other brain regions that might be affected by elevated iron levels, future studies should focus on larger datasets investigating the whole brain instead of ROIs and use longitudinal designs to detect changes in disease progression. Previous work has demonstrated that iron accumulation co-localizes with AD pathology (Ayton et al., 2020; Bulk et al., 2018; Spotorno et al., 2020; Van Bergen et al., 2018; Van Duijn et al., 2017). Additionally, iron promotes oxidative stress and facilitates the aggregation of Aβ peptides. Both iron and oxidative stress are assumed to be mediators of Aβ-toxicity (Rottkamp et al., 2001). Considering this, future work could be based on the AT(N) framework, allowing a more precise exploration of changes in iron levels.

The central role of volumetric changes in the BF (**study 1**), and MTL brain regions (**study 1** and **2**) with AD progression highlights the importance of the neurodegeneration component in the AT(N) framework. Moreover, our studies expand upon the framework by emphasizing the crucial involvement of the amygdala (**studies 1** and **2**). This aligns with previous research indicating an early structural degeneration of the amygdala in AD (Kilimann et al., 2014; Planche et al., 2022; Poulin et al., 2011; da Silva Filho et al., 2017) and suggests this region as a potential imaging biomarker, further supported in a recent review article (Stouffer et al., 2024). Therefore, future research may benefit from focusing on the amygdala and its putative role in AD diagnosis and progression. Additionally, our findings suggest that iron accumulations in the basal ganglia could be explored as an emerging biomarker in following studies. Besides the structural findings, functional local alterations also appear promising for AD research, as observed in **study 4,** which might be regarded in the future by applying the AT(N) framework. Finally, the (N) component offers crucial pathologic staging information,

supported by our results based on structural MRI (**studies 1-3**), emphasizing the necessity of including the (N) in the categorization of AT(N) and investigating it further in future studies.

8.5 Further implications

Considering all four studies, we observed that structural and functional changes occur along the progression of AD in various brain regions. This supports the notion that structural and functional MRI can serve as relevant biomarkers for detecting AD changes. Moreover, our findings align with previous studies demonstrating the importance of structural MRI and rsfMRI for diagnosing MCI and AD (e.g., Ju et al., 2019; Khatri & Kwon, 2022; Van Maurik et al., 2017). Given that MRI is a non-invasive technique, it allows repeated measurements to monitor the disease progression without negative consequences for the patient. This offers a valuable tool for the early detection and tracking of AD, which is crucial for clinicians in providing appropriate individual treatment for patients (Dubois et al., 2023).

Our focus on structural and functional brain changes in AD offers novel insights into the disease's underlying mechanisms, which is particularly important for developing effective therapeutic approaches. Current anti-AD drugs slow cognitive decline and postpone AD's onset but do not offer a cure (Peng et al., 2023). Detailed information on current drug treatment and its advances can be found elsewhere (Briggs et al., 2016; Conti Filho et al., 2023). Our findings suggest an early degeneration of the NbM, the largest cholinergic nuclei within the BF (Mesulam & Geula, 1988), that may provoke disrupted cholinergic signaling. This supports the relevance of treatments with AChE inhibitors (Sharma, 2019). Interestingly, previous studies provided hints towards structural and functional differences associated with AChE inhibitors (e.g., Blautzik et al., 2016; Goveas et al., 2011; P. Müller et al., 2021; Richter et al., 2018), indicating a link between ACh pathology and functional as well structural alterations in AD. However, it is important to note that AChE inhibition drugs showed a modest symptomatic benefit (Mohammad et al., 2017) of cognitive decline with side effects for the patients (Briggs et al., 2016; Mohammad et al., 2017), emphasizing the need for further development. Here, our results may help to shape future investigations by showing the relevance of the BF and the utility of MRI in detecting changes due to AD.

The importance of CSF assays for diagnostic classification and decreasing NbM activity with disease progression, as observed by our studies, supports the advances of anti-Aβ drugs as well as anti-tau drugs, addressing their production, preventing deposition, and accelerating their clearance (Peng et al., 2023). Although the efficacy of drugs targeting Aβ and tau in AD

has been limited (Briggs et al., 2016; Conti Filho et al., 2023), understanding the impact of Aβ and tau pathology on FC and brain atrophy in the early stages of the disease could inform future drug trials. Furthermore, our findings highlight iron as a hallmark of AD, suggesting further investigation into iron chelation therapy that focuses on the reduction of iron overload (see Mobarra et al. (2016) for an overview). Cell culture studies have shown promising findings demonstrating that an iron chelator reduces APP (Avramovich-Tirosh et al., 2007; Reznichenko et al., 2006). However, clinical evidence requires deeper investigation (Crichton et al., 2019), which could be facilitated through iron-sensitive MRI monitoring.

Previous findings indicated that single-target drugs (e.g., AChE inhibitors) focusing on a single pathology could not effectively treat AD (Mohammad et al., 2017). Consequently, there is a need to investigate multi-target drugs that address multiple symptoms of AD (Peng et al., 2023). Our findings support the potential of multi-target drugs, as indicated by observed MRI alterations associated with the BFCS, Aβ, pTau, and iron. Finally, future research needs to investigate the extent to which MRI changes are associated with therapeutic approaches and cognitive performance.

8.6 Limitations

Our studies demonstrate several strengths, including the use of multiple powerful approaches such as meta-analyses (V. I. Müller et al., 2018), ML based classification (Franciotti et al., 2023), and the extensive database ADNI. These are based on elaborated and reviewed measurements, large sample sizes, various MRI measurements and markers, CSF drawings, and longitudinal assessments of AD progression. Moreover, our studies address the need to investigate the overlap of the cholinergic and amyloid hypothesis as well as the underlying neuronal mechanisms of the onset and progression of AD that are not fully understood (e.g., Berry & Harrison, 2023). Despite these strengths, it is crucial to acknowledge certain limitations that need to be considered in future work. While the study-specific aspects have been presented in their respective sections (4-7), the following section will discuss the main limitations that apply to all.

The studies included in this thesis independently examined structural and functional changes using different methodologies and samples. Therefore, we cannot conclude their link with AD progression. Since we observed both types of changes along the progression of AD, there might be a correlation in the specific brain regions. This is supported by a recent multi-modal meta-analysis that identified overlapping functional and structural alterations in the

posterior cingulate gyrus/precuneus and parahippocampal gyrus in AD (Tang et al., 2024). Notably, functional changes were observed preceding structural changes (Johnson et al., 2012; Sperling, 2011; Warren & Moustafa, 2023) and compensating for them (see Bunzeck et al. (2024) for an overview). However, the exact interrelationship between both is not well understood. Future studies may combine both to gain a deeper understanding of the relationship during the progression of AD.

We exclusively focused on the study-specific modalities (i.e., brain volumetric information, iron accumulation, and local activity), but other sensitive biomarkers for AD, such as PET or DTI were not included (Chapleau et al., 2022; Esrael et al., 2021). Different modalities might capture distinct aspects of AD pathology and offer a more comprehensive understanding of the pathophysiology (J. Kim et al., 2022). Along these lines, it has been revealed that the combination of MRI with other biomarkers, such as PET and cognitive tests improves the diagnostic accuracy of MCI and AD (Aberathne et al., 2023; Odusami et al., 2023). Therefore, future studies should focus on combining MRI with other techniques using a multimodal approach to investigate the role of BF, MTL, and basal ganglia in AD. Here, adopting a longitudinal design might be beneficial for understanding the underlying mechanisms driving AD progression.

Subsequent studies might investigate structural and functional changes based on the AT(N) framework (Jack et al., 2018). While participants in **studies 1, 2,** and **3** were included based on their clinical diagnosis, and in **study 4** based on their CSF status, utilizing the AT(N) framework could allow a more detailed investigation (Jack et al., 2018). The reasons the AT(N) framework was not chosen in our studies are brief: in most of the included original studies the AT(N) markers were not assessed (**studies 1** and **3**), the number of subjects was limited (**studies 2** and **4**), the groups (A-T-, A+T-, A+T+) show typically unequal distributions (see, e.g., Zeng et al. (2022)), cut-off values are inadequately defined (Jack et al., 2018) (all four studies).

8.7 Conclusion

The findings presented in this thesis offer novel insights into the pathophysiology of AD, emphasizing the central role of the BF, MTL, and basal ganglia in AD progression. Our investigation revealed structural and functional alterations in the cholinergic BF's NbM and interconnected MTL, supporting an early degeneration of the NbM followed by the EC. Importantly, our results suggest a novel dissociation regarding the disease progression: the hippocampus seems particularly relevant for the progression from HC to MCI, while the EC is

prominent for the conversion from MCI to AD. Additionally, iron accumulation, particularly in the basal ganglia, was identified as a hallmark of AD, associated with cognitive impairment. These findings suggest a potential complex interplay of structural and functional alterations in the BF, MTL, and basal ganglia along AD progression. Future studies should further explore this relationship as well as possible underlying pathological mechanisms. Longitudinal multimodal studies may present a promising approach to address this.

References

2023 Alzheimer's disease facts and figures. (2023). *Alzheimer's & Dementia*, *19*(4), 1598–1695. https://doi.org/10.1002/alz.13016

Aberathne, I., Kulasiri, D., & Samarasinghe, S. (2023). Detection of Alzheimer's disease onset using MRI and PET neuroimaging: Longitudinal data analysis and machine learning. *Neural Regeneration Research*, *18*(10), 2134. https://doi.org/10.4103/1673-5374.367840

Acquas, E., Wilson, C., & Fibiger, H. C. (1996). Conditioned and Unconditioned Stimuli Increase Frontal Cortical and Hippocampal Acetylcholine Release: Effects of Novelty, Habituation, and Fear. *Journal of Neuroscience*, *16*(9), 3089–3096. https://doi.org/10.1523/JNEUROSCI.16-09-03089.1996

Agosta, F., Pievani, M., Sala, S., Geroldi, C., Galluzzi, S., Frisoni, G., & Filippi, M. (2011). White Matter Damage in Alzheimer Disease and Its Relationship to Gray Matter Atrophy. *Radiology*, *258*, 853–863. https://doi.org/10.1148/radiol.10101284

Aigner, T. G., & Mishkin, M. (1986). The effects of physostigmine and scopolamine on recognition memory in monkeys. *Behav Neural Biol*, *45*(1), 81–87.

Aisen, P. S., Petersen, R. C., Donohue, M. C., Gamst, A., Raman, R., Thomas, R. G., Walter, S., Trojanowski, J. Q., Shaw, L. M., Beckett, L. A., Jack, C. R., Jagust, W., Toga, A. W., Saykin, A. J., Morris, J. C., Green, R. C., Weiner, M. W., & Alzheimer's Disease Neuroimaging Initiative. (2010). Clinical core of the Alzheimer's disease neuroimaging initiative: Progress and plans. *Alzheimer's & Dementia*, *6*(3), 239–246. https://doi.org/10.1016/j.jalz.2010.03.006

Aisen, P. S., Petersen, R. C., Donohue, M., Weiner, M. W., & Alzheimer's Disease Neuroimaging Initiative. (2015). Alzheimer's Disease Neuroimaging Initiative 2 Clinical Core: Progress and plans. *Alzheimer's & Dementia*, *11*(7), 734–739. https://doi.org/10.1016/j.jalz.2015.05.005

Albert, M. S., DeKosky, S. T., Dickson, D., Dubois, B., Feldman, H. H., Fox, N. C., Gamst, A., Holtzman, D. M., Jagust, W. J., Petersen, R. C., Snyder, P. J., Carrillo, M. C., Thies, B., & Phelps, C. H. (2011). The diagnosis of mild cognitive impairment due to Alzheimer's disease: Recommendations from the National Institute on Aging-Alzheimer's Association workgroups on diagnostic guidelines for Alzheimer's disease. *Alzheimer's & Dementia*, *7*(3), 270–279. https://doi.org/10.1016/j.jalz.2011.03.008

Albert, M., Zhu, Y., Moghekar, A., Mori, S., Miller, M. I., Soldan, A., Pettigrew, C., Selnes, O., Li, S., & Wang, M.-C. (2018). Predicting progression from normal cognition to mild cognitive impairment for individuals at 5 years. *Brain*, *141*(3), 877–887. https://doi.org/10.1093/brain/awx365

Altamura, S., & Muckenthaler, M. U. (2009). Iron Toxicity in Diseases of Aging: Alzheimer's Disease, Parkinson's Disease and Atherosclerosis. *Journal of Alzheimer's Disease*, *16*(4), 879–895. https://doi.org/10.3233/JAD-2009-1010

Alzheimer's Association. (2021). Alzheimer's disease facts and figures. *Alzheimer's & Dementia*, *17*(3), 327–406. https://doi.org/10.1002/alz.12328

Amalric, M., Pattij, T., Sotiropoulos, I., Silva, J. M., Sousa, N., Ztaou, S., Chiamulera, C.,

Wahlberg, L. U., Emerich, D. F., & Paolone, G. (2021). Where Dopaminergic and Cholinergic Systems Interact: A Gateway for Tuning Neurodegenerative Disorders. *Frontiers in Behavioral Neuroscience*, *15*. https://www.frontiersin.org/articles/10.3389/fnbeh.2021.661973

Amunts, K., Kedo, O., Kindler, M., Pieperhoff, P., Mohlberg, H., Shah, N. J., Habel, U., Schneider, F., & Zilles, K. (2005). Cytoarchitectonic mapping of the human amygdala, hippocampal region and entorhinal cortex: Intersubject variability and probability maps. *Anatomy and Embryology*, *210*(5–6), 343–352. https://doi.org/10.1007/s00429-005-0025-5

Aquino, D., Bizzi, A., Grisoli, M., Garavaglia, B., Bruzzone, M. G., Nardocci, N., Savoiardo, M., & Chiapparini, L. (2009). Age-related Iron Deposition in the Basal Ganglia: Quantitative Analysis in Healthy Subjects. *Radiology*, *252*(1), 165–172. https://doi.org/10.1148/radiol.2522081399

Arendt, T., Bigl, V., Tennstedt, A., & Arendt, A. (1985). Neuronal loss in different parts of the nucleus basalis is related to neuritic plaque formation in cortical target areas in alzheimer's disease. *Neuroscience*, *14*(1), 1–14. https://doi.org/10.1016/0306-4522(85)90160-5

Arendt, T., Brückner, M. K., Morawski, M., Jäger, C., & Gertz, H.-J. (2015). Early neurone loss in Alzheimer's disease: Cortical or subcortical? *Acta Neuropathologica Communications*, *3*, 10. https://doi.org/10.1186/s40478-015-0187-1

Arrondo, P., Elía-Zudaire, Ó., Martí-Andrés, G., Fernández-Seara, M. A., & Riverol, M. (2022). Grey matter changes on brain MRI in subjective cognitive decline: A systematic review. *Alzheimer's Research & Therapy*, *14*(1), 98. https://doi.org/10.1186/s13195-022-01031-6

Ashburner, J. (2007). A fast diffeomorphic image registration algorithm. *NeuroImage*, *38*(1), 95–113. https://doi.org/10.1016/j.neuroimage.2007.07.007

Ashburner, J., & Friston, K. J. (2000). Voxel-Based Morphometry—The Methods. *NeuroImage*, *11*(6), 805–821. https://doi.org/10.1006/nimg.2000.0582

Atri, A., Sherman, S., Norman, K. A., Kirchhoff, B. A., Nicolas, M. M., Greicius, M. D., Cramer, S. C., Breiter, H. C., Hasselmo, M. E., & Stern, C. E. (2004). Blockade of central cholinergic receptors impairs new learning and increases proactive interference in a word paired-associate memory task. *Behav Neurosci*, *118*(1), 223–236.

Augustine, J. (1996). Circuitry and functional aspects of the insular lobe in primates including humans. *Brain Research Reviews*, *22*(3), 229–244. https://doi.org/10.1016/S0165-0173(96)00011-2

Avramovich-Tirosh, Y., Reznichenko, L., Amit, T., Zheng, H., Fridkin, M., Weinreb, O., Mandel, S., & Youdim, M. (2007). Neurorescue Activity, APP Regulation and Amyloid-β Peptide Reduction by Novel Multi-Functional Brain Permeable Iron- Chelating-Antioxidants,M-30 and Green Tea Polyphenol, EGCG. *Current Alzheimer Research*, *4*(4), 403–411. https://doi.org/10.2174/156720507781788927

Aydin, O., & Yassikaya, M. Y. (2022). Validity and Reliability Analysis of the PlotDigitizer Software Program for Data Extraction from Single-Case Graphs. *Perspectives on Behavior Science*, *45*(1), 239–257. https://doi.org/10.1007/s40614-021-00284-0

Ayton, S., Fazlollahi, A., Bourgeat, P., Raniga, P., Ng, A., Lim, Y. Y., Diouf, I., Farquharson, S., Fripp, J., Ames, D., Doecke, J., Desmond, P., Ordidge, R., Masters, C. L., Rowe, C. C., Maruff, P., Villemagne, V. L., Australian Imaging Biomarkers and Lifestyle (AIBL) Research Group, Salvado, O., & Bush, A. I. (2017). Cerebral quantitative susceptibility mapping predicts amyloid-β-related cognitive decline. *Brain: A Journal of Neurology*, *140*(8), 2112–2119. https://doi.org/10.1093/brain/awx137

Ayton, S., Wang, Y., Diouf, I., Schneider, J. A., Brockman, J., Morris, M. C., & Bush, A. I. (2020). Brain iron is associated with accelerated cognitive decline in people with Alzheimer pathology. *Molecular Psychiatry*, *25*(11), 2932–2941. https://doi.org/10.1038/s41380-019-0375-7

Backman, L., Nyberg, L., Lindenberger, U., Li, S. C., & Farde, L. (2006). The correlative triad among aging, dopamine, and cognition: Current status and future prospects. *Neurosci Biobehav Rev*, *30*(6), 791–807.

Badhwar, A., Collin-Verreault, Y., Orban, P., Urchs, S., Chouinard, I., Vogel, J., Potvin, O., Duchesne, S., & Bellec, P. (2020). Multivariate consistency of resting-state fMRI connectivity maps acquired on a single individual over 2.5 years, 13 sites and 3 vendors. *NeuroImage*, *205*, 116210. https://doi.org/10.1016/j.neuroimage.2019.116210

Bai, F., Zhang, Z., Yu, H., Shi, Y., Yuan, Y., Zhu, W., Zhang, X., & Qian, Y. (2008). Default-mode network activity distinguishes amnestic type mild cognitive impairment from healthy aging: A combined structural and resting-state functional MRI study. *Neuroscience Letters*, *438*(1), 111–115. https://doi.org/10.1016/j.neulet.2008.04.021

Baker-Nigh, A., Vahedi, S., Davis, E. G., Weintraub, S., Bigio, E. H., Klein, W. L., & Geula, C. (2015). Neuronal amyloid-β accumulation within cholinergic basal forebrain in ageing and Alzheimer's disease. *Brain*, *138*(6), 1722–1737. https://doi.org/10.1093/brain/awv024

Ballinger, E. C., Ananth, M., Talmage, D. A., & Role, L. W. (2016). Basal Forebrain Cholinergic Circuits and Signaling in Cognition and Cognitive Decline. *Neuron*, *91*(6), 1199–1218. https://doi.org/10.1016/j.neuron.2016.09.006

Bamidis, P. D., Vivas, A. B., Styliadis, C., Frantzidis, C., Klados, M., Schlee, W., Siountas, A., & Papageorgiou, S. G. (2014). A review of physical and cognitive interventions in aging. *Neuroscience & Biobehavioral Reviews*, *44*, 206–220. https://doi.org/10.1016/j.neubiorev.2014.03.019

Banks, S. J., Zhuang, X., Bayram, E., Bird, C., Cordes, D., Caldwell, J. Z. K., & Cummings, J. L. (2018). Default Mode Network Lateralization and Memory in Healthy Aging and Alzheimer's Disease. *Journal of Alzheimer's Disease*, *66*(3), 1223–1234. https://doi.org/10.3233/JAD-180541

Barbeau, E. J., Ranjeva, J. P., Didic, M., Confort-Gouny, S., Felician, O., Soulier, E., Cozzone, P. J., Ceccaldi, M., & Poncet, M. (2008). Profile of memory impairment and gray matter loss in amnestic mild cognitive impairment. *Neuropsychologia*, *46*(4), 1009–1019. https://doi.org/10.1016/j.neuropsychologia.2007.11.019

Bari, B., Chokshi, V., & Schmidt, K. (2020). Locus coeruleus-norepinephrine: Basic functions and insights into Parkinson's disease. *Neural Regeneration Research*, *15*(6), 1006. https://doi.org/10.4103/1673-5374.270297

Baron, J. C., Chételat, G., Desgranges, B., Perchey, G., Landeau, B., de la Sayette, V., & Eustache, F. (2001). In vivo mapping of gray matter loss with voxel-based morphometry in mild Alzheimer's disease. *NeuroImage*, *14*(2), 298–309. https://doi.org/10.1006/nimg.2001.0848

Bartus, R. T. (2000). On Neurodegenerative Diseases, Models, and Treatment Strategies: Lessons Learned and Lessons Forgotten a Generation Following the Cholinergic Hypothesis. *Experimental Neurology*, *163*(2), 495–529. https://doi.org/10.1006/exnr.2000.7397

Bartus, R. T., Dean, R. L., Beer, B., & Lippa, A. S. (1982). The Cholinergic Hypothesis of Geriatric Memory Dysfunction. *Science*, *217*(4558), 408–414. https://doi.org/10.1126/science.7046051

Bartzokis, G. (2011). Alzheimer's disease as homeostatic responses to age-related myelin breakdown. *Neurobiology of Aging*, *32*(8), 1341–1371. https://doi.org/10.1016/j.neurobiolaging.2009.08.007

Bartzokis, G., Beckson, M., Hance, D. B., Marx, P., Foster, J. A., & Marder, S. R. (1997). MR evaluation of age-related increase of brain iron in young adult and older normal males. *Magnetic Resonance Imaging*, *15*(1), 29–35. https://doi.org/10.1016/S0730-725X(96)00234-2

Bartzokis, G., Sultzer, D., Cummings, J., Holt, L. E., Hance, D. B., Henderson, V. W., & Mintz, J. (2000). In Vivo Evaluation of Brain Iron in Alzheimer Disease Using Magnetic Resonance Imaging. *Archives of General Psychiatry*, *57*(1), 47–53. https://doi.org/10.1001/archpsyc.57.1.47

Bartzokis, G., Sultzer, D., Mintz, J., Holt, L. E., Marx, P., Kelly Phelan, C., & Marder, S. R. (1994). In vivo evaluation of brain iron in Alzheimer's disease and normal subjects using MRI. *Biological Psychiatry*, *35*(7), 480–487. https://doi.org/10.1016/0006-3223(94)90047-7

Bartzokis, G., Tishler, T. A., Shin, I.-S., Lu, P. H., & Cummings, J. L. (2004). Brain Ferritin Iron as a Risk Factor for Age at Onset in Neurodegenerative Diseases. *Annals of the New York Academy of Sciences*, *1012*(1), 224–236. https://doi.org/10.1196/annals.1306.019

Basaia, S., Agosta, F., Wagner, L., Canu, E., Magnani, G., Santangelo, R., & Filippi, M. (2019). Automated classification of Alzheimer's disease and mild cognitive impairment using a single MRI and deep neural networks. *NeuroImage: Clinical*, *21*, 101645. https://doi.org/10.1016/j.nicl.2018.101645

Bateman, R. J., Aisen, P. S., De Strooper, B., Fox, N. C., Lemere, C. A., Ringman, J. M., Salloway, S., Sperling, R. A., Windisch, M., & Xiong, C. (2010). Autosomal-dominant Alzheimer's disease: A review and proposal for the prevention of Alzheimer's disease. *Alzheimer's Research & Therapy*, *3*(1), 1. https://doi.org/10.1186/alzrt59

Bauer, M., Kluge, C., Bach, D., Bradbury, D., Heinze, H. J., Dolan, R. J., & Driver, J. (2012). Cholinergic Enhancement of Visual Attention and Neural Oscillations in the Human Brain. *Current Biology*, *22*(5), 397–402. https://doi.org/10.1016/j.cub.2012.01.022

Baxter, L. C., Sparks, D. L., Johnson, S. C., Lenoski, B., Lopez, J. E., Connor, D. J., & Sabbagh, M. N. (2006). Relationship of cognitive measures and gray and white matter in Alzheimer's disease. *Journal of Alzheimer's Disease: JAD*, *9*(3), 253–260. https://doi.org/10.3233/jad-2006-9304

Beardmore, R., Hou, R., Darekar, A., Holmes, C., & Boche, D. (2021). The Locus Coeruleus in Aging and Alzheimer's Disease: A Postmortem and Brain Imaging Review. *Journal of Alzheimer's Disease*, *83*(1), 5–22. https://doi.org/10.3233/JAD-210191

Beheshti, I., Demirel, H., & Matsuda, H. (2017). Classification of Alzheimer's disease and prediction of mild cognitive impairment-to-Alzheimer's conversion from structural magnetic resource imaging using feature ranking and a genetic algorithm. *Computers in Biology and Medicine*, *83*, 109–119. https://doi.org/10.1016/j.compbiomed.2017.02.011

Beissner, F. (2015). Functional MRI of the Brainstem: Common Problems and their Solutions. *Clinical Neuroradiology*, *25*(S2), 251–257. https://doi.org/10.1007/s00062-015-0404-0

Bejanin, A., Schonhaut, D. R., La Joie, R., Kramer, J. H., Baker, S. L., Sosa, N., Ayakta, N., Cantwell, A., Janabi, M., Lauriola, M., O'Neil, J. P., Gorno-Tempini, M. L., Miller, Z. A., Rosen, H. J., Miller, B. L., Jagust, W. J., & Rabinovici, G. D. (2017). Tau pathology and neurodegeneration contribute to cognitive impairment in Alzheimer's disease. *Brain*, *140*(12), 3286–3300. https://doi.org/10.1093/brain/awx243

Bellenguez, C., Grenier-Boley, B., & Lambert, J.-C. (2020). Genetics of Alzheimer's disease: Where we are, and where we are going. *Current Opinion in Neurobiology*, *61*, 40–48. https://doi.org/10.1016/j.conb.2019.11.024

Bellenguez, C., Küçükali, F., Jansen, I. E., Kleineidam, L., Moreno-Grau, S., Amin, N., Naj, A. C., Campos-Martin, R., Grenier-Boley, B., Andrade, V., Holmans, P. A., Boland, A., Damotte, V., Van Der Lee, S. J., Costa, M. R., Kuulasmaa, T., Yang, Q., De Rojas, I., Bis, J. C., … Lambert, J.-C. (2022). New insights into the genetic etiology of Alzheimer's disease and related dementias. *Nature Genetics*, *54*(4), 412–436. https://doi.org/10.1038/s41588-022-01024-z

Bell-McGinty, S., Lopez, O. L., Meltzer, C. C., Scanlon, J. M., Whyte, E. M., Dekosky, S. T., & Becker, J. T. (2005). Differential cortical atrophy in subgroups of mild cognitive impairment. *Archives of Neurology*, *62*(9), 1393–1397. https://doi.org/10.1001/archneur.62.9.1393

Berry, A. S., & Harrison, T. M. (2023). New perspectives on the basal forebrain cholinergic system in Alzheimer's disease. *Neuroscience & Biobehavioral Reviews*, *150*, 105192. https://doi.org/10.1016/j.neubiorev.2023.105192

Biel, D., Steiger, T. K., & Bunzeck, N. (2021). Age-related iron accumulation and demyelination in the basal ganglia are closely related to verbal memory and executive functioning. *Scientific Reports*, *11*(1), 9438. https://doi.org/10.1038/s41598-021-88840-1

Bilgel, M., Wong, D. F., Moghekar, A. R., Ferrucci, L., Resnick, S. M., & the Alzheimer's Disease Neuroimaging Initiative. (2022). Causal links among amyloid, tau, and neurodegeneration. *Brain Communications*, *4*(4), fcac193. https://doi.org/10.1093/braincomms/fcac193

Bischoff-Grethe, A., & Fennema-Notestine, C. (2023). Structural magnetic resonance imaging. In G. G. Brown, B. Crosson, K. Y. Haaland, & T. Z. King (Eds.), *APA handbook of neuropsychology, Volume 2: Neuroscience and neuromethods (Vol. 2).* (pp. 535–550). American Psychological Association. https://doi.org/10.1037/0000308-026

Biswal, B., Zerrin Yetkin, F., Haughton, V. M., & Hyde, J. S. (1995). Functional connectivity in the motor cortex of resting human brain using echo-planar mri. *Magnetic Resonance*

in Medicine, *34*(4), 537–541. https://doi.org/10.1002/mrm.1910340409

Blautzik, J., Keeser, D., Paolini, M., Kirsch, V., Berman, A., Coates, U., Reiser, M., Teipel, S. J., & Meindl, T. (2016). Functional connectivity increase in the default-mode network of patients with Alzheimer's disease after long-term treatment with Galantamine. *European Neuropsychopharmacology*, *26*(3), 602–613. https://doi.org/10.1016/j.euroneuro.2015.12.006

Böhle, M., Eitel, F., Weygandt, M., & Ritter, K. (2019). Layer-Wise Relevance Propagation for Explaining Deep Neural Network Decisions in MRI-Based Alzheimer's Disease Classification. *Frontiers in Aging Neuroscience*, *11*, 194. https://doi.org/10.3389/fnagi.2019.00194

Bonthius, D. J., Solodkin, A., & Van Hoesen, G. W. (2005). Pathology of the Insular Cortex in Alzheimer Disease Depends on Cortical Architecture: *Journal of Neuropathology and Experimental Neurology*, *64*(10), 910–922. https://doi.org/10.1097/01.jnen.0000182983.87106.d1

Borenstein, M., Hedges, L. V., Higgins, J. P. T., & Rothstein, H. R. (Eds.). (2009). *Introduction to meta-analysis*. John Wiley & Sons.

Boxer, A. L., Rankin, K. P., Miller, B. L., Schuff, N., Weiner, M., Gorno-Tempini, M.-L., & Rosen, H. J. (2003). Cinguloparietal atrophy distinguishes Alzheimer disease from semantic dementia. *Archives of Neurology*, *60*(7), 949–956. https://doi.org/10.1001/archneur.60.7.949

Bozzali, M., Filippi, M., Magnani, G., Cercignani, M., Franceschi, M., Schiatti, E., Castiglioni, S., Mossini, R., Falautano, M., Scotti, G., Comi, G., & Falini, A. (2006). The contribution of voxel-based morphometry in staging patients with mild cognitive impairment. *Neurology*, *67*(3), 453–460. https://doi.org/10.1212/01.wnl.0000228243.56665.c2

Bozzali, M., Giulietti, G., Basile, B., Serra, L., Spanò, B., Perri, R., Giubilei, F., Marra, C., Caltagirone, C., & Cercignani, M. (2012). Damage to the cingulum contributes to Alzheimer's disease pathophysiology by deafferentation mechanism. *Human Brain Mapping*, *33*(6), 1295–1308. https://doi.org/10.1002/hbm.21287

Braak, H., & Braak, E. (1991). Neuropathological stageing of Alzheimer-related changes. *Acta Neuropathologica*, *82*(4), 239–259. https://doi.org/10.1007/BF00308809

Braak, H., & Del Tredici, K. (2011). The pathological process underlying Alzheimer's disease in individuals under thirty. *Acta Neuropathologica*, *121*(2), 171–181. https://doi.org/10.1007/s00401-010-0789-4

Braak, H., & Del Tredici, K. (2015). The preclinical phase of the pathological process underlying sporadic Alzheimer's disease. *Brain*, *138*(10), 2814–2833. https://doi.org/10.1093/brain/awv236

Brenneis, C., Wenning, G., Egger, K., Schocke, M., Trieb, T., Seppi, K., Marksteiner, J., Ransmayr, G., Benke, T., & Poewe, W. (2004). Basal forebrain atrophy is a distinctive pattern in dementia with Lewy bodies. *Neuroreport*, *15*, 1711–1714. https://doi.org/10.1097/01.wnr.0000136736.73895.03

Brenowitz, W. D., Hubbard, R. A., Keene, C. D., Hawes, S. E., Longstreth, W. T., Woltjer, R. L., & Kukull, W. A. (2017). Mixed neuropathologies and estimated rates of clinical progression in a large autopsy sample. *Alzheimer's & Dementia*, *13*(6), 654–662.

https://doi.org/10.1016/j.jalz.2016.09.015

Brett, M., Anton, J. L., Valabrgue, R., & Poline, J.-B. (2002). Region of interest analysis using an SPM toolbox. Presented at the 8th International Conference on Functional Mapping of the Human Brain, June 2-6, 2002, Sendai, Japan. *Neuroimage*, *13*, 210–217.

Briggs, R., Kennelly, S. P., & O'Neill, D. (2016). Drug treatments in Alzheimer's disease. *Clinical Medicine*, *16*(3), 247–253. https://doi.org/10.7861/clinmedicine.16-3-247

Broks, P., Preston, G. C., Traub, M., Poppleton, P., Ward, C., & Stahl, S. M. (1988). Modelling dementia: Effects of scopolamine on memory and attention. *Neuropsychologia*, *26*(5), 685–700. https://doi.org/10.1016/0028-3932(88)90004-8

Brossollet, I., Gallet, Q., Favre, P., & Houenou, J. (2023). Machine Learning and Brain Imaging for Psychiatric Disorders: New Perspectives. In O. Colliot (Ed.), *Machine Learning for Brain Disorders* (pp. 1009–1036). Springer US. https://doi.org/10.1007/978-1-0716-3195-9_32

Buccafusco, J. J., Letchworth, S. R., Bencherif, M., & Lippiello, P. M. (2005). Long-lasting cognitive improvement with nicotinic receptor agonists: Mechanisms of pharmacokinetic-pharmacodynamic discordance. *Trends Pharmacol Sci*, *26*(7), 352–360.

Bulk, M., Kenkhuis, B., Van Der Graaf, L. M., Goeman, J. J., Natté, R., & Van Der Weerd, L. (2018). Postmortem T2*- Weighted MRI Imaging of Cortical Iron Reflects Severity of Alzheimer's Disease. *Journal of Alzheimer's Disease*, *65*(4), 1125–1137. https://doi.org/10.3233/JAD-180317

Bunzeck, N., Guitart-Masip, M., Dolan, R. J., & Duzel, E. (2014). Pharmacological Dissociation of Novelty Responses in the Human Brain. *Cerebral Cortex*, *24*(5), 1351–1360. https://doi.org/10.1093/cercor/bhs420

Bunzeck, N., Schütze, H., Stallforth, S., Kaufmann, J., Düzel, S., Heinze, H.-J., & Düzel, E. (2007). Mesolimbic Novelty Processing in Older Adults. *Cerebral Cortex*, *17*(12), 2940–2948. https://doi.org/10.1093/cercor/bhm020

Bunzeck, N., Steiger, T. K., Krämer, U. M., Luedtke, K., Marshall, L., Obleser, J., & Tune, S. (2024). Trajectories and contributing factors of neural compensation in healthy and pathological aging. *Neuroscience & Biobehavioral Reviews*, *156*, 105489. https://doi.org/10.1016/j.neubiorev.2023.105489

Button, K. S., Ioannidis, J. P. A., Mokrysz, C., Nosek, B. A., Flint, J., Robinson, E. S. J., & Munafò, M. R. (2013). Power failure: Why small sample size undermines the reliability of neuroscience. *Nature Reviews Neuroscience*, *14*(5), 365–376. https://doi.org/10.1038/nrn3475

Cabeza, R., Albert, M., Belleville, S., Craik, F. I. M., Duarte, A., Grady, C. L., Lindenberger, U., Nyberg, L., Park, D. C., Reuter-Lorenz, P. A., Rugg, M. D., Steffener, J., & Rajah, M. N. (2018). Maintenance, reserve and compensation: The cognitive neuroscience of healthy ageing. *Nature Reviews Neuroscience*, 1. https://doi.org/10.1038/s41583-018-0068-2

Cabeza, R., Dolcos, F., Graham, R., & Nyberg, L. (2002). Similarities and Differences in the Neural Correlates of Episodic Memory Retrieval and Working Memory. *NeuroImage*, *16*(2), 317–330. https://doi.org/10.1006/nimg.2002.1063

Cai, Y., Xie, M., Su, Y., Tong, Z., Wu, X., Xu, W., Li, J., Zhao, F., Dang, C., Chen, G., Lan, L., Shen, J., & Zheng, Y. (2020). Aberrant Functional and Causal Connectivity in Acute Tinnitus With Sensorineural Hearing Loss. *Frontiers in Neuroscience*, *14*, 592. https://doi.org/10.3389/fnins.2020.00592

Cantero, J. L., Atienza, M., Lage, C., Zaborszky, L., Vilaplana, E., Lopez-Garcia, S., Pozueta, A., Rodriguez-Rodriguez, E., Blesa, R., Alcolea, D., Lleo, A., Sanchez-Juan, P., Fortea, J., & Alzheimer's Disease Neuroimaging Initiative. (2020). Atrophy of Basal Forebrain Initiates with Tau Pathology in Individuals at Risk for Alzheimer's Disease. *Cerebral Cortex*, *30*(4), 2083–2098. https://doi.org/10.1093/cercor/bhz224

Cantero, J. L., Zaborszky, L., & Atienza, M. (2016). Volume Loss of the Nucleus Basalis of Meynert is Associated with Atrophy of Innervated Regions in Mild Cognitive Impairment. *Cerebral Cortex*, cercor;bhw195v1. https://doi.org/10.1093/cercor/bhw195

Caroli, A., Testa, C., Geroldi, C., Nobili, F., Barnden, L. R., Guerra, U. P., Bonetti, M., & Frisoni, G. B. (2007). Cerebral perfusion correlates of conversion to Alzheimer's disease in amnestic mild cognitive impairment. *Journal of Neurology*, *254*(12), 1698–1707. https://doi.org/10.1007/s00415-007-0631-7

Cavedo, E., Grothe, M. J., Colliot, O., Lista, S., Chupin, M., Dormont, D., Houot, M., Lehéricy, S., Teipel, S., Dubois, B., & Hampel, H. (2017). Reduced basal forebrain atrophy progression in a randomized Donepezil trial in prodromal Alzheimer's disease. *Scientific Reports*, *7*(1), 11706. https://doi.org/10.1038/s41598-017-09780-3

Chapleau, M., Iaccarino, L., Soleimani-Meigooni, D., & Rabinovici, G. D. (2022). The Role of Amyloid PET in Imaging Neurodegenerative Disorders: A Review. *Journal of Nuclear Medicine*, *63*(Supplement 1), 13S-19S. https://doi.org/10.2967/jnumed.121.263195

Chapman, C. A., Yeomans, J. S., Blaha, C. D., & Blackburn, J. R. (1997). Increased striatal dopamine efflux follows scopolamine administered systemically or to the tegmental pedunculopontine nucleus. *Neuroscience*, *76*(1), 177–186.

Chen, G., Xu, T., Yan, Y., Zhou, Y., Jiang, Y., Melcher, K., & Xu, H. E. (2017). Amyloid beta: Structure, biology and structure-based therapeutic development. *Acta Pharmacologica Sinica*, *38*(9), 1205–1235. https://doi.org/10.1038/aps.2017.28

Chen, T., & Guestrin, C. (2016). XGBoost: A Scalable Tree Boosting System. *Proceedings of the 22nd ACM SIGKDD International Conference on Knowledge Discovery and Data Mining*, 785–794. https://doi.org/10.1145/2939672.2939785

Chen, Y., & Yu, Y. (2023). Tau and neuroinflammation in Alzheimer's disease: Interplay mechanisms and clinical translation. *Journal of Neuroinflammation*, *20*(1), 165. https://doi.org/10.1186/s12974-023-02853-3

Cheng, C. P.-W., Cheng, S.-T., Tam, C. W.-C., Chan, W.-C., Chu, W. C.-W., & Lam, L. C.-W. (2018). Relationship between Cortical Thickness and Neuropsychological Performance in Normal Older Adults and Those with Mild Cognitive Impairment. *Aging and Disease*, *9*(6), 1020. https://doi.org/10.14336/AD.2018.0125

Chételat, G., Desgranges, B., Sayette, V., Viader, F., Eustache, F., & Baron, J.-C. (2002). Mapping gray matter loss with voxel-based morphometry in mild cognitive impairment. *Neuroreport*, *13*, 1939–1943. https://doi.org/10.1097/00001756-200210280-00022

Chiang, G. C., Cho, J., Dyke, J., Zhang, H., Zhang, Q., Tokov, M., Nguyen, T., Kovanlikaya, I., Amoashiy, M., De Leon, M., & Wang, Y. (2022). Brain oxygen extraction and neural tissue susceptibility are associated with cognitive impairment in older individuals. *Journal of Neuroimaging*, *32*(4), 697–709. https://doi.org/10.1111/jon.12990

Choi, J. Y., Cho, H., Ahn, S. J., Lee, J. H., Ryu, Y. H., Lee, M. S., & Lyoo, C. H. (2018). Off-Target ^{18} F-AV-1451 Binding in the Basal Ganglia Correlates with Age-Related Iron Accumulation. *Journal of Nuclear Medicine*, *59*(1), 117–120. https://doi.org/10.2967/jnumed.117.195248

Christen-Zaech, S., Kraftsik, R., Pillevuit, O., Kiraly, M., Martins, R., Khalili, K., & Miklossy, J. (2003). Early Olfactory Involvement in Alzheimer's Disease. *Canadian Journal of Neurological Sciences / Journal Canadien Des Sciences Neurologiques*, *30*(1), 20–25. https://doi.org/10.1017/S0317167100002389

Clavaguera, F., Bolmont, T., Crowther, R. A., Abramowski, D., Frank, S., Probst, A., Fraser, G., Stalder, A. K., Beibel, M., Staufenbiel, M., Jucker, M., Goedert, M., & Tolnay, M. (2009). Transmission and spreading of tauopathy in transgenic mouse brain. *Nature Cell Biology*, *11*(7), 909–913. https://doi.org/10.1038/ncb1901

Cogswell, P. M., & Fan, A. P. (2023). Multimodal comparisons of QSM and PET in neurodegeneration and aging. *NeuroImage*, *273*, 120068. https://doi.org/10.1016/j.neuroimage.2023.120068

Cogswell, P. M., Wiste, H. J., Senjem, M. L., Gunter, J. L., Weigand, S. D., Schwarz, C. G., Arani, A., Therneau, T. M., Lowe, V. J., Knopman, D. S., Botha, H., Graff-Radford, J., Jones, D. T., Kantarci, K., Vemuri, P., Boeve, B. F., Mielke, M. M., Petersen, R. C., & Jack, C. R. (2021). Associations of quantitative susceptibility mapping with Alzheimer's disease clinical and imaging markers. *NeuroImage*, *224*, 117433. https://doi.org/10.1016/j.neuroimage.2020.117433

Cohen, J. (2013). *Statistical Power Analysis for the Behavioral Sciences* (0 ed.). Routledge. https://doi.org/10.4324/9780203771587

Colloby, S. J., O'Brien, J. T., & Taylor, J.-P. (2014). Patterns of cerebellar volume loss in dementia with Lewy bodies and Alzheimer's disease: A VBM-DARTEL study. *Psychiatry Research*, *223*(3), 187–191. https://doi.org/10.1016/j.pscychresns.2014.06.006

Colovic, M. B., Krstic, D. Z., Lazarevic-Pasti, T. D., Bondzic, A. M., & Vasic, V. M. (2013). Acetylcholinesterase Inhibitors: Pharmacology and Toxicology. *Current Neuropharmacology*, *11*(3), 315–335. https://doi.org/10.2174/1570159X11311030006

Contestabile, A. (2011). The history of the cholinergic hypothesis. *Behavioural Brain Research*, *221*(2), 334–340. https://doi.org/10.1016/j.bbr.2009.12.044

Conti Filho, C. E., Loss, L. B., Marcolongo-Pereira, C., Rossoni Junior, J. V., Barcelos, R. M., Chiarelli-Neto, O., Silva, B. S. D., Passamani Ambrosio, R., Castro, F. C. D. A. Q., Teixeira, S. F., & Mezzomo, N. J. (2023). Advances in Alzheimer's disease's pharmacological treatment. *Frontiers in Pharmacology*, *14*, 1101452. https://doi.org/10.3389/fphar.2023.1101452

Corder, E. H., Saunders, A. M., Strittmatter, W. J., Schmechel, D. E., Gaskell, P. C., Small, G. W., Roses, A. D., Haines, J. L., & Pericak-Vance, M. A. (1993). Gene Dose of Apolipoprotein E Type 4 Allele and the Risk of Alzheimer's Disease in Late Onset Families. *Science*,

261(5123), 921–923. https://doi.org/10.1126/science.8346443

Corder, E. H., Woodbury, M. A., Volkmann, I., Madsen, D. K., Bogdanovic, N., & Winblad, B. (2000). Density profiles of Alzheimer disease regional brain pathology for the Huddinge brain bank: Pattern recognition emulates and expands upon Braak staging. *Experimental Gerontology*, *35*(6–7), 851–864. https://doi.org/10.1016/S0531-5565(00)00147-9

Counts, S. E., Ikonomovic, M. D., Mercado, N., Vega, I. E., & Mufson, E. J. (2017). Biomarkers for the Early Detection and Progression of Alzheimer's Disease. *Neurotherapeutics*, *14*(1), 35–53. https://doi.org/10.1007/s13311-016-0481-z

Crane, P. K., Carle, A., Gibbons, L. E., Insel, P., Mackin, R. S., Gross, A., Jones, R. N., Mukherjee, S., Curtis, S. M., Harvey, D., Weiner, M., & Mungas, D. (2012). Development and assessment of a composite score for memory in the Alzheimer's Disease Neuroimaging Initiative (ADNI). *Brain Imaging and Behavior*, *6*(4), 502–516. https://doi.org/10.1007/s11682-012-9186-z

Crichton, R. (2001). *Inorganic Biochemistry of Iron Metabolism: From Molecular Mechanisms to Clinical Consequences* (1st ed.). Wiley. https://doi.org/10.1002/0470845791

Crichton, R. R., Ward, R. J., & Hider, R. C. (2019). The Efficacy of Iron Chelators for Removing Iron from Specific Brain Regions and the Pituitary—Ironing out the Brain. *Pharmaceuticals*, *12*(3), 138. https://doi.org/10.3390/ph12030138

Crowther, R. A. (1991). Straight and paired helical filaments in Alzheimer disease have a common structural unit. *Proceedings of the National Academy of Sciences*, *88*(6), 2288–2292. https://doi.org/10.1073/pnas.88.6.2288

Cummings, J. (2021). New approaches to symptomatic treatments for Alzheimer's disease. *Molecular Neurodegeneration*, *16*(1), 2. https://doi.org/10.1186/s13024-021-00424-9

Da Costa, J. P., Vitorino, R., Silva, G. M., Vogel, C., Duarte, A. C., & Rocha-Santos, T. (2016). A synopsis on aging—Theories, mechanisms and future prospects. *Ageing Research Reviews*, *29*, 90–112. https://doi.org/10.1016/j.arr.2016.06.005

Dale, A. M., Fischl, B., & Sereno, M. I. (1999). Cortical Surface-Based Analysis. *NeuroImage*, *9*(2), 179–194. https://doi.org/10.1006/nimg.1998.0395

Dale, A. M., & Sereno, M. I. (1993). Improved Localizadon of Cortical Activity by Combining EEG and MEG with MRI Cortical Surface Reconstruction: A Linear Approach. *Journal of Cognitive Neuroscience*, *5*(2), 162–176. https://doi.org/10.1162/jocn.1993.5.2.162

Damulina, A., Pirpamer, L., Soellradl, M., Sackl, M., Tinauer, C., Hofer, E., Enzinger, C., Gesierich, B., Duering, M., Ropele, S., Schmidt, R., & Langkammer, C. (2020). Cross-sectional and Longitudinal Assessment of Brain Iron Level in Alzheimer Disease Using 3-T MRI. *Radiology*, *296*(3), 619–626. https://doi.org/10.1148/radiol.2020192541

Dashjamts, T., Yoshiura, T., Hiwatashi, A., Yamashita, K., Monji, A., Ohyagi, Y., Kamano, H., Kawashima, T., Kira, J.-I., & Honda, H. (2011). Simultaneous arterial spin labeling cerebral blood flow and morphological assessments for detection of Alzheimer's disease. *Academic Radiology*, *18*(12), 1492–1499. https://doi.org/10.1016/j.acra.2011.07.015

Daugherty, A., & Raz, N. (2013). Age-related differences in iron content of subcortical nuclei observed in vivo: A meta-analysis. *NeuroImage*, *70*, 113–121.

https://doi.org/10.1016/j.neuroimage.2012.12.040

Davies, P., & Maloney, A. J. (1976). Selective loss of central cholinergic neurons in Alzheimer's disease. *Lancet (London, England)*, *2*(8000), 1403. https://doi.org/10.1016/s0140-6736(76)91936-x

Davis, M., O`Connell, T., Johnson, S., Cline, S., Merikle, E., Martenyi, F., & Simpson, K. (2018). Estimating Alzheimer's Disease Progression Rates from Normal Cognition Through Mild Cognitive Impairment and Stages of Dementia. *Current Alzheimer Research*, *15*(8), 777–788. https://doi.org/10.2174/1567205015666180119092427

de Lacalle, S., Cooper, J. D., Svendsen, C. N., Dunnett, S. B., & Sofroniew, M. V. (1996). Reduced retrograde labelling with fluorescent tracer accompanies neuronal atrophy of basal forebrain cholinergic neurons in aged rats. *Neuroscience*, *75*(1), 19–27. https://doi.org/10.1016/0306-4522(96)00239-4

Deary, I. J., Corley, J., Gow, A. J., Harris, S. E., Houlihan, L. M., Marioni, R. E., Penke, L., Rafnsson, S. B., & Starr, J. M. (2009). Age-associated cognitive decline. *British Medical Bulletin*, *92*(1), 135–152. https://doi.org/10.1093/bmb/ldp033

de Calignon, A., Polydoro, M., Suárez-Calvet, M., William, C., Adamowicz, D. H., Kopeikina, K. J., Pitstick, R., Sahara, N., Ashe, K. H., Carlson, G. A., Spires-Jones, T. L., & Hyman, B. T. (2012). Propagation of Tau Pathology in a Model of Early Alzheimer's Disease. *Neuron*, *73*(4), 685–697. https://doi.org/10.1016/j.neuron.2011.11.033

Delaby, C., Alcolea, D., Hirtz, C., Vialaret, J., Kindermans, J., Morichon, L., Fortea, J., Belbin, O., Gabelle, A., Blennow, K., Zetterberg, H., Lleó, A., & Lehmann, S. (2022). Blood amyloid and tau biomarkers as predictors of cerebrospinal fluid profiles. *Journal of Neural Transmission*, *129*(2), 231–237. https://doi.org/10.1007/s00702-022-02474-9

Dennis, E. L., & Thompson, P. M. (2014). Functional Brain Connectivity Using fMRI in Aging and Alzheimer's Disease. *Neuropsychology Review*, *24*(1), 49–62. https://doi.org/10.1007/s11065-014-9249-6

Denver, P., & McClean, P. (2018). Distinguishing normal brain aging from the development of Alzheimer's disease: Inflammation, insulin signaling and cognition. *Neural Regeneration Research*, *13*(10), 1719. https://doi.org/10.4103/1673-5374.238608

Dermody, N., Hornberger, M., Piguet, O., Hodges, J. R., & Irish, M. (2016). Prospective Memory Impairments in Alzheimer's Disease and Behavioral Variant Frontotemporal Dementia: Clinical and Neural Correlates. *Journal of Alzheimer's Disease: JAD*, *50*(2), 425–441. https://doi.org/10.3233/JAD-150871

Dermody, N., Wong, S., Ahmed, R., Piguet, O., Hodges, J. R., & Irish, M. (2016). Uncovering the Neural Bases of Cognitive and Affective Empathy Deficits in Alzheimer's Disease and the Behavioral-Variant of Frontotemporal Dementia. *Journal of Alzheimer's Disease: JAD*, *53*(3), 801–816. https://doi.org/10.3233/JAD-160175

Desikan, R. S., Ségonne, F., Fischl, B., Quinn, B. T., Dickerson, B. C., Blacker, D., Buckner, R. L., Dale, A. M., Maguire, R. P., Hyman, B. T., Albert, M. S., & Killiany, R. J. (2006). An automated labeling system for subdividing the human cerebral cortex on MRI scans into gyral based regions of interest. *NeuroImage*, *31*(3), 968–980. https://doi.org/10.1016/j.neuroimage.2006.01.021

Di Paola, M., Macaluso, E., Carlesimo, G. A., Tomaiuolo, F., Worsley, K. J., Fadda, L., &

Caltagirone, C. (2007). Episodic memory impairment in patients with Alzheimer's disease is correlated with entorhinal cortex atrophy. A voxel-based morphometry study. *Journal of Neurology*, *254*(6), 774–781. https://doi.org/10.1007/s00415-006-0435-1

Dickstein, D. L., Kabaso, D., Rocher, A. B., Luebke, J. I., Wearne, S. L., & Hof, P. R. (2007). Changes in the structural complexity of the aged brain. *Aging Cell*, *6*(3), 275–284. https://doi.org/10.1111/j.1474-9726.2007.00289.x

Diedenhof, B., & Musch, J. (2015). Correction: Cocor: A Comprehensive Solution for the Statistical Comparison of Correlations. *PLOS ONE*, *10*(6), e0131499. https://doi.org/10.1371/journal.pone.0131499

Ding, B., Chen, K.-M., Ling, H.-W., Sun, F., Li, X., Wan, T., Chai, W.-M., Zhang, H., Zhan, Y., & Guan, Y.-J. (2009). Correlation of iron in the hippocampus with MMSE in patients with Alzheimer's disease. *Journal of Magnetic Resonance Imaging*, *29*(4), 793–798. https://doi.org/10.1002/jmri.21730

Diogo, V. S., Ferreira, H. A., Prata, D., & for the Alzheimer's Disease Neuroimaging Initiative. (2022). Early diagnosis of Alzheimer's disease using machine learning: A multi-diagnostic, generalizable approach. *Alzheimer's Research & Therapy*, *14*(1), 107. https://doi.org/10.1186/s13195-022-01047-y

Dixon, S. J., Lemberg, K. M., Lamprecht, M. R., Skouta, R., Zaitsev, E. M., Gleason, C. E., Patel, D. N., Bauer, A. J., Cantley, A. M., Yang, W. S., Morrison, B., & Stockwell, B. R. (2012). Ferroptosis: An Iron-Dependent Form of Nonapoptotic Cell Death. *Cell*, *149*(5), 1060–1072. https://doi.org/10.1016/j.cell.2012.03.042

Dolan, R. J. (2002). Emotion, Cognition, and Behavior. *Science*, *298*(5596), 1191–1194. https://doi.org/10.1126/science.1076358

Doll, S., & Conrad, M. (2017). Iron and ferroptosis: A still ill-defined liaison. *IUBMB Life*, *69*(6), 423–434. https://doi.org/10.1002/iub.1616

Doucette, R., Fisman, M., Hachinski, V. C., & Mersky, H. (1986). Cell Loss from the Nucleus Basalis of Meynert in Alzheimer's Disease. *Canadian Journal of Neurological Sciences / Journal Canadien Des Sciences Neurologiques*, *13*(S4), 435–440. https://doi.org/10.1017/S0317167100037070

Du, L., Zhao, Z., Cui, A., Zhu, Y., Zhang, L., Liu, J., Shi, S., Fu, C., Han, X., Gao, W., Song, T., Xie, L., Wang, L., Sun, S., Guo, R., & Ma, G. (2018). Increased Iron Deposition on Brain Quantitative Susceptibility Mapping Correlates with Decreased Cognitive Function in Alzheimer's Disease. *ACS Chemical Neuroscience*, *9*(7), 1849–1857. https://doi.org/10.1021/acschemneuro.8b00194

Dubois, B., Von Arnim, C. A. F., Burnie, N., Bozeat, S., & Cummings, J. (2023). Biomarkers in Alzheimer's disease: Role in early and differential diagnosis and recognition of atypical variants. *Alzheimer's Research & Therapy*, *15*(1), 175. https://doi.org/10.1186/s13195-023-01314-6

Dunn, A. R., O'Connell, K. M. S., & Kaczorowski, C. C. (2019). Gene-by-environment interactions in Alzheimer's disease and Parkinson's disease. *Neuroscience & Biobehavioral Reviews*, *103*, 73–80. https://doi.org/10.1016/j.neubiorev.2019.06.018

Dusek, P., Hofer, T., Alexander, J., Roos, P. M., & Aaseth, J. O. (2022). Cerebral Iron Deposition

in Neurodegeneration. *Biomolecules*, *12*(5), 714. https://doi.org/10.3390/biom12050714

Duyckaerts, C., Delaère, P., Hauw, J.-J., Abbamondi-Pinto, A. L., Sorbi, S., Allen, I., Brion, J. P., Flament-Durand, J., Duchen, L., Kauss, J., Schlote, W., Lowe, J., Probst, A., Ravid, R., Swaab, D. F., Renkawek, K., & Tomlinson, B. (1990). Rating of the lesions in senile dementia of the Alzheimer type: Concordance between laboratories A European multicenter study under the auspices of EURAGE. *Journal of the Neurological Sciences*, *97*(2–3), 295–323. https://doi.org/10.1016/0022-510X(90)90226-D

Düzel, S., Münte, T. F., Lindenberger, U., Bunzeck, N., Schütze, H., Heinze, H.-J., & Düzel, E. (2010). Basal forebrain integrity and cognitive memory profile in healthy aging. *Brain Research*, *1308*, 124–136. https://doi.org/10.1016/j.brainres.2009.10.048

Düzel, S., Schütze, H., Stallforth, S., Kaufmann, J., Bodammer, N., Bunzeck, N., Münte, T. F., Lindenberger, U., Heinze, H.-J., & Düzel, E. (2008). A close relationship between verbal memory and SN/VTA integrity in young and older adults. *Neuropsychologia*, *46*(13), 3042–3052. https://doi.org/10.1016/j.neuropsychologia.2008.06.001

Eckart, C., & Bunzeck, N. (2013). Dopamine modulates processing speed in the human mesolimbic system. *NeuroImage*, *66*, 293–300. https://doi.org/10.1016/j.neuroimage.2012.11.001

Eckart, C., Woźniak-Kwaśniewska, A., Herweg, N. A., Fuentemilla, L., & Bunzeck, N. (2016). Acetylcholine modulates human working memory and subsequent familiarity based recognition via alpha oscillations. *NeuroImage*, *137*, 61–69. https://doi.org/10.1016/j.neuroimage.2016.05.049

Egger, M., Smith, G. D., Schneider, M., & Minder, C. (1997). Bias in meta-analysis detected by a simple, graphical test. *BMJ*, *315*(7109), 629–634. https://doi.org/10.1136/bmj.315.7109.629

Eickhoff, S. B., Bzdok, D., Laird, A. R., Kurth, F., & Fox, P. T. (2012). Activation likelihood estimation meta-analysis revisited. *NeuroImage*, *59*(3), 2349–2361. https://doi.org/10.1016/j.neuroimage.2011.09.017

Eickhoff, S. B., Bzdok, D., Laird, A. R., Roski, C., Caspers, S., Zilles, K., & Fox, P. T. (2011). Co-activation patterns distinguish cortical modules, their connectivity and functional differentiation. *NeuroImage*, *57*(3), 938–949. https://doi.org/10.1016/j.neuroimage.2011.05.021

Eickhoff, S. B., Heim, S., Zilles, K., & Amunts, K. (2006). Testing anatomically specified hypotheses in functional imaging using cytoarchitectonic maps. *NeuroImage*, *32*(2), 570–582. https://doi.org/10.1016/j.neuroimage.2006.04.204

Eickhoff, S. B., Laird, A. R., Grefkes, C., Wang, L. E., Zilles, K., & Fox, P. T. (2009). Coordinate-based activation likelihood estimation meta-analysis of neuroimaging data: A random-effects approach based on empirical estimates of spatial uncertainty. *Human Brain Mapping*, *30*(9), 2907–2926. https://doi.org/10.1002/hbm.20718

Eickhoff, S. B., Nichols, T. E., Laird, A. R., Hoffstaedter, F., Amunts, K., Fox, P. T., Bzdok, D., & Eickhoff, C. R. (2016). Behavior, sensitivity, and power of activation likelihood estimation characterized by massive empirical simulation. *NeuroImage*, *137*, 70–85. https://doi.org/10.1016/j.neuroimage.2016.04.072

Eickhoff, S. B., Paus, T., Caspers, S., Grosbras, M.-H., Evans, A. C., Zilles, K., & Amunts, K. (2007). Assignment of functional activations to probabilistic cytoarchitectonic areas revisited. *NeuroImage*, *36*(3), 511–521. https://doi.org/10.1016/j.neuroimage.2007.03.060

Eickhoff, S. B., Stephan, K. E., Mohlberg, H., Grefkes, C., Fink, G. R., Amunts, K., & Zilles, K. (2005). A new SPM toolbox for combining probabilistic cytoarchitectonic maps and functional imaging data. *NeuroImage*, *25*(4), 1325–1335. https://doi.org/10.1016/j.neuroimage.2004.12.034

Eklund, A., Nichols, T. E., & Knutsson, H. (2016). Cluster failure: Why fMRI inferences for spatial extent have inflated false-positive rates. *Proceedings of the National Academy of Sciences*, *113*(28), 7900–7905. https://doi.org/10.1073/pnas.1602413113

Esrael, S. M. A. M., Hamed, A. M. M., Khedr, E. M., & Soliman, R. K. (2021). Application of diffusion tensor imaging in Alzheimer's disease: Quantification of white matter microstructural changes. *Egyptian Journal of Radiology and Nuclear Medicine*, *52*(1), 89. https://doi.org/10.1186/s43055-021-00460-x

Ezzati, A., Zammit, A. R., Habeck, C., Hall, C. B., & Lipton, R. B. (2020). Detecting biological heterogeneity patterns in ADNI amnestic mild cognitive impairment based on volumetric MRI. *Brain Imaging and Behavior*, *14*(5), 1792–1804. https://doi.org/10.1007/s11682-019-00115-6

Farrow, T. F. D., Thiyagesh, S. N., Wilkinson, I. D., Parks, R. W., Ingram, L., & Woodruff, P. W. R. (2007). Fronto-temporal-lobe atrophy in early-stage Alzheimer's disease identified using an improved detection methodology. *Psychiatry Research*, *155*(1), 11–19. https://doi.org/10.1016/j.pscychresns.2006.12.013

Feng, F., Huang, W., Meng, Q., Hao, W., Yao, H., Zhou, B., Guo, Y., Zhao, C., An, N., Wang, L., Huang, X., Zhang, X., & Shu, N. (2021). Altered Volume and Structural Connectivity of the Hippocampus in Alzheimer's Disease and Amnestic Mild Cognitive Impairment. *Frontiers in Aging Neuroscience*, *13*, 705030. https://doi.org/10.3389/fnagi.2021.705030

Fernández-Blázquez, M. A., Ávila-Villanueva, M., Maestú, F., & Medina, M. (2016). Specific Features of Subjective Cognitive Decline Predict Faster Conversion to Mild Cognitive Impairment. *Journal of Alzheimer's Disease*, *52*(1), 271–281. https://doi.org/10.3233/JAD-150956

Fernández-Cabello, S., Kronbichler, M., Van Dijk, K. R. A., Goodman, J. A., Spreng, R. N., Schmitz, T. W., & on behalf of the Alzheimer's Disease Neuroimaging Initiative. (2020). Basal forebrain volume reliably predicts the cortical spread of Alzheimer's degeneration. *Brain*, *143*(3), 993–1009. https://doi.org/10.1093/brain/awaa012

Ferrucci, L., Cooper, R., Shardell, M., Simonsick, E. M., Schrack, J. A., & Kuh, D. (2016). Age-Related Change in Mobility: Perspectives From Life Course Epidemiology and Geroscience. *The Journals of Gerontology Series A: Biological Sciences and Medical Sciences*, *71*(9), 1184–1194. https://doi.org/10.1093/gerona/glw043

Ferrucci, L., Gonzalez-Freire, M., Fabbri, E., Simonsick, E., Tanaka, T., Moore, Z., Salimi, S., Sierra, F., & De Cabo, R. (2020). Measuring biological aging in humans: A quest. *Aging Cell*, *19*(2), e13080. https://doi.org/10.1111/acel.13080

Ficiarà, E., Munir, Z., Boschi, S., Caligiuri, M. E., & Guiot, C. (2021). Alteration of Iron Concentration in Alzheimer's Disease as a Possible Diagnostic Biomarker Unveiling

Ferroptosis. *International Journal of Molecular Sciences*, *22*(9), 4479. https://doi.org/10.3390/ijms22094479

Fischer, W., Gage, F. H., & Björklund, A. (1989). Degenerative Changes in Forebrain Cholinergic Nuclei Correlate with Cognitive Impairments in Aged Rats. *The European Journal of Neuroscience*, *1*(1), 34–45. https://doi.org/10.1111/j.1460-9568.1989.tb00772.x

Fischl, B. (2012). FreeSurfer. *NeuroImage*, *62*(2), 774–781. https://doi.org/10.1016/j.neuroimage.2012.01.021

Fischl, B., & Dale, A. M. (2000). Measuring the thickness of the human cerebral cortex from magnetic resonance images. *Proceedings of the National Academy of Sciences*, *97*(20), 11050–11055. https://doi.org/10.1073/pnas.200033797

Fischl, B., Liu, A., & Dale, A. M. (2001). Automated manifold surgery: Constructing geometrically accurate and topologically correct models of the human cerebral cortex. *IEEE Transactions on Medical Imaging*, *20*(1), 70–80. https://doi.org/10.1109/42.906426

Fischl, B., Salat, D. H., Busa, E., Albert, M., Dieterich, M., Haselgrove, C., van der Kouwe, A., Killiany, R., Kennedy, D., Klaveness, S., Montillo, A., Makris, N., Rosen, B., & Dale, A. M. (2002). Whole Brain Segmentation. *Neuron*, *33*(3), 341–355. https://doi.org/10.1016/S0896-6273(02)00569-X

Fischl, B., Salat, D. H., Van Der Kouwe, A. J. W., Makris, N., Ségonne, F., Quinn, B. T., & Dale, A. M. (2004a). Sequence-independent segmentation of magnetic resonance images. *NeuroImage*, *23*, S69–S84. https://doi.org/10.1016/j.neuroimage.2004.07.016

Fischl, B., Salat, D., Van Der Kouwe, Makris, N., Ségonne, F., Quinn, B., & Dale, A. M. (2004b). Automatically Parcellating the Human Cerebral Cortex. *Cerebral Cortex*, *14*(1), 11–22. https://doi.org/10.1093/cercor/bhg087

Floyd, R. A., & Carney, J. M. (1993). The Role of Metal Ions in Oxidative Processes and Aging. *Toxicology and Industrial Health*, *9*(1–2), 197–214. https://doi.org/10.1177/0748233793009001-214

Foerde, K., & Shohamy, D. (2011). The role of the basal ganglia in learning and memory: Insight from Parkinson's disease. *Neurobiology of Learning and Memory*, *96*(4), 624–636. https://doi.org/10.1016/j.nlm.2011.08.006

Fotuhi, M., Do, D., & Jack, C. (2012). Modifiable factors that alter the size of the hippocampus with ageing. *Nature Reviews Neurology*, *8*(4), 189–202. https://doi.org/10.1038/nrneurol.2012.27

Fox, P. T., Laird, A. R., Fox, S. P., Fox, P. M., Uecker, A. M., Crank, M., Koenig, S. F., & Lancaster, J. L. (2005). Brainmap taxonomy of experimental design: Description and evaluation. *Human Brain Mapping*, *25*(1), 185–198. https://doi.org/10.1002/hbm.20141

Fox, P. T., & Lancaster, J. L. (2002). Mapping context and content: The BrainMap model. *Nature Reviews Neuroscience*, *3*(4), 319–321. https://doi.org/10.1038/nrn789

Franceschi, C., Garagnani, P., Morsiani, C., Conte, M., Santoro, A., Grignolio, A., Monti, D., Capri, M., & Salvioli, S. (2018). The Continuum of Aging and Age-Related Diseases: Common Mechanisms but Different Rates. *Frontiers in Medicine*, *5*, 61. https://doi.org/10.3389/fmed.2018.00061

Franciotti, R., Nardini, D., Russo, M., Onofrj, M., & Sensi, S. L. (2023). Comparison of Machine

Learning-based Approaches to Predict the Conversion to Alzheimer's Disease from Mild Cognitive Impairment. *Neuroscience*, *514*, 143–152. https://doi.org/10.1016/j.neuroscience.2023.01.029

Freitas, S., Simões, M. R., Alves, L., & Santana, I. (2013). Montreal Cognitive Assessment: Validation Study for Mild Cognitive Impairment and Alzheimer Disease. *Alzheimer Disease & Associated Disorders*, *27*(1), 37–43. https://doi.org/10.1097/WAD.0b013e3182420bfe

Frisoni, G. B. (2005). Structural correlates of early and late onset Alzheimer's disease: Voxel based morphometric study. *Journal of Neurology, Neurosurgery & Psychiatry*, *76*(1), 112–114. https://doi.org/10.1136/jnnp.2003.029876

Frisoni, G. B., Fox, N. C., Jack, C. R., Scheltens, P., & Thompson, P. M. (2010). The clinical use of structural MRI in Alzheimer disease. *Nature Reviews Neurology*, *6*(2), 67–77. https://doi.org/10.1038/nrneurol.2009.215

Frisoni, G. B., Testa, C., Zorzan, A., Sabattoli, F., Beltramello, A., Soininen, H., & Laakso, M. P. (2002). Detection of grey matter loss in mild Alzheimer's disease with voxel based morphometry. *Journal of Neurology, Neurosurgery, and Psychiatry*, *73*(6), 657–664. https://doi.org/10.1136/jnnp.73.6.657

Friston, K. J., Williams, S., Howard, R., Frackowiak, R. S. J., & Turner, R. (1996). Movement-Related effects in fMRI time-series: Movement Artifacts in fMRI. *Magnetic Resonance in Medicine*, *35*(3), 346–355. https://doi.org/10.1002/mrm.1910350312

Futami, T., Takakusaki, K., & Kitai, S. T. (1995). Glutamatergic and cholinergic inputs from the pedunculopontine tegmental nucleus to dopamine neurons in the substantia nigra pars compacta. *Neurosci Res*, *21*(4), 331–342.

Gais, S., & Born, J. (2004). Low acetylcholine during slow-wave sleep is critical for declarative memory consolidation. *Proc Natl Acad Sci U S A*, *101*(7), 2140–2144.

Gallardo, G., & Holtzman, D. M. (2019). Amyloid-β and Tau at the Crossroads of Alzheimer's Disease. In A. Takashima, B. Wolozin, & L. Buee (Eds.), *Tau Biology* (Vol. 1184, pp. 187–203). Springer Singapore. https://doi.org/10.1007/978-981-32-9358-8_16

Gao, L., Jiang, Z., Cai, Z., Cai, M., Zhang, Q., Ma, Y., Li, G., Zhao, F., & Ma, Q. (2017). Brain iron deposition analysis using susceptibility weighted imaging and its association with body iron level in patients with mild cognitive impairment. *Molecular Medicine Reports*, *16*(6), 8209–8215. https://doi.org/10.3892/mmr.2017.7668

García, V., Mollineda, R. A., & Sánchez, J. S. (2009). Index of Balanced Accuracy: A Performance Measure for Skewed Class Distributions. In H. Araujo, A. M. Mendonça, A. J. Pinho, & M. I. Torres (Eds.), *Pattern Recognition and Image Analysis* (pp. 441–448). Springer. https://doi.org/10.1007/978-3-642-02172-5_57

Gassenmaier, S., Küstner, T., Nickel, D., Herrmann, J., Hoffmann, R., Almansour, H., Afat, S., Nikolaou, K., & Othman, A. E. (2021). Deep Learning Applications in Magnetic Resonance Imaging: Has the Future Become Present? *Diagnostics*, *11*(12), 2181. https://doi.org/10.3390/diagnostics11122181

Gaykema, R. P. A., & Zaborszky, L. (1997). Parvalbumin-containing neurons in the basal forebrain receive direct input from the substantia nigra-ventral tegmental area. *Brain Research*, *747*(1), 173–179. https://doi.org/10.1016/S0006-8993(96)01309-1

Gerardin, E., Chételat, G., Chupin, M., Cuingnet, R., Desgranges, B., Kim, H.-S., Niethammer, M., Dubois, B., Lehéricy, S., Garnero, L., Eustache, F., & Colliot, O. (2009). Multidimensional classification of hippocampal shape features discriminates Alzheimer's disease and mild cognitive impairment from normal aging. *NeuroImage*, *47*(4), 1476–1486. https://doi.org/10.1016/j.neuroimage.2009.05.036

Geula, C., Dunlop, S. R., Ayala, I., Kawles, A. S., Flanagan, M. E., Gefen, T., & Mesulam, M.-M. (2021). Basal forebrain cholinergic system in the dementias: Vulnerability, resilience, and resistance. *Journal of Neurochemistry*, *158*(6), 1394–1411. https://doi.org/10.1111/jnc.15471

Geula, C., & Mesulam, M.-M. (1996). Systematic Regional Variations in the Loss of Cortical Cholinergic Fibers in Alzheimer's Disease. *Cerebral Cortex*, *6*(2), 165–177. https://doi.org/10.1093/cercor/6.2.165

Ghisletta, P., Rabbitt, P., Lunn, M., & Lindenberger, U. (2012). Two thirds of the age-based changes in fluid and crystallized intelligence, perceptual speed, and memory in adulthood are shared. *Intelligence*, *40*(3), 260–268. https://doi.org/10.1016/j.intell.2012.02.008

Gibbons, L. E., Carle, A. C., Mackin, R. S., Harvey, D., Mukherjee, S., Insel, P., Curtis, S. M., Mungas, D., & Crane, P. K. (2012). A composite score for executive functioning, validated in Alzheimer's Disease Neuroimaging Initiative (ADNI) participants with baseline mild cognitive impairment. *Brain Imaging and Behavior*, *6*(4), 517–527. https://doi.org/10.1007/s11682-012-9176-1

Gili, T., Cercignani, M., Serra, L., Perri, R., Giove, F., Maraviglia, B., Caltagirone, C., & Bozzali, M. (2011). Regional brain atrophy and functional disconnection across Alzheimer's disease evolution. *Journal of Neurology, Neurosurgery, and Psychiatry*, *82*(1), 58–66. https://doi.org/10.1136/jnnp.2009.199935

Glover, G. H. (2011). Overview of Functional Magnetic Resonance Imaging. *Neurosurgery Clinics of North America*, *22*(2), 133–139. https://doi.org/10.1016/j.nec.2010.11.001

Goate, A., Chartier-Harlin, M.-C., Mullan, M., Brown, J., Crawford, F., Fidani, L., Giuffra, L., Haynes, A., Irving, N., James, L., Mant, R., Newton, P., Rooke, K., Roques, P., Talbot, C., Pericak-Vance, M., Roses, A., Williamson, R., Rossor, M., … Hardy, J. (1991). Segregation of a missense mutation in the amyloid precursor protein gene with familial Alzheimer's disease. *Nature*, *349*(6311), 704–706. https://doi.org/10.1038/349704a0

Gold, B. T., Jiang, Y., Jicha, G. A., & Smith, C. D. (2010). Functional response in ventral temporal cortex differentiates mild cognitive impairment from normal aging. *Human Brain Mapping*, *31*(8), 1249–1259. https://doi.org/10.1002/hbm.20932

Good, C. D., Scahill, R. I., Fox, N. C., Ashburner, J., Friston, K. J., Chan, D., Crum, W. R., Rossor, M. N., & Frackowiak, R. S. J. (2002). Automatic Differentiation of Anatomical Patterns in the Human Brain: Validation with Studies of Degenerative Dementias. *NeuroImage*, *17*(1), 29–46. https://doi.org/10.1006/nimg.2002.1202

Goutte, C., & Gaussier, E. (2005). A Probabilistic Interpretation of Precision, Recall and F-Score, with Implication for Evaluation. In D. E. Losada & J. M. Fernández-Luna (Eds.), *Advances in Information Retrieval* (Vol. 3408, pp. 345–359). Springer Berlin Heidelberg. https://doi.org/10.1007/978-3-540-31865-1_25

Goveas, J. S., Xie, C., Ward, B. D., Wu, Z., Li, W., Franczak, M., Jones, J. L., Antuono, P. G., & Li,

S. (2011). Recovery of hippocampal network connectivity correlates with cognitive improvement in mild alzheimer's disease patients treated with donepezil assessed by resting-state fMRI. *Journal of Magnetic Resonance Imaging*, *34*(4), 764–773. https://doi.org/10.1002/jmri.22662

Grieder, M., Crinelli, R. M., Jann, K., Federspiel, A., Wirth, M., Koenig, T., Stein, M., Wahlund, L.-O., & Dierks, T. (2013). Correlation between Topographic N400 Anomalies and Reduced Cerebral Blood Flow in the Anterior Temporal Lobes of Patients with Dementia. *Journal of Alzheimer's Disease: JAD*, *36*(4), 711–731. https://doi.org/10.3233/JAD-121690

Grothe, M., Heinsen, H., & Teipel, S. (2013). Longitudinal measures of cholinergic forebrain atrophy in the transition from healthy aging to Alzheimer's disease. *Neurobiology of Aging*, *34*(4), 1210–1220. https://doi.org/10.1016/j.neurobiolaging.2012.10.018

Grothe, M., Heinsen, H., & Teipel, S. J. (2012). Atrophy of the Cholinergic Basal Forebrain Over the Adult Age Range and in Early Stages of Alzheimer's Disease. *Biological Psychiatry*, *71*(9), 805–813. https://doi.org/10.1016/j.biopsych.2011.06.019

Grothe, M. J., Sepulcre, J., Gonzalez-Escamilla, G., Jelistratova, I., Schöll, M., Hansson, O., Teipel, S. J., & Alzheimer's Disease Neuroimaging Initiative. (2018). Molecular properties underlying regional vulnerability to Alzheimer's disease pathology. *Brain*. https://doi.org/10.1093/brain/awy189

Grueso, S., & Viejo-Sobera, R. (2021). Machine learning methods for predicting progression from mild cognitive impairment to Alzheimer's disease dementia: A systematic review. *Alzheimer's Research & Therapy*, *13*(1), 162. https://doi.org/10.1186/s13195-021-00900-w

Guan, X., Guo, T., Zhou, C., Wu, J., Zeng, Q., Li, K., Luo, X., Bai, X., Wu, H., Gao, T., Gu, L., Liu, X., Cao, Z., Wen, J., Chen, J., Wei, H., Zhang, Y., Liu, C., Song, Z., … Zhang, M. (2022). Altered brain iron depositions from aging to Parkinson's disease and Alzheimer's disease: A quantitative susceptibility mapping study. *NeuroImage*, *264*, 119683. https://doi.org/10.1016/j.neuroimage.2022.119683

Guitart-Masip, M., Salami, A., Garrett, D., Rieckmann, A., Lindenberger, U., & Bäckman, L. (2016). BOLD Variability is Related to Dopaminergic Neurotransmission and Cognitive Aging. *Cerebral Cortex*, *26*(5), 2074–2083. https://doi.org/10.1093/cercor/bhv029

Guo, X., Wang, Z., Li, K., Li, Z., Qi, Z., Jin, Z., Yao, L., & Chen, K. (2010). Voxel-based assessment of gray and white matter volumes in Alzheimer's disease. *Neuroscience Letters*, *468*(2), 146–150. https://doi.org/10.1016/j.neulet.2009.10.086

Gupta, Y., Lama, R. K., Kwon, G.-R., & Alzheimer's Disease Neuroimaging Initiative. (2019). Prediction and Classification of Alzheimer's Disease Based on Combined Features From Apolipoprotein-E Genotype, Cerebrospinal Fluid, MR, and FDG-PET Imaging Biomarkers. *Frontiers in Computational Neuroscience*, *13*, 72. https://doi.org/10.3389/fncom.2019.00072

Gutteridge, J. M. C. (1992). Iron and oxygen radicals in brain. *Annals of Neurology*, *32*(S1), S16–S21. https://doi.org/10.1002/ana.410320705

Haacke, E. M., Cheng, N. Y. C., House, M. J., Liu, Q., Neelavalli, J., Ogg, R. J., Khan, A., Ayaz, M., Kirsch, W., & Obenaus, A. (2005). Imaging iron stores in the brain using magnetic resonance imaging. *Magnetic Resonance Imaging*, *23*(1), 1–25.

https://doi.org/10.1016/j.mri.2004.10.001

Halberstadt, A. L., & Balaban, C. D. (2008). Selective anterograde tracing of nonserotonergic projections from dorsal raphe nucleus to the basal forebrain and extended amygdala. *Journal of Chemical Neuroanatomy*, *35*(4), 317–325. https://doi.org/10.1016/j.jchemneu.2008.02.006

Hall, A. M., Moore, R. Y., Lopez, O. L., Kuller, L., & Becker, J. T. (2008). Basal forebrain atrophy is a presymptomatic marker for Alzheimer's disease. *Alzheimer's & Dementia: The Journal of the Alzheimer's Association*, *4*(4), 271–279. https://doi.org/10.1016/j.jalz.2008.04.005

Hallgren, B., & Sourander, P. (1958). The effect of age on the non-haemin iron in the human brain. *Journal of Neurochemistry*, *3*(1), 41–51. https://doi.org/10.1111/j.1471-4159.1958.tb12607.x

Hämäläinen, A., Pihlajamäki, M., Tanila, H., Hänninen, T., Niskanen, E., Tervo, S., Karjalainen, P. A., Vanninen, R. L., & Soininen, H. (2007). Increased fMRI responses during encoding in mild cognitive impairment. *Neurobiology of Aging*, *28*(12), 1889–1903. https://doi.org/10.1016/j.neurobiolaging.2006.08.008

Hampel, H., Mesulam, M.-M., Cuello, A. C., Khachaturian, A. S., Vergallo, A., Farlow, M. R., Snyder, P. J., Giacobini, E., & Khachaturian, Z. S. (2018). REVISITING THE CHOLINERGIC HYPOTHESIS IN ALZHEIMER'S DISEASE: EMERGING EVIDENCE FROM TRANSLATIONAL AND CLINICAL RESEARCH. *The Journal Of Prevention of Alzheimer's Disease*, 1–14. https://doi.org/10.14283/jpad.2018.43

Han, X., Jovicich, J., Salat, D., Van Der Kouwe, A., Quinn, B., Czanner, S., Busa, E., Pacheco, J., Albert, M., Killiany, R., Maguire, P., Rosas, D., Makris, N., Dale, A., Dickerson, B., & Fischl, B. (2006). Reliability of MRI-derived measurements of human cerebral cortical thickness: The effects of field strength, scanner upgrade and manufacturer. *NeuroImage*, *32*(1), 180–194. https://doi.org/10.1016/j.neuroimage.2006.02.051

Hanseeuw, B. J., Betensky, R. A., Jacobs, H. I. L., Schultz, A. P., Sepulcre, J., Becker, J. A., Cosio, D. M. O., Farrell, M., Quiroz, Y. T., Mormino, E. C., Buckley, R. F., Papp, K. V., Amariglio, R. A., Dewachter, I., Ivanoiu, A., Huijbers, W., Hedden, T., Marshall, G. A., Chhatwal, J. P., … Johnson, K. (2019). Association of Amyloid and Tau With Cognition in Preclinical Alzheimer Disease: A Longitudinal Study. *JAMA Neurology*, *76*(8), 915. https://doi.org/10.1001/jamaneurol.2019.1424

Hansson, O., Seibyl, J., Stomrud, E., Zetterberg, H., Trojanowski, J. Q., Bittner, T., Lifke, V., Corradini, V., Eichenlaub, U., Batrla, R., Buck, K., Zink, K., Rabe, C., Blennow, K., Shaw, L. M., for the Swedish BioFINDER study group, & Alzheimer's Disease Neuroimaging Initiative. (2018). CSF biomarkers of Alzheimer's disease concord with amyloid-β PET and predict clinical progression: A study of fully automated immunoassays in BioFINDER and ADNI cohorts. *Alzheimer's & Dementia*, *14*(11), 1470–1481. https://doi.org/10.1016/j.jalz.2018.01.010

Harada, C. N., Natelson Love, M. C., & Triebel, K. L. (2013). Normal Cognitive Aging. *Clinics in Geriatric Medicine*, *29*(4), 737–752. https://doi.org/10.1016/j.cger.2013.07.002

Hare, D. J., & Double, K. L. (2016). Iron and dopamine: A toxic couple. *Brain*, *139*(4), 1026–1035. https://doi.org/10.1093/brain/aww022

Harvey, R. J. (2003). The prevalence and causes of dementia in people under the age of 65

years. *Journal of Neurology, Neurosurgery & Psychiatry*, *74*(9), 1206–1209. https://doi.org/10.1136/jnnp.74.9.1206

Hashmi, A., & Osman, A. H. (2022). Brain Tumor Classification Using Conditional Segmentation with Residual Network and Attention Approach by Extreme Gradient Boost. *Applied Sciences*, *12*(21), 10791. https://doi.org/10.3390/app122110791

Hasselmo, M. E. (2006). The role of acetylcholine in learning and memory. *Current Opinion in Neurobiology*, *16*(6), 710–715. https://doi.org/10.1016/j.conb.2006.09.002

Hasselmo, M. E., & Sarter, M. (2011). Modes and models of forebrain cholinergic neuromodulation of cognition. *Neuropsychopharmacology*, *36*(1), 52–73.

Hayes, A. F. (2017). *Introduction to mediation, moderation, and conditional process analysis: A regression-based approach*. Guilford publications.

He, Y., Wang, L., Zang, Y., Tian, L., Zhang, X., Li, K., & Jiang, T. (2007). Regional coherence changes in the early stages of Alzheimer's disease: A combined structural and resting-state functional MRI study. *NeuroImage*, *35*(2), 488–500. https://doi.org/10.1016/j.neuroimage.2006.11.042

Heckner, M. K., Cieslik, E. C., Küppers, V., Fox, P. T., Eickhoff, S. B., & Langner, R. (2021). Delineating visual, auditory and motor regions in the human brain with functional neuroimaging: A BrainMap-based meta-analytic synthesis. *Scientific Reports*, *11*(1), 9942. https://doi.org/10.1038/s41598-021-88773-9

Hedden, T., & Gabrieli, J. D. E. (2004). Insights into the ageing mind: A view from cognitive neuroscience. *Nature Reviews Neuroscience*, *5*(2), 87–96. https://doi.org/10.1038/nrn1323

Hedges, L. V., & Olkin, I. (1985). *Statistical Methods for Meta-Analysis*. Academic Press, Inc. https://doi.org/10.1016/C2009-0-03396-0

Hett, K., Ta, V.-T., Catheline, G., Tourdias, T., Manjón, J. V., Coupé, P., Alzheimer's Disease Neuroimaging Initiative, Weiner, M. W., Aisen, P., Petersen, R., Jack, C. R., Jagust, W., Trojanowki, J. Q., Toga, A. W., Beckett, L., Green, R. C., Saykin, A. J., Morris, J., Shaw, L. M., … Fargher, K. (2019). Multimodal Hippocampal Subfield Grading For Alzheimer's Disease Classification. *Scientific Reports*, *9*(1), 13845. https://doi.org/10.1038/s41598-019-49970-9

Heys, J. G., Giocomo, L. M., & Hasselmo, M. E. (2010). Cholinergic Modulation of the Resonance Properties of Stellate Cells in Layer II of Medial Entorhinal Cortex. *Journal of Neurophysiology*, *104*(1), 258–270. https://doi.org/10.1152/jn.00492.2009

Hicks, S. A., Strümke, I., Thambawita, V., Hammou, M., Riegler, M. A., Halvorsen, P., & Parasa, S. (2022). On evaluation metrics for medical applications of artificial intelligence. *Scientific Reports*, *12*(1), 5979. https://doi.org/10.1038/s41598-022-09954-8

Higgins, J. P., Thompson, S. G., Deeks, J. J., & Altman, D. G. (2003). Measuring inconsistency in meta-analyses. *BMJ*, *327*(7414), 557–560. https://doi.org/10.1136/bmj.327.7414.557

Hirao, K., Ohnishi, T., Matsuda, H., Nemoto, K., Hirata, Y., Yamashita, F., Asada, T., & Iwamoto, T. (2006). Functional interactions between entorhinal cortex and posterior cingulate cortex at the very early stage of Alzheimer's disease using brain perfusion single-photon emission computed tomography. *Nuclear Medicine Communications*, *27*(2), 151–156. https://doi.org/10.1097/01.mnm.0000189783.39411.ef

Honea, R. A., Thomas, G. P., Harsha, A., Anderson, H. S., Donnelly, J. E., Brooks, W. M., & Burns, J. M. (2009). Cardiorespiratory fitness and preserved medial temporal lobe volume in Alzheimer disease. *Alzheimer Disease and Associated Disorders*, *23*(3), 188–197. https://doi.org/10.1097/WAD.0b013e31819cb8a2

Hornung, J.-P. (2003). The human raphe nuclei and the serotonergic system. *Journal of Chemical Neuroanatomy*, *26*(4), 331–343. https://doi.org/10.1016/j.jchemneu.2003.10.002

Horowitz, M. P., & Greenamyre, J. T. (2010). Mitochondrial Iron Metabolism and Its Role in Neurodegeneration. *Journal of Alzheimer's Disease*, *20*(s2), S551–S568. https://doi.org/10.3233/JAD-2010-100354

Hou, Y., Dan, X., Babbar, M., Wei, Y., Hasselbalch, S. G., Croteau, D. L., & Bohr, V. A. (2019). Ageing as a risk factor for neurodegenerative disease. *Nature Reviews Neurology*, *15*(10), 565–581. https://doi.org/10.1038/s41582-019-0244-7

Huang, Y., Xu, L., Kuang, L., Wang, W., Cao, J., & Xiao, M.-N. (2020). Abnormal brain activity in adolescents with Internet addiction who attempt suicide: An assessment using functional magnetic resonance imaging. *Neural Regeneration Research*, *15*(8), 1554. https://doi.org/10.4103/1673-5374.274346

Husain, M. A., Laurent, B., & Plourde, M. (2021). APOE and Alzheimer's Disease: From Lipid Transport to Physiopathology and Therapeutics. *Frontiers in Neuroscience*, *15*, 630502. https://doi.org/10.3389/fnins.2021.630502

Hussain, S., Mubeen, I., Ullah, N., Shah, S. S. U. D., Khan, B. A., Zahoor, M., Ullah, R., Khan, F. A., & Sultan, M. A. (2022). Modern Diagnostic Imaging Technique Applications and Risk Factors in the Medical Field: A Review. *BioMed Research International*, *2022*, 1–19. https://doi.org/10.1155/2022/5164970

Insel, P. S., Mormino, E. C., Aisen, P. S., Thompson, W. K., & Donohue, M. C. (2020). Neuroanatomical spread of amyloid β and tau in Alzheimer's disease: Implications for primary prevention. *Brain Communications*, *2*(1), fcaa007. https://doi.org/10.1093/braincomms/fcaa007

Irish, M., Eyre, N., Dermody, N., O'Callaghan, C., Hodges, J. R., Hornberger, M., & Piguet, O. (2016). Neural Substrates of Semantic Prospection—Evidence from the Dementias. *Frontiers in Behavioral Neuroscience*, *10*, 96. https://doi.org/10.3389/fnbeh.2016.00096

Irish, M., Hodges, J. R., & Piguet, O. (2013). Episodic future thinking is impaired in the behavioural variant of frontotemporal dementia. *Cortex; a Journal Devoted to the Study of the Nervous System and Behavior*, *49*(9), 2377–2388. https://doi.org/10.1016/j.cortex.2013.03.002

Irish, M., Hornberger, M., El Wahsh, S., Lam, B. Y. K., Lah, S., Miller, L., Hsieh, S., Hodges, J. R., & Piguet, O. (2014). Grey and white matter correlates of recent and remote autobiographical memory retrieval-insights from the dementias. *PloS One*, *9*(11), e113081. https://doi.org/10.1371/journal.pone.0113081

Ishii, K., Sasaki, H., Kono, A. K., Miyamoto, N., Fukuda, T., & Mori, E. (2005). Comparison of gray matter and metabolic reduction in mild Alzheimer's disease using FDG-PET and voxel-based morphometric MR studies. *European Journal of Nuclear Medicine and Molecular Imaging*, *32*(8), 959–963. https://doi.org/10.1007/s00259-004-1740-5

Jack, C. R., Bennett, D. A., Blennow, K., Carrillo, M. C., Dunn, B., Haeberlein, S. B., Holtzman, D. M., Jagust, W., Jessen, F., Karlawish, J., Liu, E., Molinuevo, J. L., Montine, T., Phelps, C., Rankin, K. P., Rowe, C. C., Scheltens, P., Siemers, E., Snyder, H. M., … Silverberg, N. (2018). NIA-AA Research Framework: Toward a biological definition of Alzheimer's disease. *Alzheimer's & Dementia*, *14*(4), 535–562. https://doi.org/10.1016/j.jalz.2018.02.018

Jack, C. R., Bennett, D. A., Blennow, K., Carrillo, M. C., Feldman, H. H., Frisoni, G. B., Hampel, H., Jagust, W. J., Johnson, K. A., Knopman, D. S., Petersen, R. C., Scheltens, P., Sperling, R. A., & Dubois, B. (2016). A/T/N: An unbiased descriptive classification scheme for Alzheimer disease biomarkers. *Neurology*, *87*(5), 539–547. https://doi.org/10.1212/WNL.0000000000002923

Jack, C. R., Bernstein, M. A., Borowski, B. J., Gunter, J. L., Fox, N. C., Thompson, P. M., Schuff, N., Krueger, G., Killiany, R. J., DeCarli, C. S., Dale, A. M., Carmichael, O. W., Tosun, D., Weiner, M. W., & Alzheimer's Disease Neuroimaging Initiative. (2010). Update on the Magnetic Resonance Imaging core of the Alzheimer's Disease Neuroimaging Initiative. *Alzheimer's & Dementia*, *6*(3), 212–220. https://doi.org/10.1016/j.jalz.2010.03.004

Jack, C. R., & Holtzman, D. M. (2013). Biomarker Modeling of Alzheimer's Disease. *Neuron*, *80*(6), 1347–1358. https://doi.org/10.1016/j.neuron.2013.12.003

Jack, C. R., Knopman, D. S., Jagust, W. J., Petersen, R. C., Weiner, M. W., Aisen, P. S., Shaw, L. M., Vemuri, P., Wiste, H. J., Weigand, S. D., Lesnick, T. G., Pankratz, V. S., Donohue, M. C., & Trojanowski, J. Q. (2013). Tracking pathophysiological processes in Alzheimer's disease: An updated hypothetical model of dynamic biomarkers. *The Lancet Neurology*, *12*(2), 207–216. https://doi.org/10.1016/S1474-4422(12)70291-0

Jack, C. R., Knopman, D. S., Jagust, W. J., Shaw, L. M., Aisen, P. S., Weiner, M. W., Petersen, R. C., & Trojanowski, J. Q. (2010). Hypothetical model of dynamic biomarkers of the Alzheimer's pathological cascade. *The Lancet Neurology*, *9*(1), 119–128. https://doi.org/10.1016/S1474-4422(09)70299-6

Jagust, W. (2018). Imaging the evolution and pathophysiology of Alzheimer disease. *Nature Reviews Neuroscience*, *19*(11), 687–700. https://doi.org/10.1038/s41583-018-0067-3

Jessen, F., Amariglio, R. E., van Boxtel, M., Breteler, M., Ceccaldi, M., Chételat, G., Dubois, B., Dufouil, C., Ellis, K. A., van der Flier, W. M., Glodzik, L., van Harten, A. C., de Leon, M. J., McHugh, P., Mielke, M. M., Molinuevo, J. L., Mosconi, L., Osorio, R. S., Perrotin, A., … Group, S. C. D. I. (SCD-I. W. (2014). A conceptual framework for research on subjective cognitive decline in preclinical Alzheimer's disease. *Alzheimer's & Dementia*, *10*(6), 844–852. https://doi.org/10.1016/j.jalz.2014.01.001

Jessen, F., Feyen, L., Freymann, K., Tepest, R., Maier, W., Heun, R., Schild, H.-H., & Scheef, L. (2006). Volume reduction of the entorhinal cortex in subjective memory impairment. *Neurobiology of Aging*, *27*(12), 1751–1756. https://doi.org/10.1016/j.neurobiolaging.2005.10.010

Jiang, L., & Zuo, X.-N. (2016). Regional Homogeneity: A Multimodal, Multiscale Neuroimaging Marker of the Human Connectome. *The Neuroscientist*, *22*(5), 486–505. https://doi.org/10.1177/1073858415595004

Johnson, K. A., Fox, N. C., Sperling, R. A., & Klunk, W. E. (2012). Brain Imaging in Alzheimer Disease. *Cold Spring Harbor Perspectives in Medicine*, *2*(4), a006213–a006213.

https://doi.org/10.1101/cshperspect.a006213

Jovicich, J., Czanner, S., Greve, D., Haley, E., Van Der Kouwe, A., Gollub, R., Kennedy, D., Schmitt, F., Brown, G., MacFall, J., Fischl, B., & Dale, A. (2006). Reliability in multi-site structural MRI studies: Effects of gradient non-linearity correction on phantom and human data. *NeuroImage*, *30*(2), 436–443. https://doi.org/10.1016/j.neuroimage.2005.09.046

Ju, R., Hu, C., Zhou, P., & Li, Q. (2019). Early Diagnosis of Alzheimer's Disease Based on Resting-State Brain Networks and Deep Learning. *IEEE/ACM Transactions on Computational Biology and Bioinformatics*, *16*(1), 244–257. https://doi.org/10.1109/TCBB.2017.2776910

Julkunen, V., Niskanen, E., Koikkalainen, J., Herukka, S.-K., Pihlajamäki, M., Hallikainen, M., Kivipelto, M., Muehlboeck, S., Evans, A. C., Vanninen, R., & Soininen, H. (2010). Differences in Cortical Thickness in Healthy Controls, Subjects with Mild Cognitive Impairment, and Alzheimer's Disease Patients: A Longitudinal Study. *Journal of Alzheimer's Disease*, *21*(4), 1141–1151. https://doi.org/10.3233/JAD-2010-100114

Kabasawa, H. (2022). MR Imaging in the 21st Century: Technical Innovation over the First Two Decades. *Magnetic Resonance in Medical Sciences*, *21*(1), 71–82. https://doi.org/10.2463/mrms.rev.2021-0011

Kanda, T., Ishii, K., Uemura, T., Miyamoto, N., Yoshikawa, T., Kono, A. K., & Mori, E. (2008). Comparison of grey matter and metabolic reductions in frontotemporal dementia using FDG-PET and voxel-based morphometric MR studies. *European Journal of Nuclear Medicine and Molecular Imaging*, *35*(12), 2227–2234. https://doi.org/10.1007/s00259-008-0871-5

Kapasi, A., DeCarli, C., & Schneider, J. A. (2017). Impact of multiple pathologies on the threshold for clinically overt dementia. *Acta Neuropathologica*, *134*(2), 171–186. https://doi.org/10.1007/s00401-017-1717-7

Karaman, B. K., Mormino, E. C., Sabuncu, M. R., & for the Alzheimer's Disease Neuroimaging Initiative. (2022). Machine learning based multi-modal prediction of future decline toward Alzheimer's disease: An empirical study. *PLOS ONE*, *17*(11), e0277322. https://doi.org/10.1371/journal.pone.0277322

Karas, G. B., Scheltens, P., Rombouts, S. A. R. B., Visser, P. J., Van Schijndel, R. A., Fox, N. C., & Barkhof, F. (2004). Global and local gray matter loss in mild cognitive impairment and Alzheimer's disease. *NeuroImage*, *23*(2), 708–716. https://doi.org/10.1016/j.neuroimage.2004.07.006

Kaufmann, T., van der Meer, D., Doan, N. T., Schwarz, E., Lund, M. J., Agartz, I., Alnæs, D., Barch, D. M., Baur-Streubel, R., Bertolino, A., Bettella, F., Beyer, M. K., Bøen, E., Borgwardt, S., Brandt, C. L., Buitelaar, J., Celius, E. G., Cervenka, S., Conzelmann, A., … Westlye, L. T. (2019). Common brain disorders are associated with heritable patterns of apparent aging of the brain. *Nature Neuroscience*, *22*(10), Article 10. https://doi.org/10.1038/s41593-019-0471-7

Kendall, M. G., & Gibbons, J., D. (1990). *Rank correlation methods.* NY: Oxford University Press.

Kent, S. A., Spires-Jones, T. L., & Durrant, C. S. (2020). The physiological roles of tau and Aβ: Implications for Alzheimer's disease pathology and therapeutics. *Acta Neuropathologica*, *140*(4), 417–447. https://doi.org/10.1007/s00401-020-02196-w

Kerbler, G. M., Fripp, J., Rowe, C. C., Villemagne, V. L., Salvado, O., Rose, S., & Coulson, E. J. (2015). Basal forebrain atrophy correlates with amyloid β burden in Alzheimer's disease. *NeuroImage: Clinical*, *7*, 105–113. https://doi.org/10.1016/j.nicl.2014.11.015

Khan, U. A., Liu, L., Provenzano, F. A., Berman, D. E., Profaci, C. P., Sloan, R., Mayeux, R., Duff, K. E., & Small, S. A. (2014). Molecular drivers and cortical spread of lateral entorhinal cortex dysfunction in preclinical Alzheimer's disease. *Nature Neuroscience*, *17*(2), 304–311. https://doi.org/10.1038/nn.3606

Khatri, U., & Kwon, G.-R. (2022). Alzheimer's Disease Diagnosis and Biomarker Analysis Using Resting-State Functional MRI Functional Brain Network With Multi-Measures Features and Hippocampal Subfield and Amygdala Volume of Structural MRI. *Frontiers in Aging Neuroscience*, *14*, 818871. https://doi.org/10.3389/fnagi.2022.818871

Khattar, N., Triebswetter, C., Kiely, M., Ferrucci, L., Resnick, S. M., Spencer, R. G., & Bouhrara, M. (2021). Investigation of the association between cerebral iron content and myelin content in normative aging using quantitative magnetic resonance neuroimaging. *NeuroImage*, *239*, 118267. https://doi.org/10.1016/j.neuroimage.2021.118267

Kilimann, I., Grothe, M., Heinsen, H., Alho, E. J. L., Grinberg, L., Amaro Jr., E., dos Santos, G. A. B., da Silva, R. E., Mitchell, A. J., Frisoni, G. B., Bokde, A. L. W., Fellgiebel, A., Filippi, M., Hampel, H., Klöppel, S., & Teipel, S. J. (2014). Subregional Basal Forebrain Atrophy in Alzheimer's Disease: A Multicenter Study. *Journal of Alzheimer's Disease*, *40*(3), 687–700. https://doi.org/10.3233/JAD-132345

Kim, H.-G., Park, S., Rhee, H. Y., Lee, K. M., Ryu, C.-W., Rhee, S. J., Lee, S. Y., Wang, Y., & Jahng, G.-H. (2017). Quantitative susceptibility mapping to evaluate the early stage of Alzheimer's disease. *NeuroImage. Clinical*, *16*, 429–438. https://doi.org/10.1016/j.nicl.2017.08.019

Kim, J., Jeong, M., Stiles, W. R., & Choi, H. S. (2022). Neuroimaging Modalities in Alzheimer's Disease: Diagnosis and Clinical Features. *International Journal of Molecular Sciences*, *23*(11), 6079. https://doi.org/10.3390/ijms23116079

Kim, S., Youn, Y. C., Hsiung, G.-Y. R., Ha, S.-Y., Park, K.-Y., Shin, H.-W., Kim, D.-K., Kim, S.-S., & Kee, B. S. (2011). Voxel-based morphometric study of brain volume changes in patients with Alzheimer's disease assessed according to the Clinical Dementia Rating score. *Journal of Clinical Neuroscience: Official Journal of the Neurosurgical Society of Australasia*, *18*(7), 916–921. https://doi.org/10.1016/j.jocn.2010.12.019

Kirkwood, T. B. L. (2005). Understanding the Odd Science of Aging. *Cell*, *120*(4), 437–447. https://doi.org/10.1016/j.cell.2005.01.027

Kluyver, T., Ragan-Kelley, B., P&#233, Rez, F., Granger, B., Bussonnier, M., Frederic, J., Kelley, K., Hamrick, J., Grout, J., Corlay, S., Ivanov, P., Avila, D., n, Abdalla, S., Willing, C., & Team, J. D. (2016). Jupyter Notebooks – a publishing format for reproducible computational workflows. *Positioning and Power in Academic Publishing: Players, Agents and Agendas*, 87–90. https://doi.org/10.3233/978-1-61499-649-1-87

Ko, S. -u., Hausdorff, J. M., & Ferrucci, L. (2010). Age-associated differences in the gait pattern changes of older adults during fast-speed and fatigue conditions: Results from the Baltimore longitudinal study of ageing. *Age and Ageing*, *39*(6), 688–694. https://doi.org/10.1093/ageing/afq113

Koeppen, A. H. (1995). The history of iron in the brain. *Journal of the Neurological Sciences*,

134, 1–9. https://doi.org/10.1016/0022-510X(95)00202-D

Kolb, B., & Whishaw, I. Q. (2003). *Fundamentals of human neuropsychology* (5th ed). Worth Publishers.

Kuchcinski, G., Patin, L., Lopes, R., Leroy, M., Delbeuck, X., Rollin-Sillaire, A., Lebouvier, T., Wang, Y., Spincemaille, P., Tourdias, T., Hacein-Bey, L., Devos, D., Pasquier, F., Leclerc, X., Pruvo, J.-P., & Verclytte, S. (2022). Quantitative susceptibility mapping demonstrates different patterns of iron overload in subtypes of early-onset Alzheimer's disease. *European Radiology*, *33*(1), 184–195. https://doi.org/10.1007/s00330-022-09014-9

Kukolja, J., Thiel, C. M., & Fink, G. R. (2009). Cholinergic Stimulation Enhances Neural Activity Associated with Encoding but Reduces Neural Activity Associated with Retrieval in Humans. *The Journal of Neuroscience*, *29*(25), 8119–8128. https://doi.org/10.1523/JNEUROSCI.0203-09.2009

Kulason, S., Xu, E., Tward, D. J., Bakker, A., Albert, M., Younes, L., & Miller, M. I. (2020). Entorhinal and Transentorhinal Atrophy in Preclinical Alzheimer's Disease. *Frontiers in Neuroscience*, *14*, 804. https://doi.org/10.3389/fnins.2020.00804

Laird, A. R., Eickhoff, S. B., Kurth, F., Fox, P. M., Uecker, A. M., Turner, J. A., Robinson, J. L., Lancaster, J. L., & Fox, P. T. (2009). ALE Meta-Analysis Workflows Via the Brainmap Database: Progress Towards A Probabilistic Functional Brain Atlas. *Frontiers in Neuroinformatics*, *3*, 23. https://doi.org/10.3389/neuro.11.023.2009

Laird, A. R., Fox, P. M., Price, C. J., Glahn, D. C., Uecker, A. M., Lancaster, J. L., Turkeltaub, P. E., Kochunov, P., & Fox, P. T. (2005). ALE meta-analysis: Controlling the false discovery rate and performing statistical contrasts. *Human Brain Mapping*, *25*(1), 155–164. https://doi.org/10.1002/hbm.20136

Laird, A. R., Robinson, J. L., McMillan, K. M., Tordesillas-Gutiérrez, D., Moran, S. T., Gonzales, S. M., Ray, K. L., Franklin, C., Glahn, D. C., Fox, P. T., & Lancaster, J. L. (2010). Comparison of the disparity between Talairach and MNI coordinates in functional neuroimaging data: Validation of the Lancaster transform. *NeuroImage*, *51*(2), 677–683. https://doi.org/10.1016/j.neuroimage.2010.02.048

Lancaster, J. L., Tordesillas-Gutiérrez, D., Martinez, M., Salinas, F., Evans, A., Zilles, K., Mazziotta, J. C., & Fox, P. T. (2007). Bias between MNI and Talairach coordinates analyzed using the ICBM-152 brain template. *Human Brain Mapping*, *28*(11), 1194–1205. https://doi.org/10.1002/hbm.20345

Lane, C. A., Hardy, J., & Schott, J. M. (2018). Alzheimer's disease. *European Journal of Neurology*, *25*(1), 59–70. https://doi.org/10.1111/ene.13439

Lange, A. G., Barth, C., Kaufmann, T., Anatürk, M., Suri, S., Ebmeier, K. P., & Westlye, L. T. (2020). The maternal brain: Region-specific patterns of brain aging are traceable decades after childbirth. *Human Brain Mapping*, *41*(16), 4718–4729. https://doi.org/10.1002/hbm.25152

Langkammer, C., Krebs, N., Goessler, W., Scheurer, E., Ebner, F., Yen, K., Fazekas, F., & Ropele, S. (2010). Quantitative MR Imaging of Brain Iron: A Postmortem Validation Study. *Radiology*, *257*(2), 455–462. https://doi.org/10.1148/radiol.10100495

Langkammer, C., Ropele, S., Pirpamer, L., Fazekas, F., & Schmidt, R. (2014). MRI for Iron

Mapping in Alzheimer's Disease. *Neurodegenerative Diseases*, *13*(2–3), 189–191. https://doi.org/10.1159/000353756

Langkammer, C., Schweser, F., Krebs, N., Deistung, A., Goessler, W., Scheurer, E., Sommer, K., Reishofer, G., Yen, K., Fazekas, F., Ropele, S., & Reichenbach, J. R. (2012). Quantitative susceptibility mapping (QSM) as a means to measure brain iron? A post mortem validation study. *NeuroImage*, *62*(3), 1593–1599. https://doi.org/10.1016/j.neuroimage.2012.05.049

LeDoux, J. (2003). The emotional brain, fear, and the amygdala. *Cell Mol Neurobiol*, *23*(4–5), 727–738.

Lee, J., & Kim, H.-J. (2022). Normal Aging Induces Changes in the Brain and Neurodegeneration Progress: Review of the Structural, Biochemical, Metabolic, Cellular, and Molecular Changes. *Frontiers in Aging Neuroscience*, *14*, 931536. https://doi.org/10.3389/fnagi.2022.931536

Lee, M. H., Smyser, C. D., & Shimony, J. S. (2013). Resting-State fMRI: A Review of Methods and Clinical Applications. *American Journal of Neuroradiology*, *34*(10), 1866–1872. https://doi.org/10.3174/ajnr.A3263

Leutritz, T., Seif, M., Helms, G., Samson, R. S., Curt, A., Freund, P., & Weiskopf, N. (2020). Multiparameter mapping of relaxation (R1, R2*), proton density and magnetization transfer saturation at 3 T: A multicenter dual-vendor reproducibility and repeatability study. *Human Brain Mapping*, *41*(15), 4232–4247. https://doi.org/10.1002/hbm.25122

Li, D., Liu, Y., Zeng, X., Xiong, Z., Yao, Y., Liang, D., Qu, H., Xiang, H., Yang, Z., Nie, L., Wu, P.-Y., & Wang, R. (2020). Quantitative Study of the Changes in Cerebral Blood Flow and Iron Deposition During Progression of Alzheimer's Disease. *Journal of Alzheimer's Disease: JAD*, *78*(1), 439–452. https://doi.org/10.3233/JAD-200843

Li, X., Feng, X., Sun, X., Hou, N., Han, F., & Liu, Y. (2022). Global, regional, and national burden of Alzheimer's disease and other dementias, 1990–2019. *Frontiers in Aging Neuroscience*, *14*, 937486. https://doi.org/10.3389/fnagi.2022.937486

Li, X., Yu, B., Sun, Q., Zhang, Y., Ren, M., Zhang, X., Li, A., Yuan, J., Madisen, L., Luo, Q., Zeng, H., Gong, H., & Qiu, Z. (2018). Generation of a whole-brain atlas for the cholinergic system and mesoscopic projectome analysis of basal forebrain cholinergic neurons. *Proceedings of the National Academy of Sciences*, *115*(2), 415–420. https://doi.org/10.1073/pnas.1703601115

Li, Z., Zhang, Z., Ren, Y., Wang, Y., Fang, J., Yue, H., Ma, S., & Guan, F. (2021). Aging and age-related diseases: From mechanisms to therapeutic strategies. *Biogerontology*, *22*(2), 165–187. https://doi.org/10.1007/s10522-021-09910-5

Lillig, C. H., Berndt, C., & Holmgren, A. (2008). Glutaredoxin systems. *Biochimica et Biophysica Acta (BBA) - General Subjects*, *1780*(11), 1304–1317. https://doi.org/10.1016/j.bbagen.2008.06.003

Lim, B. Y., Lai, K. W., Haiskin, K., Kulathilake, K. A. S. H., Ong, Z. C., Hum, Y. C., Dhanalakshmi, S., Wu, X., & Zuo, X. (2022). Deep Learning Model for Prediction of Progressive Mild Cognitive Impairment to Alzheimer's Disease Using Structural MRI. *Frontiers in Aging Neuroscience*, *14*, 876202. https://doi.org/10.3389/fnagi.2022.876202

Lin, L., & Chu, H. (2018). Quantifying Publication Bias in Meta-Analysis. *Biometrics*, *74*(3), 785–794. https://doi.org/10.1111/biom.12817

Lisman, J. E., & Grace, A. A. (2005). The Hippocampal-VTA Loop: Controlling the Entry of Information into Long-Term Memory. *Neuron*, *46*(5), 703–713. https://doi.org/10.1016/j.neuron.2005.05.002

Lisman, J. E., Grace, A. A., & Duzel, E. (2011). A neoHebbian framework for episodic memory; role of dopamine-dependent late LTP. *Trends in Neurosciences*, *34*(10), 536–547. https://doi.org/10.1016/j.tins.2011.07.006

Liu, A. K. L., Chang, R. C.-C., Pearce, R. K. B., & Gentleman, S. M. (2015). Nucleus basalis of Meynert revisited: Anatomy, history and differential involvement in Alzheimer's and Parkinson's disease. *Acta Neuropathologica*, *129*(4), 527–540. https://doi.org/10.1007/s00401-015-1392-5

Liu, H., Zhang, L., Xi, Q., Zhao, X., Wang, F., Wang, X., Men, W., & Lin, Q. (2018). Changes in Brain Lateralization in Patients with Mild Cognitive Impairment and Alzheimer's Disease: A Resting-State Functional Magnetic Resonance Study from Alzheimer's Disease Neuroimaging Initiative. *Frontiers in Neurology*, *9*, 3. https://doi.org/10.3389/fneur.2018.00003

Liu, L., Drouet, V., Wu, J. W., Witter, M. P., Small, S. A., Clelland, C., & Duff, K. (2012). Trans-synaptic spread of tau pathology in vivo. *PloS One*, *7*(2), e31302. https://doi.org/10.1371/journal.pone.0031302

Liu, X., Du, L., Zhang, B., Zhao, Z., Gao, W., Liu, B., Liu, J., Chen, Y., Wang, Y., Yu, H., & Ma, G. (2021). Alterations and Associations Between Magnetic Susceptibility of the Basal Ganglia and Diffusion Properties in Alzheimer's Disease. *Frontiers in Neuroscience*, *15*, 616163. https://doi.org/10.3389/fnins.2021.616163

Liu, Y., Yu, C., Zhang, X., Liu, J., Duan, Y., Alexander-Bloch, A. F., Liu, B., Jiang, T., & Bullmore, E. (2014). Impaired Long Distance Functional Connectivity and Weighted Network Architecture in Alzheimer's Disease. *Cerebral Cortex*, *24*(6), 1422–1435. https://doi.org/10.1093/cercor/bhs410

Loeffler, D. A., Connor, J. R., Juneau, P. L., Snyder, B. S., Kanaley, L., DeMaggio, A. J., Nguyen, H., Brickman, C. M., & LeWitt, P. A. (1995). Transferrin and Iron in Normal, Alzheimer's Disease, and Parkinson's Disease Brain Regions. *Journal of Neurochemistry*, *65*(2), 710–716. https://doi.org/10.1046/j.1471-4159.1995.65020710.x

Logothetis, N. K., & Wandell, B. A. (2004). Interpreting the BOLD Signal. *Annual Review of Physiology*, *66*(1), 735–769. https://doi.org/10.1146/annurev.physiol.66.082602.092845

Lombardi, G., Crescioli, G., Cavedo, E., Lucenteforte, E., Casazza, G., Bellatorre, A.-G., Lista, C., Costantino, G., Frisoni, G., Virgili, G., & Filippini, G. (2020). Structural magnetic resonance imaging for the early diagnosis of dementia due to Alzheimer's disease in people with mild cognitive impairment. *Cochrane Database of Systematic Reviews*. https://doi.org/10.1002/14651858.CD009628.pub2

Long, H., Zhu, W., Wei, L., & Zhao, J. (2023). Iron homeostasis imbalance and ferroptosis in brain diseases. *MedComm*, *4*(4), e298. https://doi.org/10.1002/mco2.298

Long, Z., Jing, B., Yan, H., Dong, J., Liu, H., Mo, X., Han, Y., & Li, H. (2016). A support vector

machine-based method to identify mild cognitive impairment with multi-level characteristics of magnetic resonance imaging. *Neuroscience*, *331*, 169–176. https://doi.org/10.1016/j.neuroscience.2016.06.025

López-Otín, C., Blasco, M. A., Partridge, L., Serrano, M., & Kroemer, G. (2013). The Hallmarks of Aging. *Cell*, *153*(6), 1194–1217. https://doi.org/10.1016/j.cell.2013.05.039

Lowe, M. J., Dzemidzic, M., Lurito, J. T., Mathews, V. P., & Phillips, M. D. (2000). Correlations in Low-Frequency BOLD Fluctuations Reflect Cortico-Cortical Connections. *NeuroImage*, *12*(5), 582–587. https://doi.org/10.1006/nimg.2000.0654

Lowe, M. J., Mock, B. J., & Sorenson, J. A. (1998). Functional Connectivity in Single and Multislice Echoplanar Imaging Using Resting-State Fluctuations. *NeuroImage*, *7*(2), 119–132. https://doi.org/10.1006/nimg.1997.0315

Luo, D., Wan, X., Liu, J., & Tong, T. (2018). Optimally estimating the sample mean from the sample size, median, mid-range, and/or mid-quartile range. *Statistical Methods in Medical Research*, *27*(6), 1785–1805. https://doi.org/10.1177/0962280216669183

Makino, Y., Yokosawa, K., Takeda, Y., & Kumada, T. (2004). Visual search and memory search engage extensive overlapping cerebral cortices: An fMRI study. *NeuroImage*, *23*(2), 525–533. https://doi.org/10.1016/j.neuroimage.2004.06.026

Mantyh, P. W., Ghilardi, J. R., Rogers, S., DeMaster, E., Allen, C. J., Stimson, E. R., & Maggio, J. E. (1993). Aluminum, Iron, and Zinc Ions Promote Aggregation of Physiological Concentrations of Beta-Amyloid Peptide. *Journal of Neurochemistry*, *61*(3), 1171–1174. https://doi.org/10.1111/j.1471-4159.1993.tb03639.x

Mark, G. P., Shabani, S., Dobbs, L. K., & Hansen, S. T. (2011). Cholinergic modulation of mesolimbic dopamine function and reward. *Physiology & Behavior*, *104*(1), 76–81. https://doi.org/10.1016/j.physbeh.2011.04.052

Martinez, R., Morsch, P., Soliz, P., Hommes, C., Ordunez, P., & Vega, E. (2021). Life expectancy, healthy life expectancy, and burden of disease in older people in the Americas, 1990–2019: A population-based study. *Revista Panamericana de Salud Pública*, *45*, 1–14. https://doi.org/10.26633/RPSP.2021.114

Martínez-Florez, J. F., Osorio, J. D., Cediel, J. C., Rivas, J. C., Granados-Sánchez, A. M., López-Peláez, J., Jaramillo, T., & Cardona, J. F. (2021). Short-Term Memory Binding Distinguishing Amnestic Mild Cognitive Impairment from Healthy Aging: A Machine Learning Study. *Journal of Alzheimer's Disease*, *81*(2), 729–742. https://doi.org/10.3233/JAD-201447

Maruszak, A., & Thuret, S. (2014). Why looking at the whole hippocampus is not enoughâ€"a critical role for anteroposterior axis, subfield and activation analyses to enhance predictive value of hippocampal changes for Alzheimerâ€™s disease diagnosis. *Frontiers in Cellular Neuroscience*, *8*. https://doi.org/10.3389/fncel.2014.00095

Massimo, L., Libon, D. J., Chandrasekaran, K., Dreyfuss, M., McMillan, C. T., Rascovsky, K., Boller, A., & Grossman, M. (2013). Self-appraisal in behavioural variant frontotemporal degeneration. *Journal of Neurology, Neurosurgery, and Psychiatry*, *84*(2), 148–153. https://doi.org/10.1136/jnnp-2012-303153

Mastroberardino, P. G., Hoffman, E. K., Horowitz, M. P., Betarbet, R., Taylor, G., Cheng, D., Na, H. M., Gutekunst, C.-A., Gearing, M., Trojanowski, J. Q., Anderson, M., Chu, C. T., Peng,

J., & Greenamyre, J. T. (2009). A novel transferrin/TfR2-mediated mitochondrial iron transport system is disrupted in Parkinson's disease. *Neurobiology of Disease*, *34*(3), 417–431. https://doi.org/10.1016/j.nbd.2009.02.009

Matsuda, H., Kitayama, N., Ohnishi, T., Asada, T., Nakano, S., Sakamoto, S., Imabayashi, E., & Katoh, A. (2002). Longitudinal evaluation of both morphologic and functional changes in the same individuals with Alzheimer's disease. *Journal of Nuclear Medicine: Official Publication, Society of Nuclear Medicine*, *43*(3), 304–311.

Mattson, M. P., & Arumugam, T. V. (2018). Hallmarks of Brain Aging: Adaptive and Pathological Modification by Metabolic States. *Cell Metabolism*, *27*(6), 1176–1199. https://doi.org/10.1016/j.cmet.2018.05.011

Mattson, M. P., & Magnus, T. (2006). Ageing and neuronal vulnerability. *Nature Reviews Neuroscience*, *7*(4), Article 4. https://doi.org/10.1038/nrn1886

Mazère, J., Prunier, C., Barret, O., Guyot, M., Hommet, C., Guilloteau, D., Dartigues, J. F., Auriacombe, S., Fabrigoule, C., & Allard, M. (2008). In vivo SPECT imaging of vesicular acetylcholine transporter using [(123)I]-IBVM in early Alzheimer's disease. *NeuroImage*, *40*(1), 280–288. https://doi.org/10.1016/j.neuroimage.2007.11.028

McKhann, G. M., Drachman, D., Folstein, M., Katzman, R., Price, D., & Stadlan, E. M. (1984). Clinical diagnosis of Alzheimer's disease: Report of the NINCDS-ADRDA Work Group under the auspices of Department of Health and Human Services Task Force on Alzheimer's Disease. *Neurology*, *34*(7), 939–939. https://doi.org/10.1212/WNL.34.7.939

McKhann, G. M., Knopman, D. S., Chertkow, H., Hyman, B. T., Jack, C. R., Kawas, C. H., Klunk, W. E., Koroshetz, W. J., Manly, J. J., Mayeux, R., Mohs, R. C., Morris, J. C., Rossor, M. N., Scheltens, P., Carrillo, M. C., Thies, B., Weintraub, S., & Phelps, C. H. (2011). The diagnosis of dementia due to Alzheimer's disease: Recommendations from the National Institute on Aging-Alzheimer's Association workgroups on diagnostic guidelines for Alzheimer's disease. *Alzheimer's & Dementia*, *7*(3), 263–269. https://doi.org/10.1016/j.jalz.2011.03.005

Mechelli, A., Price, C., Friston, K., & Ashburner, J. (2005). Voxel-Based Morphometry of the Human Brain: Methods and Applications. *Current Medical Imaging Reviews*, *1*(2), 105–113. https://doi.org/10.2174/1573405054038726

Mendez, M. F. (2019). Early-onset Alzheimer Disease and Its Variants. *CONTINUUM: Lifelong Learning in Neurology*, *25*(1), 34–51. https://doi.org/10.1212/CON.0000000000000687

Mesulam, M. (2004a). The cholinergic innervation of the human cerebral cortex. *Progress in Brain Research*, *145*, 67–78. https://doi.org/10.1016/S0079-6123(03)45004-8

Mesulam, M. (2004b). The Cholinergic Lesion of Alzheimer's Disease: Pivotal Factor or Side Show? *Learning & Memory*, *11*(1), 43–49. https://doi.org/10.1101/lm.69204

Mesulam, M. (2012). Cholinergic Aspects of Aging and Alzheimer's Disease. *Biological Psychiatry*, *71*(9), 760–761. https://doi.org/10.1016/j.biopsych.2012.02.025

Mesulam, M., & Geula. (1988). Nucleus basalis (Ch4) and cortical cholinergic innervation in the human brain: Observations based on the distribution of acetylcholinesterase and choline acetyltransferase. *Journal of Comparative Neurology*, *275*(2), 216–240.

https://doi.org/10.1002/cne.902750205

Mesulam, M., Mufson, E. J., Levey, A. I., & Wainer, B. H. (1983). Cholinergic innervation of cortex by the basal forebrain: Cytochemistry and cortical connections of the septal area, diagonal band nuclei, nucleus basalis (Substantia innominata), and hypothalamus in the rhesus monkey. *Journal of Comparative Neurology*, *214*(2), 170–197. https://doi.org/10.1002/cne.902140206

Mesulam, M., Shaw, P., Mash, D., & Weintraub, S. (2004). Cholinergic nucleus basalis tauopathy emerges early in the aging-MCI-AD continuum. *Annals of Neurology*, *55*(6), 815–828. https://doi.org/10.1002/ana.20100

Mesulam, M.-M., Hersh, L. B., Mash, D. C., & Geula, C. (1992). Differential cholinergic innervation within functional subdivisions of the human cerebral cortex: A choline acetyltransferase study. *The Journal of Comparative Neurology*, *318*(3), 316–328. https://doi.org/10.1002/cne.903180308

Mieling, M., Göttlich, M., Yousuf, M., & Bunzeck, N. (2023). Basal forebrain activity predicts functional degeneration in the entorhinal cortex in Alzheimer's disease. *Brain Communications*, *5*(5), fcad262. https://doi.org/10.1093/braincomms/fcad262

Mieling, M., Meier, H., & Bunzeck, N. (2023). Structural Degeneration of the Nucleus basalis of Meynert in Mild Cognitive Impairment and Alzheimer's Disease – Evidence from an MRI-based Meta-Analysis. *Neuroscience & Biobehavioral Reviews*, 105393. https://doi.org/10.1016/j.neubiorev.2023.105393

Mieling, M., Wiskow, C., & Bunzeck, N. (2024). *Globus pallidus iron relates to cognitive impairment in Alzheimer's disease: Evidence from MRI-based meta-analysis*. https://doi.org/10.31219/osf.io/xta8m

Mieling, M., Yousuf, M., & Bunzeck, N. (2023). *Predicting MCI and Alzheimer's disease on structural brain integrity with machine learning*. https://doi.org/10.31219/osf.io/8dtcm

Migliore, L., & Coppedè, F. (2009). Genetics, environmental factors and the emerging role of epigenetics in neurodegenerative diseases. *Mutation Research/Fundamental and Molecular Mechanisms of Mutagenesis*, *667*(1–2), 82–97. https://doi.org/10.1016/j.mrfmmm.2008.10.011

Migliore, L., & Coppedè, F. (2022). Gene–environment interactions in Alzheimer disease: The emerging role of epigenetics. *Nature Reviews Neurology*, *18*(11), 643–660. https://doi.org/10.1038/s41582-022-00714-w

Miller, A. D., & Blaha, C. D. (2004). Nigrostriatal dopamine release modulated by mesopontine muscarinic receptors. *Neuroreport*, *15*(11), 1805–1808.

Mills, E., Dong, X., Wang, F., & Xu, H. (2010). Mechanisms of brain iron transport: Insight into neurodegeneration and CNS disorders. *Future Medicinal Chemistry*, *2*(1), 51–64. https://doi.org/10.4155/fmc.09.140

Mitsushima, D., Sano, A., & Takahashi, T. (2013). A cholinergic trigger drives learning-induced plasticity at hippocampal synapses. *Nature Communications*, *4*. https://doi.org/10.1038/ncomms3760

Mobarra, N., Shanaki, M., Ehteram, H., Nasiri, H., Sahmani, M., Saeidi, M., Goudarzi, M., Pourkarim, H., & Azad, M. (2016). A Review on Iron Chelators in Treatment of Iron

Overload Syndromes. *International Journal of Hematology-Oncology and Stem Cell Research*, *10*(4), 239–247.

Mofrad, S. A., Lundervold, A. J., Vik, A., & Lundervold, A. S. (2021). Cognitive and MRI trajectories for prediction of Alzheimer's disease. *Scientific Reports*, *11*(1), 2122. https://doi.org/10.1038/s41598-020-78095-7

Mofrad, S. A., Lundervold, A., & Lundervold, A. S. (2021). A predictive framework based on brain volume trajectories enabling early detection of Alzheimer's disease. *Computerized Medical Imaging and Graphics*, *90*, 101910. https://doi.org/10.1016/j.compmedimag.2021.101910

Mohammad, D., Chan, P., Bradley, J., Lanctôt, K., & Herrmann, N. (2017). Acetylcholinesterase inhibitors for treating dementia symptoms—A safety evaluation. *Expert Opinion on Drug Safety*, *16*(9), 1009–1019. https://doi.org/10.1080/14740338.2017.1351540

Montalà-Flaquer, M., Cañete-Massé, C., Vaqué-Alcázar, L., Bartrés-Faz, D., Peró-Cebollero, M., & Guàrdia-Olmos, J. (2023). Spontaneous brain activity in healthy aging: An overview through fluctuations and regional homogeneity. *Frontiers in Aging Neuroscience*, *14*, 1002811. https://doi.org/10.3389/fnagi.2022.1002811

Moon, W.-J., Kim, H.-J., Roh, H. G., Choi, J. W., & Han, S.-H. (2012). Fluid-attenuated inversion recovery hypointensity of the pulvinar nucleus of patients with Alzheimer disease: Its possible association with iron accumulation as evidenced by the t2(*) map. *Korean Journal of Radiology*, *13*(6), 674–683. https://doi.org/10.3348/kjr.2012.13.6.674

Moon, Y., Han, S.-H., & Moon, W.-J. (2016). Patterns of Brain Iron Accumulation in Vascular Dementia and Alzheimer's Dementia Using Quantitative Susceptibility Mapping Imaging. *Journal of Alzheimer's Disease*, *51*(3), 737–745. https://doi.org/10.3233/JAD-151037

Moon, Y., Moon, W.-J., Kim, H., & Han, S.-H. (2014). Regional Atrophy of the Insular Cortex Is Associated with Neuropsychiatric Symptoms in Alzheimer's Disease Patients. *European Neurology*, *71*(5–6), 223–229. https://doi.org/10.1159/000356343

Moreno-Ibarra, M.-A., Villuendas-Rey, Y., Lytras, M. D., Yáñez-Márquez, C., & Salgado-Ramírez, J.-C. (2021). Classification of Diseases Using Machine Learning Algorithms: A Comparative Study. *Mathematics*, *9*(15), 1817. https://doi.org/10.3390/math9151817

Morris, G. P., Clark, I. A., & Vissel, B. (2018). Questions concerning the role of amyloid-β in the definition, aetiology and diagnosis of Alzheimer's disease. *Acta Neuropathologica*, *136*(5), 663–689. https://doi.org/10.1007/s00401-018-1918-8

Mosca, E., Szigeti, F., Tragianni, S., Gallagher, D., & Groh, G. (2022). SHAP-Based Explanation Methods: A Review for NLP Interpretability. *Proceedings of the 29th International Conference on Computational Linguistics*, 4593–4603. https://aclanthology.org/2022.coling-1.406

Moscovitch, M., Cabeza, R., Winocur, G., & Nadel, L. (2016). Episodic Memory and Beyond: The Hippocampus and Neocortex in Transformation. *Annual Review of Psychology*, *67*(1), 105–134. https://doi.org/10.1146/annurev-psych-113011-143733

Muhammed Niyas, K. P., & Thiyagarajan, P. (2023). A systematic review on early prediction of Mild cognitive impairment to alzheimers using machine learning algorithms. *International Journal of Intelligent Networks*, *4*, 74–88.

https://doi.org/10.1016/j.ijin.2023.03.004

Muir, J. L. (1997). Acetylcholine, Aging, and Alzheimer's Disease. *Pharmacology Biochemistry and Behavior*, *56*(4), 687–696. https://doi.org/10.1016/S0091-3057(96)00431-5

Müller, P., Vellage, A., Schmicker, M., Menze, I., Grothe, M. J., Teipel, S. J., & Müller, N. G. (2021). Structural MRI of the basal forebrain as predictor of cognitive response to galantamine in healthy older adults—A randomized controlled double-blinded crossover study. *Alzheimer's & Dementia: Translational Research & Clinical Interventions*, *7*(1), e12153. https://doi.org/10.1002/trc2.12153

Müller, V. I., Edna C. Cieslik, Laird, A. R., Fox, P. T., Radua, J., Mataix-Cols, D., Tench, C. R., Yarkoni, T., Nichols, T. E., Turkeltaub, P. E., Wager, T. D., & Eickhoff, S. B. (2018). Ten simple rules for neuroimaging meta-analysis. *Neuroscience and Biobehavioral Reviews*, *84*, 151–161. https://doi.org/10.1016/j.neubiorev.2017.11.012

Murman, D. (2015). The Impact of Age on Cognition. *Seminars in Hearing*, *36*(03), 111–121. https://doi.org/10.1055/s-0035-1555115

Muth, K., Schönmeyer, R., Matura, S., Haenschel, C., Schröder, J., & Pantel, J. (2010). Mild Cognitive Impairment in the Elderly is Associated with Volume Loss of the Cholinergic Basal Forebrain Region. *Biological Psychiatry*, *67*(6), 588–591. https://doi.org/10.1016/j.biopsych.2009.02.026

Nemy, M., Dyrba, M., Brosseron, F., Buerger, K., Dechent, P., Dobisch, L., Ewers, M., Fliessbach, K., Glanz, W., Goerss, D., Heneka, M. T., Hetzer, S., Incesoy, E. I., Janowitz, D., Kilimann, I., Laske, C., Maier, F., Munk, M. H., Perneczky, R., … Ferreira, D. (2023). Cholinergic white matter pathways along the Alzheimer's disease continuum. *Brain*, *146*(5), 2075–2088. https://doi.org/10.1093/brain/awac385

Nichols, E., Szoeke, C. E. I., Vollset, S. E., Abbasi, N., Abd-Allah, F., Abdela, J., Aichour, M. T. E., Akinyemi, R. O., Alahdab, F., Asgedom, S. W., Awasthi, A., Barker-Collo, S. L., Baune, B. T., Béjot, Y., Belachew, A. B., Bennett, D. A., Biadgo, B., Bijani, A., Bin Sayeed, M. S., … Murray, C. J. L. (2019). Global, regional, and national burden of Alzheimer's disease and other dementias, 1990–2016: A systematic analysis for the Global Burden of Disease Study 2016. *The Lancet Neurology*, *18*(1), 88–106. https://doi.org/10.1016/S1474-4422(18)30403-4

Nikseresht, S., Bush, A. I., & Ayton, S. (2019). Treating Alzheimer's disease by targeting iron. *British Journal of Pharmacology*, *176*(18), 3622–3635. https://doi.org/10.1111/bph.14567

Niu, H., Álvarez-Álvarez, I., Guillén-Grima, F., & Aguinaga-Ontoso, I. (2017). Prevalence and incidence of Alzheimer's disease in Europe: A meta-analysis. *Neurología (English Edition)*, *32*(8), 523–532. https://doi.org/10.1016/j.nrleng.2016.02.009

Oakman, S. A., Faris, P. L., Kerr, P. E., Cozzari, C., & Hartman, B. K. (1995). Distribution of pontomesencephalic cholinergic neurons projecting to substantia nigra differs significantly from those projecting to ventral tegmental area. *J Neurosci*, *15*(9), 5859–5869.

Ocasio, E., & Duong, T. Q. (2021). Deep learning prediction of mild cognitive impairment conversion to Alzheimer's disease at 3 years after diagnosis using longitudinal and whole-brain 3D MRI. *PeerJ Computer Science*, *7*, e560. https://doi.org/10.7717/peerj-cs.560

Odusami, M., Maskeliūnas, R., Damaševičius, R., & Misra, S. (2023). Explainable Deep-Learning-Based Diagnosis of Alzheimer's Disease Using Multimodal Input Fusion of PET and MRI Images. *Journal of Medical and Biological Engineering*, *43*(3), 291–302. https://doi.org/10.1007/s40846-023-00801-3

Ogawa, S., Lee, T. M., Kay, A. R., & Tank, D. W. (1990). Brain magnetic resonance imaging with contrast dependent on blood oxygenation. *Proceedings of the National Academy of Sciences*, *87*(24), 9868–9872. https://doi.org/10.1073/pnas.87.24.9868

Ohnishi, T., Matsuda, H., Tabira, T., Asada, T., & Uno, M. (2001). Changes in brain morphology in Alzheimer disease and normal aging: Is Alzheimer disease an exaggerated aging process? *AJNR. American Journal of Neuroradiology*, *22*(9), 1680–1685.

Olman, C. A., Davachi, L., & Inati, S. (2009). Distortion and Signal Loss in Medial Temporal Lobe. *PLoS ONE*, *4*(12), e8160. https://doi.org/10.1371/journal.pone.0008160

Olsson, B., Lautner, R., Andreasson, U., Öhrfelt, A., Portelius, E., Bjerke, M., Hölttä, M., Rosén, C., Olsson, C., Strobel, G., Wu, E., Dakin, K., Petzold, M., Blennow, K., & Zetterberg, H. (2016). CSF and blood biomarkers for the diagnosis of Alzheimer's disease: A systematic review and meta-analysis. *The Lancet Neurology*, *15*(7), 673–684. https://doi.org/10.1016/S1474-4422(16)00070-3

Ostrerova-Golts, N., Petrucelli, L., Hardy, J., Lee, J. M., Farer, M., & Wolozin, B. (2000). The A53T α-Synuclein Mutation Increases Iron-Dependent Aggregation and Toxicity. *Journal of Neuroscience*, *20*(16), 6048–6054. https://doi.org/10.1523/JNEUROSCI.20-16-06048.2000

Page, M. J., McKenzie, J. E., Bossuyt, P. M., Boutron, I., Hoffmann, T. C., Mulrow, C. D., Shamseer, L., Tetzlaff, J. M., Akl, E. A., Brennan, S. E., Chou, R., Glanville, J., Grimshaw, J. M., Hróbjartsson, A., Lalu, M. M., Li, T., Loder, E. W., Mayo-Wilson, E., McDonald, S., … Moher, D. (2021). The PRISMA 2020 statement: An updated guideline for reporting systematic reviews. *BMJ*, n71. https://doi.org/10.1136/bmj.n71

Palmqvist, S., Mattsson, N., Hansson, O., & for the Alzheimer's Disease Neuroimaging Initiative. (2016). Cerebrospinal fluid analysis detects cerebral amyloid-β accumulation earlier than positron emission tomography. *Brain*, *139*(4), 1226–1236. https://doi.org/10.1093/brain/aww015

Pan, D., Zeng, A., Jia, L., Huang, Y., Frizzell, T., & Song, X. (2020). Early Detection of Alzheimer's Disease Using Magnetic Resonance Imaging: A Novel Approach Combining Convolutional Neural Networks and Ensemble Learning. *Frontiers in Neuroscience*, *14*, 259. https://doi.org/10.3389/fnins.2020.00259

Pedregosa, F., Varoquaux, G., Gramfort, A., Michel, V., Thirion, B., Grisel, O., Blondel, M., Müller, A., Nothman, J., Louppe, G., Prettenhofer, P., Weiss, R., Dubourg, V., Vanderplas, J., Passos, A., Cournapeau, D., Brucher, M., Perrot, M., & Duchesnay, É. (2012). *Scikit-learn: Machine Learning in Python*. https://doi.org/10.48550/ARXIV.1201.0490

Pellegrini, E., Ballerini, L., Hernandez, M. D. C. V., Chappell, F. M., González-Castro, V., Anblagan, D., Danso, S., Muñoz-Maniega, S., Job, D., Pernet, C., Mair, G., MacGillivray, T. J., Trucco, E., & Wardlaw, J. M. (2018). Machine learning of neuroimaging for assisted diagnosis of cognitive impairment and dementia: A systematic review. *Alzheimer's & Dementia: Diagnosis, Assessment & Disease Monitoring*, *10*(1), 519–535.

https://doi.org/10.1016/j.dadm.2018.07.004

Peng, Y., Jin, H., Xue, Y., Chen, Q., Yao, S., Du, M., & Liu, S. (2023). Current and future therapeutic strategies for Alzheimer's disease: An overview of drug development bottlenecks. *Frontiers in Aging Neuroscience*, *15*, 1206572. https://doi.org/10.3389/fnagi.2023.1206572

Pennanen, C., Testa, C., Laakso, M. P., Hallikainen, M., Helkala, E.-L., Hänninen, T., Kivipelto, M., Könönen, M., Nissinen, A., Tervo, S., Vanhanen, M., Vanninen, R., Frisoni, G. B., & Soininen, H. (2005). A voxel based morphometry study on mild cognitive impairment. *Journal of Neurology, Neurosurgery, and Psychiatry*, *76*(1), 11–14. https://doi.org/10.1136/jnnp.2004.035600

Peters, J. L., Sutton, A. J., Jones, D. R., Abrams, K. R., & Rushton, L. (2007). Performance of the trim and fill method in the presence of publication bias and between-study heterogeneity. *Statistics in Medicine*, *26*(25), 4544–4562. https://doi.org/10.1002/sim.2889

Petersen, R. C., Lopez, O., Armstrong, M. J., Getchius, T. S. D., Ganguli, M., Gloss, D., Gronseth, G. S., Marson, D., Pringsheim, T., Day, G. S., Sager, M., Stevens, J., & Rae-Grant, A. (2018). Practice guideline update summary: Mild cognitive impairment: Report of the Guideline Development, Dissemination, and Implementation Subcommittee of the American Academy of Neurology. *Neurology*, *90*(3), 126–135. https://doi.org/10.1212/WNL.0000000000004826

Picciotto, M. R., Higley, M. J., & Mineur, Y. S. (2012). Acetylcholine as a Neuromodulator: Cholinergic Signaling Shapes Nervous System Function and Behavior. *Neuron*, *76*(1), 116–129. https://doi.org/10.1016/j.neuron.2012.08.036

Planche, V., Manjon, J. V., Mansencal, B., Lanuza, E., Tourdias, T., Catheline, G., & Coupé, P. (2022). Structural progression of Alzheimer's disease over decades: The MRI staging scheme. *Brain Communications*, *4*(3), fcac109. https://doi.org/10.1093/braincomms/fcac109

PlotDigitizer: Free Online App. (n.d.). https://plotdigitizer.com

Plotkin, D. A., & Jarvik, L. F. (1986). Cholinergic Dysfunction in Alzheimer Disease: Cause or Effect? In *Progress in Brain Research* (Vol. 65, pp. 91–103). Elsevier. https://doi.org/10.1016/S0079-6123(08)60644-5

Poulin, S. P., Dautoff, R., Morris, J. C., Barrett, L. F., & Dickerson, B. C. (2011). Amygdala atrophy is prominent in early Alzheimer's disease and relates to symptom severity. *Psychiatry Research*, *194*(1), 7–13. https://doi.org/10.1016/j.pscychresns.2011.06.014

Power, J. D., Barnes, K. A., Snyder, A. Z., Schlaggar, B. L., & Petersen, S. E. (2012). Spurious but systematic correlations in functional connectivity MRI networks arise from subject motion. *NeuroImage*, *59*(3), 2142–2154. https://doi.org/10.1016/j.neuroimage.2011.10.018

Prieto del Val, L., Cantero, J. L., & Atienza, M. (2016). Atrophy of amygdala and abnormal memory-related alpha oscillations over posterior cingulate predict conversion to Alzheimer's disease. *Scientific Reports*, *6*(1), Article 1. https://doi.org/10.1038/srep31859

Purves, D. (Ed.). (2008). *Neuroscience* (4th ed). Sinauer.

Qin, Y., Zhu, W., Zhan, C., Zhao, L., Wang, J., Tian, Q., & Wang, W. (2011). Investigation on positive correlation of increased brain iron deposition with cognitive impairment in Alzheimer disease by using quantitative MR R2' mapping. *Journal of Huazhong University of Science and Technology. Medical Sciences = Hua Zhong Ke Ji Da Xue Xue Bao. Yi Xue Ying De Wen Ban = Huazhong Keji Daxue Xuebao. Yixue Yingdewen Ban*, *31*(4), 578. https://doi.org/10.1007/s11596-011-0493-1

Quevenco, F. C., Preti, M. G., Van Bergen, J. M. G., Hua, J., Wyss, M., Li, X., Schreiner, S. J., Steininger, S. C., Meyer, R., Meier, I. B., Brickman, A. M., Leh, S. E., Gietl, A. F., Buck, A., Nitsch, R. M., Pruessmann, K. P., Van Zijl, P. C. M., Hock, C., Van De Ville, D., & Unschuld, P. G. (2017). Memory performance-related dynamic brain connectivity indicates pathological burden and genetic risk for Alzheimer's disease. *Alzheimer's Research & Therapy*, *9*(1), 24. https://doi.org/10.1186/s13195-017-0249-7

Rabin, L. A., Smart, C. M., & Amariglio, R. E. (2017). Subjective Cognitive Decline in Preclinical Alzheimer's Disease. *Annual Review of Clinical Psychology*, *13*(1), 369–396. https://doi.org/10.1146/annurev-clinpsy-032816-045136

Rabinovici, G. D., Seeley, W. W., Kim, E. J., Gorno-Tempini, M. L., Rascovsky, K., Pagliaro, T. A., Allison, S. C., Halabi, C., Kramer, J. H., Johnson, J. K., Weiner, M. W., Forman, M. S., Trojanowski, J. Q., Dearmond, S. J., Miller, B. L., & Rosen, H. J. (2007). Distinct MRI atrophy patterns in autopsy-proven Alzheimer's disease and frontotemporal lobar degeneration. *American Journal of Alzheimer's Disease and Other Dementias*, *22*(6), 474–488. https://doi.org/10.1177/1533317507308779

Rajmohan, R., & Reddy, P. H. (2017). Amyloid Beta and Phosphorylated Tau Accumulations Cause Abnormalities at Synapses of Alzheimer's disease Neurons. *Journal of Alzheimer's Disease : JAD*, *57*(4), 975–999. https://doi.org/10.3233/JAD-160612

Ram, N., Gerstorf, D., Lindenberger, U., & Smith, J. (2011). Developmental change and intraindividual variability: Relating cognitive aging to cognitive plasticity, cardiovascular lability, and emotional diversity. *Psychology and Aging*, *26*(2), 363–371. https://doi.org/10.1037/a0021500

Rami, L., Gómez-Anson, B., Monte, G. C., Bosch, B., Sánchez-Valle, R., & Molinuevo, J. L. (2009). Voxel based morphometry features and follow-up of amnestic patients at high risk for Alzheimer's disease conversion. *International Journal of Geriatric Psychiatry*, *24*(8), 875–884. https://doi.org/10.1002/gps.2216

Ramos Bernardes da Silva Filho, S., Oliveira Barbosa, J. H., Rondinoni, C., dos Santos, A. C., Garrido Salmon, C. E., da Costa Lima, N. K., Ferriolli, E., & Moriguti, J. C. (2017). Neuro-degeneration profile of Alzheimer's patients: A brain morphometry study. *NeuroImage: Clinical*, *15*, 15–24. https://doi.org/10.1016/j.nicl.2017.04.001

Rao, S. S., & Adlard, P. A. (2018). Untangling Tau and Iron: Exploring the Interaction Between Iron and Tau in Neurodegeneration. *Frontiers in Molecular Neuroscience*, *11*, 276. https://doi.org/10.3389/fnmol.2018.00276

Rao, Y. L., Ganaraja, B., Murlimanju, B. V., Joy, T., Krishnamurthy, A., & Agrawal, A. (2022). Hippocampus and its involvement in Alzheimer's disease: A review. *3 Biotech*, *12*(2), 55. https://doi.org/10.1007/s13205-022-03123-4

Rathore, S., Habes, M., Iftikhar, M. A., Shacklett, A., & Davatzikos, C. (2017). A review on neuroimaging-based classification studies and associated feature extraction methods

for Alzheimer's disease and its prodromal stages. *NeuroImage*, *155*, 530–548. https://doi.org/10.1016/j.neuroimage.2017.03.057

Reinert, A., Morawski, M., Seeger, J., Arendt, T., & Reinert, T. (2019). Iron concentrations in neurons and glial cells with estimates on ferritin concentrations. *BMC Neuroscience*, *20*(1), 25. https://doi.org/10.1186/s12868-019-0507-7

Rémy, F., Mirrashed, F., Campbell, B., & Richter, W. (2005). Verbal episodic memory impairment in Alzheimer's disease: A combined structural and functional MRI study. *NeuroImage*, *25*(1), 253–266. https://doi.org/10.1016/j.neuroimage.2004.10.045

Reuter, M., Rosas, H. D., & Fischl, B. (2010). Highly accurate inverse consistent registration: A robust approach. *NeuroImage*, *53*(4), 1181–1196. https://doi.org/10.1016/j.neuroimage.2010.07.020

Reuter, M., Schmansky, N. J., Rosas, H. D., & Fischl, B. (2012). Within-subject template estimation for unbiased longitudinal image analysis. *NeuroImage*, *61*(4), 1402–1418. https://doi.org/10.1016/j.neuroimage.2012.02.084

Reznichenko, L., Amit, T., Zheng, H., Avramovich-Tirosh, Y., Youdim, M. B. H., O. Weinreb, & Mandel, S. (2006). Reduction of iron-regulated amyloid precursor protein and β-amyloid peptide by (–)-epigallocatechin-3-gallate in cell cultures: Implications for iron chelation in Alzheimer's disease. *Journal of Neurochemistry*, *97*(2), 527–536. https://doi.org/10.1111/j.1471-4159.2006.03770.x

Rho, H.-J., Kim, J.-H., & Lee, S.-H. (2018). Function of Selective Neuromodulatory Projections in the Mammalian Cerebral Cortex: Comparison Between Cholinergic and Noradrenergic Systems. *Frontiers in Neural Circuits*, *12*, 47. https://doi.org/10.3389/fncir.2018.00047

Richter, N., Beckers, N., Onur, O. A., Dietlein, M., Tittgemeyer, M., Kracht, L., Neumaier, B., Fink, G. R., & Kukolja, J. (2018). Effect of cholinergic treatment depends on cholinergic integrity in early Alzheimer's disease. *Brain*, *141*(3), 903–915. https://doi.org/10.1093/brain/awx356

Rogaev, E. I., Sherrington, R., Rogaeva, E. A., Levesque, G., Ikeda, M., Liang, Y., Chi, H., Lin, C., Holman, K., Tsuda, T., Mar, L., Sorbi, S., Nacmias, B., Piacentini, S., Amaducci, L., Chumakov, I., Cohen, D., Lannfelt, L., Fraser, P. E., … George-Hyslop, P. H. S. (1995). Familial Alzheimer's disease in kindreds with missense mutations in a gene on chromosome 1 related to the Alzheimer's disease type 3 gene. *Nature*, *376*(6543), 775–778. https://doi.org/10.1038/376775a0

Rogers, J. T., Bush, A. I., Cho, H.-H., Smith, D. H., Thomson, A. M., Friedrlich, A. L., Lahiri, D. K., Leedman, P. J., Huang, X., & Cahill, C. M. (2008). Iron and the translation of the amyloid precursor protein (APP) and ferritin mRNAs: Riboregulation against neural oxidative damage in Alzheimer's disease. *Biochemical Society Transactions*, *36*(6), 1282–1287. Scopus. https://doi.org/10.1042/BST0361282

Rombouts, S. A. R. B., Barkhof, F., Witter, M. P., & Scheltens, P. (2000). Unbiased whole-brain analysis of gray matter loss in Alzheimer's disease. *Neuroscience Letters*, *285*(3), 231–233. https://doi.org/10.1016/S0304-3940(00)01067-3

Rondina, J. M., Ferreira, L. K., De Souza Duran, F. L., Kubo, R., Ono, C. R., Leite, C. C., Smid, J., Nitrini, R., Buchpiguel, C. A., & Busatto, G. F. (2018). Selecting the most relevant brain regions to discriminate Alzheimer's disease patients from healthy controls using

multiple kernel learning: A comparison across functional and structural imaging modalities and atlases. *NeuroImage: Clinical*, *17*, 628–641. https://doi.org/10.1016/j.nicl.2017.10.026

Rosano, C., Simonsick, E. M., Harris, T. B., Kritchevsky, S. B., Brach, J., Visser, M., Yaffe, K., & Newman, A. B. (2005). Association between Physical and Cognitive Function in Healthy Elderly: The Health, Aging and Body Composition Study. *Neuroepidemiology*, *24*(1–2), 8–14. https://doi.org/10.1159/000081043

Rossum, G. van, & Drake, F. L. (2010). *The Python language reference* (Release 3.0.1 [Repr.]). Python Software Foundation.

Rottkamp, C. A., Raina, A. K., Zhu, X., Gaier, E., Bush, A. I., Atwood, C. S., Chevion, M., Perry, G., & Smith, M. A. (2001). Redox-active iron mediates amyloid-β toxicity. *Free Radical Biology and Medicine*, *30*(4), 447–450. https://doi.org/10.1016/S0891-5849(00)00494-9

Rousselet, G. A., & Pernet, C. R. (2012). Improving standards in brain-behavior correlation analyses. *Frontiers in Human Neuroscience*, *6*. https://doi.org/10.3389/fnhum.2012.00119

Rutishauser, U., Ross, I. B., Mamelak, A. N., & Schuman, E. M. (2010). Human memory strength is predicted by theta-frequency phase-locking of single neurons. *Nature*, *464*(7290), 903–907. https://doi.org/10.1038/nature08860

Safer, D. J., & Allen, R. P. (1971). The central effects of scopolamine in man. *Biological Psychiatry*, *3*(4), 347–355.

Sarica, A., Cerasa, A., & Quattrone, A. (2017). Random Forest Algorithm for the Classification of Neuroimaging Data in Alzheimer's Disease: A Systematic Review. *Frontiers in Aging Neuroscience*, *9*, 329. https://doi.org/10.3389/fnagi.2017.00329

Sato, C., Barthélemy, N. R., Mawuenyega, K. G., Patterson, B. W., Gordon, B. A., Jockel-Balsarotti, J., Sullivan, M., Crisp, M. J., Kasten, T., Kirmess, K. M., Kanaan, N. M., Yarasheski, K. E., Baker-Nigh, A., Benzinger, T. L. S., Miller, T. M., Karch, C. M., & Bateman, R. J. (2018). Tau Kinetics in Neurons and the Human Central Nervous System. *Neuron*, *97*(6), 1284-1298.e7. https://doi.org/10.1016/j.neuron.2018.02.015

Sato, J. R., Fujita, A., Cardoso, E. F., Thomaz, C. E., Brammer, M. J., & Amaro, E. (2010). Analyzing the connectivity between regions of interest: An approach based on cluster Granger causality for fMRI data analysis. *NeuroImage*, *52*(4), 1444–1455. https://doi.org/10.1016/j.neuroimage.2010.05.022

Saykin, A. J., Shen, L., Foroud, T. M., Potkin, S. G., Swaminathan, S., Kim, S., Risacher, S. L., Nho, K., Huentelman, M. J., Craig, D. W., Thompson, P. M., Stein, J. L., Moore, J. H., Farrer, L. A., Green, R. C., Bertram, L., Jack, C. R., Weiner, M. W., & Alzheimer's Disease Neuroimaging Initiative. (2010). Alzheimer's Disease Neuroimaging Initiative biomarkers as quantitative phenotypes: Genetics core aims, progress, and plans. *Alzheimer's & Dementia*, *6*(3), 265–273. https://doi.org/10.1016/j.jalz.2010.03.013

Schaeverbeke, J., Delmotte, K., Vandenberghe, R., & Poesen, K. (2021). Prognostic value of amyloid/tau/neurodegeneration (ATN) classification based on diagnostic cerebrospinal fluid samples for Alzheimer's disease. *Alzheimer's & Dementia*, *17*(S5). https://doi.org/10.1002/alz.051036

Scheiblich, H., Trombly, M., Ramirez, A., & Heneka, M. T. (2020). Neuroimmune Connections in Aging and Neurodegenerative Diseases. *Trends in Immunology*, *41*(4), 300–312. https://doi.org/10.1016/j.it.2020.02.002

Schellenberg, G. D., Bird, T. D., Wijsman, E. M., Orr, H. T., Anderson, L., Nemens, E., White, J. A., Bonnycastle, L., Weber, J. L., Alonso, M. E., Potter, H., Heston, L. L., & Martin, G. M. (1992). Genetic Linkage Evidence for a Familial Alzheimer's Disease Locus on Chromosome 14. *Science*, *258*(5082), 668–671. https://doi.org/10.1126/science.1411576

Schindler, S. E., Gray, J. D., Gordon, B. A., Xiong, C., Batrla-Utermann, R., Quan, M., Wahl, S., Benzinger, T. L. S., Holtzman, D. M., Morris, J. C., & Fagan, A. M. (2018). Cerebrospinal fluid biomarkers measured by Elecsys assays compared to amyloid imaging. *Alzheimer's & Dementia*, *14*(11), 1460–1469. https://doi.org/10.1016/j.jalz.2018.01.013

Schliebs, R., & Arendt, T. (2011). The cholinergic system in aging and neuronal degeneration. *Behavioural Brain Research*, *221*(2), 555–563. https://doi.org/10.1016/j.bbr.2010.11.058

Schmidt-Wilcke, T., Poljansky, S., Hierlmeier, S., Hausner, J., & Ibach, B. (2009). Memory performance correlates with gray matter density in the ento-/perirhinal cortex and posterior hippocampus in patients with mild cognitive impairment and healthy controls—A voxel based morphometry study. *NeuroImage*, *47*(4), 1914–1920. https://doi.org/10.1016/j.neuroimage.2009.04.092

Schmitz, T. W., & Duncan, J. (2018). Normalization and the Cholinergic Microcircuit: A Unified Basis for Attention. *Trends in Cognitive Sciences*, *22*(5), 422–437. https://doi.org/10.1016/j.tics.2018.02.011

Schmitz, T. W., Mur, M., Aghourian, M., Bedard, M.-A., & Spreng, R. N. (2018). Longitudinal Alzheimer's Degeneration Reflects the Spatial Topography of Cholinergic Basal Forebrain Projections. *Cell Reports*, *24*(1), 38–46. https://doi.org/10.1016/j.celrep.2018.06.001

Schmitz, T. W., Soreq, H., Poirier, J., & Spreng, R. N. (2020). Longitudinal Basal Forebrain Degeneration Interacts with TREM2/C3 Biomarkers of Inflammation in Presymptomatic Alzheimer's Disease. *The Journal of Neuroscience*, *40*(9), 1931–1942. https://doi.org/10.1523/JNEUROSCI.1184-19.2019

Schmitz, T. W., & Spreng, R. N. (2016). Basal forebrain degeneration precedes and predicts the cortical spread of Alzheimer's pathology. *Nature Communications*, *7*(1), 13249. https://doi.org/10.1038/ncomms13249

Schneider, B. A., Avivi-Reich, M., & Mozuraitis, M. (2015). A cautionary note on the use of the Analysis of Covariance (ANCOVA) in classification designs with and without within-subject factors. *Frontiers in Psychology*, *6*. https://doi.org/10.3389/fpsyg.2015.00474

Schultz, A. P., Chhatwal, J. P., Hedden, T., Mormino, E. C., Hanseeuw, B. J., Sepulcre, J., Huijbers, W., LaPoint, M., Buckley, R. F., Johnson, K. A., & Sperling, R. A. (2017). Phases of Hyperconnectivity and Hypoconnectivity in the Default Mode and Salience Networks Track with Amyloid and Tau in Clinically Normal Individuals. *The Journal of Neuroscience*, *37*(16), 4323–4331. https://doi.org/10.1523/JNEUROSCI.3263-16.2017

Schultz, H., Sommer, T., & Peters, J. (2015). The Role of the Human Entorhinal Cortex in a

Representational Account of Memory. *Frontiers in Human Neuroscience*, *9*. https://doi.org/10.3389/fnhum.2015.00628

Schumacher, J., Ray, N. J., Hamilton, C. A., Donaghy, P. C., Firbank, M., Roberts, G., Allan, L., Durcan, R., Barnett, N., O'Brien, J. T., Taylor, J.-P., & Thomas, A. J. (2022). Cholinergic white matter pathways in dementia with Lewy bodies and Alzheimer's disease. *Brain*, *145*(5), 1773–1784. https://doi.org/10.1093/brain/awab372

Ségonne, F., Dale, A. M., Busa, E., Glessner, M., Salat, D., Hahn, H. K., & Fischl, B. (2004). A hybrid approach to the skull stripping problem in MRI. *NeuroImage*, *22*(3), 1060–1075. https://doi.org/10.1016/j.neuroimage.2004.03.032

Self, W. K., & Holtzman, D. M. (2023). Emerging diagnostics and therapeutics for Alzheimer disease. *Nature Medicine*, *29*(9), 2187–2199. https://doi.org/10.1038/s41591-023-02505-2

Semsei, I. (2000). On the nature of aging. *Mechanisms of Ageing and Development*, *117*(1–3), 93–108. https://doi.org/10.1016/S0047-6374(00)00147-0

Sepulcre, J., Grothe, M. J., d'Oleire Uquillas, F., Ortiz-Terán, L., Diez, I., Yang, H.-S., Jacobs, H. I. L., Hanseeuw, B. J., Li, Q., El-Fakhri, G., Sperling, R. A., & Johnson, K. A. (2018). Neurogenetic contributions to amyloid beta and tau spreading in the human cortex. *Nature Medicine*, *24*(12), Article 12. https://doi.org/10.1038/s41591-018-0206-4

Serai, S. D., Ho, M.-L., Artunduaga, M., Chan, S. S., & Chavhan, G. B. (2021). Components of a magnetic resonance imaging system and their relationship to safety and image quality. *Pediatric Radiology*, *51*(5), 716–723. https://doi.org/10.1007/s00247-020-04894-9

Serrano-Pozo, A., Frosch, M. P., Masliah, E., & Hyman, B. T. (2011). Neuropathological Alterations in Alzheimer Disease. *Cold Spring Harbor Perspectives in Medicine*, *1*(1), a006189–a006189. https://doi.org/10.1101/cshperspect.a006189

Sharma, K. (2019). Cholinesterase inhibitors as Alzheimer's therapeutics (Review). *Molecular Medicine Reports*. https://doi.org/10.3892/mmr.2019.10374

Shaw, L. M., Vanderstichele, H., Knapik-Czajka, M., Clark, C. M., Aisen, P. S., Petersen, R. C., Blennow, K., Soares, H., Simon, A., Lewczuk, P., Dean, R., Siemers, E., Potter, W., Lee, V. M.-Y., Trojanowski, J. Q., & Alzheimer's Disease Neuroimaging Initiative. (2009). Cerebrospinal fluid biomarker signature in Alzheimer's disease neuroimaging initiative subjects. *Annals of Neurology*, *65*(4), 403–413. https://doi.org/10.1002/ana.21610

Sherman, S. J., Atri, A., Hasselmo, M. E., Stern, C. E., & Howard, M. W. (2003). Scopolamine impairs human recognition memory: Data and modeling. *Behav Neurosci*, *117*(3), 526–539.

Shiino, A., Watanabe, T., Maeda, K., Kotani, E., Akiguchi, I., & Matsuda, M. (2006). Four subgroups of Alzheimer's disease based on patterns of atrophy using VBM and a unique pattern for early-onset disease. *NeuroImage*, *33*, 17–26. https://doi.org/10.1016/j.neuroimage.2006.06.010

Sian-Hülsmann, J., Mandel, S., Youdim, M. B. H., & Riederer, P. (2011). The relevance of iron in the pathogenesis of Parkinson's disease. *Journal of Neurochemistry*, *118*(6), 939–957. https://doi.org/10.1111/j.1471-4159.2010.07132.x

Sikora, E., Bielak-Zmijewska, A., Dudkowska, M., Krzystyniak, A., Mosieniak, G., Wesierska, M., & Wlodarczyk, J. (2021). Cellular Senescence in Brain Aging. *Frontiers in Aging*

Neuroscience, *13*, 646924. https://doi.org/10.3389/fnagi.2021.646924

Silver, N. C., Hittner, J. B., & May, K. (2004). Testing Dependent Correlations With Nonoverlapping Variables: A Monte Carlo Simulation. *The Journal of Experimental Education*, *73*(1), 53–69. https://doi.org/10.3200/JEXE.71.1.53-70

Singh, V., Chertkow, H., Lerch, J. P., Evans, A. C., Dorr, A. E., & Kabani, N. J. (2006). Spatial patterns of cortical thinning in mild cognitive impairment and Alzheimer's disease. *Brain*, *129*(11), 2885–2893. https://doi.org/10.1093/brain/awl256

Slavin, M. J., Brodaty, H., Kochan, N. A., Crawford, J. D., Trollor, J. N., Draper, B., & Sachdev, P. S. (2010). Prevalence and Predictors of "Subjective Cognitive Complaints" in the Sydney Memory and Ageing Study. *The American Journal of Geriatric Psychiatry*, *18*(8), 701–710. https://doi.org/10.1097/JGP.0b013e3181df49fb

Sled, J. G., Zijdenbos, A. P., & Evans, A. C. (1998). A nonparametric method for automatic correction of intensity nonuniformity in MRI data. *IEEE Transactions on Medical Imaging*, *17*(1), 87–97. https://doi.org/10.1109/42.668698

Son, S.-J., Kim, J., & Park, H. (2017). Structural and functional connectional fingerprints in mild cognitive impairment and Alzheimer's disease patients. *PLOS ONE*, *12*(3), e0173426. https://doi.org/10.1371/journal.pone.0173426

Spampinato, M. V., Rumboldt, Z., Hosker, R. J., Mintzer, J. E., & For the Alzheimer's Disease Neuroimaging Initiative. (2011). Apolipoprotein E and Gray Matter Volume Loss in Patients with Mild Cognitive Impairment and Alzheimer Disease. *Radiology*, *258*(3), 843–852. https://doi.org/10.1148/radiol.10100307

Sperling, R. (2011). The potential of functional MRI as a biomarker in early Alzheimer's disease. *Neurobiology of Aging*, *32*, S37–S43. https://doi.org/10.1016/j.neurobiolaging.2011.09.009

Sperling, R. A., Aisen, P. S., Beckett, L. A., Bennett, D. A., Craft, S., Fagan, A. M., Iwatsubo, T., Jack, C. R., Kaye, J., Montine, T. J., Park, D. C., Reiman, E. M., Rowe, C. C., Siemers, E., Stern, Y., Yaffe, K., Carrillo, M. C., Thies, B., Morrison-Bogorad, M., … Phelps, C. H. (2011). Toward defining the preclinical stages of Alzheimer's disease: Recommendations from the National Institute on Aging-Alzheimer's Association workgroups on diagnostic guidelines for Alzheimer's disease. *Alzheimer's & Dementia*, *7*(3), 280–292. https://doi.org/10.1016/j.jalz.2011.03.003

Spotorno, N., Acosta-Cabronero, J., Stomrud, E., Lampinen, B., Strandberg, O. T., Van Westen, D., & Hansson, O. (2020). Relationship between cortical iron and tau aggregation in Alzheimer's disease. *Brain*, *143*(5), 1341–1349. https://doi.org/10.1093/brain/awaa089

Steiger, T. K., & Bunzeck, N. (2017). Reward Dependent Invigoration Relates to Theta Oscillations and Is Predicted by Dopaminergic Midbrain Integrity in Healthy Elderly. *Frontiers in Aging Neuroscience*, *9*. https://doi.org/10.3389/fnagi.2017.00001

Steiger, T. K., Weiskopf, N., & Bunzeck, N. (2016). Iron Level and Myelin Content in the Ventral Striatum Predict Memory Performance in the Aging Brain. *The Journal of Neuroscience*, *36*(12), 3552–3558. https://doi.org/10.1523/JNEUROSCI.3617-15.2016

Sterne, J. A. C., & Egger, M. (2001). Funnel plots for detecting bias in meta-analysis. *Journal of Clinical Epidemiology*, *54*(10), 1046–1055. https://doi.org/10.1016/S0895-

4356(01)00377-8

Stolz, E., Mayerl, H., Muniz-Terrera, G., & Gill, T. M. (2024). Terminal Decline in Physical Function in Older Adults. *The Journals of Gerontology: Series A*, *79*(1), glad119. https://doi.org/10.1093/gerona/glad119

Stouffer, K. M., Grande, X., Düzel, E., Johansson, M., Creese, B., Witter, M. P., Miller, M. I., Wisse, L. E. M., & Berron, D. (2024). Amidst an amygdala renaissance in Alzheimer's disease. *Brain*, *147*(3), 816–829. https://doi.org/10.1093/brain/awad411

Suh, J., Rivest, A. J., Nakashiba, T., Tominaga, T., & Tonegawa, S. (2011). Entorhinal Cortex Layer III Input to the Hippocampus Is Crucial for Temporal Association Memory. *Science*, *334*(6061), 1415–1420. https://doi.org/10.1126/science.1210125

Suk, H.-I., Lee, S.-W., & Shen, D. (2015). Latent feature representation with stacked auto-encoder for AD/MCI diagnosis. *Brain Structure and Function*, *220*(2), 841–859. https://doi.org/10.1007/s00429-013-0687-3

Sutton, A. J. (2000). Empirical assessment of effect of publication bias on meta-analyses. *BMJ*, *320*(7249), 1574–1577. https://doi.org/10.1136/bmj.320.7249.1574

Sutton, H. C., & Winterbourn, C. C. (1989). On the participation of higher oxidation states of iron and copper in fenton reactions. *Free Radical Biology and Medicine*, *6*(1), 53–60. https://doi.org/10.1016/0891-5849(89)90160-3

Suurmond, R., Van Rhee, H., & Hak, T. (2017). Introduction, comparison, and validation of *META-ESSENTIALS* : A free and simple tool for meta-analysis. *Research Synthesis Methods*, *8*(4), 537–553. https://doi.org/10.1002/jrsm.1260

Suzuki, H., Venkataraman, A. V., Bai, W., Guitton, F., Guo, Y., Dehghan, A., Matthews, P. M., & for the Alzheimer's Disease Neuroimaging Initiative. (2019). Associations of Regional Brain Structural Differences With Aging, Modifiable Risk Factors for Dementia, and Cognitive Performance. *JAMA Network Open*, *2*(12), e1917257. https://doi.org/10.1001/jamanetworkopen.2019.17257

Swerdlow, R. H. (2011). Brain aging, Alzheimer's disease, and mitochondria. *Biochimica et Biophysica Acta (BBA) - Molecular Basis of Disease*, *1812*(12), 1630–1639. https://doi.org/10.1016/j.bbadis.2011.08.012

Tahami Monfared, A. A., Phan, N. T. N., Pearson, I., Mauskopf, J., Cho, M., Zhang, Q., & Hampel, H. (2023). A Systematic Review of Clinical Practice Guidelines for Alzheimer's Disease and Strategies for Future Advancements. *Neurology and Therapy*, *12*(4), 1257–1284. https://doi.org/10.1007/s40120-023-00504-6

Tang, X., Guo, Z., Chen, G., Sun, S., Xiao, S., Chen, P., Tang, G., Huang, L., & Wang, Y. (2024). A Multimodal Meta-Analytical Evidence of Functional and Structural Brain Abnormalities Across Alzheimer's Disease Spectrum. *Ageing Research Reviews*, *95*, 102240. https://doi.org/10.1016/j.arr.2024.102240

Tanveer, M., Richhariya, B., Khan, R. U., Rashid, A. H., Khanna, P., Prasad, M., & Lin, C. T. (2020). Machine Learning Techniques for the Diagnosis of Alzheimer's Disease: A Review. *ACM Transactions on Multimedia Computing, Communications, and Applications*, *16*(1s), 1–35. https://doi.org/10.1145/3344998

Tao, Y., Wang, Y., Rogers, J. T., & Wang, F. (2014). Perturbed Iron Distribution in Alzheimer's Disease Serum, Cerebrospinal Fluid, and Selected Brain Regions: A Systematic Review

and Meta-Analysis. *Journal of Alzheimer's Disease*, *42*(2), 679–690. https://doi.org/10.3233/JAD-140396

Tardif, C. L., Collins, D. L., & Pike, G. B. (2009). Regional impact of field strength on voxel-based morphometry results. *Human Brain Mapping*, *31*(7), 943–957. https://doi.org/10.1002/hbm.20908

Teipel, S. J., Wohlert, A., Metzger, C., Grimmer, T., Sorg, C., Ewers, M., Meisenzahl, E., Klöppel, S., Borchardt, V., Grothe, M. J., Walter, M., & Dyrba, M. (2017). Multicenter stability of resting state fMRI in the detection of Alzheimer's disease and amnestic MCI. *NeuroImage: Clinical*, *14*, 183–194. https://doi.org/10.1016/j.nicl.2017.01.018

Thal, D. R., Rüb, U., Orantes, M., & Braak, H. (2002). Phases of Aβ-deposition in the human brain and its relevance for the development of AD. *Neurology*, *58*(12), 1791–1800. https://doi.org/10.1212/WNL.58.12.1791

The jamovi project (2023). Jamovi (Version 2.3) [Computer Software]. (2.3). (2023). [Computer software]. https://www.jamovi.org

Therriault, J., Zimmer, E. R., Benedet, A. L., Pascoal, T. A., Gauthier, S., & Rosa-Neto, P. (2022). Staging of Alzheimer's disease: Past, present, and future perspectives. *Trends in Molecular Medicine*, *28*(9), 726–741. https://doi.org/10.1016/j.molmed.2022.05.008

Threlfell, S., Lalic, T., Platt, N. J., Jennings, K. A., Deisseroth, K., & Cragg, S. J. (2012). Striatal Dopamine Release Is Triggered by Synchronized Activity in Cholinergic Interneurons. *Neuron*, *75*(1), 58–64. https://doi.org/10.1016/j.neuron.2012.04.038

Tian, Y., Tian, Y., Yuan, Z., Zeng, Y., Wang, S., Fan, X., Yang, D., & Yang, M. (2022). Iron Metabolism in Aging and Age-Related Diseases. *International Journal of Molecular Sciences*, *23*(7), 3612. https://doi.org/10.3390/ijms23073612

Tiepolt, S., Rullmann, M., Jochimsen, T. H., Gertz, H.-J., Schroeter, M. L., Patt, M., Sabri, O., & Barthel, H. (2020). Quantitative susceptibility mapping in β-Amyloid PET-stratified patients with dementia and healthy controls—A hybrid PET/MRI study. *European Journal of Radiology*, *131*, 109243. https://doi.org/10.1016/j.ejrad.2020.109243

Todorich, B., Pasquini, J. M., Garcia, C. I., Paez, P. M., & Connor, J. R. (2009). Oligodendrocytes and myelination: The role of iron. *Glia*, *57*(5), 467–478. https://doi.org/10.1002/glia.20784

Toniolo, S., Zhao, S., Scholcz, A., Amein, B., Ganse-Dumrath, A., Heslegrave, A. J., Thompson, S., Manohar, S., Zetterberg, H., & Husain, M. (2024). Relationship of plasma biomarkers to digital cognitive tests in Alzheimer's disease. *Alzheimer's & Dementia: Diagnosis, Assessment & Disease Monitoring*, *16*(2), e12590. https://doi.org/10.1002/dad2.12590

Tran, D., DiGiacomo, P., Born, D. E., Georgiadis, M., & Zeineh, M. (2022). Iron and Alzheimer's Disease: From Pathology to Imaging. *Frontiers in Human Neuroscience*, *16*, 838692. https://doi.org/10.3389/fnhum.2022.838692

Tukey, J. W. (1977). *Exploratory data analysis*. Addison-Wesley Pub. Co.

Tuovinen, T., Rytty, R., Moilanen, V., Abou Elseoud, A., Veijola, J., Remes, A. M., & Kiviniemi, V. J. (2016). The Effect of Gray Matter ICA and Coefficient of Variation Mapping of BOLD Data on the Detection of Functional Connectivity Changes in Alzheimer's Disease and bvFTD. *Frontiers in Human Neuroscience*, *10*, 680.

https://doi.org/10.3389/fnhum.2016.00680

Turkeltaub, P. E., Eickhoff, S. B., Laird, A. R., Fox, M., Wiener, M., & Fox, P. (2012). Minimizing within-experiment and within-group effects in activation likelihood estimation meta-analyses. *Human Brain Mapping*, *33*(1), 1–13. https://doi.org/10.1002/hbm.21186

Van Bergen, J. M. G., Li, X., Hua, J., Schreiner, S. J., Steininger, S. C., Quevenco, F. C., Wyss, M., Gietl, A. F., Treyer, V., Leh, S. E., Buck, F., Nitsch, R. M., Pruessmann, K. P., Van Zijl, P. C. M., Hock, C., & Unschuld, P. G. (2016). Colocalization of cerebral iron with Amyloid beta in Mild Cognitive Impairment. *Scientific Reports*, *6*(1), 35514. https://doi.org/10.1038/srep35514

Van Bergen, J. M. G., Li, X., Quevenco, F. C., Gietl, A. F., Treyer, V., Meyer, R., Buck, A., Kaufmann, P. A., Nitsch, R. M., Van Zijl, P. C. M., Hock, C., & Unschuld, P. G. (2018). Simultaneous quantitative susceptibility mapping and Flutemetamol-PET suggests local correlation of iron and β-amyloid as an indicator of cognitive performance at high age. *NeuroImage*, *174*, 308–316. https://doi.org/10.1016/j.neuroimage.2018.03.021

Van Broeckhoven, C., Backhovens, H., Cruts, M., De Winter, G., Bruyland, M., Cras, P., & Martin, J.-J. (1992). Mapping of a gene predisposing to early–onset Alzheimer's disease to chromosome 14q24.3. *Nature Genetics*, *2*(4), 335–339. https://doi.org/10.1038/ng1292-335

van den Heuvel, M. P., & Hulshoff Pol, H. E. (2010). Exploring the brain network: A review on resting-state fMRI functional connectivity. *European Neuropsychopharmacology*, *20*(8), 519–534. https://doi.org/10.1016/j.euroneuro.2010.03.008

Van Der Kant, R., Goldstein, L. S. B., & Ossenkoppele, R. (2020). Amyloid-β-independent regulators of tau pathology in Alzheimer disease. *Nature Reviews Neuroscience*, *21*(1), 21–35. https://doi.org/10.1038/s41583-019-0240-3

Van Duijn, S., Bulk, M., Van Duinen, S. G., Nabuurs, R. J. A., Van Buchem, M. A., Van Der Weerd, L., & Natté, R. (2017). Cortical Iron Reflects Severity of Alzheimer's Disease. *Journal of Alzheimer's Disease*, *60*(4), 1533–1545. https://doi.org/10.3233/JAD-161143

Van Maurik, I. S., Zwan, M. D., Tijms, B. M., Bouwman, F. H., Teunissen, C. E., Scheltens, P., Wattjes, M. P., Barkhof, F., Berkhof, J., Van Der Flier, W. M., & for the Alzheimer's Disease Neuroimaging Initiative. (2017). Interpreting Biomarker Results in Individual Patients With Mild Cognitive Impairment in the Alzheimer's Biomarkers in Daily Practice (ABIDE) Project. *JAMA Neurology*, *74*(12), 1481. https://doi.org/10.1001/jamaneurol.2017.2712

Vanasse, T. J., Fox, P. M., Barron, D. S., Robertson, M., Eickhoff, S. B., Lancaster, J. L., & Fox, P. T. (2018). BrainMap VBM: An environment for structural meta-analysis. *Human Brain Mapping*, *39*(8), 3308–3325. https://doi.org/10.1002/hbm.24078

Vemuri, P., & Jack, C. R. (2010). Role of structural MRI in Alzheimer's disease. *Alzheimer's Research & Therapy*, *2*(4), 23. https://doi.org/10.1186/alzrt47

Vemuri, P., Wiste, H. J., Weigand, S. D., Shaw, L. M., Trojanowski, J. Q., Weiner, M. W., Knopman, D. S., Petersen, R. C., Jack, C. R., & On behalf of the Alzheimer's Disease Neuroimaging Initiative. (2009). MRI and CSF biomarkers in normal, MCI, and AD subjects: Predicting future clinical change. *Neurology*, *73*(4), 294–301. https://doi.org/10.1212/WNL.0b013e3181af79fb

Verghese, P. B., Castellano, J. M., & Holtzman, D. M. (2011). Apolipoprotein E in Alzheimer's disease and other neurological disorders. *The Lancet Neurology*, *10*(3), 241–252. https://doi.org/10.1016/S1474-4422(10)70325-2

Vieira, S., Pinaya, W. H. L., & Mechelli, A. (2017). Using deep learning to investigate the neuroimaging correlates of psychiatric and neurological disorders: Methods and applications. *Neuroscience & Biobehavioral Reviews*, *74*, 58–75. https://doi.org/10.1016/j.neubiorev.2017.01.002

Vogels, O. J. M., Broere, C. A. J., Ter Laak, H. J., Ten Donkelaar, H. J., Nieuwenhuys, R., & Schulte, B. P. M. (1990). Cell loss and shrinkage in the nucleus basalis Meynert complex in Alzheimer's disease. *Neurobiology of Aging*, *11*(1), 3–13. https://doi.org/10.1016/0197-4580(90)90056-6

Wager, T. D., Lindquist, M., & Kaplan, L. (2007). Meta-analysis of functional neuroimaging data: Current and future directions. *Social Cognitive and Affective Neuroscience*, *2*(2), 150–158. https://doi.org/10.1093/scan/nsm015

Walker, L. C., Diamond, M. I., Duff, K. E., & Hyman, B. T. (2013). Mechanisms of Protein Seeding in Neurodegenerative Diseases. *JAMA Neurology*, *70*(3), 10.1001/jamaneurol.2013.1453. https://doi.org/10.1001/jamaneurol.2013.1453

Wan, W., Cao, L., Kalionis, B., Murthi, P., Xia, S., & Guan, Y. (2019). Iron Deposition Leads to Hyperphosphorylation of Tau and Disruption of Insulin Signaling. *Frontiers in Neurology*, *10*, 607. https://doi.org/10.3389/fneur.2019.00607

Wang, D., Li, Y.-Y., Luo, J.-H., & Li, Y.-H. (2014). Age-related iron deposition in the basal ganglia of controls and Alzheimer disease patients quantified using susceptibility weighted imaging. *Archives of Gerontology and Geriatrics*, *59*(2), 439–449. https://doi.org/10.1016/j.archger.2014.04.002

Wang, D., Zhu, D., Wei, X.-E., Li, Y.-H., & Li, W.-B. (2013). Using susceptibility-weighted images to quantify iron deposition differences in amnestic mild cognitive impairment and Alzheimer's disease. *Neurology India*, *61*(1), 26–34. https://doi.org/10.4103/0028-3886.107924

Wang, H., Yang, F., Zhang, S., Xin, R., & Sun, Y. (2021). Genetic and environmental factors in Alzheimer's and Parkinson's diseases and promising therapeutic intervention via fecal microbiota transplantation. *Npj Parkinson's Disease*, *7*(1), 70. https://doi.org/10.1038/s41531-021-00213-7

Wang, L., Benzinger, T. L., Hassenstab, J., Blazey, T., Owen, C., Liu, J., Fagan, A. M., Morris, J. C., & Ances, B. M. (2015). Spatially distinct atrophy is linked to β-amyloid and tau in preclinical Alzheimer disease. *Neurology*, *84*(12), 1254–1260. https://doi.org/10.1212/WNL.0000000000001401

Wang, Q., He, C., Wang, Z., Zhang, Z., Xie, C., & for the Alzheimer's Disease Neuroimaging Initiative. (2021). Dynamic Connectivity Alteration Facilitates Cognitive Decline in Alzheimer's Disease Spectrum. *Brain Connectivity*, *11*(3), 213–224. https://doi.org/10.1089/brain.2020.0823

Wang, S.-M., Kim, N.-Y., Kang, D. W., Um, Y. H., Na, H.-R., Woo, Y. S., Lee, C. U., Bahk, W.-M., & Lim, H. K. (2021). A Comparative Study on the Predictive Value of Different Resting-State Functional Magnetic Resonance Imaging Parameters in Preclinical Alzheimer's Disease. *Frontiers in Psychiatry*, *12*, 626332.

https://doi.org/10.3389/fpsyt.2021.626332

Ward, R. J., Dexter, D. T., & Crichton, R. R. (2022). Iron, Neuroinflammation and Neurodegeneration. *International Journal of Molecular Sciences*, *23*(13), 7267. https://doi.org/10.3390/ijms23137267

Ward, R. J., Zucca, F. A., Duyn, J. H., Crichton, R. R., & Zecca, L. (2014). The role of iron in brain ageing and neurodegenerative disorders. *The Lancet Neurology*, *13*(10), 1045–1060. https://doi.org/10.1016/S1474-4422(14)70117-6

Warren, J. D., Rohrer, J. D., Schott, J. M., Fox, N. C., Hardy, J., & Rossor, M. N. (2013). Molecular nexopathies: A new paradigm of neurodegenerative disease. *Trends in Neurosciences*, *36*(10), 561–569. https://doi.org/10.1016/j.tins.2013.06.007

Warren, S. L., & Moustafa, A. A. (2023). Functional magnetic resonance imaging, deep learning, and Alzheimer's disease: A systematic review. *Journal of Neuroimaging*, *33*(1), 5–18. https://doi.org/10.1111/jon.13063

Wegmann, S., Jung, Y. J., Chinnathambi, S., Mandelkow, E.-M., Mandelkow, E., & Muller, D. J. (2010). Human Tau Isoforms Assemble into Ribbon-like Fibrils That Display Polymorphic Structure and Stability. *Journal of Biological Chemistry*, *285*(35), 27302–27313. https://doi.org/10.1074/jbc.M110.145318

Wei, G., Irish, M., Hodges, J. R., Piguet, O., & Kumfor, F. (2020). Disease-specific profiles of apathy in Alzheimer's disease and behavioural-variant frontotemporal dementia differ across the disease course. *Journal of Neurology*, *267*(4), 1086–1096. https://doi.org/10.1007/s00415-019-09679-1

Weiner, M. W., Veitch, D. P., Aisen, P. S., Beckett, L. A., Cairns, N. J., Green, R. C., Harvey, D., Jack, C. R., Jagust, W., Morris, J. C., Petersen, R. C., Salazar, J., Saykin, A. J., Shaw, L. M., Toga, A. W., Trojanowski, J. Q., & Alzheimer's Disease Neuroimaging Initiative. (2017). The Alzheimer's Disease Neuroimaging Initiative 3: Continued innovation for clinical trial improvement. *Alzheimer's & Dementia*, *13*(5), 561–571. https://doi.org/10.1016/j.jalz.2016.10.006

Weishaupt, D., Köchli, V. D., Marincek, B., Froehlich, J. M., Nanz, D., & Prüßmann, K. P. (2014). *Wie funktioniert MRI? Eine Einführung in Physik und Funktionsweise der Magnetresonanzbildgebung* (7., überarbeitete und ergänzte Auflage). Springer.

Wen, Q., & Chklovskii, D. B. (2005). Segregation of the Brain into Gray and White Matter: A Design Minimizing Conduction Delays. *PLoS Computational Biology*, *1*(7), e78. https://doi.org/10.1371/journal.pcbi.0010078

Whitehouse, P. J., Price, D. L., Clark, A. W., Coyle, J. T., & DeLong, M. R. (1981). Alzheimer disease: Evidence for selective loss of cholinergic neurons in the nucleus basalis. *Annals of Neurology*, *10*(2), 122–126. https://doi.org/10.1002/ana.410100203

Whitehouse, P., Price, D., Struble, R., Clark, A., Coyle, J., & DeLong, M. R. (1982). Alzheimer's Disease and Senile Dementia: Loss of Neurons in the Basal Forebrain. *Science*, *215*(4537), 1237–1239. https://doi.org/10.1126/science.7058341

Whitwell, J. L. (2009). Voxel-Based Morphometry: An Automated Technique for Assessing Structural Changes in the Brain. *Journal of Neuroscience*, *29*(31), 9661–9664. https://doi.org/10.1523/JNEUROSCI.2160-09.2009

Whitwell, J. L., Jack, C. R., Kantarci, K., Weigand, S. D., Boeve, B. F., Knopman, D. S., Drubach,

D. A., Tang-Wai, D. F., Petersen, R. C., & Josephs, K. A. (2007). Imaging correlates of posterior cortical atrophy. *Neurobiology of Aging*, *28*(7), 1051–1061. https://doi.org/10.1016/j.neurobiolaging.2006.05.026

WHO|Ageing and Health. (2022, October 1). Https://Www.Who.Int/News-Room/Fact-Sheets/Detail/Ageing-and-Health.

WHO|Dementia. (2021, January 27). Https://Www.Who.Int/News-Room/Facts-in-Pictures/Detail/Dementia.

Wilson, F. A., & Rolls, E. T. (1990). Neuronal responses related to the novelty and familarity of visual stimuli in the substantia innominata, diagonal band of Broca and periventricular region of the primate basal forebrain. *Exp Brain Res*, *80*(1), 104–120.

Winters, B. D., & Bussey, T. J. (2005). Removal of cholinergic input to perirhinal cortex disrupts object recognition but not spatial working memory in the rat. *Eur J Neurosci*, *21*(8), 2263–2270.

Winters, B. D., Saksida, L. M., & Bussey, T. J. (2006). Paradoxical facilitation of object recognition memory after infusion of scopolamine into perirhinal cortex: Implications for cholinergic system function. *J Neurosci*, *26*(37), 9520–9529.

Wolz, R., Julkunen, V., Koikkalainen, J., Niskanen, E., Zhang, D. P., Rueckert, D., Soininen, H., Lötjönen, J., & the Alzheimer's Disease Neuroimaging Initiative. (2011). Multi-Method Analysis of MRI Images in Early Diagnostics of Alzheimer's Disease. *PLoS ONE*, *6*(10), e25446. https://doi.org/10.1371/journal.pone.0025446

Woolf, N. (1991). Cholinergic systems in mammalian brain and spinal cord. *Progress in Neurobiology*, *37*(6), 475–524. https://doi.org/10.1016/0301-0082(91)90006-M

Wu, B.-S., Zhang, Y.-R., Li, H.-Q., Kuo, K., Chen, S.-D., Dong, Q., Liu, Y., & Yu, J.-T. (2021). Cortical structure and the risk for Alzheimer's disease: A bidirectional Mendelian randomization study. *Translational Psychiatry*, *11*(1), 476. https://doi.org/10.1038/s41398-021-01599-x

Wu, H., Williams, J., & Nathans, J. (2014). Complete morphologies of basal forebrain cholinergic neurons in the mouse. *eLife*, *3*, e02444. https://doi.org/10.7554/eLife.02444

Wu, J. W., Hussaini, S. A., Bastille, I. M., Rodriguez, G. A., Mrejeru, A., Rilett, K., Sanders, D. W., Cook, C., Fu, H., Boonen, R. A. C. M., Herman, M., Nahmani, E., Emrani, S., Figueroa, Y. H., Diamond, M. I., Clelland, C. L., Wray, S., & Duff, K. E. (2016). Neuronal activity enhances tau propagation and tau pathology in vivo. *Nature Neuroscience*, *19*(8), 1085–1092. https://doi.org/10.1038/nn.4328

Wu, Z., Peng, Y., Hong, M., & Zhang, Y. (2021). Gray Matter Deterioration Pattern During Alzheimer's Disease Progression: A Regions-of-Interest Based Surface Morphometry Study. *Frontiers in Aging Neuroscience*, *13*, 593898. https://doi.org/10.3389/fnagi.2021.593898

Xie, L., Das, S. R., Wisse, L. E. M., Ittyerah, R., De Flores, R., Shaw, L. M., Yushkevich, P. A., Wolk, D. A., & for the Alzheimer's Disease Neuroimaging Initiative. (2023). Baseline structural MRI and plasma biomarkers predict longitudinal structural atrophy and cognitive decline in early Alzheimer's disease. *Alzheimer's Research & Therapy*, *15*(1), 79. https://doi.org/10.1186/s13195-023-01210-z

Xie, S., Xiao, J. X., Gong, G. L., Zang, Y. F., Wang, Y. H., Wu, H. K., & Jiang, X. X. (2006). Voxel-based detection of white matter abnormalities in mild Alzheimer disease. *Neurology*, *66*(12), 1845–1849. https://doi.org/10.1212/01.wnl.0000219625.77625.aa

Xing, X.-X., Zheng, M.-X., Hua, X.-Y., Ma, S.-J., Ma, Z.-Z., & Xu, J.-G. (2021). Brain plasticity after peripheral nerve injury treatment with massage therapy based on resting-state functional magnetic resonance imaging. *Neural Regeneration Research*, *16*(2), 388. https://doi.org/10.4103/1673-5374.290912

Xu, J., Jia, Z., Knutson, M. D., & Leeuwenburgh, C. (2012). Impaired Iron Status in Aging Research. *International Journal of Molecular Sciences*, *13*(2), 2368–2386. https://doi.org/10.3390/ijms13022368

Xu, X., Wang, Q., & Zhang, M. (2008). Age, gender, and hemispheric differences in iron deposition in the human brain: An in vivo MRI study. *NeuroImage*, *40*(1), 35–42. https://doi.org/10.1016/j.neuroimage.2007.11.017

Yamamoto, A., Shin, R., Hasegawa, K., Naiki, H., Sato, H., Yoshimasu, F., & Kitamoto, T. (2002). Iron (III) induces aggregation of hyperphosphorylated τ and its reduction to iron (II) reverses the aggregation: Implications in the formation of neurofibrillary tangles of Alzheimer's disease. *Journal of Neurochemistry*, *82*(5), 1137–1147. https://doi.org/10.1046/j.1471-4159.2002.t01-1-01061.x

Yamazaki, Y., Zhao, N., Caulfield, T. R., Liu, C.-C., & Bu, G. (2019). Apolipoprotein E and Alzheimer disease: Pathobiology and targeting strategies. *Nature Reviews Neurology*, *15*(9), 501–518. https://doi.org/10.1038/s41582-019-0228-7

Yan. (2010). DPARSF: A MATLAB toolbox for "pipeline" data analysis of resting-state fMRI. *Frontiers in System Neuroscience*. https://doi.org/10.3389/fnsys.2010.00013

Yan, C.-G., Cheung, B., Kelly, C., Colcombe, S., Craddock, R. C., Di Martino, A., Li, Q., Zuo, X.-N., Castellanos, F. X., & Milham, M. P. (2013). A comprehensive assessment of regional variation in the impact of head micromovements on functional connectomics. *NeuroImage*, *76*, 183–201. https://doi.org/10.1016/j.neuroimage.2013.03.004

Yang, A., Du, L., Gao, W., Liu, B., Chen, Y., Wang, Y., Liu, X., Lv, K., Zhang, W., Xia, H., Wu, K., & Ma, G. (2022). Associations of cortical iron accumulation with cognition and cerebral atrophy in Alzheimer's disease. *Quantitative Imaging in Medicine and Surgery*, *12*(9), 4570–4586. https://doi.org/10.21037/qims-22-7

Yang, L., Yan, Y., Wang, Y., Hu, X., Lu, J., Chan, P., Yan, T., & Han, Y. (2018). Gradual Disturbances of the Amplitude of Low-Frequency Fluctuations (ALFF) and Fractional ALFF in Alzheimer Spectrum. *Frontiers in Neuroscience*, *12*, 975. https://doi.org/10.3389/fnins.2018.00975

Yim, Y., Choi, J. D., Cho, J. H., Moon, Y., Han, S.-H., & Moon, W.-J. (2022). Magnetic susceptibility in the deep gray matter may be modulated by apolipoprotein E4 and age with regional predilections: A quantitative susceptibility mapping study. *Neuroradiology*, *64*(7), 1331–1342. https://doi.org/10.1007/s00234-021-02859-9

Yin, C., Yi, L., Jia, L., Wang, J., Liu, P., Guo, Y., & Han, Y. (2014). Early morphological brain abnormalities in patients with amnestic mild cognitive impairment. *Translational Neuroscience*, *5*(4), 253–259. https://doi.org/10.2478/s13380-014-0234-6

Yousuf, M., Packard, P. A., Fuentemilla, L., & Bunzeck, N. (2021). Functional coupling between

CA3 and laterobasal amygdala supports schema dependent memory formation. *NeuroImage*, *244*, 118563. https://doi.org/10.1016/j.neuroimage.2021.118563

Yuan, L.-X., Zhao, N., Wang, X.-Q., Lv, Y.-T., & He, H. (2021). Echo Time Dependency of Local Activity Metrics of Resting-State Functional MRI. *Frontiers in Neuroscience*, *15*, 619412. https://doi.org/10.3389/fnins.2021.619412

Yue, L., Hu, D., Zhang, H., Wen, J., Wu, Y., Li, W., Sun, L., Li, X., Wang, J., Li, G., Wang, T., Shen, D., & Xiao, S. (2021). Prediction of 7-year's conversion from subjective cognitive decline to mild cognitive impairment. *Human Brain Mapping*, *42*(1), 192–203. https://doi.org/10.1002/hbm.25216

Zaborszky, L., & Cullinan, W. E. (1996). Direct catecholaminergic-cholinergic interactions in the basal forebrain. I. Dopamine-?-hydroxylase- and tyrosine hydroxylase input to cholinergic neurons. *The Journal of Comparative Neurology*, *374*(4), 535–554. https://doi.org/10.1002/(SICI)1096-9861(19961028)374:4<535::AID-CNE5>3.0.CO;2-2

Záborszky, L., Gombkoto, P., Varsanyi, P., Gielow, M. R., Poe, G., Role, L. W., Ananth, M., Rajebhosale, P., Talmage, D. A., Hasselmo, M. E., Dannenberg, H., Minces, V. H., & Chiba, A. A. (2018). Specific Basal Forebrain–Cortical Cholinergic Circuits Coordinate Cognitive Operations. *The Journal of Neuroscience*, *38*(44), 9446–9458. https://doi.org/10.1523/JNEUROSCI.1676-18.2018

Zaborszky, L., Hoemke, L., Mohlberg, H., Schleicher, A., Amunts, K., & Zilles, K. (2008). Stereotaxic probabilistic maps of the magnocellular cell groups in human basal forebrain. *NeuroImage*, *42*(3), 1127–1141. https://doi.org/10.1016/j.neuroimage.2008.05.055

Zang, Y., Jiang, T., Lu, Y., He, Y., & Tian, L. (2004). Regional homogeneity approach to fMRI data analysis. *NeuroImage*, *22*(1), 394–400. https://doi.org/10.1016/j.neuroimage.2003.12.030

Zarow, C., Lyness, S. A., Mortimer, J. A., & Chui, H. C. (2003). Neuronal Loss Is Greater in the Locus Coeruleus Than Nucleus Basalis and Substantia Nigra in Alzheimer and Parkinson Diseases. *Archives of Neurology*, *60*(3), 337. https://doi.org/10.1001/archneur.60.3.337

Zecca, L., Youdim, M. B. H., Riederer, P., Connor, J. R., & Crichton, R. R. (2004). Iron, brain ageing and neurodegenerative disorders. *Nature Reviews Neuroscience*, *5*(11), 863–873. https://doi.org/10.1038/nrn1537

Zeng, Q., Luo, X., Li, K., Wang, S., Zhang, R., Hong, H., Huang, P., Jiaerken, Y., Xu, X., Xu, J., Wang, C., Zhou, J., & Zhang, M. (2019). Distinct Spontaneous Brain Activity Patterns in Different Biologically-Defined Alzheimer's Disease Cognitive Stage: A Preliminary Study. *Frontiers in Aging Neuroscience*, *11*, 350. https://doi.org/10.3389/fnagi.2019.00350

Zeng, Q., Qiu, T., Li, K., Luo, X., Wang, S., Xu, X., Liu, X., Hong, L., Li, J., Huang, P., & Zhang, M. (2022). Increased functional connectivity between nucleus basalis of Meynert and amygdala in cognitively intact elderly along the Alzheimer's continuum. *NeuroImage: Clinical*, *36*, 103256. https://doi.org/10.1016/j.nicl.2022.103256

Zhang, T., Liao, Q., Zhang, D., Zhang, C., Yan, J., Ngetich, R., Zhang, J., Jin, Z., & Li, L. (2021). Predicting MCI to AD Conversation Using Integrated sMRI and rs-fMRI: Machine Learning and Graph Theory Approach. *Frontiers in Aging Neuroscience*, *13*, 688926.

https://doi.org/10.3389/fnagi.2021.688926

Zhang, X., Xue, C., Cao, X., Yuan, Q., Qi, W., Xu, W., Zhang, S., & Huang, Q. (2021). Altered Patterns of Amplitude of Low-Frequency Fluctuations and Fractional Amplitude of Low-Frequency Fluctuations Between Amnestic and Vascular Mild Cognitive Impairment: An ALE-Based Comparative Meta-Analysis. *Frontiers in Aging Neuroscience*, *13*, 711023. https://doi.org/10.3389/fnagi.2021.711023

Zhang, X.-D. (2020). Machine Learning. In X.-D. Zhang, *A Matrix Algebra Approach to Artificial Intelligence* (pp. 223–440). Springer Singapore. https://doi.org/10.1007/978-981-15-2770-8_6

Zhang, Z., Liu, Y., Jiang, T., Zhou, B., An, N., Dai, H., Wang, P., Niu, Y., Wang, L., & Zhang, X. (2012). Altered spontaneous activity in Alzheimer's disease and mild cognitive impairment revealed by Regional Homogeneity. *NeuroImage*, *59*(2), 1429–1440. https://doi.org/10.1016/j.neuroimage.2011.08.049

Zhao, Z., Lu, J., Jia, X., Chao, W., Han, Y., Jia, J., & Li, K. (2014). Selective Changes of Resting-State Brain Oscillations in aMCI: An fMRI Study Using ALFF. *BioMed Research International*, *2014*, 1–7. https://doi.org/10.1155/2014/920902

Zou, Q.-H., Zhu, C.-Z., Yang, Y., Zuo, X.-N., Long, X.-Y., Cao, Q.-J., Wang, Y.-F., & Zang, Y.-F. (2008). An improved approach to detection of amplitude of low-frequency fluctuation (ALFF) for resting-state fMRI: Fractional ALFF. *Journal of Neuroscience Methods*, *172*(1), 137–141. https://doi.org/10.1016/j.jneumeth.2008.04.012

Zuo, X.-N., Di Martino, A., Kelly, C., Shehzad, Z. E., Gee, D. G., Klein, D. F., Castellanos, F. X., Biswal, B. B., & Milham, M. P. (2010). The oscillating brain: Complex and reliable. *NeuroImage*, *49*(2), 1432–1445. https://doi.org/10.1016/j.neuroimage.2009.09.037

Zuo, X.-N., & Xing, X.-X. (2014). Test-retest reliabilities of resting-state FMRI measurements in human brain functional connectomics: A systems neuroscience perspective. *Neuroscience & Biobehavioral Reviews*, *45*, 100–118. https://doi.org/10.1016/j.neubiorev.2014.05.009

Appendix

Supplementary Material S1: Structural degeneration of the nucleus basalis of Meynert in mild cognitive impairment and Alzheimer's disease – Evidence from an MRI-based meta-analysis

This supplementary material corresponds to **study 1** (see section 4). It has been formally integrated into the dissertation's style for consistency. The content corresponds to the following publication:

Mieling, M., Göttlich, M., Yousuf, M., & Bunzeck, N. (2023). Basal forebrain activity predicts functional degeneration in the entorhinal cortex in Alzheimer's disease. Brain Communications, 5(5), fcad262. https://doi.org/10.1093/braincomms/fcad262

Table S1.1. Checklist for Neuroimaging Meta-Analyses after Müller et al. (2018).

The research question was specifically defined	YES, and it includes the following contrasts: 1) HC>MCI 2) HC>AD
The literature search was systematic	YES, it included the following search criteria in the BrainMap database: HC>MCI ALE meta-analysis 1) Experiments contrast *is* gray matter 2) Experiments context *is* disease 3) Experiments observed changes *is* control>patients 4) Subjects diagnosis *is* mild cognitive impairment 5) Subjects diagnosis *is* not dementia HC>AD ALE meta-analysis 1) Experiments contrast *is* gray matter 2) Experiments context *is* disease 3) Experiments observed changes *is* control>patients 4) Subjects diagnosis *is* Alzheimer's disease 5) Subjects diagnosis *is* not frontotemporal dementia 6) Subjects diagnosis *is not* Lewy body dementia 7) Subjects diagnosis *is not* Parkinson's disease 8) Subjects diagnosis *is not* behavioral variant frontotemporal dementia 9) Subjects diagnosis *is not* non-aphasic frontotemporal dementia
Detailed inclusion and exclusion criteria were applied	YES, see Table 4.1 for more information.
Sample overlap was taken into account	YES, experiments were carefully checked regarding the inclusion of possible analysis including subgroups of MCI or AD.
All experiments use the same search overage (state how brain coverage is assessed and how small volume corrections and conjunctions are taken into account)	YES, the search coverage was the following: - Only whole-brain coverage - ROI studies were excluded
Studies are converted to a common reference space	YES, using the following conversion: - Sleuth's implemented automated tool of using the icbm2tal conversion (converting reported Talairach coordinates to MNI coordinates).
The study protocol and all analyses was planned beforehand, including the methods and	YES, 1) Any non-planned analyses are clearly stated as post-hoc in the paper.

parameters used for inference, correction for multiple testing, etc.	2) The meta-analysis used the default methods and parameters of the software.
The meta-analysis includes diagnostics	YES, the following: Mild cognitive impairment and Alzheimer's disease

Table S1.2. Overview of included studies for the contrast HC > MCI. Abbreviations: aMCI: amnestic type mild cognitive impairment; HC: healthy controls.

Title, authors & date of publication	Groups, mean age, sample size	Included experiment / contrast	Statistical threshold and thresholding method	MRI field strength, reference space, analysis software
White Matter Damage in Alzheimer Disease and Its Relationship to Gray Matter Atrophy (Agosta et al., 2011)	aMCI, 70 years, n = 15 HC, 70 years, n = 15	HC > aMCI	p < 0.001 Cluster-wise corrected for multiple comparisons	1.5 T MNI SPM5
Default-mode network activity distinguishes amnestic type mild cognitive impairment from healthy aging: A combined structural and resting-state functional MRI study (Bai et al., 2008)	aMCI, 71 years, n = 20 HC, 69 years, n = 20	HC > aMCI	p < 0.05 Voxel-wise corrected for multiple comparisons	1.5 T Talairach SPM5
Profile of memory impairment and gray matter loss in amnestic mild cognitive impairment (Barbeau et al., 2008)	aMCI unimpaired in a visual recognition memory test (DMS48), 72 years, n = 12 aMCI impaired in a visual recognition memory test (DMS48), 67 years, n = 16 HC, 63 years, n = 28	HC > aMCI (unimpaired & impaired performance)	p < 0.05 FDR corrected for multiple comparisons	1.5 T Talairach SPM2
Differential cortical atrophy in subgroups of mild cognitive impairment (Bell-McGinty et al., 2005)	aMCI converters to AD during follow-up, 76 years, n = 4	HC > MCI (MCI-A converters, MCI-A non-converters, MCI-MCD	p < 0.001	1.5 T MNI

	aMCI non-converters during follow-up, 72 years, n = 5 MCI-MCD (multiple cognitive domain) converters during follow up, 71 years, n = 10 MCI-MCD (multiple cognitive domain) non-converters during follow up (ICD: G31.84),72 years, n = 18 HC, 67 years, n = 47	converters, MCI-MCD non-converters)		SPM99
The contribution of voxel-based morphometry in staging patients with mild cognitive impairment (Bozzali et al., 2006)	MCI converters to AD, 71 years, n = 14 HC, 66 years, n = 20	HC > MCI converters	$p < 0.001$	1.5 T MNI SPM2
The contribution of voxel-based morphometry in staging patients with mild cognitive impairment (Bozzali et al., 2006)	MCI non-converters to AD, 71 years, n = 8 HC, 66 years, n = 20	HC > MCI non-converters	$p < 0.001$	1.5 T MNI SPM2
Cerebral perfusion correlates of conversion to Alzheimer's disease in amnestic mild cognitive impairment (Caroli et al., 2007)	Non-converters aMCI, 71 years, n = 14 HC, 69 years, n = 17	HC > Non-converters aMCI to AD	$p < 0.001$	1.0 T MNI SPM2

Mapping gray matter loss with voxel-based morphometry in mild cognitive impairment (Chételat et al., 2002)	MCI, 71 years, n = 22 HC, 67 years, n = 22	HC > MCI	p < 0.01 Corrected for multiple comparisons	1.5 T Talairach SPM99
Functional response in ventral temporal cortex differentiates mild cognitive impairment from normal aging (Gold et al., 2010)	MCI, 78 years, n = 12 HC, 77 years, n = 14	HC > MCI	p < 0.001	3.0 T MNI SPM5
Increased fMRI responses during encoding in mild cognitive impairment (Hämäläinen et al., 2007)	MCI, 72 years, n = 14 HC, 71 years, n = 21	HC > MCI	p < 0.05 Cluster-wise corrected for multiple comparisons	1.5 T MNI SPM2
A support vector machine-based method to identify mild cognitive impairment with multi-level characteristics of magnetic resonance imaging (Z. Long et al., 2016)	MCI, 66 years, n = 29 HC, 62 years, n = 33	HC > MCI	p < 0.01 Voxel-wise corrected for multiple comparisons	3.0 T MNI SPM8
A voxel-based morphometry study on mild cognitive impairment (Pennanen et al., 2005)	MCI, 72 years, n = 51 HC, 74 years, n = 32	HC > MCI	p < 0.001	1.5 T MNI

				SPM99
Voxel based morphometry features and follow-up of amnestic patients at high risk for Alzheimer's disease conversion (Rami et al., 2009)	aMCI, 73 years, n = 14 HC, 74 years, n = 27	HC > aMCI	p < 0.001	1.5 T MNI SPM2
Memory performance correlates with gray matter density in the ento-/perirhinal cortex and posterior hippocampus in patients with mild cognitive impairment and healthy controls — A voxel based morphometry study (Schmidt-Wilcke et al., 2009)	MCI, 66 years, n = 18 HC, 63 years, n = 18	HC > MCI	p < 0.05 FWE corrected for multiple comparisons	1.5 T MNI SPM2
Four subgroups of Alzheimer's disease based on patterns of atrophy using VBM and a unique pattern for early-onset disease (Shiino et al., 2006)	MCI, 68 years, n = 20 HC, 69 years, n = 88	HC > MCI	p < 0.05 Voxel-wise corrected for multiple comparisons	1.5 T Talairach MedX
Early morphological brain abnormalities in patients with amnestic mild cognitive impairment (Yin et al., 2014)	aMCI, 67 years, n = 11 HC, 62 years, n = 22	HC > aMCI	p < 0.05 Cluster-wise corrected for multiple comparisons	3.0 T MNI SPM5
Selective Changes of Resting-State Brain Oscillations in aMCI: An fMRI Study Using ALFF (Zhao et al., 2014)	aMCI, 65 years, n = 20 HC, 67 years, n = 18	HC > aMCI	p < 0.01 Voxel-wise corrected for multiple comparisons	3.0 T MNI SPM5

Table S1.3. Overview of included studies for the experimental condition HC > AD. Abbreviations: AD: Alzheimer's disease; HC: healthy controls.

Title, authors & date of publication	Groups, mean age, sample size	Included experiments	Statistical threshold and thresholding method	MRI field strength, reference space, analysis software
In vivo mapping of gray matter loss with voxel-based morphometry in mild Alzheimer's disease (Baron et al., 2001)	AD, 73 years, n = 19 HC, 66 years, n = 16	HC > AD	p < 0.001	1.5 T Talairach SPM2
Relationship of cognitive measures and gray and white matter in Alzheimer's disease (Baxter et al., 2006)	AD, 76 years, n = 15 HC, 76 years, n = 15	HC > AD	p < 0.0001	1.5 T MNI SPM2
Cinguloparietal atrophy distinguishes Alzheimer disease from semantic dementia (Boxer et al., 2003)	AD, 70 years, n = 11 HC, 65 years, n = 15	HC > AD	p < 0.05 Voxel-wise corrected for multiple comparisons	1.5 T MNI SPM99
The contribution of voxel-based morphometry in staging patients with mild cognitive impairment (Bozzali et al., 2006)	AD, 68 years, n = 22 HC, 66 years, n = 20	HC > AD	p < 0.05 Voxel-wise corrected for multiple comparisons	1.5 T MNI SPM2
Damage to the cingulum contributes to Alzheimer's disease pathophysiology by deafferentation mechanism (Bozzali et al., 2012)	Probable AD, 73 years, n = 31 HC, 68 years, n = 14	HC > AD	p < 0.05 Voxel-wise corrected for	3.0 T MNI

			multiple comparisons	SPM8
Basal forebrain atrophy is a distinctive pattern in dementia with Lewy bodies (Brenneis et al., 2004)	AD, 73 years, n = 10 HC, 65 years, n = 10	HC > AD	p < 0.05 Corrected or multiple comparisons	1.5 T MNI SPM99
Patterns of cerebellar volume loss in dementia with Lewy bodies and Alzheimer's disease: A VBM-DARTEL study (Colloby et al., 2014)	AD, 79 years, n = 47 HC, 77 years, n = 39	HC > AD	p < 0.05 Voxel-wise corrected for multiple comparisons	3.0 T MNI SPM8
Simultaneous arterial spin labeling cerebral blood flow and morphological assessments for detection of Alzheimer's disease (Dashjamts et al., 2011)	AD, 75 years, n = 23 HC, 73 years, n = 23	HC > AD	p < 0.001	3.0 T MNI SPM8
Prospective Memory Impairments in Alzheimer's Disease and Behavioral Variant Frontotemporal Dementia: Clinical and Neural Correlates (Dermody, Hornberger, et al., 2016)	AD, 63 years, n = 12 HC, 69 years, n = 12	HC > AD	p < 0.05 Voxel-wise corrected for multiple comparisons	3.0 T MNI FSL
Uncovering the Neural Bases of Cognitive and Affective Empathy Deficits in Alzheimer's Disease and the Behavioral-Variant of Frontotemporal Dementia (Dermody, Wong, et al., 2016)	AD, 66 years, n = 25 HC, 68 years, n = 22	HC > AD	p < 0.05 Voxel-wise corrected for multiple comparisons	3.0 T MNI FSL

Episodic memory impairment in patients with Alzheimer's disease is correlated with entorhinal cortex atrophy. A voxel-based morphometry study (Di Paola et al., 2007)	AD, 64 years, n = 18 HC, 65 years, n = 18	HC > AD	p < 0.05 Corrected for multiple comparisons	1.5 T Talairach SPM2
Fronto-temporal-lobe atrophy in early-stage Alzheimer's disease identified using an improved detection methodology (Farrow et al., 2007)	Early stage AD, First scan (AD1), 77 years, n = 7 HC, 70 years, n = 11	HC > AD1	p < 0.05 Corrected for multiple comparisons	1.5 T Talairach SPM2
Detection of grey matter loss in mild Alzheimer's disease with voxel based morphometry (Frisoni et al., 2002)	AD, 74 years, n = 29 HC, 74 years, n = 26	HC > AD	p < 0.05 Corrected for multiple comparisons	1.5 T MNI SPM99
Regional brain atrophy and functional disconnection across Alzheimer's disease evolution (Gili et al., 2011)	AD, 72 years, n = 11 HC, 64 years, n = 10	HC > AD	p < 0.001 Cluster-wise corrected for multiple comparisons	3.0 T MNI SPM5
Correlation between Topographic N400 Anomalies and Reduced Cerebral Blood Flow in the Anterior Temporal Lobes of Patients with Dementia (Grieder et al., 2013)	AD, 66 years, n = 14 HC, 69 years, n = 19	HC > AD	p < 0.01 Voxel-wise corrected for multiple comparisons	3.0 T MNI SPM8
Voxel-based assessment of gray and white matter volumes in Alzheimer's disease (Guo et al., 2010)	AD, 72 years, n = 13 HC, 70 years, n = 14	HC > AD	p < 0.05	3.0 T MNI

			Corrected for multiple comparisons	SPM2
Basal forebrain atrophy is a presymptomatic marker for Alzheimer's disease (Hall et al., 2008)	Probable AD, 83 years, n = 26 HC, 77 years, n = 127	HC > Probable AD	p < 0.05 Voxel-wise corrected for multiple comparisons	1.5 T MNI SPM2
Increased fMRI responses during encoding in mild cognitive impairment (Hämäläinen et al., 2007)	AD, 73 years, n = 15 HC, 71 years, n = 21	HC > AD	p < 0.01 Cluster-wise corrected for multiple comparisons	1.5 T MNI SPM2
Cardiorespiratory fitness and preserved medial temporal lobe volume in Alzheimer disease (Honea et al., 2009)	Early AD, 74 years, n = 60 HC, 73 years, n = 56	HC > Early AD	p < 0.05 Corrected for multiple comparisons	3.0 T MNI SPM5
*Neural Substrates of Semantic Prospection - Evidence from the Dementia*s (Irish et al., 2016)	AD, 65 years, n = 15 HC, 67 years, n = 20	HC > AD	p < 0.05 Voxel-wise corrected for multiple comparisons	3.0 T MNI FSL
Episodic future thinking is impaired in the behavioral variant of frontotemporal dementia (Irish et al., 2013)	AD, 65 years, n = 10 HC, 69 years, n = 10	HC > AD	p < 0.001 Voxel-wise corrected for multiple comparisons	3.0 T MNI FSL

Grey and white matter correlates of recent and remote autobiographical memory retrieval-insights from the dementias (Irish et al., 2014)	AD, 68 years, n = 15 HC, 72 years, n = 14	HC > AD	p < 0.001 Voxel-wise corrected for multiple comparisons	3.0 T MNI FSL
Comparison of gray matter and metabolic reduction in mild Alzheimer's disease using FDG-PET and voxel-based morphometric MR studies (Ishii et al., 2005)	Mild AD, 67 years, n = 30 HC, 67 years, n = 30	HC > Mild AD	p < 0.05 Voxel-wise corrected for multiple comparisons	1.5 T MNI SPM99
Comparison of grey matter and metabolic reductions in frontotemporal dementia using FDG-PET and voxel-based morphometric MR studies (Kanda et al., 2008)	AD, 65 years, n = 20 HC, 65 years, n = 20	HC > AD	p < 0.01 Voxel-wise corrected for multiple comparisons	1.5 T MNI SPM2
Voxel-based morphometric study of brain volume changes in patients with Alzheimer's disease assessed according to the Clinical Dementia Rating score (S. Kim et al., 2011)	AD, 69 years, n = 61 HC, 70 years, n = 33	HC > AD	p < 0.01 Corrected for multiple comparisons	3.0 T MNI SPM2
Self-appraisal in behavioral variant frontotemporal degeneration (Massimo et al., 2013)	AD, 71 years, n = 17 HC, 64 years, n = 30	HC > AD	p < 0.05 Cluster-wise corrected for multiple comparisons	Unknown MRI field strength Talairach SPM5
Longitudinal evaluation of both morphologic and functional changes in the same individuals with Alzheimer's disease (Matsuda et al., 2002)	AD, 71 years, n = 15 HC, 71 years, n = 25	HC > AD	p < 0.05	1.0 T MNI SPM99

			Corrected for multiple comparisons	
In vivo SPECT imaging of vesicular acetylcholine transporter using [(123)I]-IBVM in early Alzheimer's disease (Mazère et al., 2008)	AD, 81 years, n = 8 HC, 74 years, n = 8	HC > AD	p < 0.01 Cluster-wise corrected for multiple comparisons	1.5 T Talairach Unknown software system
Changes in brain morphology in Alzheimer disease and normal aging: Is Alzheimer disease an exaggerated aging process? (Ohnishi et al., 2001)	AD, 72 years, n = 26 HC, 71 years, n = 22	HC > AD	p < 0.001	1.0 T MNI SPM96
Distinct MRI atrophy patterns in autopsy-proven Alzheimer's disease and frontotemporal lobar degeneration (Rabinovici et al., 2007)	AD, 65 years, n = 11 HC, 64 years, n = 40	HC > AD	p < 0.001	1.5 T MNI SPM2
Voxel based morphometry features and follow-up of amnestic patients at high risk for Alzheimer's disease conversion (Rami et al., 2009)	AD, 76 years, n = 31 HC, 74 years, n = 27	HC > AD	p < 0.001	1.5 T MNI SPM2
Verbal episodic memory impairment in Alzheimer's disease: a combined structural and functional MRI study (Rémy et al., 2005)	AD, 72 years, n = 8 HC, 66 years, n = 11	HC > AD	p < 0.001	1.5 T MNI SPM2
Four subgroups of Alzheimer's disease based on patterns of atrophy using VBM and a unique	AD, 71 years, n = 40	HC > AD	p < 0.05	1.5 T

pattern for early onset disease (Shiino et al., 2006)	HC, 69 years, n = 88		Corrected for multiple comparisons	Talairach MedX
The Effect of Gray Matter ICA and Coefficient of Variation Mapping of BOLD Data on the Detection of Functional Connectivity Changes in Alzheimer's Disease and bvFTD (Tuovinen et al., 2016)	AD, 61 years, n = 23 HC, 59 years, n = 25	HC > AD	p < 0.05 Voxel-wise corrected for multiple comparisons	1.5 T MNI FSL
Disease-specific profiles of apathy in Alzheimer's disease and behavioral-variant frontotemporal dementia differ across the disease course (Wei et al., 2020)	Early AD, 64 years, n = 10 HC, 64 years, n = 28	HC > Early AD	p < 0.05 Voxel-wise corrected for multiple comparisons	3.0 T MNI FSL
Imaging correlates of posterior cortical atrophy (Whitwell et al., 2007)	AD, 65 years, n = 38 HC, 66 years, n = 38	HC > AD	p < 0.05 Corrected for multiple comparisons	1.5 T MNI SPM2
Voxel-based detection of white matter abnormalities in mild Alzheimer disease (S. Xie et al., 2006)	AD, 72 years, n = 13 HC, 71 years, n = 16	HC > AD	p < 0.001 Cluster-wise corrected for multiple comparisons	1.5 T MNI SPM2

Supplementary material S2: Predicting MCI and Alzheimer's disease on structural brain integrity with machine learning

This supplementary material corresponds to **study 2** (see section 5). It has been formally integrated into the dissertation's style for consistency. The manuscript has been submitted to a peer-reviewed journal. The content corresponds to the following preprint:

Mieling, M., Yousuf, M., & Bunzeck, N. (2023). Predicting MCI and Alzheimer's disease on structural brain integrity with machine learning. https://doi.org/10.31219/osf.io/8dtcm

Table S2.1. Demographics, information on APOE4 genotype and harmonized CSF assays.

Analysis 1	**HC**	**MCI**	**AD**	**Test - χ^2/ Fisher's F**
n (total)=568	271	193	104	χ^2=73.8, p<.001***
ADNI-GO/2 (n=334) / 3 (n=234)	128/142	132/61	73/31	χ^2=94.1, p<.001***
Manufacturer Philips (n=95) / Siemens (n=362) / GE (n=111)	36/184/51	33/123/37	26/55/23	χ^2=9.29, p=0.054
FreeSurfer versions (5.1, 6.0)	129/142	132/61	73/31	χ^2=26.9, p<.001***
Age	71.0 (5.99)	70.8 (7.47)	73.9 (8.24)	F(2,565)=7.89, p<.001***
Female (n=288) / Male (n=280)	164/107	89/104	35/69	χ^2=24.2, p<.001***
Education (in years)	16.7 (2.28)	16.1 (2.72)	15.9 (2.59)	F(2,565)=5.77, p=0.003**
APOE 4 (0/1/2)	182/82/7	123/53/17	33/47/24	χ^2=61.3 p<.001***
Aβ	1415 (656)	1181 (582)	664 (394)	F(2,565)= 60.8, p<.001***
pTau	20.4 (8.52)	24.5 (13.1)	36.8 (14.4)	F(2,565)=76.4, p<.001***
pTau/Amyloid ratio	0.0184 (0.0147)	0.0269 (0.0221)	0.0661 (0.0361)	F(2,565)=171, p<.001***

Analysis 2	**HC stable**	**HC converter**	**Test - χ^2/ t**
n (total)=92	46	46	χ^2=0.00, p=1.0
ADNI1 (n=30) / ADNI-GO/2 (n=38) / 3 (n=24)	15/19/12	15/19/12	χ^2=90.00, p=1.0
Manufacturer	6/20/20	8/19/19	χ^2=0.337, p=0.845

Philips (n=6) / Siemens (n=20) / GE (n=20)			
Scanner fieldstrength (1.5 / 3.0)	25/21	25/21	χ^2=0.00, p=1.0
FreeSurfer versions (4.3, 5.1, 6.0)	25/9/12	25/9/12	χ^2=0.00, p=1.0
Age	73.6 (6.37)	78.5 (5.94)	t=-3.34, p<.001***
Female (n=42) / Male (n=50)	23/23	19/27	χ^2=0.701, p=0.402
Education (in years)	16.5 (2.61)	16.3 (2.61)	t=0.28, p=0.78
APOE 4 (0/1/2)	29/15/2	28/15/3	χ^2=0.218 p=0.897
Aβ if available (n=16)	1129.55 (465.18)	969.69 (680.58)	t=0.776, p=0.444
pTau if available (n=16)	20.61 (6.72)	25.96 (8.11)	t=-3.27, p=0.002**
pTau/Amyloid ratio if available (n=16)	0.0231 (0.0372)	0.0372 (0.0224)	t=-4.59, p<.001***
Stable time for non-converters; time until next follow-up for converters (in months)	31.1 (31.2)	15.0 (8.35)	t=-3.39, p<.001***

Analysis 3	**MCI stable**	**MCI converters**	**Test - χ^2/ t**
n (total)=378	189	189	χ^2=0.00, p=1.0
ADNI1 (n=228) / ADNI-GO/2 (n=113) / 3 (n=37)	112/58/19	116/55/18	χ^2=0.177, p=0.915
Manufacturer	32/91/66	25/89/75	χ^2=1.46, p=0.483

Philips (n=57) / Siemens (n=180) / GE (n=141)			
Scanner field strength (1.5 / 3.0)	111/78	125/64	χ^2=2.21, p=0.137
FreeSurfer versions (4.3, 5.1, 6.0)	111/59/19	125/46/18	χ^2=0.00, p=0.291
Age	73.6 (7.44)	74.4 (6.89)	t=-1.09, p=0.276
Female (n=155) / Male (n=223)	77/112	78/111	χ^2=0.011, p=0.917
Education (in years)	15.6 (3.05)	15.9 (2.88)	t=-0.935, p=0.35
APOE 4 (0/1/2)	101/68/20	52/109/28	χ^2=26.5 p<.001***
Aβ if available (n=44)	1145 (572)	719 (339)	t=4.25, p<.001***
pTau if available (n=44)	25.1 (12.7)	35.1 (15.9)	t=-3.27, p=0.002**
pTau/Amyloid ratio if available (n=44, SD)	0.0307 (0.0256)	0.0576 (0.0291)	t=-4.59, p<.001***
Stable for non-converters; time until next follow-up for converters (in months)	52.5 (93.5)	9.53 (5.85)	t=-6.3, p<.001***

Information of the final sample from analysis 1, 2 and 3 grouped by diagnoses. Means and standard deviation (SD) are represented and the respective t-test or chi-square test to investigate possible group differences. Baseline clinical diagnosis: HC=cognitive normal; MCI=mild cognitive impairment; AD=Alzheimer's Disease. Age and education were assessed in years. APOE4 status: no allel / 1 allel / 2 allels. Aβ=amyloid-β in pg/ml as concentration of the amyloid-β 1-42 peptide. pTau=in pg/ml as CSF concentration of hyperphosphorylated tau. *p<0.05, **p<0.01, ***p<0.001

Table S2.2. Included brain regions with volume and thickness for all analyses based on the cortical and subcortical parcellation

Regions with volume	Regions with thickness
Pallidum_volume	Paracentral_thickness
Paracentral_volume	Parahippocampal_thickness
Parahippocampal_volume	Opercularis_thickness
ParsOpercularis_volume	ParsOrbitalis_thickness
ParsOrbitalis_volume	ParsTriangularis_thickness
ParsTriangularis_volume	Pericalcarine_thickness
Pericalcarine_volume	Postcentral_thickness
Postcentral_volume	PosteriorCingulate_thickness
PosteriorCingulate_volume	Precentral_thickness
Precentral_volume	Precuneus_thickness
Precuneus_volume	RostralAnteriorCingulate_thickness
Putamen_volume	RostralMiddleFrontal_thickness
RostralAnteriorCingulate_volume	SuperiorFrontal_thickness
RostralMiddleFrontal_volume	SuperiorParietal_thickness
SuperiorFrontal_volume	SuperiorTemporal_thickness
SuperiorParietal_volume	Supramarginal_thickness
SuperiorTemporal_volume	TemporalPole_thickness
Supramarginal_volume	TransverseTemporal_thickness
TemporalPole_volume	Insula_thickness
Thalamus_volume	Bankssts_thickness
TransverseTemporal_volume	CaudalAnteriorCingulate_thickness
VentralDC_volume	CaudalMiddleFrontal_thickness
Insula_volume	Cuneus_thickness
Amygdala_volume	Entorhinal_thickness
Bankssts_volume	FrontalPole_thickness
CaudalAnteriorCingulate_volume	Fusiform_thickness
CaudalMiddleFrontal_volume	InferiorParietal_thickness
Caudate_volume	InferiorTemporal_thickness
CerebellumCortex_volume	IsthmusCingulate_thickness
CerebellumWM_volume	LateralOccipital_thickness
ChoroidPlexus_volume	LateralOrbitofrontal_thickness
Cuneus_volume	Lingual_thickness
Entorhinal_volume	MedialOrbitofrontal_thickness
FrontalPole_volume	MiddleTemporal_thickness
Fusiform_volume	
Hippocampus_volume	
InferiorParietal_volume	
InferiorTemporal_volume	
IsthmusCingulate_volume	
LateralOccipital_volume	

LateralOrbitofrontal_volume
Lingual_volume
MedialOrbitofrontal_volume
MiddleTemporal_volume
AccumbensArea_volume
Brainstem_volume

Table S2.3. Neuropsychological test results at the first measurement, for analysis 1 HC vs. MCI vs. AD, analysis 2 HC-stable vs. HC-converter and analysis 3 MCI-stable vs. MCI-converter. Shown are mean values and numbers in brackets represent one SD.

Neuropsychological test	**mean values (SD)**			**F- value**	**P- value**
Analysis 1					
	HC	**MCI**	**AD**		
MEM score	1.13 (0.57)	0.487 (0.61)	-0.88 (0.5)	F(2,562)=410.4	<0.001*
EF score	1.16 (0.81)	0.538 (0.87)	-0.78(1.02)[1]	F(2,561)=161.96	<0.001*
MMSE	29.2(1.05)	28.2 (1.64)[1]	23.1(1.96)	F(2,561)=591.29	<0.001*
ADAS-Cog 13	8.01 (4.07)[2]	13.3(5.56)	30.7(7.78)[3]	F(2,557)=583.24	<0.001*
CDRSB	0.02 (0.12)	1.36 (0.88)	4.59 (1.63)	F(2,562)=961.92	<0.001*
MoCA	26.4 (2.34)[6]	23.8(2.87)	17.5 (4.29)[5]	F(2,551)=297.01	<0.001*
Clock drawing	4.7 (0.59)[1]	4.48 (0.8)	3.42 (1.48)	F(2,561)=70.971	<0.001*
Analysis 2					
	HC stable	**HC converters**			
MEM score	1.09 (0.54)	0.6 (0.58)		F(1,87)=9.88	=0.002*
EF score	0.91 (0.84)	0.53 (0.67)		F(1,87)=2.76	=0.1
MMSE	29 (1.19)	28.8 (1.4)		F(1,87)=0.1	=0.75
ADAS-Cog 13	7.91 (3.73)	12.5 (5.42)		F(1,87)=14.44	<0.001*
CDRSB	0.01 (0.07)	0.174 (0.41)		F(1,87)=7.24	=0.009
MoCA	26.2 (2.29)[15]	24.3 (2.52)[16]		F(1,87)=7.31	=0.009
Clock drawing	4.74 (0.49)	4.59 (0.65)		F(1,87)=2.1	=0.151
Analysis 3	**MCI stable**	**MCI converters**			
MEM score	0.229(0.66)	-0.478 (0.52)[1]		F(1,371)=142.71	<0.001*
EF score	0.205 (0.85)	0.314 (0.831)[2]		F(1,371)=38.42	<0.001*
MMSE	27.4 (2.21)[1]	25.8(2.4)[1]		F(1,371)=45.32	<0.001*
ADAS-Cog 13	15.7 (6.5)[1]	23.5 (6.59)[1]		F(1,371)=136.59	<0.001*
CDRSB	1.43 (0.8)[1]	2.57 (1.06)		F(1,372)=135.05	<0.001*
MoCA	23.08 (3.25)[113]	20.8 (3.18)[118]		F(1,142)=32.926	<0.001*
Clock drawing	4.39 (0.8)	4.02 (1.03)[1]		F(1,372)=15.04	<0.001*

The mean values with standard deviation (SD) for cognitive normal (HC); Mild cognitive impairment (MCI) and Alzheimer's disease (AD). The upper numbers represent the missing values that were excluded. The AD groups showed worse performance in all neuropsychological tests followed by MCI and HC. MEM: memory function score; EF: executive function score; MMSE: Mini-Mental State Examination; ADAS-Cog 13: Alzheimer's Disease Assessment Scale- Cognition Subscale, 13 tasks; CDRSB: Clinical Dementia Rating Scale; MoCA: Montreal-Cognitive-Assessment; Clock drawing: clock drawing test

* significant after Bonferroni correction $p<0.05/n$ (n=7 tests).

Supplementary material S3: Basal forebrain activity predicts functional degeneration in the entorhinal cortex in Alzheimer's disease

This supplementary material corresponds to **study 4** (see section 7). It has been formally integrated into the dissertation's style for consistency. The content corresponds to the following publication:

Mieling, M., Göttlich, M., Yousuf, M., & Bunzeck, N. (2023). Basal forebrain activity predicts functional degeneration in the entorhinal cortex in Alzheimer's disease. Brain Communications, 5(5), fcad262. https://doi.org/10.1093/braincomms/fcad262

Material and methods

Image acquisition

Participants were scanned at multiple sites equipped with 3-Tesla MRI scanners according to unified ADNI monitoring protocols (Jack, Bernstein, et al., 2010). All scanner sites had to pass strict scanner validation tests before contributing. To ensure maximum compatibility between the measurements, we adhered ADNI's recommendations including only the basic rsfMRI version of ADNI 3 since the advanced version is not compatible with ADNI-GO/2. Moreover, all participants included in our analysis were examined with the same scanner using the same type of head coil for both timepoints, t1 and t2 (https://adni.loni.usc.edu/methods/mri-tool/mri-analysis/), this led to the exclusion of 3 participants in ADNI-GO/2 and 16 in ADNI 3 data. Furthermore, for the inclusion of images, the quality criteria by ADNI were adhered by only including measurements with excellent, good, or fair quality, thus, we excluded n=8 ADNI-GO/2 and n=14 ADNI 3 data sets.

T1- weighted sagittal images were obtained using a magnetization-prepared rapid gradient echo (MP-RAGE) with ~1mm isotropic voxel size and TR(ms)/TE(ms)/flip angle(degree)=6.5-2300/2.93-3.12/9° for Philips and Siemens, 11° for GE. rsfMRI was acquired using axial echo-planar imaging (EPI). For each subject's measurement, volumes between 140 and 200 were recorded in ~3.3mm isotropic voxel resolution with a TR(ms)/TE(ms)/flip angle(degree)=3000-3025/ 30-30.001/ 80° for ADNI-GO/2, 90° for ADNI 3. Fieldmaps were included if available to correct for B0 inhomogeneities. The following protocol parameters were applied: Philips: TR(ms)/TE1(ms)/TE2(ms)/flip angle (degree)=20/2.3/4.6/10°; Siemens: TR(ms)/TE1(ms)/ TE2(ms)/flip angle (degree)=571-581/4.92/7.38/60°. For GE no fieldmapping was conducted. Detailed descriptions of image acquisition can be found on http://adni.loni.usc.edu.

Data preprocessing

Considering their specific scanning parameters such as TR, slice order, and volume number, all data were preprocessed with the Data Processing Assistant for Resting-State fMRI Advanced (DPARSFA, http://rfmri.org/dpabi) toolbox version 5 (release 5.2_210501), which is based on the Statistical Parametric Mapping toolbox (SPM 12, https://www.fil.ion.ucl.ac.uk/spm/) for MATLAB®. The preprocessing pipeline started with removing the first ten volumes for the signal to reach T1 equilibrium and the subject to adjust to the scanner's environment. Further steps included a) slice time correction; b) spatial realignment using a six-parameter rigid-body spatial transformation and unwarping using B_0 fieldmaps if available to mitigate spurious effects of head motions during the measurement; c) T1 co-registration to the mean functional image; d) CSF, gray and white matter tissue class segmentation, as well as spatial normalization using diffeomorphic anatomical registration using exponential lie algebra (DARTEL) (Ashburner, 2007) for T1 images; e) regression of nuisance variables, including CSF and white matter signal, the first order polynomial trend and the Friston 24-parameter model (Friston et al., 1996) to mitigate the influence of spurious physiological effects and head motion; f) functional images were normalized to MNI space and resampled to an isotropic voxel size of 3 mm using the parameters estimated by DARTEL.

For ReHo and FC measures, the normalized images were bandpass filtered (0.01-0.1 Hz). In a next step, scrubbing was applied to detect and remove single frames affected by head motion, so-called "bad" time points. Frames exceeding a frame-to-frame displacement of 1 mm have been removed along with the previous and the two subsequent frames (Power et al., 2012). Only scans with >70% remaining EPI volumes after scrubbing were included to ensure a sufficiently high number of volumes for the subsequent analysis (Yan et al., 2013). Consequently, we excluded these participants who did not meet this criterion (ADNI-GO/2: n=16, ADNI 3: n=4). For fALFF, no filtering and scrubbing were applied (Yan, 2010).

To reduce the influence of excessive head motion, participants exhibiting more than 3.0 mm of maximum movement and a 3.0-degree rotation angle were discarded (n=3 for ADNI 3).

Further, images were visually inspected after co-registration, segmentation, and normalization to guarantee high quality. This included a specific focus on signal loss and artifacts in the regions of interest (NbM, EC) by overlaying the ROI mask in standardized space;

especially, the EC represents a region that might often be affected by artifacts (Olman et al., 2009). This check resulted in a final sample size of n=71 (Table 7.1).

Since head motion strongly influences FC measures (Power et al., 2012), we compared head motion in an independent t-test with CSF group as a grouping factor to ensure no confounding effect on groups. Consequently, the comparison in the 6 parameters of rigid body transformation of maximum and mean motion revealed no significant differences between normal CSF and abnormal CSF, except for measurement 2 the mean rotation in z-axis ($t(69)=2.425$, $p=0.018$). Furthermore, the root mean square of head motion, same as the relative root mean square of framewise displacement (FD) Vanijk showed no significant differences between the two groups. In measurement 1 there was a significant difference between nCSF and aCSF in the mean FD Power ($t(69)=-2.276$, $p=0.026$) and in measurement 2 ($t(69)=-3.228$, $p=0.002$). Because the groups only differed regarding their mean FD Power and the other tests revealed no significant differences, we minimized the influence of head motions by excluding participants with excessive head motions and utilizing scrubbing.

Region of interest definition

The regions of interest NbM and EC were created in MNI space combined across both hemispheres with the SPM Anatomy Toolbox Version 3.0 (Eickhoff et al., 2005, 2006, 2007) (available from https://www.fz-juelich.de/en/inm/inm-7/resources/jubrain-anatomy-toolbox, Fig. 7.1A) The NbM is defined as the Ch4 according to previous published probabilistic maps (Zaborszky et al., 2008). The EC was defined based on the previously published probability map (Amunts et al., 2005) .

We used the toolbox MarsBaR (Brett et al., 2002) to extract the mean rsfMRI signal intensity for each ROI at a threshold of 50% probability and each subject individually.

rsfMRI analyses

The fractional amplitude of low-frequency fluctuations analysis (fALFF)

Spontaneous local brain activity based on the amplitude of BOLD signals can be assessed by the amplitude of low-frequency fluctuations (ALFF) and its improved measure of fractional amplitude of low-frequency fluctuations (fALFF) (Biswal et al., 1995; Zou et al., 2008; Zuo et al., 2010). ALFF assesses the amplitude in the low-frequency range, and fALFF represents the ratio of total amplitude within the low-frequency range (here, 0.01-0.1 Hz) to the amplitude across the entire detectable frequency range. Importantly, fALFF shows a higher specificity

with regard to the detection of local spontaneous brain activity and is more robust against nonspecific signals (e.g., physiological noise) as compared to ALFF (Zou et al., 2008; Zuo et al., 2010). Therefore, fALFF is recommended (Zuo & Xing, 2014) and used here.

Regional Homogeneity (ReHo)

Regional homogeneity (ReHo) refers to local connectivity within brain regions to measure regional synchronization among brain voxels and their neighboring voxels (Zang et al., 2004). The central assumption of ReHo is that structural neighboring voxels represent a functional homogeneity of time series defining it a network centrality metric (Jiang & Zuo, 2016). In this study, ReHo is quantified by Kendall's coefficient of concordance (KCC) (Kendall & Gibbons, 1990) of a given voxel with its nearest neighbors. Thus, a larger ReHo value indicates higher local synchronization.

ROI to ROI functional connectivity

FC is defined by a temporal dependence across anatomically separated brain regions regarding patterns of neuronal activity (Biswal et al., 1995; Lowe et al., 1998, 2000). FC is supposed to reflect functional communication and a shared function between brain regions (van den Heuvel & Hulshoff Pol, 2010). Therefore, Pearson's correlation coefficient between both time courses extracted from the NbM and EC was calculated and a Fisher’s z transformation was applied.

Results

ReHo

Regions differ regarding their regional homogeneity (ReHo), however, not CSF group

The 2x2 mixed ANCOVA revealed a significant main effect of region ($F(1,69)=8.387$, $p=0.005$, partial $\eta^2=0.108$, Fig. S3.2A), no main effect of group ($F(1,63)=0.003$, $p=0.960$, partial $\eta^2=0.000$, Fig. S3.2A) and no significant interaction between group and region ($F(1,63)=1.706$, $p=0.196$, partial $\eta^2=0.026$, Fig. S3.2A).

Annual percentage signal change in ReHo does not differentiate between CSF groups or regions

We used a 2x2 mixed ANCOVA to investigate whether the longitudinal indices of APSC in ReHo of the NbM and EC differentiated between CSF normal vs. abnormal groups. There was no

significant main effect of region (F(1,69)=0.001, p=0.974, partial η^2=0.000, Fig. S3.2B), no main effect of CSF group (F(1,63)=0.218, p=0.642, partial η^2=0.003, Fig. S3.2B), and no interaction of region and CSF group (F(1,63)=0.394, p=0.532 , partial η^2=0.006, Fig. S3.2B).

The baseline signal in NbM does not predict the annual percentage signal change in ReHo of EC

The robust regression modeling did not reveal any significant results (see Fig. S3.3, Table S3.2).

CSF group does not moderate the functional spread of degeneration in ReHo

The moderation analysis included baseline ReHo NbM as independent variable, ReHo EC APSC as dependent variable and CSF group as moderator. The model was not statistically significant (R^2=0.2135, F(9,61)=1.2677, p=0.2728), with no significant direct effect of NbM→EC (t(61)=-0.5922, p=0.5559), and no significant moderator effect (t(61)=-0.5067, p=0.6142), which is in line with the robust regression analysis.

The moderation analysis included baseline ReHo EC as independent variable, ReHo NbM APSC as dependent variable and CSF group as moderator. The model was also not statistically significant (R^2=0.0544, F(9,61)=0.3712, p=0.9445), with no significant direct effect of EC→NbM (t(61)=-0.4040, p=0.6876), and no significant moderator effect (t(61)=-0.7685, p=0.4451, which, again, is in line with the robust regression analysis.

Functional connectivity between NbM and EC

NbM and EC show functional connectivity independent from CSF status

To investigate FC between NbM and EC, we used a 2x2 mixed ANCOVA with time (timepoint 1 and timepoint 2) and group (aCSF, nCSF) as within and between group variables. There was no significant effect of time (F(1,69)=1.221, p=0.273, partial η^2=0.017, Fig. S3.2C), no main effect of CSF group (F(1,63)=1.467, p=0.23, partial η^2=0.023, Fig. S3.2C), and no significant interaction between time and group (F(1,63)=0.571, p=0.453, partial η^2=0.009, Fig. S3.2C).

However, given our a priori hypotheses of a FC between both regions, we carried out post-hoc t-tests for each time point separately across both groups. These revealed a significant effect, and therefore functional connectivity, for timepoint 1 in nCSF (t(36)=2.667, p=0.011) and timepoint 2 (t(36)=3.054, p=0.004). In aCSF there was only a borderline significant effect at timepoint 1 (t(33)=1.999, p=0.054) but a highly significant effect in timepoint 2 (t(33)=3.535, p=0.001).

Figure S3.1

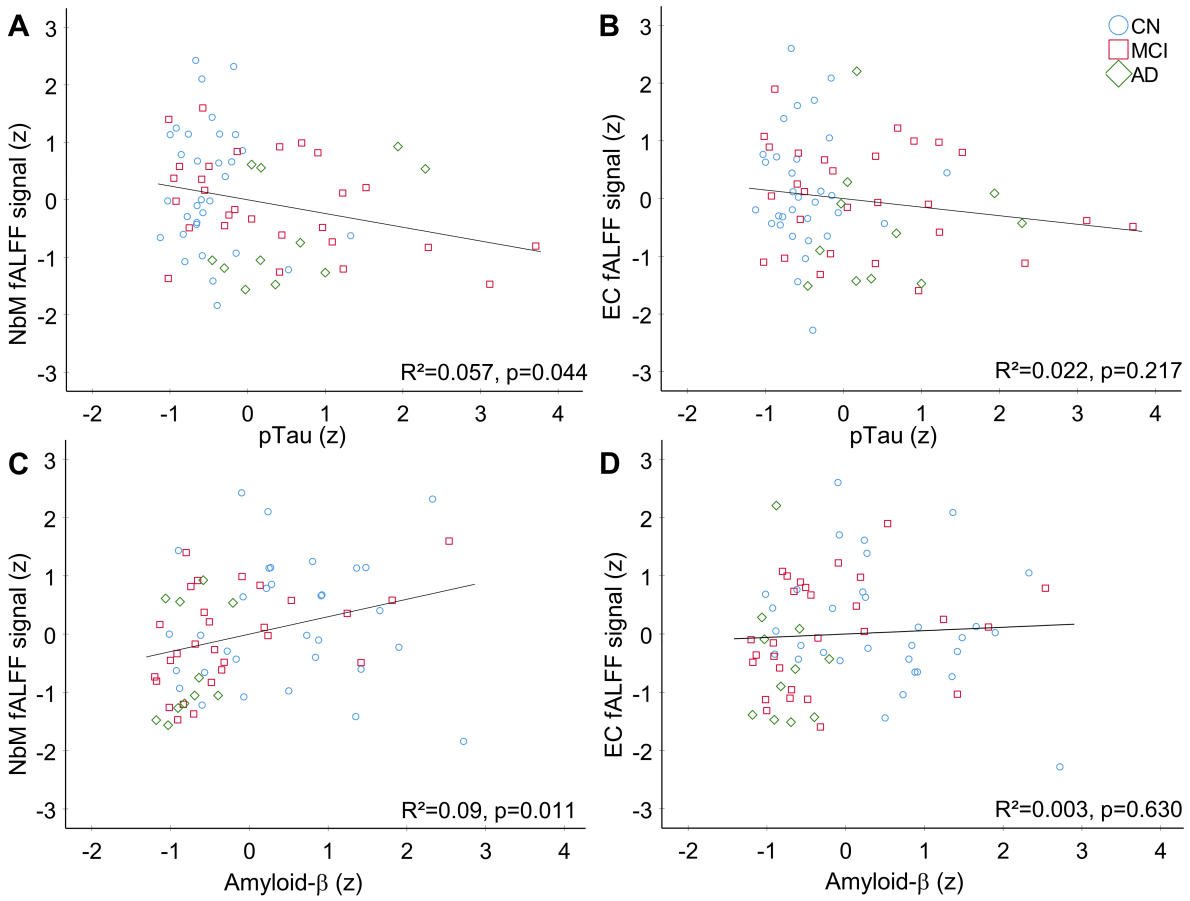

Figure S3.1. **Linear regression models for fALFF signals in the nucleus basalis of Meynert (NbM) and entorhinal cortex (EC) separately for Aβ and pTau.** A) and B) show linear regressions for z-scored fALFF signal at baseline (t1) in A) NbM and B) EC against the z-scored pTau. In C) the relationship is shown for NbM and in D) EC against amyloid-β. A significant linear regression was observed only in the NbM for pTau and amyloid-β (A and C) (pTAu: R^2=0.057, F(1, 69)=4.19, p=0.044; amyloid-β: R^2=0.09, F(1, 69)=6.784, p=0.011), but not EC (B and D) (pTau: R^2=0.022, F(1, 69)=1.556, p=0.217; amyloid-β: R^2=0.003, F(1, 69)=0.234, p=0.63), supporting the linear regression models with only the CSF status. For the sake of visualization, groups are shown in blue circle for HC (n=32), red square for MCI (n=28), and green rhombus for AD (n=11)).

Figure S3.2

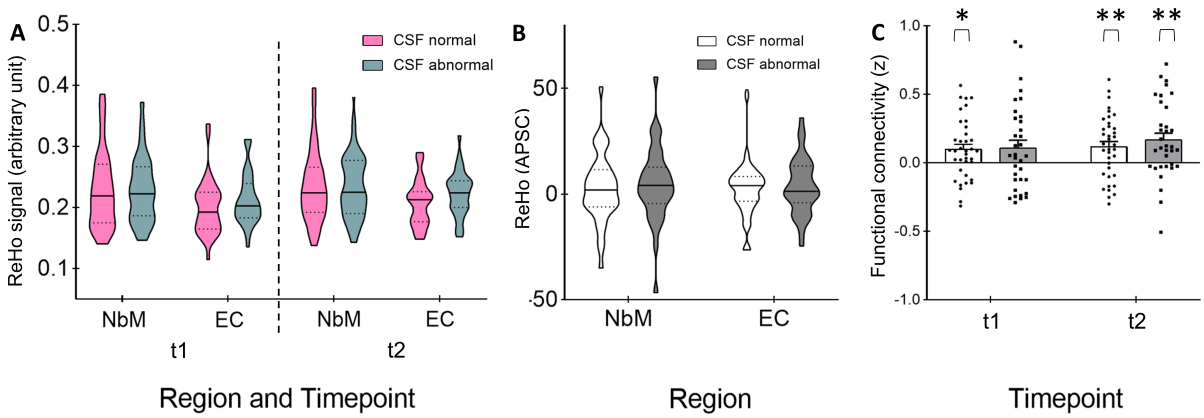

Figure S3.2. ReHo signals and annual percentage change and functional connectivity between the nucleus basalis of Meynert (NbM) and entorhinal cortex (EC). A) Violin plots representing the participants' baseline signals (t1) and signals at the follow-up measurement (t2) in ReHo for normal CSF (n=37) and abnormal CSF (n=34). The mixed ANCOVA revealed a significant effect of region at t1 ($F(1,69)=8.387$, $p=0.005$), shown in A). B) showing the annual percentage signal change (APSC) in both regions for ReHo; here, mixed ANCOVA revealed no significant effects. The horizontal lines show the median and the dotted lines the interquartile range. C) Functional connectivity between NbM and EC at t1 and t2, analyzed using post-hoc t-tests. It revealed a significant effect in nCSF at t1 ($t(36)=2.667$, $p=0.011$) and t2 ($t(36)=3.054$, $p=0.004$). In the aCSF group, there was a borderline significant effect at t1 ($t(33)=1.999$, $p=0.054$) and a highly significant effect at t2 ($t(33)=3.535$, $p=0.001$). Dots represent individual data points, and error bars represent standard deviations. *$p<0.05$, **$p<0.01$.

Figure S3.3

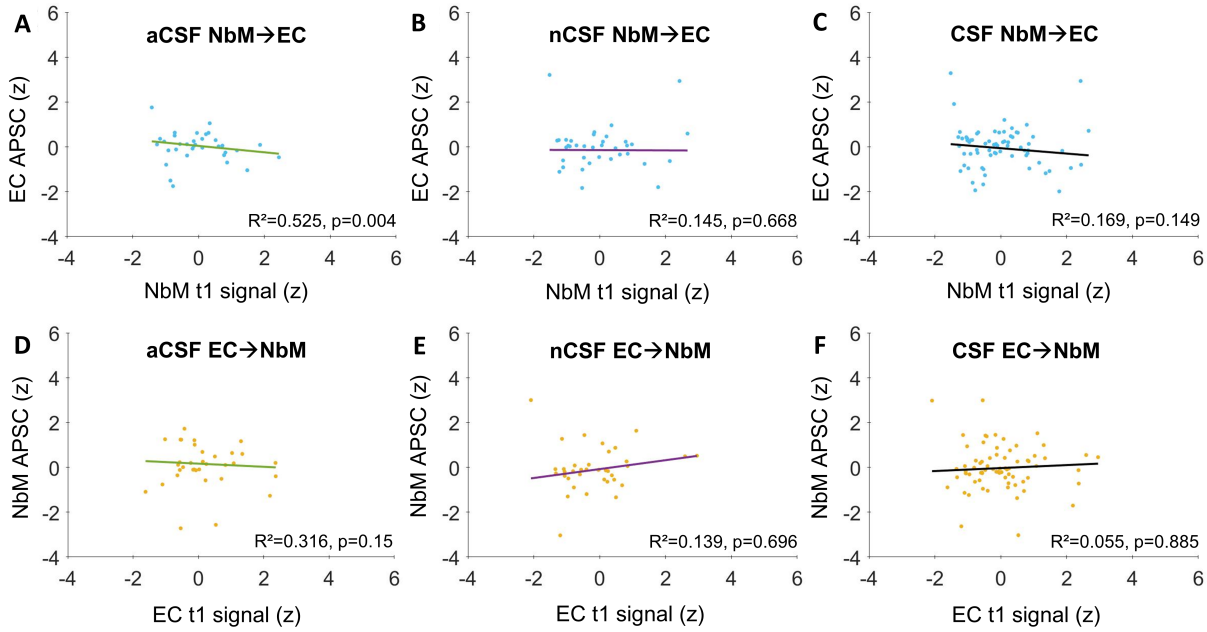

Figure S3.3. Robust regression models in ReHo. Plots for the robust regression models for NbM→EC (A, B, C), and EC→NbM (D, E, F) separately for both groups and averaged across groups (C, F). X-axis represent z-scored baseline (t1) signal, y-axis represent z-scored annual percentage signal change (APSC) in ReHo. Dots represent individual data. No significant effects were found. NbM=nucleus basalis of Meyert. EC=entorhinal cortex. aCSF=abnormal CSF (n=34); nCSF=normal CSF (n=37); CSF=CSF normal and abnormal included as a variable (n=71).

Table S3.1.

Output of the robust regression models of fALFF with the covariates age, sex, ADNI cohort, scanner and education.

aCSF NbM → EC (n= 34)

	Estimate	SE	t	p
Intercept	3.74	2.88	1.3	0.205
Baseline NbM	-0.3	0.22	-1.36	0.185
Sex	-0.05	0.45	-0.11	0.91
Age	-0.06	0.03	-2.28	0.031
ADNI Group	1.28	1.1	1.17	0.251
Scanner: Siemens	-0.63	1.24	-0.51	0.615
Scanner: GE	-1.8	1.23	-1.46	0.155
Education	0.06	0.1	0.6	0.551

R-Squared: 0.263; Adjusted R- Squared: 0.0649; df= 26; F-statistics vs. constant model: 1.33; p-value: 0.277

nCSF NbM → EC (n= 37)

	Estimate	SE	t	p
Intercept	0.95	2.15	0.44	0.662
Baseline NbM	-0.43	0.15	-2.81	0.009
Sex	-0.11	0.33	-0.34	0.738
Age	-0.01	0.02	-0.38	0.708
ADNI Group	0.13	0.46	0.28	0.78
Scanner: Siemens	0.42	0.48	0.88	0.388
Scanner: GE	-0.34	0.54	-0.63	0.536
Education	-0.02	0.07	-0.24	0.813

R-Squared: 0.296; Adjusted R- Squared: 0.126; df=29; F-statistics vs. constant model: 1.74; p-value: 0.138

aCSF EC → NbM (n= 34)

	Estimate	SE	t	p
Intercept	-2.24	3.11	-0.72	0.478
Baseline EC	-0.26	0.25	-1.03	0.314
Sex	0.06	0.53	0.12	0.908
Age	0.02	0.03	0.5	0.623
ADNI Group	1.28	1.2	1.07	0.296
Scanner: Siemens	-0.83	1.36	-0.61	0.545
Scanner: GE	-1.08	1.36	-0.8	0.433
Education	0.05	0.11	0.51	0.614

R-Squared: 0.137; Adjusted R- Squared: -0.0959; df= 26; F-statistics vs. constant model: 0.587; p-value: 0.76

nCSF EC → NbM (n= 37)

	Estimate	SE	t	p
Intercept	2.15	1.89	1.14	0.264
Baseline EC	-0.21	0.13	-1.58	0.125
Sex	0.03	0.3	0.09	0.926
Age	-0.02	0.02	-1.14	0.262
ADNI Group	-0.01	0.4	-0.02	0.984
Scanner: Siemens	0.54	0.42	1.27	0.214
Scanner: GE	-0.03	0.47	-0.07	0.944
Education	-0.04	0.06	-0.58	0.565

R-Squared: 0.175; Adjusted R- Squared: -0.0239; df=29; F-statistics vs. constant model: 0.88; p-value: 0.534

With CSF NbM → EC (n= 71)

	Estimate	SE	t	p
Intercept	2.2	1.61	1.36	0.178
Baseline NbM	-0.38	0.12	-3.14	0.003
Sex	-0.19	0.25	-0.78	0.44
CSF	0.18	0.26	0.72	0.477
Age	-0.03	0.02	-1.99	0.051
ADNI Group	0.32	0.39	0.81	0.42
Scanner: Siemens	0.12	0.43	0.27	0.788
Scanner: GE	-0.69	0.47	-1.48	0.145
Education	0.01	0.05	0.28	0.783

R-Squared: 0.235; Adjusted R- Squared: 0.137; df=62; F-statistics vs. constant model: 2.39; p-value: 0.026

With CSF EC → NbM (n= 71)

	Estimate	SE	t	p
Intercept	0.04	1.62	0.03	0.98
Baseline EC	-0.21	0.11	-1.8	0.077
Sex	-0.04	0.25	-0.17	0.866
CSF	0.08	0.25	0.33	0.741
Age	-0.004	0.02	-0.22	0.823
ADNI Group	0.16	0.38	0.41	0.685
Scanner: Siemens	0.32	0.43	0.73	0.466
Scanner: GE	-0.06	0.47	-0.12	0.905
Education	0.003	0.05	0.06	0.951

R-Squared: 0.0884; Adjusted R- Squared: -0.0293; df=62; F-statistics vs. constant model: 0.751; p-value: 0.646

Table S3.2.

The output of the robust regression models of ReHo with the covariates age, sex, ADNI cohort, scanner and education.

aCSF NbM → EC (n= 34)

	Estimate	SE	t	p
Intercept	-5.07	1.97	-2.58	0.016
Baseline NbM	-0.14	0.15	-0.98	0.337
Sex	0.4	0.3	1.31	0.201
Age	0.04	0.02	2.28	0.031
ADNI Group	-1.33	0.75	-1.78	0.087
Scanner: Siemens	1.12	0.85	1.32	0.198
Scanner: GE	3.06	0.84	3.66	0.001
Education	0.1	0.07	1.53	0.137

R-Squared: 0.525; Adjusted R- Squared: 0.397; df=26; F-statistics vs. constant model: 4.1; p-value: 0.00373

nCSF NbM→ EC (n= 37)

	Estimate	SE	t	p
Intercept	0.83	2.3	0.36	0.722
Baseline NbM	-0.01	0.15	-0.04	0.971
Sex	0.12	0.36	0.33	0.743
Age	-0.03	0.03	-1.03	0.313
ADNI Group	-0.09	0.47	-0.19	0.851
Scanner: Siemens	-0.43	0.51	-0.86	0.399
Scanner: GE	0.34	0.59	0.57	0.57
Education	0.06	0.07	0.78	0.442

R-Squared: 0.145; Adjusted R- Squared: -0.0608; df= 29; F-statistics vs. constant model: 0.705; p-value: 0.668

aCSF EC → NbM (n= 34)

	Estimate	SE	t	p
Intercept	-2.38	3.15	-0.76	0.455
Baseline EC	-0.07	0.21	-0.33	0.744
Sex	0.14	0.46	0.31	0.757
Age	0.02	0.03	0.64	0.526
ADNI Group	0.08	1.11	0.07	0.946
Scanner: Siemens	1.87	1.27	1.48	0.152
Scanner: GE	0.49	1.25	0.39	0.7
Education	0.05	0.1	0.52	0.608

R-Squared: 0.316; Adjusted R- Squared: 0.131; df=26; F-statistics vs. constant model: 1.71; p-value: 0.15

nCSF EC → NbM (n= 37)

	Estimate	SE	t	p
Intercept	1.65	2.4	0.69	0.497
Baseline EC	0.2	0.16	1.21	0.237
Sex	-0.06	0.37	-0.17	0.863
Age	-0.02	0.03	-0.9	0.377
ADNI Group	0.56	0.48	1.16	0.254
Scanner: Siemens	-0.36	0.52	-0.68	0.501
Scanner: GE	0.15	0.59	0.25	0.804
Education	-0.01	0.08	-0.17	0.863

R-Squared: 0.139; Adjusted R- Squared: -0.0688; df=29; F-statistics vs. constant model: 0.669; p-value: 0.696

With CSF NbM → EC (n= 71)

	Estimate	SE	t	p
Intercept	-2.02	1.6	-1.27	0.21
Baseline NbM	-0.12	0.11	-1.05	0.297
Sex	0.19	0.24	0.78	0.441
CSF	0.1	0.24	0.42	0.678
Age	0.02	0.02	0.89	0.376
ADNI Group	-0.22	0.38	-0.58	0.566
Scanner: Siemens	-0.13	0.42	-0.3	0.763
Scanner: GE	1.18	0.47	2.53	0.014
Education	0.04	0.05	0.84	0.403

R-Squared: 0.169; Adjusted R- Squared: 0.0623; df=62; F-statistics vs. constant model: 1.58; p-value: 0.149

With CSF EC→ NbM (n= 71)

	Estimate	SE	t	p
Intercept	0.14	1.77	0.08	0.939
Baseline EC	0.07	0.12	0.54	0.59
Sex	-0.1	0.27	-0.36	0.723
CSF	0.26	0.26	1.01	0.317
Age	-0.01	0.02	-0.3	0.768
ADNI Group	0.41	0.42	1.0	0.323
Scanner: Siemens	-0.29	0.47	-0.63	0.531
Scanner: GE	0.17	0.51	0.33	0.743
Education	0.002	0.06	0.04	0.972

R-Squared: 0.055; Adjusted R- Squared: -0.0669; df=62; F-statistics vs. constant model: 0.451; p-value: 0.885